Modelling and numerical methods for the study of particle transport in a hot plasma

Sébastien Guisset

▶ **To cite this version:**

Sébastien Guisset. Modelling and numerical methods for the study of particle transport in a hot plasma. General Mathematics [math.GM]. Université de Bordeaux, 2016. English. NNT : 2016BORD0117 . tel-01376087

HAL Id: tel-01376087
https://theses.hal.science/tel-01376087

Submitted on 4 Oct 2016

HAL is a multi-disciplinary open access archive for the deposit and dissemination of scientific research documents, whether they are published or not. The documents may come from teaching and research institutions in France or abroad, or from public or private research centers.

L'archive ouverte pluridisciplinaire **HAL**, est destinée au dépôt et à la diffusion de documents scientifiques de niveau recherche, publiés ou non, émanant des établissements d'enseignement et de recherche français ou étrangers, des laboratoires publics ou privés.

université de BORDEAUX

UNIVERSITÉ DE BORDEAUX

Année 2016

THÈSE

pour obtenir le grade de

DOCTEUR

Discipline: *Mathématiques appliquées et calcul scientifique*

École doctorale de Mathématiques et Informatique de Bordeaux

présentée et soutenue publiquement par

Sébastien GUISSET

le 23 Septembre 2016

Modélisation et méthodes numériques pour l'étude du transport de particules dans un plasma chaud

Devant la commission d'examen composée de :

M. Alain Bachelot, Professeur, Université de Bordeaux, Président du jury.
M. Bruno Després, Professeur, Université de Paris 6, Rapporteur.
M. Francis Filbet, Professeur, Université de Toulouse, Rapporteur.
M. Christophe Chalons, Professeur, Université de Versailles, Examinateur.
M. Philippe Helluy, Professeur, Université de Strasbourg, Examinateur.
M. Mohammed Lemou, Directeur de recherche CNRS, Université de Rennes 1, Examinateur.
M. Bruno Dubroca, Expert Sénior CEA/DAM, Invité.
M. Vladimir Tikhonchuk, Professeur Université de Bordeaux, Invité.
M. Stéphane Brull, Maître de Conférence, Bordeaux INP, Directeur de thèse.
M. Emmanuel d'Humières, Maître de Conférence, Université de Bordeaux, Co-Directeur de thèse.

Titre Modélisation et méthodes numériques pour l'étude du transport de particules dans un plasma chaud.

Résumé Les modèles aux moments angulaires constituent des descriptions intermédiaires entre les modèles cinétiques et les modèles fluides. Dans ce manuscrit, les modèles aux moments angulaires basés sur un principe de minimisation d'entropie sont étudiés pour des applications en physique des plasmas. Ce mémoire se découpe en trois parties. La première est une contribution à la modélisation en physique des plasmas à travers le formalisme des modèles aux moments angulaires. Dans celle-ci, le domaine de validité de ces modèles est étudié en régimes non-collisionels. Il est également montré que les opérateurs de collisions proposés pour le modèle M_1 permettent de retrouver des coefficients de transport plasma précis. La deuxième partie de ce document concerne la dérivation de méthodes numériques pour l'étude du transport de particules en temps long. Dans ce cadre, des schémas numériques appropriés pour le modèle M_1, préservant l'asymptotique, sont construits et validés numériquement. La troisième partie représente un premier pas significatif vers la modélisation multi-espèces. Ici, le modèle aux moments angulaire M_1, construit dans un référentiel mobile, est appliqué à la dynamique des gaz raréfiés. Les propriétés de ce modèle sont détaillées, un schéma numérique est proposé et une validation numérique est menée.

Mots-clés Modélisation en physique des plasmas, transport de particules, modèles aux moments angulaires, schémas préservant l'asymptotique, schémas de type Godunov, solveurs de Riemann approchés.

Laboratoire d'accueil Laboratoire Celia, 351 Cours de la Libération F-33405 Talence cedex France / Institut de Mathématiques de Bordeaux, 351 cours de la Libération F-33405 Talence cedex France.

Title Modelling and numerical methods for the study of particle transport in a hot plasma.

Abstract Angular moments models represent alternative descriptions situated in between the kinetic and the fluid models. In this work, angular moments models based on an entropy minimisation principle are considered for plasma physics applications. This manuscript is organised in three parts. The first one is a contribution to plasma physics modelling within the formalism of angular moments models. The validity domain of angular moments models in collisionless regimes is studied. It is also shown that the collisional operators proposed for the M_1 angular moments model enable to recover accurate plasma transport coefficients. The second part of this document deals with the derivation of numerical methods for the long timescales particle transport. Appropriate asymptotic-preserving numerical schemes are designed for the M_1 angular moments model and numerical validations are performed. The third part represents a first important step toward multi-species modelling. The M_1 angular moments model in a moving frame is introduced and applied to rarefied gas dynamics. The model properties are highlighted, a numerical scheme is proposed and a numerical validation is carried out.

Keywords Plasma physics modelling, particle transport, angular moments models, Asymptotic-preserving schemes, Godunov-type schemes, approximate Riemann solvers.

Host laboratories Laboratoire Celia, 351 Cours de la Libération F-33405 Talence cedex France / Institut de Mathématiques de Bordeaux, 351 cours de la Libération F-33405 Talence cedex France.

Remerciements

Tout d'abord, je remercie Bruno Després et Francis Filbet d'avoir accepté de rapporter cette thèse. Je les remercie pour leurs remarques, commentaires, critiques, suggestions suite à la lecture de ce manuscrit. Je remercie également Christophe Chalons, pour les discussions lors du congrès SMAI puis lors de sa venue à Bordeaux, Philippe Helluy pour le Cemracs 2014 à Luminy et Mohammed Lemou pour les échanges lors de l'été 2015 à Beijing. Je les remercie tous les trois d'avoir accepté le rôle d'examinateur dans ce jury. Je remercie Alain Bachelot d'avoir accepté de présider ce jury et pour sa sympathie.

J'adresse un grand "Merci!" à Stéphane Brull et Bruno Dubroca pour leur encadrement et pour tout ce qu'ils m'ont apporté lors de cette thèse. Je les remercie pour leur patience malgré mes interminables questions et mon entêtement, pour leur pédagogie, leurs critiques et leurs conseils. Au-delà du travail de thèse, je les remercie pour leur bonne humeur et leur humour communicatif qui était toujours présent au quotidien. Malgré les difficultés rencontrées cela m'a permis de relativiser certaines situations et de rester optimiste.

Je remercie mon co-directeur de thèse Emmanuel d'Humières pour ses conseils avisés et sa gentillesse. Échanger avec lui m'a appris à être plus diplômate et à garder une ouverture d'esprit vis à vis de thèmes de recherches différents ou de nouvelles idées.

Je tiens à remercier Vladimir Tikhonchuk pour sa disponibilité et pour le partage de son expérience. J'ai souvent été impressionné par la précision et la profondeur de ses remarques. Ceci m'a amené à me poser de nombreuses questions et à effectuer de nombreux calculs relatifs à la compréhension de la physique des plasmas.

Je remercie Denise Aregba pour toutes les explications concernant les schémas de relaxation, les problèmes de Riemann et bien d'autres choses. Je la remercie pour les séances de travail et pour ses conseils clairs et avisés sur la thèse et bien au-delà.

Merci à Rodolphe Turpault d'avoir pris du temps pour discuter des limites de diffusion et plus généralement des schémas asymptotic-preserving. Je le remercie aussi pour son écoute et ses conseils lors de mon activité d'enseignement.

Je remercie Rachel Nuter pour toutes les discussions portant sur la physique des plasmas et pour avoir eu le courage de vérifier mes calculs des taux d'absorption laser-plasma!

Je remercie Thanh-Ha Nguyen-Bui pour les discussions sur la physique en général

et pour sa sympathie.

Je remercie Jean-Luc Feugeas pour les discussions sur les modèles aux moments et les fermetures entropiques.

Je remercie Jérome Breil pour notre projet TER, pour sa sympathie et pour m'avoir permis de rencontrer les membres du laboratoire Celia.

Je remercie les permanents du groupe Fusion au Celia et tous les gens qui ont pris de leur temps pour moi. Je remercie en particulier Emmanuelle Lesage (pour le chef-d'oeuvre de sa carrière), Céline Oum et Sophie Heurtebise pour tout leur travail. Plus généralement, je remercie toutes les personnes qui contribuent à améliorer nos conditions de travail et qui permettent cette liberté qui est si importante pour la production scientifique.

Je remercie mes anciens enseignants rencontrés lors de mes années d'études. Ils ont, pour certains, marqué ma manière de travailler, de réfléchir et de voir les choses.

Je remercie mes amis du laboratoire et ceux extérieur, pour tous les moments passés ensemble et les nombreux à venir j'espère.

Je remercie toute ma famille et en particulier mes parents et ma soeur pour leur soutien inconditionnel. Au-delà de leur soutien, ils m'ont permis de développer un grand intérêt pour les sciences et je leur dois énormément.

Je remercie la famille Lhomme pour son affection et son accueil lors des weekends à Angoulême. Enfin, je remercie Lucie qui me supporte et me soutient.

Contents

Introduction

Intention

This manuscript is a contribution to the modelling and numerical methods for the transport of charged particles in dense plasmas. We are interested in hot plasmas created by lasers and the general context is the understanding of the processes leading to ignition of the fusion reactions. This issue constitutes the main motivation of this work and is followed as a general research direction. However, many other research areas are closely related to this work since they present a similar physics. They extend to hypersonic flows [5], radiotherapy [11, 12, 13], magnetic confinement fusion (MCF) [145, 146], astrophysics [59], studies of lighting and flames, engines for space propulsion [103] or plasma remediation processes.

Context

Nowadays, everybody knows the emergency to tackle the issues related to energetic resources exhaustion and global warming. Several research axes are dealing with measures permitting significant energy savings. Other approaches consider new energy production methods based on nuclear fusion reactions. Stars are powered by nuclear fusion in their cores and the control of such processes on earth represents a great perspective for abondant energy production. A nearly inexhaustible combustible in addition to a small quantity of long-life time radioactive waste and greenhouse gas make this approach very attractive.

Nuclear fusion reactions are based on the fusion of light atomic nuclei, which releases large quantities of energic particles or radiation. In the case of the fusion of deuterium and tritium (D-T), an alpha particle and a neutron are produced. A large kinetic energy is carried out by these two reaction products (3.5 MeV for the alpha particle and 14.1 Mev for the neutron). The use of deuterium and tritium (D-T) nuclei is currently the nominal way chosen to achieve fusion with a minimum of energy provided to the system. The cross section of D-T reaction fusion is indeed several times larger compared to the other fusion reactions (D-^{3}He, D-Dp, D-Dn, etc). The D-T reaction, producing the 14 MeV neutrons, is the following

$$\mathrm{D} + \mathrm{T} \rightarrow {}^4\mathrm{He}\ (3.52\ \mathrm{MeV}) + \mathrm{n}\ (14.06\ \mathrm{MeV}).$$

The main difficulty in the initiation of the fusion reaction lies in the fact that both parent nuclei have the same positive charge and repulse each other. In order to achieve the fusion of two nuclei one has to overcome the Coulomb repulsive forces

between them. The amount of energy released and the number of reactions in the volume of plasma depend on the density of particles and their temperature. The reaction gain becomes higher than one when the energy released by fusion reactions becomes greater than the one invested in the plasma heating and confinement. This condition can be expressed in terms of the density n, temperature T of the plasma and its confinement time τ through the Lawson criterion [153]. For a Deuterium-Tritium plasma heated to the temperature of 10 keV or 10^8K, this criteria writes as

$$n\tau > 10^{20}\mathrm{m}^{-3}\mathrm{s}.$$

There exist different ways to satisfy this criterion. An enormous mass insures through the gravitation forces a very large confinement time in stars. The confinement time is the major factor of success. On Earth, two approaches are considered to achieve a large gain in fusion reactions: the magnetic and inertial confinement. The first method consists in using strong magnetic fields to maintain the combustible at a very high temperature. The plasma can be stabilised and confined away from the walls by the magnetic field, to obtain a continuous production of the fusion energy: this is the process of magnetic confinement fusion [145, 146]. The devices considered to study the feasibility of magnetic confinement fusion are the tokamaks, stellarators and other magnetic traps, which confine a plasma mixture of hydrogen isotopes in a magnetic field produced by supra-conducting coils. The confinement is achieved by choosing a toroidal geometry for the magnetic fusion reactor.
The second approach consists in bringing to very high density and temperature a small volume of fuel within an extremely short time by the use of very powerful lasers. In this case the confinement is achieved by the inertia of imploding mass: this is the process of inertial confinement fusion [89, 152, 163]. The idea of inertial confinement appeared in 1960 with the invention of the laser. This new source of radiation brought new attractive perspectives for fusion since high energy fluxes could be reached (of the order of 10^{14}-10^{15} W/cm^2). One of the first ideas was to transfer the laser beams energy to a small spherical target, in order to heat it sufficiently and to ignite a thermonuclear flame. In this context, Russian, American and French laboratories started to study laser-matter interactions in the sixties. However, the idea to directly use the laser energy to ignite the target was quickly given up and in 1972 an "ablative" implosion scheme was proposed. This scheme, based on the action-reaction principle, consists in the irradiation of a deuterium-tritium spherical shell by the use of powerful laser beam carefully set to obtain a symmetric illumination. Under the effect of the laser-radiation, the external face of a spherical shell is vaporised and the plasma produced expands toward the exterior: this is called the ablation process. By action-reaction, the external plasma expansion thrusts the internal part of the shell toward the center. The ablative pressure compresses and heats the shell while the gas contained inside the shell creates the hot spot in the center where the ignition conditions can be created. In that case, a nuclear combustion ignited in the hot spot propagates radially and consumes the fuel in the compressed

shell. To access such a laser energy, two facilities were built: the Laser Mégajoule (LMJ) in Bordeaux and the National Ignition Facility (NIF) in Livermore (USA). The NIF is operational since 2009. The ignition process described here supposes a perfectly isotropic irradiation with a high number of laser beams perfectly balanced and synchronised, which makes the direct drive approach particularly challenging. Also, in order to overcome the contradictory conditions of heating and compressing the target at the same time, another ignition scheme called the fast ignition scheme was proposed in 1994. The idea is to separate the fuel compression and heating. One starts by compressing the target by using the direct drive scheme, then launches a short highly energetic beam of particles to ignite the compressed fuel.
Another way to ensure an isotropic illumination is to use the indirect drive approach. It consists in the irradiation, of a hollow cylindrical metallic cavity (usually made of gold) of a few millimetres in diameter and one centimer long called "hohlraum" from inside by using many intense laser beams. The energy deposited in the holraum is converted in X-rays and creates an isotropic illumination of the target inside the cavity.

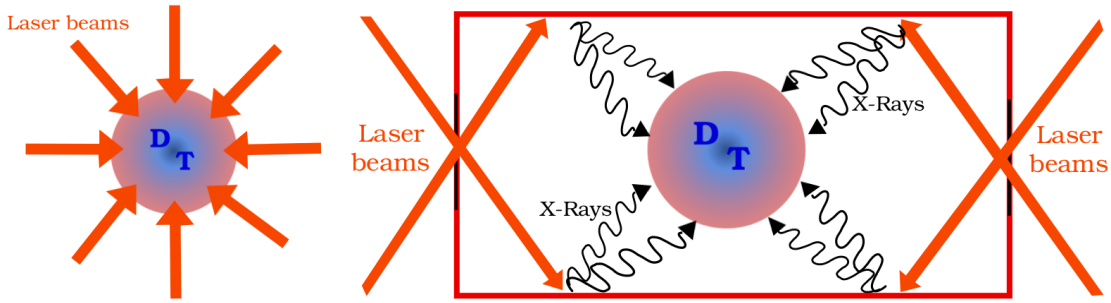

Figure 1: Irradiation scheme of a target by intense laser light in the case of the direct drive approach (left) and the indirect drive approach (right).

The understanding of the processes involved in inertial confinement fusion requires a deep and challenging study of the collisional kinetic transport of multiple species of charged particles. In addition, a rigorous mastering of the coupling with other phenomena involved in the ignition process such as radiative transfer [18, 104, 174], neutron production [78] or laser-plasma absorption processes [190] is also required. The present document mainly focuses on the modelling and the numerical study of the transport of charged particles created in the zone of laser plasma interaction at the outer part of the target [67].
In order to take into account different aspects of the particle transport numerous contributions have been made. We refer here to [198] for a review of Vlasov-Fokker-Planck numerical modelling for inertial confinement fusion plasmas. We mention here, the work of N. Crouseilles and F. Filbet [65] who developed in 2004 a Maxwell-Fokker-Planck-Landau numerical code integrating important developments dealing with the discretisation of collisional operators [39, 40, 48, 72, 73]. We also mention

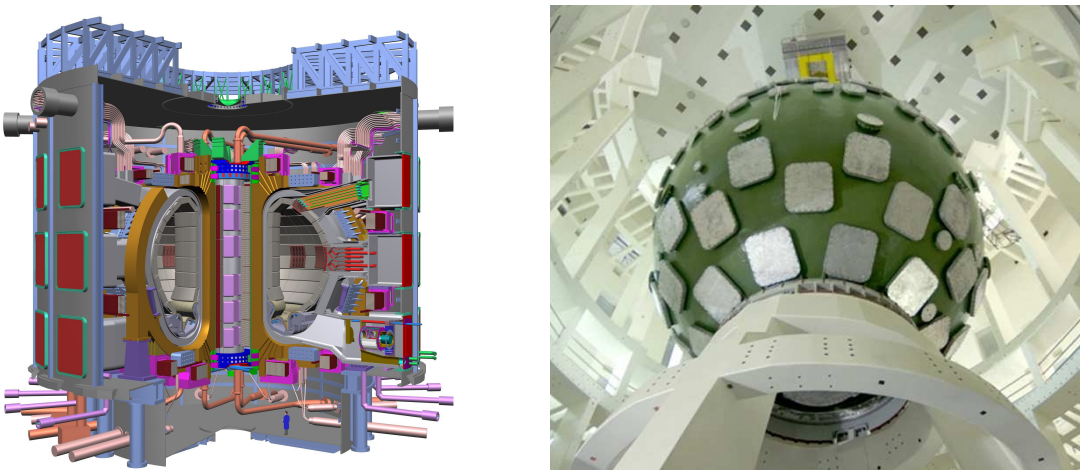

Figure 2: "International Thermonuclear Experiment Reactor" project (ITER - Cadarache) for the magnetic confinement fusion (left) and the laser installation "Laser MegaJoule" (LMJ - Bordeaux) for Inertial Confinement Fusion (right).

[41, 93, 156, 157]. These work were largely pursued in [86, 168] permitting to include the contribution of magnetic fields and explore relativistic regimes.

Research directions and objectives

Kinetic descriptions are known to be very accurate to describe the transport of charged particles in a plasma. However, they are also known to be computationally expensive to describe most realistic physical applications. An alternative way consists in considering fluid descriptions based on averaged physical quantities. However, such a macroscopic description is not sufficiently accurate. For example, in the context of inertial confinement fusion, the plasma particles may have an energy distribution far from the thermodynamic equilibrium so that the fluid description is not adapted. Moreover kinetic effects like the non local transport [33, 170], wave damping or the development of instabilities [82] can be important over time scales shorter than the collisional time so that fluid simulations are insufficient and kinetic codes have to be considered to capture the physical processes. Kinetic approaches are usually limited to times and lengths much shorter than those studied with fluid simulations. It is therefore an important challenge to describe kinetic effects using reduced kinetic codes operating on fluid time scales [94, 122].

The angular moments models represent an alternative method situated in between the kinetic and the fluid models. They require computational times shorter than kinetic models and provide results with a higher accuracy than fluid models. They originate from an angular moments average [175, 182] of the kinetic equations. The idea is to keep the velocity modulus (denoted ζ in this work) as a variable. That allows to consider the particle distributions in energy far from equilibrium, while using a simplified description of particle angular distribution. Such models are obtained by integration of the kinetic equation in angle (integration on the unit

sphere). Thus a hierarchy of moments equations can be obtained. There exist several moment models whose differences come from the choice of the closure relation. In this document we consider the angular moments models [83] based on an entropy minimisation principle. The entropy minimisation problems have been widely studied in [4, 160, 175, 177, 195]. The underlying distribution function is given by an exponential of a polynomial function depending on the particle energy and it is therefore non negative. Moreover, these closures verify the fundamental mathematical properties [112, 160, 172] such as hyperbolicity and entropy dissipation. However, their solutions could be rather different from the solution of the full kinetic equation. Moreover, from the numerical point of view, even if the closure is well defined, computational challenges remain. In particular, the resolution of the entropy minimisation problem can be very computationally costly and we refer to [4] for a specific treatment.
The angular M_1 model is largely used in the context of radiative transfer [20, 57, 84, 186, 187, 201, 202], however it is relatively new in applications to the transport of charged particles in plasma [83]. Therefore the first objective of this work is to provide a better understanding of the advantages and the limits of these reduced models for plasma physics modelling. Since angular moments models can be seen as a compromise between kinetic and fluid descriptions, they represent attractive natural candidates for capturing kinetic effects on large time scale. Therefore, another important objective is to propose appropriate numerical methods for computing the numerical solutions of angular moments models in long time regimes. Indeed, in the case where the characteristic quantities of the problem become large compared to the plasma parameters or the collisional parameters, stiffnesses appear in the considered set of equations and the model degenerates. In general, classical numerical schemes used for angular moments models are not able to correctly capture the asymptotic limit under suitable conditions on the time and space step. Also, in addition to correctly behaving in asymptotic regimes, the numerical methods also should preserve the fundamental properties of the angular moments models such as the preservation of the admissible sets for instance. This point is investigated in details in this document. Another objective concerns the simulation of multi-species particle transport. The electronic transport studies are often performed considering immobile ions [86, 168]. Indeed, because of their large mass compared to electrons, the ion motion is often neglected considering small time intervals. However, working on long time scales requires to take the ion motion into account. This will give access to a more general and interesting physics related to inertial confinement fusion applications. A significant work is then required for the use of the angular moments models to the multi-species particle transport studies.

Structure of the manuscript

This work is situated in between the plasmas physics modelling, applied mathematics and numerical analysis. This manuscript is organised in three parts. The first part is a contribution to plasma modelling through the scope of angular moments

models. The second part of this document deals with the derivation of numerical methods for the description of the long time particle transport. Common schemes usually used for angular moments models preserve the admissibility of the numerical solutions. However, such schemes are in general not able to capture the correct solution when considering asymptotic regimes. The aim is to propose numerical schemes which handle the asymptotic limit under resonable constraints on the space and time steps. The third part is a contribution to multi-species modelling. The final goal is the study of the electron and ion dynamics with an accurate model which is also numerically affordable for applications. In this work a simpler problem is investigated considering non-charged particles. The angular model is derived in a moving framework where the mean velocity is defined by the rarefied gas dynamics.

Chapter 1. In this first chapter we introduce the basic concepts essential for plasma physics modelling. These elements are used in the following chapters.

Chapter 2. In this chapter, we start recalling the principle of the angular moments closures. Angular moments models are widely used in numerical solutions of kinetic equations. While in the strongly collisional limit they are providing a good approximation of the full kinetic equation, their validity domain in the weakly collisional limit is unknown. The work of this chapter is devoted to define the validity domain of the M_1 model and its extensions, the two populations M_1 and the M_2 angular moments models for the collisionless kinetic physics applications. Three typical kinetic plasmas effects are considered, which are the charged particle beams interaction, the Landau damping and the electromagnetic wave absorption in an overdense semi-infinite plasma. For each case, a perturbative analysis is performed and the dispersion relation is established using the moments models. These relations are compared with those computed by considering the Vlasov equation. The validity limits of each model are demonstrated.

Chapter 3. In this chapter, the electronic M_1 model introduced in chapter 1 is applied here for electron transport studies in a hot collisional plasma. The moment extraction of the electron-electron collision operator from the kinetic collision operator, for this angular moments model, is challenging and some approximations are required. Firstly, we recall the collisional operators used for the electronic M_1 model proposed in [166, 167]. Then, a characterisation of the electron-electron and electron-ion collision operators is given and following [32] the electron plasma transport coefficients are derived. It is shown that in the high Z limit the electronic M_1 model and the Fokker-Planck-Landau equation coincide near equilibrium. Also, in general, the electron-electron collision operator proposed for the electronic M_1 model recovers accurate electron transport plasma coefficients.

Chapter 4. Angular moments models are nonlinear hyperbolic systems. For this purpose, in this chapter, some concepts of numerical methods for nonlinear sys-

tems are recalled following the ideas introduced in [52, 101, 102, 118, 159]. These methods directly apply to angular moments model and are used in the next chapters.

Chapter 5. This section deals with the numerical resolution of the M_1-Maxwell system in the quasi-neutral regime [63, 74]. In this regime the stiffness of the stability constraints of classical schemes implies long calculation times. That is why we introduce a stable numerical scheme consistent with the transitional and limit models. This scheme is able to handle the quasi-neutrality limit regime without any restrictions on time and space steps. This approach can be easily applied to angular moment models by using a moments extraction. Finally, two physically relevant numerical test cases are presented for the asymptotic-preserving scheme in different regimes. The first one corresponds to a regime where electromagnetic effects are predominant. The second one on the contrary shows the efficiency of the asymptotic-preserving scheme in the quasi-neutral regime. In the latter case the illustrative simulations are compared with kinetic and hydrodynamic numerical results.

Chapter 6. This chapter is devoted to the derivation of an asymptotic-preserving scheme for the electronic M_1 model in the diffusive regime. In the first part of this section, the case without electric field and the homogeneous case are studied. The derivation of the scheme is based on an approximate Riemann solver where the intermediate states are chosen consistent with the integral form of the approximate Riemann solver. This choice can be modified to enable the derivation of a numerical scheme which also satisfies the admissible conditions and is well-suited for capturing steady states. Moreover, it enjoys asymptotic-preserving properties and handles the diffusive limit recovering the correct diffusion equation. Numerical tests cases are presented, in each case, the asymptotic-preserving scheme is compared to the classical HLL [118] scheme usually used for the electronic M_1 model. It is shown that the new scheme gives comparable results with respect to the HLL scheme in the classical regime. On the contrary, in the diffusive regime, the asymptotic-preserving scheme coincides with the expected diffusion equation, while the HLL scheme suffers from a severe lack of accuracy because of its unphysical numerical viscosity. The second part of this section is devoted to the extension of the proposed numerical scheme proposed to the general case. The goal is to deal with the mixed derivatives which arise in the diffusive limit leading to an anisotropic diffusion. The derived numerical scheme preserves the realisibility domain and enjoys asymptotic-preserving properties correctly handling the diffusive limit recovering the relevant limit equation. In addition, the cases with electric field and varying collisional parameter are naturally taken into account with the present approach. Numerical test cases validate the considered scheme in the non-collisional and diffusive limits.

Chapter 7. This study is a first step towards the multi-species charged particles modelling. Before considering complex configurations dealing with charged

particles interactions, in the present chapter, we only consider non-charged particles and apply the angular M_1 model in a moving frame to rarefied gas dynamics. In the present work, the velocity framework is centered on the particle mean velocity. First of all, the derivation of the angular M_1 moments model in the mean velocity frame is introduced. The choice of the mean velocity framework in order to enforce the Galilean invariance property of the model is highlighted. In addition, it is shown that the model rewritten in terms of the entropic variables is Friedrichs-symmetric. Also, the derivation of the associated conservation laws and the zero mean velocity condition are detailed. Secondly, a suitable numerical scheme, preserving the realisable requirement of the numerical solution for the angular M_1 moments model in the mean velocity frame is proposed. Thirdly, some numerical results obtained considering several test cases in different collisional regimes are displayed.

Conclusion We present our conclusions and some short and long time perspectives.

Résumé en français

Ce manuscrit est une contribution à la modélisation et aux méthodes numériques pour l'étude du transport de particules dans un plasma dense. Nous sommes intéressés par des plasmas chauds crées par lasers et le contexte général est la compréhension des processus conduisant à l'allumage des réactions de fusion. Cette thématique constitue la principale motivation de ce travail et est suivie comme direction de recherche générale. Cependant, de nombreux thèmes de recherche sont étroitement reliés à ce travail puisqu'ils présentent une physique similaire. Nous pouvons citer par exemple l'étude des écoulements hypersoniques [5], la radiothérapie [11, 12, 13], la fusion par confinement magnétique [145, 146], l'astrophysique [59], l'étude des éclairs et des flammes, la propulsion pour engin spatiaux [103] ou les processus de décontamination plasma.

Directions de recherches et objectifs

Les descriptions cinétiques sont connues pour être très précisent pour décrire le transport de particules chargées dans un plasma. Cependant, elles sont aussi connues pour êtres particulièrement coûteuse en terme de ressources informatiques lorsqu'elles sont utilisées pour décrire la plupart des applications physiques. Une approche alternative consiste à considérer une description basée sur des quantités physique moyennées. Cependant ce type de description macroscopique peut ne pas être suffisamment précise. Par exemple, dans le contexte de la fusion par confinement inertielle, les particules constituant le plasma peuvent posséder une distribution énergétique éloignée d'une distribution énergétique à l'équilibre thermodynamique telle qu'une description fluide n'est pas adaptée. De plus, les effets cinétiques comme le transport non-local [33, 170], l'amortissement d'ondes ou le développement d'instabilités [82] peuvent être important sur des échelles de temps plus courtes que les périodes de collisions. Ainsi les simulations fluides sont insuffisamment précisent et des codes cinétiques doivent êtres considérés pour capturer correctement le processus physique. Les approches cinétiques sont souvent limitées à des échelles de temps et de longueurs bien plus petites que celles étudiées avec des simulations fluides. La description d'effets cinétiques par l'utilisation de modèles réduits opérant sur des échelles fluides constitue un défi considérable [94, 122].

Les modèles aux moments angulaires représentent une méthode alternative située entres les modèles cinétiques et les modèles fluides. Ils nécessitent un coût informatique moins important que les modèles cinétiques et fournissent des résultats de plus grande précision que les modèles fluides. Ils sont basés sur une moyenne angulaire [175, 182] des équations cinétiques tout en conservant le module de la vitesse (noté ζ dans ce travail) comme variable. Ceci permet de considérer des distributions énergétiques de particules éloignés de l'équilibre tout en travaillant avec une description réduite. De tels modèles sont obtenus par l'intégration angulaire de l'équation cinétique (intégration sur la sphère unité). Ainsi une hiérarchie d'équations aux moments peut être obtenue. Il existe plusieurs modèles aux moments dont les différences proviennent de choix de la relation de fermeture. Dans ce document nous

considérons les modèles aux moments angulaires basés sur un principe de minimisation d'entropie [83]. Les problèmes de minimisations d'entropie ont été largement étudiés [4, 160, 175, 177, 195]. La fonction de distribution sous-jacente est donnée par l'exponentielle d'une fonction polynomiale dépendant du module de vitesse et est ainsi non négative. De plus les modèles aux moments basés sur des fermetures entropiques satisfont des propriétés mathématiques fondamentales [112, 160, 172] comme l'hyperbolicité et la dissipation d'entropie. Cependant, d'un point de vue numérique, même si la fermeture est bien définie, des difficultés numériques demeurent. En particulier, la résolution de problèmes de minimisation d'entropie sous contraintes peuvent êtres particulièrement complexes et nous renvoyons à [4] pour un traitement spécifique.
Le modèle aux moments angulaires M_1 est largement utilisé dans le contexte du transfert radiatif [20, 57, 84, 186, 187, 201, 202], cependant, il est relativement nouveau de l'utiliser pour des applications en physiques des plasmas [83]. Ainsi, le premier objectif de ce travail est de fournir une meilleure compréhension des avantages et des limites de ce modèle réduit pour la modélisation en physique des plasmas. Puisque les modèles aux moments angulaires peuvent êtres considérés comme un compromis entres les descriptions fluides et cinétiques, ils représentent des candidats naturels pour capturer des effets cinétiques sur de longues échelles de temps. Ainsi, un autre objectif important est de proposer des méthodes numériques appropriées pour calculer des solutions numériques de modèles aux moments angulaires pour l'étude de régimes en temps longs. En effet, dans le cas où les grandeurs caractéristiques du problème considéré deviennent grandes devant les paramètres plasmas ou les paramètres collisionnels, des raideurs apparaissent dans le système d'équation étudié et le modèle dégénère. En général, les schémas numériques classiques utilisés pour les modèles aux moments angulaires ne sont pas capables de correctement capturer les bonnes limites asymptotiques sous des conditions acceptables sur les pas de temps et d'espace. Aussi, en plus de se comporter correctement dans les régimes asymptotiques, les méthodes numériques doivent êtres capables de préserver les propriétés fondamentales des modèles aux moments angulaires comme la préservation des ensembles admissibles. Ce point est étudié en détail dans ce document. Un autre objectif concerne la simulation du transport multi-espèce. Les études portant sur le transport électronique sont souvent effectuées en considérant les ions immobiles [86, 168]. En effet, en raison de leur masse importante comparée aux électrons, le mouvement des ions est souvent négligé car de petits intervalles de temps sont considérés. Cependant, lors des études sur de longues échelles, le mouvement ionique doit être considéré. Ceci donnerait accès à une physique plus générale et plus riche pour des applications en fusion par confinement inertiel. Un travail important est donc requis pour l'utilisation des modèles aux moments angulaires pour l'étude de transport de particules multi-espèces.

Structure du manuscrit

Ce travail se situe entre la modélisation en physique des plasmas, les mathématiques

appliquées et l'analyse numérique. Ce manuscrit est organisé en trois parties. La première partie est une contribution à la modélisation en physique des plasmas à travers les modèles aux moments angulaires. La deuxième partie de ce document traite de la dérivation de méthodes numériques pour l'étude du transport de particules en temps long. Les schémas classiques utilisés pour les modèles aux moments angulaires préservent l'admissibilité de la solutions numérique. Cependant, de tels schémas ne sont, en général, pas capables de capturer la bonne solution numérique lorsque l'on considère des régimes asymptotiques. Le but est de proposer des schémas numériques qui capturent la bonne limite asymptotique sous des contraintes raisonnables sur le pas de temps et d'espace. La troisième partie est une contribution à la modélisation multi-espèce. L'objectif final est d'étudier les dynamiques électronique et ionique avec un modèle précis qui est aussi numériquement peu coûteux pour les applications. Dans ce travail un problème plus simple est étudié considérant des particules non-chargées.

Chapitre 1. Dans ce premier chapitre nous introduisons les concepts de bases essentiels en modélisation pour la physique des plasmas. Ces éléments sont utilisés dans les chapitres suivants.

Chapitre 2. Dans ce chapitre, nous commençons par rappeler le principe de construction des modèles aux moments basés sur une fermeture par minimisation d'entropie. Alors qu'en limite fortement collisionnelle les modèles aux moments angulaires fournissent une bonne approximation d'une équation cinétique complète, leur domaine de validité en limite non-collisionnelle est inconnu. Le travail ce chapitre est dévoué à l'étude du domaine de validité du modèle M_1 et de ces extensions, le modèle M_1 double population et le modèle M_2 pour des applications cinétiques non-collisionnelle. Trois effets sont étudiés, l'interaction de faisceaux de particules chargées, l'amortissement Landau et l'absorption d'une onde électromagnétique dans un plasma semi-infini très dense. Pour chaque phénomène une analyse perturbative est conduite et une relation de dispersion est établie en utilisant les modèles aux moments angulaires. Ces relations sont comparées avec celles obtenues en considérant l'équation de Vlasov. Les domaines de validité de chaque modèle sont étudiés.

Chapitre 3. Dans ce chapitre, le modèle M_1 électronique est utilisé pour l'étude du transport électronique dans un plasma collisionnel. La prise aux moments de l'opérateur de collision électron-électron de Landau est difficile et des approximations sont nécessaires. Premièrement, les opérateurs de collisions utilisés pour le modèle M_1 électronique sont détaillés [166, 167]. Les propriétés de ces opérateurs sont données puis suivant [32] les coefficients de transport plasma sont dérivés. Il est montré que dans la limite Z élevé (degré d'ionisation élevé), le modèle M_1 électronique et l'équation de Fokker-Planck-Landau coïncide proche équilibre. Il est aussi montré que l'opérateur de collision électron-électron proposé pour le modèle

M_1 électronique permet de retrouver des coefficients de transport plasma proches de ceux obtenus avec l'équation Fokker-Planck-Landau.

Chapitre 4. Les modèles aux moments angulaires sont des systèmes hyperboliques. Dans ce chapitre, quelques concepts pour la résolution numérique de systèmes non linéaires sont rappelés en suivant les idées présentées dans [52, 101, 102, 118, 159]. Ces méthodes s'appliquent directement aux modèles aux moments angulaires et sont utilisées dans les prochains chapitres.

Chapitre 5. Cette partie traite de la résolution numérique du système M_1-Maxwell dans le régime quasi-neutre [63, 74]. Dans ce régime les équations permettant de calculer le champ électrique deviennent singulières. Une reformulation de l'équation de Maxwell-Ampère est alors considérée puis un schéma numérique est proposé. Ce schéma est consistent avec le modèle intermédiaire et le modèle limite. Ce schéma se comporte correctement en régime quasi-neutre sans restrictions sur le pas de temps ni d'espace. Deux cas tests numériques sont enfin présentés.

Chapitre 6. Ce chapitre est dédié à la dérivation d'un schéma préservant l'asymptotique pour le modèle M_1 électronique en régime de diffusion. Dans la première partie de cette section, le cas sans champ électrique puis le cas homogène avec champ électrique sont étudiés. La construction du schéma est basée sur un solveur de Riemann approché dont les états intermédiaires sont choisis consistent avec la forme intégrale du modèle M_1. Le schéma proposé préserve l'admissibilité de la solution numérique et capture la bonne limite asymptotique. Différents cas test numériques sont présentés. La deuxième partie de ce travail concerne l'extension de la méthode proposée au modèle général. Dans ce cas, des dérivés croisées apparaissent en limites de diffusion et une modification du schéma est nécessaire. Différents cas tests numériques sont enfin présentés dans le cas général.

Chapitre 7. Cette étude représente un premier important vers la modélisation de particules chargées multi-espèces. Avant de considérer des configurations complexes traitant de l'intéraction de particules chargées, dans ce chapitre, nous considérons seulement des particules non-chargées et présentons le modèle aux moments angulaires M_1 pour l'étude de la dynamique des gaz raréfiés. Dans ce travail, l'origine du repère en vitesse est centrée sur la vitesse moyenne des particules. Premièrement, la dérivation du modèle au moment M_1 dans le référentiel de vitesse moyenne est présentée. Il est montré que le choix de ce référentiel permet d'assurer la propriété d'invariance galiléenne du modèle. Il est aussi montré que le modèle écrit en fonctions des variables entropiques est symétrique au sens de Friedrichs. La dérivation de lois des conservations associées est aussi détaillée. Deuxièmement, un schéma numérique préservant l'admissibilité de la solution numérique est proposé. Finalement, plusieurs cas tests numériques menés en considérant différents régimes collisionnels sont présentés.

Conclusion. Nous présentons nos conclusions et plusieurs perspectives à ces travaux.

Modelling in plasma physics

Chapter 1

Basic concepts for plasma physics modelling

In this first chapter, we introduce some basics concepts necessary for plasma physics modelling. These notions will be used in the next chapters.

1.1 Kinetic description of a plasma

The rigorous derivation of kinetic models to describe the transport of particles is particularly challenging and is still an active field of research. Indeed, two main problems remain opens in kinetic theory. The first one deals with the rigorous derivation of the Boltzmann equation [26] starting from a set of particles evolving according to Newton's laws. This important problem has been partially solved (only for short times) by Lanford [124] considering the Boltzmann-Grad limit [109] for hard spheres. Important related results have been obtained in [51, 99, 125, 126, 137, 183]. The second problem deals with the rigorous derivation of the Vlasov-Poisson system starting from a set of charged particles interacting through a Coulombian potential. This issue has been solved in the case of a regular potential by Braun and Hep [34] and Dobrushin [81] and for singular potentials by Hauray and Jabin [121] but the case of Coulombian potentials remains open.

In combination with the Vlasov equation, the Landau kinetic equation [149] is the most important kinetic model in the theory of collisional plasma physics. This equation is often called the Fokker-Planck-Landau equation because the Landau equation was derived in the Fokker-Planck form [188] in 1957. The first formal derivation of the Landau equation from the BBGKY hierarchy was performed by Bogolyubov in 1946 [25]. The Landau collisional term can be seen as an approximation of the Boltzmann collision integral or the Balescu-Lenard collision integral [8, 158]. Therefore, it is reasonable to consider the Vlasov or the Fokker-Planck-Landau equation to describe the transport of charged particles in a plasma.

In this chapter following [178] a formal derivation of a kinetic equation is presented. This approach enables the derivation of the Klimontovich equation and the

kinetic equation thereafter. Connections can be made between this approach and the Liouville approach [178, 196]. We refer to [204] for a review of Mathematical topics in collisional kinetic theory and the references therein for more rigorous derivations of kinetic equations.

The most complete microscopic description of a gas, considering a system of N particles in a volume V, is to describe the coordinates $\vec{r}_i(t)$ and the momenta $\vec{p}_i(t)$ of the N^{th} particles over time. One can introduce a microscopic distribution function $f_{\text{micro}}(t, \vec{r}, \vec{p})$ characterising the number of particles at the time t, in the phase volume $d^3\vec{r}d^3\vec{p}$

$$dN = f_{\text{micro}}(t, \vec{r}, \vec{p})d^3\vec{r}d^3\vec{p}. \tag{1.1}$$

When the positions and velocities of each particle are known, the microscopic distribution function is completely defined by an exact expression. The microscopic distribution can be seen as a product of Dirac functions of all particles coordinates

$$f_{\text{micro}}(t, \vec{r}, \vec{p}) = \sum_{i=1}^{N} \delta(\vec{r} - \vec{r}_i(t))\delta(\vec{p} - \vec{p}_i(t)), \tag{1.2}$$

with $\delta(\vec{r}) = \delta(\vec{x})\delta(\vec{y})\delta(\vec{z})$ the Dirac function in three dimensions. Here in the phase space the distribution function is singular, it represents the coordinates of all particles in the phase space.
In order to derive a more employable model one introduces a continuous description considering a spatial average of the microscopic distribution function. The following continuous distribution is defined

$$f(t, \vec{r}, \vec{p}) = \langle f_{\text{micro}}(t, \vec{r}, \vec{p})\rangle_{V_a}, \tag{1.3}$$

where the operation $\langle\rangle_{V_a}$ represents the spatial average on a volume V_a. Obviously, the volume V_a must be sufficiently large compared to mean volume attributed to each particle $V_a >> V/N$. According to the statistical theory, the fluctuation amplitudes of the average value is of order $N_a^{-1/2}$, where N_a is the number of particles in the volume V_a. However, the volume V_a must also be small compared to the total volume V, $V_a << V$, in order to describe the system with sufficient accuracy. In practice, the volume V_a is defined by the spatial resolution of the measurement techniques and numerical simulations. The temporal evolution equation of the distribution function is now derived. According to the definition (1.2), the temporal evolution of the distribution function is due to the motion of all the particles. Therefore, the temporal derivative of the microscopic distribution function writes

$$\partial_t f_{micro} = d_t \sum_{i=1}^{N} \delta(\vec{r} - \vec{r}_i(t))\delta(\vec{p} - \vec{p}_i(t)),$$

where $\partial_t = \partial/\partial t$ is the temporal partial derivative and $d_t = d/dt$ the temporal total derivative. The previous equation rewrites

$$\partial_t f_{micro} = -\sum_{i=1}^{N} d_t \vec{r}_i . \vec{\nabla} \delta(\vec{r} - \vec{r}_i(t)) \delta(\vec{p} - \vec{p}_i(t)) - \sum_{i=1}^{N} d_t \vec{p}_i . \partial_{\vec{p}} \delta(\vec{p} - \vec{p}_i(t)) \delta(\vec{r} - \vec{r}_i(t)), \quad (1.4)$$

where $\vec{\nabla} = \partial/\partial \vec{r}$ is the spatial gradient and $\partial_{\vec{p}} = \partial/\partial \vec{p}$ is the partial derivative in term of the momentum. The derivative of $d_t \vec{r}_i$ is by definition the velocity of the particle $\vec{v}_i = p_i/m$ and the derivative of $\vec{p}_i$ satisfies the Newton law

$$\partial_t \vec{p}_i = \vec{F}_i,$$

where $\vec{F}_i$ is the force applied on the particle i. Here we can drop the indexes of the velocity $\vec{v}_i$ and the force $\vec{F}_i$ in equation (1.4) using the property of the Dirac function $a\delta(x-a) = x\delta(x-a)$. From equation (1.4), it follows that

$$\partial_t f_{micro} + \vec{v} . \vec{\nabla} f_{micro} + \vec{F}_{micro} . \partial_{\vec{p}} f_{micro} = 0. \quad (1.5)$$

This kinetic equation is known as the Klimontovich kinetic equation [142]. This equation is microscopic, describing a set a discrete particles and enables to derive an equation for the mean distribution function. In order to derive a continuous description for the mean distribution function (1.3), the Klimontovich equation (1.5) is averaged over a spatial volume V_a as prescribed above. The average of the Klimontovich equation (1.5) reads

$$\partial_t f + \vec{v} . \vec{\nabla} f + \langle \vec{F}_{micro} . \partial_{\vec{p}} f_{micro} \rangle = 0. \quad (1.6)$$

One can remark a problem arising with the average of the last term of the previous equation because of its nonlinearity. In order to develop this term a hypothesis is made called the weak particle correlation. It is supposed that the distance between particles is sufficiently large compared to the characteristic interaction distance, so that they are almost free. Their trajectories are almost regular, defined by mean forces with perturbations induced by the chaotic motion of others particles, which are of an inferior order. Here, the quantities are developed as an average quantity and a fluctuation

$$f_{micro} = f + \delta f_{micro}, \qquad \vec{F}_{micro} = \vec{F} + \delta \vec{F}_{micro}, \quad (1.7)$$

where the fluctuations are small $\delta f_{micro} << f$, with a zero mean value $< \delta f_{micro} >= 0$. These definitions enable to expand the last nonlinear term of (1.6). In a plasma, several species of particles are present. The minimum number is two: the ions and the electrons. Considering the distribution function of the species α and retaining only the term of first order one obtains the following classical kinetic equation

$$\partial_t f_\alpha + \vec{v} . \vec{\nabla} f_\alpha + \vec{F}_\alpha . \partial_{\vec{p}} f_\alpha = 0. \quad (1.8)$$

In a plasma, F_α is called the Lorentz force which is induced by self-consistent electric and magnetic fields

$$\vec{F}_\alpha = q_\alpha(\vec{E} + \vec{v} \wedge \vec{B}). \tag{1.9}$$

This kinetic equation with Lorentz self-consistent force is called the Vlasov equation and was proposed by Anatoly Vlasov in 1945. This kinetic model describes particles interacting by long range forces: electromagnetic and gravitational. The Vlasov equation describes the distribution function on large scales, greater than the Debye length and applies to low density plasmas. This equation does not take into account the fluctuations which become important when particles are close to each other therefore the Vlasov equation applies to non-collisional plasmas.
Considering the contribution of the correlation term δf_{micro} in the microscopic distribution function (1.7) it comes that

$$\partial_t f_\alpha + \vec{v}.\vec{\nabla} f_\alpha + \vec{F}_\alpha.\partial_{\vec{p}} f_\alpha = -\left\langle \delta\vec{F}_{\text{micro }\alpha}.\partial_{\vec{p}} \sum_\beta \delta f_{\text{micro }\beta} \right\rangle = \sum_\beta C_{\alpha\beta}. \tag{1.10}$$

The new term in the right side of the equation is called the collision integral. The form of this integral will be investigated in section 1.4.

1.2 Maxwell's equations and macroscopic quantities

The kinetic equation (1.10) must be completed with equations for the mean fields, $\vec{E} =< \vec{E}_{micro} >$ and $\vec{B} =< \vec{B}_{micro} >$. The microscopic fields satisfy the Maxwell's equations [171]

$$\vec{\nabla} \wedge \vec{E}_{micro} = -\partial_t \vec{B}_{micro}, \tag{1.11}$$

$$\vec{\nabla}.\vec{E}_{micro} = \varepsilon_0^{-1}\rho_{micro}, \tag{1.12}$$

$$\vec{\nabla} \wedge \vec{B}_{micro} = \mu_0 \vec{j}_{micro} + c^{-2}\partial_t \vec{E}_{micro}, \tag{1.13}$$

$$\vec{\nabla}.\vec{B}_{micro} = 0. \tag{1.14}$$

These fields are generated by the charged particles in the plasma. The microscopic charge density and the current density read

$$\rho_{micro}(t,\vec{r}) = \sum_\alpha q_\alpha \int f_{micro\,\alpha}(t,\vec{r},\vec{p})d\vec{p}, \quad j_{micro}(t,\vec{r}) = \sum_\alpha q_\alpha \int f_{micro\,\alpha}(t,\vec{r},\vec{p})\vec{v}d\vec{p}.$$

The previous microscopic Maxwell's equations can be averaged directly to obtain the following set of equations

$$\vec{\nabla} \wedge \vec{E} = -\partial_t \vec{B}, \tag{1.15}$$

$$\vec{\nabla}.\vec{E} = \varepsilon_0^{-1}(\rho + \rho^{ext}), \tag{1.16}$$

$$\vec{\nabla} \wedge \vec{B} = \mu_0(\vec{j} + \vec{j}^{ext}) + c^{-2}\partial_t \vec{E}_{micro}, \tag{1.17}$$

$$\vec{\nabla}.\vec{B} = 0. \tag{1.18}$$

where ρ^{ext} and $\vec{j}^{ext}$ are the external charge and current density. The charge density and the current density are also obtained from the distribution functions of particles

$$\rho(t,\vec{r}) = \sum_\alpha q_\alpha \int f_\alpha(t,\vec{r},\vec{p})d\vec{p}, \quad \vec{j}(t,\vec{r}) = \sum_\alpha q_\alpha \int f_\alpha(t,\vec{r},\vec{p})\vec{v}d\vec{p}.$$

Electromagnetic forces are long range interactions, each particle follows a collective electromagnetic field created by many others particles. This collective behaviour is the main difference between plasmas and neutral gas. As for the charge and current density, average quantities can be defined. For each particles species we define

- the particle density

$$n_\alpha(t,\vec{r}) = \int f_\alpha(t,\vec{r},\vec{p})d\vec{p},$$

- the mean velocity

$$\vec{u}_\alpha(t,\vec{r}) = \frac{1}{n_\alpha(t,\vec{r})}\int f_\alpha(t,\vec{r},\vec{p})\vec{v}d\vec{p},$$

- the mean energy

$$E_\alpha(t,\vec{r}) = \frac{1}{n_\alpha(t,\vec{r})}\int f_\alpha(t,\vec{r},\vec{p})\frac{m_\alpha v^2}{2}d\vec{p},$$

- the heat flux

$$\vec{q}_\alpha(t,\vec{r}) = \int f_\alpha(t,\vec{r},\vec{p})m_\alpha\frac{(\vec{v}-\vec{u}_\alpha)^2}{2}(\vec{v}-\vec{u}_\alpha)d\vec{p}. \tag{1.19}$$

1.3 Fluid Models

The kinetic description is particularly accurate. However, this description can be difficult to use and numerical calculations are only possible considering small plasma volumes and short time scales. Therefore, in many applications, one prefers to use reduced models considering that the distribution functions of particles remain close to Maxwellian distribution functions. In this case, the plasma is described with macroscopic quantities: the density, the mean velocity and the mean energy (or the temperature). This hypothesis is not always valid but can apply on very collisional plasmas. In this section, following [58, 144] the development of hydrodynamic models is introduced.

The first macroscopic equation is the particles conservation equation. This equation is derived integrating in velocity the kinetic equation and using the definitions of the density and the mean velocity, it comes that

$$\frac{\partial n_\alpha}{\partial t} + \vec{\nabla}.(n_\alpha \vec{u}_\alpha) = 0. \tag{1.20}$$

This equation is valid only considering elastic collisions. In the case of ionisation or recombination, the right side of the equation can become non-zero. The transport equation on the momentum is derived multiplying the kinetic equation by the momentum $\vec{p} = m_\alpha \vec{v}$ and integrating on the momentum. This equation reads

$$\frac{\partial n_\alpha m_\alpha \vec{u}_\alpha}{\partial t} + \vec{\nabla}.(\bar{\bar{P}}_\alpha) - q_\alpha n_\alpha (\vec{E} + \vec{u}_\alpha \wedge \vec{B}) = \sum_\beta \vec{R}_{\alpha\beta}. \tag{1.21}$$

The term in the right side comes from the integration of the collisions and is called the friction force

$$\vec{R}_{\alpha\beta} = \int \vec{p}_\alpha C_{\alpha\beta} d\vec{p}_\alpha.$$

In the case of a collision between particles of the same species, the conservation of momentum implies that $\vec{R}_{\alpha\alpha} = \vec{0}$. In addition the conservation of the total momentum implies that $\sum_{\alpha,\beta} \vec{R}_{\alpha\beta} = \vec{0}$. Therefore, it follows that

$$\vec{R}_{\alpha\beta} = -\vec{R}_{\beta\alpha}.$$

In general, the friction force $\vec{R}_{\alpha\beta}$ is proportional to the difference of mean velocities of particles α and β and is defined using the collision frequency $\nu_{\alpha\beta}$ such that

$$\vec{R}_{\alpha\beta} = -\nu_{\alpha\beta} m_\alpha n_\alpha (\vec{u}_\alpha - \vec{u}_\beta).$$

The tensor pressure is split in three parts. First, we consider the pressure of the fluid flow and the part linked with the thermal agitation

$$P_{\alpha ij} = n_\alpha m_\alpha u_i u_j + m_\alpha \int w_i w_j f_\alpha(t, \vec{r}, \vec{w}) d\vec{w}.$$

Then the kinetic part is split into a diagonal part and a symmetric part without trace

$$P_{\alpha ij} = n_\alpha m_\alpha u_i u_j + \delta_{ij} p_\alpha + \Pi_{\alpha ij},$$

where δ_{ij} is the Kronecker symbol and p_α the scalar pressure defined by

$$p_\alpha = \frac{1}{3} m_\alpha \int (\vec{v} - \vec{u}_\alpha)^2 f_\alpha d\vec{v}.$$

The term Π_α is called the stress tensor and is defined by

$$\Pi_{\alpha ij} = m_\alpha \int (w_i w_j - \frac{1}{3} w^2 \delta_{ij}) f_\alpha(t, \vec{r}, \vec{w}) d\vec{w}.$$

In the case of an isotropic plasma in the centre of mass framework, the stress tensor is zero and the pressure is a scalar quantity. A more detailed analysis shows that the stress tensor comes from the internal friction of the fluid and leads to the viscosity phenomenon. In the case of a plasma without magnetic field, the stress tensor reads

$$\Pi_{\alpha ij} = -\eta_\alpha \Big(\nabla_i u_{\alpha j} + \nabla_j u_{\alpha i} - \frac{2}{3}\delta_{ij} \vec{\nabla}.\vec{u}_\alpha \Big), \tag{1.22}$$

where η_α is coefficient of viscosity. In the case where the distribution function are close to a Maxwellian distribution function, one has the following relation between pressure and temperature $p_\alpha = n_\alpha k_B T_\alpha$. Therefore, an additional equation is required to obtain the temperature.

The equation on the temperature is derived by multiplying the kinetic equation by the particle energy $\frac{1}{2} m_\alpha v^2$ and integrating over the momentum. One obtains

$$\partial_t \Big(\frac{1}{2} n_\alpha m_\alpha u_\alpha^2 + \frac{3}{2} n_\alpha k_b T_\alpha \Big) + \vec{\nabla}.\Big(\frac{1}{2} n_\alpha m_\alpha u_\alpha^2 \vec{u}_\alpha + \frac{5}{2} n_\alpha k_b T_\alpha \vec{u}_\alpha + \vec{q}_\alpha \Big) = \vec{j}_\alpha.\vec{E} + \sum_\beta W_{\alpha\beta}. \tag{1.23}$$

The first term in the right hand side describes the energy deposition due to the Ohmic heating. The second term is due to the exchange of energy due to collisions between particles

$$W_{\alpha\beta} = \int m_\alpha \frac{v_\alpha^2}{2} C_{\alpha\beta} d\vec{p}_\alpha. \tag{1.24}$$

The conservation of the energy in elastic collisions implies the reciprocity condition $W_{\alpha\beta} = -W_{\beta\alpha}$ and $W_{\alpha\alpha} = 0$. The second term in the left side of the equation describes the convective energy transport (terms proportional to $\vec{u}_\alpha$) and diffusive energy transport due to the heat flux (1.19). Similarly to the stress tensor, the heat flux exists only in an inhomogeneous plasma. In the case of collisional plasma without magnetic field and for small deviations from equilibrium one can show the heat flux is defined by the Fourier law [194]

$$\vec{q}_\alpha = -\kappa_\alpha \vec{\nabla} T_\alpha, \tag{1.25}$$

where κ_α is the thermal conductivity. One remarks that in each equation a superior order moment appears: in (1.20) the density is linked with the velocity. Equation (1.21) links the velocity and the pressure tensor. Finally, equation (1.23) links the energy to the heat flux. One must cut somewhere this infinite chain expressing the highest order moment as a function of inferior order ones. This procedure is called the closure of the fluid equations. In this case $\vec{q}_\alpha$ and $\bar{\bar{\Pi}}_\alpha$ must be determined. The formulae (1.25) and (1.22) are examples of closure for $\vec{q}_\alpha$ and $\bar{\bar{\Pi}}_\alpha$. However, this choice is not unique and other closure can be considered.

1.4 Collisions between particles: the Landau collisional operator

1.4.1 Form of the collisional operators

As explained in the introduction of this chapter, a fundamental equation to describe a collisional plasma is the Fokker-Planck-Landau equation [149]. It is derived from the Boltzmann collisional integral which can be simplified in the case of Coulombian interactions [3]. Using the Rutherford cross section formulae for the charged particle collisions and considering that small angle collisions are dominant [73], one can neglect the large angle collisions and perform an expansion of terms in the Boltzmann collisional integral. Very often, in the classical kinetic theory, a Fokker-Planck-Landau equation coupled with the Maxwell's equation are used to describe the transport of particles in a collisional plasma [58, 75, 76, 77, 161]. It is admitted that the Fokker-Planck-Landau equation is one of the most accomplished model to describe collisional plasmas. In this section, the Landau collisional operator is briefly introduced with some of its properties. Finally, we recall the property of the system to conserve the total energy.

The Landau collisional operator was first derived by Lev Landau in 1936 and this form is the most used in the collisional plasma physics. This collision integral for charged particles reads

$$C_{\alpha\beta}(f_\alpha, f_\beta) = \frac{q_\alpha^2 q_\beta^2 \ln\Lambda}{8\pi\varepsilon_0^2}\frac{\partial}{\partial p_{\alpha i}}\int \frac{(|\vec{u}|^2\delta_{ij} - u_i u_j)}{|\vec{u}|^3}\left(\frac{\partial f_\alpha}{\partial p_{\alpha j}} f_\beta - f_\alpha \frac{\partial f_\beta}{\partial p_{\beta j}}\right) d\vec{v}_\beta, \qquad (1.26)$$

where $\vec{u} = \vec{v}_\alpha - \vec{v}_\beta$ is the relative velocity. The conservative form (1.26) is called the Landau form. Another equivalent form of this operator can be derived called the Rosenbluth form [188]. It is derived by developing (1.26) as a non-linear combination of a diffusive operator and a friction operator.

Even if the Landau collision operator is simpler than the Boltzmann integral, it is still challenging to use it. Therefore, one often uses less accurate but simpler formulations. In the case of electron-ion collisions one can take advantage of the large difference of mass to simplify the Landau collision operator and perform the integral over the ion velocity to obtain

$$C_{ei}(f_e) = \frac{Z^2 n_i e^4 \ln\Lambda}{8\pi\varepsilon_0^2 m_e^2}\frac{\partial}{\partial v_j}\frac{v^2\delta_{js} - v_s v_s}{v^3}\frac{\partial f_e}{\partial v_s},$$

where n_i is the ion density.

1.4.2 Conservation laws and entropy dissipation property

Some fundamental properties of the Landau collision integral (1.26) [39, 72, 123] are presented in this section. The Landau collision integral (1.26), leads to additional

terms into the hydrodynamic equation (1.20),(1.21) and (1.23). Firstly, integrating the kinetic equation in velocity one recovers the continuity equation (1.20). The integral of the collisional operator is zero

$$\int C_{\alpha\beta}(f,f)d\vec{v}_\alpha = 0,$$

because (1.26) is a divergence in the velocity space. Multiplying the kinetic equation by the momentum $m_\alpha\vec{v}_\alpha$ leads to equation (1.21) where the last term is the friction force $\vec{R}$, which is the loss rate of momentum of the particles α colliding the particles β. Multiplying the kinetic equation by $\frac{1}{2}m_\alpha\vec{v}_\alpha^2$ and integrating in velocity leads to energy equation (1.23). The term $W_{\alpha\beta}$ given by (1.24) represents the energy exchange due to collisions. Finally, the kinetic equation (1.10) satisfies the Boltzmann H-theorem: the entropy of a closed system decreases over time. The entropy is defined by

$$H(f_\alpha) = \sum_\alpha \int (f_\alpha \ln f_\alpha - f_\alpha)d\vec{v}_\alpha.$$

We multiply the kinetic equation (1.10) by $\ln f_\alpha$, and integrate in velocity. The first term rewrites

$$\int \ln f_\alpha \partial_t f_\alpha d\vec{v}_\alpha = \partial_t \int (f_\alpha \ln f_\alpha - f_\alpha)d\vec{v}_\alpha.$$

The right collisional term is integrated by part, and one obtains

$$-\sum_{\alpha\beta} \frac{q_\alpha^2 q_\beta^2 \ln\Lambda}{8\pi\varepsilon_0^2} \int\int \frac{\partial \ln f_\alpha}{\partial \vec{p}_\alpha} \bar{\bar{K}}_{\alpha\beta}\vec{G}_{\alpha\beta} f_\alpha f_\beta d\vec{v}_\alpha d\vec{v}_\beta,$$

where the vector $\vec{G}$ is given by

$$\vec{G}_{\alpha\beta} = \frac{\partial \ln f_\alpha}{\partial \vec{p}_\alpha} - \frac{\partial \ln f_\beta}{\partial \vec{p}_\beta},$$

and the tensor

$$\bar{\bar{K}} = (u^2 Id - \vec{u}\otimes\vec{u})/u^3, \tag{1.27}$$

is the integral kernel of the Landau collision operator (1.26). One remarks, this operator is symmetric therefore this property enables to switch the indices α and β in this formula and to rewrite it under the following form

$$\sum_{\alpha\beta} \frac{q_\alpha^2 q_\beta^2 \ln\Lambda}{8\pi\varepsilon_0^2} \int\int \frac{\partial \ln f_\beta}{\partial \vec{p}_\beta} \bar{\bar{K}}_{\alpha\beta}\vec{G}_{\alpha\beta} f_\alpha f_\beta d\vec{v}_\alpha d\vec{v}_\beta,$$

where we used the fact that $\vec{G}$ is anti-symmetric. These two forms are equivalent and summing the two expressions one obtains

$$\partial_t H(f_\alpha) + div_{\vec{x}}(F(f_\alpha)) = -\frac{1}{2}\sum_{\alpha\beta} \frac{q_\alpha^2 q_\beta^2 \ln\Lambda}{8\pi\varepsilon_0^2} \int\int \vec{G}_{\alpha\beta}\bar{\bar{K}}_{\alpha\beta}\vec{G}_{\alpha\beta} f_\alpha f_\beta d\vec{v}_\alpha d\vec{v}_\beta,$$

where the term $\vec{G}\bar{\bar{K}}\vec{G} = (u^2G^2 - (\vec{u}.\vec{G})^2)/u^3$ is positive and the entropy flux is defined by

$$F(f_\alpha) = \int (f_\alpha \ln f_\alpha - f_\alpha)\vec{v}_\alpha d\vec{v}_\alpha.$$

Therefore, the integral is negative and the total entropy decreases in time.

1.4.3 Conservation of the total energy

An important feature of the Maxwell-Fokker-Planck-Landau system is the conservation of the total energy [123]. More precisely, under conditions at the boundaries of the domain the sum of the electromagnetic energy and the plasma energy is conserved over time. The demonstration is given if only electrons are considered.

The total energy E_{tot} is defined by

$$E_{tot} = \varepsilon_0 \frac{(\vec{E})^2 + (c\vec{B})^2}{2} + \int \frac{m}{2}\vec{v}^2 f d\vec{v}.$$

Proposition 1.1. *The Maxwell-Fokker-Planck system conserves the total energy under the following conditions on the frontier $\partial\Omega$ of $\vec{\Omega}$*

$$\varepsilon_0 c^2 (\vec{E} \wedge \vec{B}).\vec{n} + \int \frac{m}{2}|\vec{v}|^2(\vec{v}.\vec{n}) f d\vec{v} = 0.$$

This property is derived multiplying the Maxwell equations (1.17) and (1.15) by $\vec{E}$ and $\vec{B}$. The sum of the two obtained equations leads to

$$\frac{1}{2}\frac{\partial}{\partial t}\Big(\frac{\vec{E}^2}{c^2} + \vec{B}^2\Big) + \vec{\nabla}_x(\vec{E} \wedge \vec{B}) = -\frac{1}{c^2\varepsilon_0}\vec{j}.\vec{E}. \tag{1.28}$$

Now, multiplying the electron kinetic equation by $m\dfrac{v^2}{2}$ and integrating in velocity one obtains

$$\frac{\partial}{\partial t}\Big(\int m\frac{\vec{v}^2}{2} f\Big)d\vec{v} + \vec{\nabla}_{\vec{x}}\Big(\int m\frac{\vec{v}^2}{2} f\vec{v} d\vec{v}\Big) + q\int \vec{\nabla}_{\vec{v}}((\vec{E} + \vec{v} \wedge \vec{B})f)\frac{\vec{v}^2}{2} d\vec{v} = 0. \tag{1.29}$$

The third term of the right side of this equation rewrites

$$\vec{\nabla}_{\vec{v}}.((\vec{E} + \vec{v} \wedge \vec{B})f)\frac{\vec{v}^2}{2} = \vec{\nabla}_{\vec{v}}.((\vec{E} + \vec{v} \wedge \vec{B})f\frac{\vec{v}^2}{2}) - f(\vec{E} + \vec{v} \wedge \vec{B}).\vec{\nabla}_{\vec{v}}\Big(\frac{\vec{v}^2}{2}\Big).$$

Therefore, equation (1.29) simplifies into

$$\frac{\partial}{\partial t}\Big(\int m\frac{\vec{v}^2}{2} f\Big)d\vec{v} + \vec{\nabla}_{\vec{x}}\Big(\int m\frac{\vec{v}^2}{2} f\vec{v} d\vec{v}\Big) - \vec{j}.\vec{E} = 0. \tag{1.30}$$

Finally, the total energy equation is obtained summing equations (1.30) and (1.28)

$$\frac{1}{2}\frac{\partial}{\partial t}\Big(\varepsilon_0(\vec{E}^2+(c\vec{B})^2)+\int m\vec{v}^2 f d\vec{v}\Big)+\vec{\nabla}_{\vec{x}}.\Big(\varepsilon_0 c^2.(\vec{E}\wedge\vec{B})+\int m\vec{v}^2 f\vec{v}d\vec{v}\Big)=0. \quad (1.31)$$

The first and second terms in the temporal derivative correspond to the electromagnetic energy and the plasma energy. The first and second term in the spatial derivative are the electromagnetic energy flux (the term $\varepsilon_0 c^2(\vec{E}\wedge\vec{B})$ is called the Poynting vector) and the plasma energy flux. Then integrating over the space domain, equation (1.31) gives

$$\frac{1}{2}\frac{\partial}{\partial t}\int_\Omega\Big(\varepsilon_0(\vec{E}^2+(c\vec{B})^2)+\int m\vec{v}^2 f d\vec{v}\Big)d\vec{\Omega}+\int_{\partial\Omega}\Big(\varepsilon_0 c^2.(\vec{E}\wedge\vec{B}).\vec{n}+\int m\vec{v}^2(\vec{v}.\vec{n})f d\vec{v}\Big)d\sigma=0,$$

which gives proposition (1.1).

Chapter 2

Angular moments models

The study introduced in this chapter has been published. The reference is:
S. Guisset, R. Nuter, J. Moreau, S. Brull, E. d'Humières, B. Dubroca, V. Tikhonchuk. *Limits of the M1 and M2 angular moments models for kinetic plasma physics studies.* J. Phys. A: Math. Theor. 48, 335501 (2015).

2.1 Introduction

The aim of this chapter is to introduce the principle of the angular moment closure and to define the validity domain of the M_1, the two populations M_1 and the M_2 angular moments models for kinetic plasma physics applications. The purpose is to investigate if these three moments models are able to capture and describe correctly the basic phenomena occurring in a collisionless plasma. It has been shown in [83] that the M_1 model is very accurate in the case of isotropic configurations or with configurations where one direction is dominant. However the model loses precision in the case of an anisotropic configuration and in the limit where the mean free path is larger than the characteristic length of the problem. The accuracy can be improved by considering the two populations M_1 model or the M_2 model [83]. However, their respective domains of validity are not defined either.
We consider here three classical kinetic effects, which are the interaction of charged particle beams, the Landau damping of a Langmuir plasma wave and the absorption of a electromagnetic wave incident normally on the boundary of an overdense plasma. Historically, the two beams instability was one of the first studied plasma physics problems [47, 143]. A beam of charged particles propagates in a plasma generating an oscillating electric field exponentially increasing in time, and reducing the beam kinetic energy. The collisionless damping of plasma waves was first discovered theoretically by Landau [148] then demonstrated in laboratory [58, 169]. The latter physical phenomenon corresponds to the collisionless absorption of an electromagnetic wave incident on an overcritical plasma. A part of the wave energy is absorbed and transferred to the plasma while the other part is reflected [190]. For these three phenomena, a perturbative analysis is performed and the dispersion

relation is established using the moments models. These relations are compared in this paper with those obtained directly from the Vlasov equation, providing the accuracy degree of the moments models.

This chapter is organised as follows: firstly in Section 2.2 we introduce the principle of the angular moment closure with the derivation of the M_1 model. Then in Section 2.3 the two populations M_1 and the M_2 moments models are briefly presented. Section 2.4 is devoted to the electron beams interaction. A dispersion relation computed with the M_1 model is compared with the one obtained with the Vlasov equation. We highlight that the M_1 model exactly captures the interaction phenomenon. The Landau damping is presented in Section 2.5. In this case the M_1 model captures the damping qualitatively, but is not able to describe it correctly. On the contrary, the two M_1 populations model and the M_2 model display results with a good accuracy. Finally, the collisionless skin effect is studied in Section 2.6. We show that the M_1 model is not able to describe the absorption phenomenon, while the two populations M_1 model and the M_2 model capture it qualitatively. In order to perform an explicit calculation of the absorption rate, the two limiting cases of a cold and hot electron plasma are studied corresponding to the low and high frequency skin effect [162]. We show that in the cold plasma limit the two populations M_1 and the M_2 moments models give inaccurate absorption coefficients. In the opposite limit the two populations M_1 model fails in describing correctly the phenomenon while the M_2 model provides an accurate result. Some conclusions are given in Section 2.7.

2.2 Principle of the angular moment closure

The purpose of angular moment models is to reduce the computational cost of the kinetic descriptions as introduced in Chapter 1. The electronic M_1 model [83, 166] is derived performing an angular moment extraction from the Fokker-Planck-Landau equation. For the sake of clarity, we omit in the following, the $\vec{x}$ and t dependence of the distribution function. If S^2 is the unit sphere $\vec{\Omega} = \vec{v}/|\vec{v}|$ represents the direction of propagation of the particle. By setting $\zeta = |\vec{v}|$, the distribution function f writes in the spherical coordinates in the phase space $f(\vec{\Omega}, \zeta)$. The first three angular moments of the distribution function are defined by

$$f_0(\zeta) = \zeta^2 \int_{S^2} f(\vec{\Omega}, \zeta) d\vec{\Omega}, \quad \vec{f}_1(\zeta) = \zeta^2 \int_{S^2} f(\vec{\Omega}, \zeta) \vec{\Omega} d\vec{\Omega}, \quad \bar{\bar{f}}_2(\zeta) = \zeta^2 \int_{S^2} f(\vec{\Omega}, \zeta) \vec{\Omega} \otimes \vec{\Omega} d\vec{\Omega}. \tag{2.1}$$

The complete angular integration of the Fokker-Planck-Landau equation, as performed in [83, 166, 200] is detailed in Appendix A. In this Section we directly give the result of this angular moment extraction and detail the closure procedure. The

angular integration of the Fokker-Planck-Landau equation reads

$$\begin{cases} \partial_t f_0 + \nabla_{\vec{x}}.(\zeta \vec{f}_1) + \frac{q}{m}\partial_\zeta(\vec{f}_1.\vec{E}) = Q_0(f_0), \\ \partial_t \vec{f}_1 + \nabla_{\vec{x}}.(\zeta \bar{\bar{f}}_2) + \frac{q}{m}\partial_\zeta(\bar{\bar{f}}_2\vec{E}) - \frac{q}{m\zeta}(f_0\vec{E} - \bar{\bar{f}}_2\vec{E}) - \frac{q}{m}(\vec{f}_1 \wedge \vec{B}) = \vec{Q}_1(\vec{f}_1), \end{cases} \tag{2.2}$$

where the collisional operators Q_0 and Q_1 are given by

$$Q_0(f_0) = \frac{2\alpha_{ee}}{3}\partial_\zeta\Big(\zeta^2 A(\zeta)\partial_\zeta(\frac{f_0}{\zeta^2}) - \zeta B(\zeta) f_0\Big), \tag{2.3}$$

$$\vec{Q}_1(\vec{f}_1) = -\frac{2\alpha_{ei}}{\zeta^3}\vec{f}_1. \tag{2.4}$$

The coefficients $A(\zeta)$ and $B(\zeta)$ write

$$A(\zeta) = \int_0^\infty \min(\frac{1}{\zeta^3}, \frac{1}{\omega^3})\omega^2 f_0(\omega) d\omega, \tag{2.5}$$

$$B(\zeta) = \int_0^\infty \min(\frac{1}{\zeta^3}, \frac{1}{\omega^3})\omega^3 \partial_\omega(\frac{f_0(\omega)}{\omega^2}) d\omega. \tag{2.6}$$

The fundamental point of the moments models is the definition of a closure, which writes the highest moment as a function of the lower ones. This closure relation corresponds to an approximation of the underlying distribution function, which the moments system is constructed from. In the M_1 model (2.2), we need to define $\bar{\bar{f}}_2$ as a function of f_0 and $\vec{f}_1$. The closure relation originates from an entropy minimisation principle [160, 175]. The underlying distribution function f is obtained as a solution of the following minimisation problem

$$\min_{f\geq 0}\{\ \mathcal{H}(f)\ /\ \forall \zeta \in \mathbb{R}^+,\ \ \zeta^2 \int_{S^2} f(\vec{\Omega},\zeta) d\vec{\Omega} = f_0(\zeta),\ \ \zeta^2 \int_{S^2} f(\vec{\Omega},\zeta)\vec{\Omega} d\vec{\Omega} = \vec{f}_1(\zeta)\ \}, \tag{2.7}$$

where $\mathcal{H}(f)$ is the angular entropy defined by

$$\mathcal{H}(f) = \zeta^2 \int_{\mathbb{S}^2} (f\ \ln\ f\ -\ f) d\vec{\Omega}. \tag{2.8}$$

The solution of (2.7) writes [85, 167]

$$f(\vec{\Omega},\zeta) = \exp(\ a_0(\zeta) + \vec{a}_1(\zeta).\vec{\Omega}\ ), \tag{2.9}$$

where $a_0(\zeta)$ is a scalar and $\vec{a}_1(\zeta)$ a real valued vector. An important parameter is the anisotropy parameter $\vec{\alpha}$ defined by

$$\vec{\alpha} = \frac{\vec{f}_1}{f_0}, \tag{2.10}$$

which is by construction less or equal than one in norm $|\vec{\alpha}| \leq 1$. If we compute the angular moments of the distribution function given by (2.9) one obtains

$$f_0 = 4\pi \exp(a_0) \frac{\sinh(|a_1|)}{|a_1|}, \; f_1 = 4\pi \exp(a_0) \frac{\sinh(|a_1|)(1 - |a_1| \coth(|a_1|))}{|a_1|^3} a_1.$$

These relations can be combined to give

$$\alpha = \frac{1 - |a_1| \coth(|a_1|)}{|a_1|^2} a_1,$$

then by taking the modulus of the previous expression

$$|\alpha| = \frac{|a_1| \coth(|a_1| - 1)}{|a_1|}. \tag{2.11}$$

The relation (2.11) cannot be inverted explicitly by hand. However, this relation determines a unique solution which can be computed numerically. Then the moment $\bar{\bar{f}}_2$ can be computed assuming we know $\vec{a}_1$

$$\bar{\bar{f}}_2 = f_0 \Big(\frac{1 - \chi}{2} \bar{\bar{I}}_d + \frac{3\chi - 1}{2} \frac{\vec{f}_1}{|\vec{f}_1|} \otimes \frac{\vec{f}_1}{|\vec{f}_1|} \Big), \tag{2.12}$$

where

$$\chi = \frac{|a_1|^2 - 2|a_1| \coth(|\vec{a}_1|) + 2}{|\vec{a}_1|^2}.$$

The χ factor can be computed as a function of the anisotropy parameter $\vec{\alpha}$

$$\chi(\vec{\alpha}) \approx \frac{1 + \vec{\alpha}^2 + \vec{\alpha}^4}{3}. \tag{2.13}$$

The definition (2.12) enables to close the problem (2.2). We note here that the choice

$$\chi(\vec{\alpha}) \approx \frac{1}{3}. \tag{2.14}$$

corresponds to the P_1 closure largely used in the context of radiative transfer [97]. Using the definitions of the angular moments (2.1), one remarks that f_0 is non-negative as the integral of a non-negative distribution function. Similarly, taking the absolute value of f_1 with the definition (2.1), one shows that $|f_1| \leq f_0$. Therefore we consider the following set of admissible states [83] defined by

$$\mathcal{A} = \Big((f_0, f_1) \in \mathbb{R}^2, \;\; f_0 \geq 0, \;\; |f_1| \leq f_0 \Big). \tag{2.15}$$

2.3 Two populations M_1 and M_2 angular moments models

The M_1 model is well adapted (2.2)-(2.12)-(2.13) to the case of a near-isotropic configuration, where $|f_1| << f_0$ ($|\vec{\alpha}| << 1$). In this case it is equivalent to the P_1 model (2.2)-(2.12)-(2.14). It provides also a good approximation in the case of one dominant direction ($|\vec{\alpha}| \approx 1$) [83]. However, for the other values of α, the M_1 model may be not sufficiently accurate [83]. In order to improve the accuracy of the model in intermediate cases one can consider the two populations M_1 model [83, 202] and the M_2 model [4, 120]. This section provides a description of the two populations M_1 model and the M_2 model.

2.3.1 Two populations M_1 model

In [83, 202], it was suggested to decompose the distribution function into two parts. One part for particles with positive velocities and another one for particles with negative velocities. The total distribution function writes

$$f = f^- + f^+,$$

where $f^- = f|_{v_x<0}$ describes the particle with negative velocities and $f^+ = f|_{v_x>0}$ the particles with positive velocities. We can now define the zeroth order angular moments f_0^- and f_0^+.

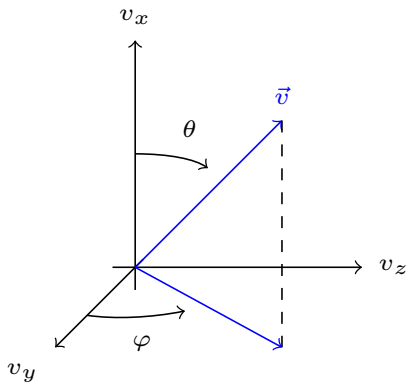

Figure 2.1: The coordinates system used for the calculation of angular moments of the electron distribution function.

According to (2.1), the expressions for angular moments write

$$f_0^+(\zeta) = \zeta^2 \int_0^{2\pi} \int_0^{\pi/2} f(\zeta, \vec{\Omega}) \, \sin(\theta) \, d\theta d\varphi,$$

and

$$f_0^-(\zeta) = \zeta^2 \int_0^{2\pi} \int_{\pi/2}^{\pi} f(\zeta, \vec{\Omega})\ \sin(\theta)\ d\theta d\varphi.$$

Similarly the first angular moments are defined as

$$\vec{f_1}^+(\zeta) = \zeta^2 \int_0^{2\pi} \int_0^{\pi/2} f(\zeta, \vec{\Omega})\ \vec{\Omega}\ \ \sin(\theta)\ d\theta d\varphi, \tag{2.16}$$

$$\vec{f_1}^-(\zeta) = \zeta^2 \int_0^{2\pi} \int_{\pi/2}^{\pi} f(\zeta, \vec{\Omega})\ \vec{\Omega}\ \ \sin(\theta)\ d\theta d\varphi, \tag{2.17}$$

where $\vec{\Omega} = (\cos\theta,\ \sin\theta\cos\phi,\ \sin\theta\sin\phi)$, see Fig.2.1. Equations (2.2) are solved for each population distribution. The sum of the two population distributions is considered to compute the electron current $\vec{j}$

$$\vec{j} = q \int_0^{+\infty} (\vec{f_1}^- + \vec{f_1}^+)\zeta d\zeta. \tag{2.18}$$

This source term is considered to solve the Maxwell's equations (1.15-1.18).

2.3.2 M_2 model

The M_2 model, similarly to the M_1 model (2.2)-(2.12)-(2.13) is also based on an entropy minimisation principle. The difference lies in the fact that an additional angular moment is considered making this model more accurate than the M_1 model. Let us introduce the tensor of order three $\vec{\vec{\vec{f}}}_3$

$$\vec{\vec{\vec{f}}}_3(\zeta) = \zeta^2 \int_{S^2} f(\vec{\Omega}, \zeta)\ \vec{\Omega} \otimes \vec{\Omega} \otimes \vec{\Omega}\ d\vec{\Omega}.$$

The entropy minimisation principle for the M_2 model [4, 120] implies that the underlying distribution function writes

$$f(\vec{\Omega}, \zeta) = \exp(\ a_0(\zeta) + \vec{a}_1(\zeta).\vec{\Omega} + \bar{\bar{a}}_2(\zeta)\ :\ \vec{\Omega} \otimes \vec{\Omega}\ ), \tag{2.19}$$

where $a_0(\zeta)$ is a scalar, $\vec{a}_1(\zeta)$ a real valued vector and $\bar{\bar{a}}_2(\zeta)$ a real valued tensor of order two. The notation $\otimes$ represents the tensor product and : is the two times contracted product. The equations of the M_2 model write

$$\begin{cases} \partial_t f_0 + \nabla_{\vec{x}}.(\zeta \vec{f_1}) + \frac{q}{m}\partial_\zeta(\vec{f_1}.\vec{E}) = 0, \\ \partial_t \vec{f_1} + \nabla_{\vec{x}}.(\zeta \bar{\bar{f}}_2) + \frac{q}{m}\partial_\zeta(\bar{\bar{f}}_2\vec{E}) - \frac{q}{m\zeta}(f_0\vec{E} - \bar{\bar{f}}_2\vec{E}) = 0, \\ \partial_t \bar{\bar{f}}_2 + \nabla_{\vec{x}}.(\zeta \vec{\vec{\vec{f}}}_3) + \frac{q}{m}\partial_\zeta(\vec{\vec{\vec{f}}}_3\vec{E}) - \frac{q}{m\zeta}(\vec{f_1} \otimes \vec{E} + 2\vec{\vec{\vec{f}}}_3\vec{E} + \vec{E} \otimes \vec{f_1}) = 0. \end{cases} \tag{2.20}$$

For clarity, the contribution of the magnetic field has been removed. The self-consistent magnetic field leads to superior order terms in the perturbative analysis performed in the next sections and can be neglected because the unperturbed distribution function is isotropic.
The aim of the next sections is to define the validity domain of the M_1, the two populations M_1 and the M_2 moments models. The purpose is to investigate if these three moments models are able to capture and describe correctly the basic phenomena occurring in a collisionless plasma.

2.4 Particle beam interaction

In this section we study the interaction of electron beams using the M_1 model. We demonstrate that the dispersion relation obtained from the M_1 model agrees exactly with the one obtained from the Vlasov equation.

2.4.1 Dispersion relation for the M_1 model in the one-dimensional electrostatic case

In the electrostatic case, only one component of the electric field is considered (E_x). The system of equations (2.2) and the Poisson equation read as follows

$$\begin{cases} \partial_t f_0 + \partial_x(\zeta f_{1x}) - \partial_\zeta(E_x f_{1x}) = 0, \\ \partial_t f_{1x} + \partial_x(\zeta f_{2xx}) - \partial_\zeta(E_x f_{2xx}) + \frac{(f_0 - f_{2xx})E_x}{\zeta} = 0, \\ \partial_x E_x = 1 - \int_0^\infty f_0(\zeta) d\zeta, \end{cases} \tag{2.21}$$

where the time is normalised to the inverse of the electron plasma frequency $\omega_{pe} = \sqrt{e^2 n_0/m\varepsilon_0}$, the velocity is normalised to the thermal velocity $v_{th} = \sqrt{T/m}$, the length to the Debye length $\lambda_D = v_{th}/\omega_{pe}$, the electric field is normalised to $E_p = m v_{th}\omega_{pe}/e$ and ϵ_0 is the vacuum dielectric permittivity. Only one component of the closure relation (2.12) is non zero. According to equation (2.10)

$$f_{2xx} = \chi(\alpha_x) f_0.$$

Let us consider a perturbation of the electric field δE_x and the corresponding perturbation of the zeroth and first moment δf_0 and δf_{1x}

$$\begin{cases} E(t,x) = 0 + \delta E_x(t,x), \\ f_0(t,x,\zeta) = F_0(\zeta) + \delta f_0(t,x,\zeta), \\ f_{1x}(t,x,\zeta) = F_{1x}(\zeta) + \delta f_{1x}(t,x,\zeta), \end{cases}$$

where F_0, F_{1x} correspond to the homogeneous stationary solution of system (2.21). For the sake of clarity, we omit in the following the arguments t, x and ζ in the

equations. The linearised system (2.21) reads

$$\begin{cases} \partial_t \delta f_0 + \partial_x(\zeta \delta f_{1x}) - \partial_\zeta(F_{1x}\delta E_x) = 0, \\ \partial_t \delta f_{1x} + \partial_x\left((\chi(\mathcal{F}) - \chi'(\mathcal{F})\mathcal{F})\zeta\ \delta f_0 + \chi'(\mathcal{F})\zeta\ \delta f_{1x}\right) - \partial_\zeta(F_{2xx}\delta E_x) + \frac{(F_0 - F_{2xx})\delta E_x}{\zeta} = 0, \\ \partial_x \delta E_x = -\int_0^\infty \delta f_0(\zeta) d\zeta, \end{cases} \tag{2.22}$$

where $F_{2xx} = \chi(\mathcal{F})F_0$ and $\mathcal{F} = F_{1x}/F_0$. We define the Fourier transform $\hat{f}$ of a function f as

$$\hat{f}(\omega, k) = \frac{1}{2\pi}\int_{-\infty}^{+\infty}\int_{-\infty}^{+\infty} f(t,x)e^{i(\omega t - kx)}dxdt.$$

The Fourier transform of the first and second equations of (2.22) results in

$$-i\omega\delta\hat{f}_0 + ik\zeta\delta\hat{f}_{1x} = \partial_\zeta(F_{1x}\delta\hat{E}_x), \tag{2.23}$$

$$-i\omega\delta\hat{f}_{1x} + ik\zeta(\chi(\mathcal{F}) - \chi'(\mathcal{F})\mathcal{F})\delta\hat{f}_0 + ik\zeta\chi'(\mathcal{F})\delta\hat{f}_{1x} = \partial_\zeta(\chi(\mathcal{F})F_0\delta\hat{E}_x) - \frac{(1-\chi(\mathcal{F}))F_0\delta\hat{E}}{\zeta}. \tag{2.24}$$

For the sake of simplicity, in the following the quantities $\delta\hat{f}$ are replaced by δf. Inserting (2.23) into (2.24) gives

$$\delta f_0 = -\frac{1}{iD}\left[(\omega - k\zeta\chi'(\mathcal{F}))\partial_\zeta F_1 + k\zeta\partial_\zeta(\chi(\mathcal{F})F_0) - k(1-\chi(\mathcal{F}))F_0\right]\delta E, \tag{2.25}$$

with

$$D = \omega^2 - \omega k\zeta\chi'(\mathcal{F}) - k^2\zeta^2[\chi(\mathcal{F}) - \chi'(\mathcal{F})\mathcal{F}].$$

The Fourier transform of the third equation of (2.21) gives $ik\delta E = -\int_0^\infty \delta f_0(\zeta)d\zeta$. Then the integration of (2.25) leads to

$$1 + \int_0^\infty \frac{1}{Dk}\left[(\omega - k\zeta\chi'(\mathcal{F}))\partial_\zeta F_1 + k\zeta\partial_\zeta(\chi(\mathcal{F})F_0) - k(1-\chi(\mathcal{F}))F_0\right]d\zeta = 0. \tag{2.26}$$

This equation is the general formulation of the dispersion relation for the M_1 model in the one dimensional electrostatic case. It is applied to the electron beams in the next subsection and to the Landau damping in the next section.

2.4.2 Electron beams

Let us consider the electron distribution function as a sum of n beams of particles aligned along the x-axis. The distribution function writes

$$f(x,v) = \frac{1}{n}\sum_{l=1}^{n}\delta(v - v_l),$$

where $v_l = \epsilon_l |v_l| = \epsilon_l \zeta_l$, with $\epsilon_l = \pm 1$ depending on the direction of propagation of electrons. Now, the corresponding zeroth and first moments F_0, F_1 are given by,

$$F_0(x,\zeta) = \zeta^2 \frac{1}{n} \sum_{l=1}^{n} \delta(\zeta - \zeta_l), \quad F_1(x,\zeta) = \zeta^2 \frac{1}{n} \sum_{l=1}^{n} \epsilon_l \delta(\zeta - \zeta_l).$$

After a simple computation using (2.13) and the definition of $\mathcal{F}$, we obtain that $\mathcal{F} = \epsilon_l$, $\chi(\mathcal{F}) = 1$ and $\chi'(\mathcal{F}) = 2\epsilon_l$ for $\zeta = \zeta_l$. Using the previous values in (2.26), we obtain that $D = (\omega - k\epsilon_l\zeta_l)^2 = (\omega - kv_l)^2$, for $\zeta = \zeta_l$, and the value of the integral in (2.26) becomes $-\frac{1}{n}\sum_{l=1}^{n} v_l^2/(\omega - kv_l)^2$. We can rewrite the dispersion relation (2.26) as,

$$1 - \frac{1}{n} \sum_{l=1}^{n} \frac{v_l^2}{(\omega - kv_l)^2} = 0,$$

which agrees exactly with the dispersion relation obtained from the Vlasov equation [58].

In this part we have shown that the M_1 model (2.2)-(2.12)-(2.13) correctly describes the particle beams interaction. In the case of different energy beams, the dispersion relation obtained using the M_1 model coincides exactly with the one obtained from the Vlasov equation. It is then evident that more accurate models such as the two populations M_1 model or the M_2 model give the same dispersion equation.
We study in the next part, the Landau damping. It is shown that even if the M_1 model captures qualitatively the phenomenon, it is not accurate enough to describe it quantitatively.

2.5 Dispersion of an electron plasma wave

Landau damping is a well-known process in plasma physics, which also presents a large interest in some other fields such as galaxy dynamics [165]. The aim of this part is to study if the M_1 model (2.2)-(2.12)-(2.13) is able to describe electron plasma waves including the Landau damping effect. We suppose that the equilibrium solution to the Vlasov equation is given by a Maxwellian function

$$f(\zeta) = (2\pi)^{-3/2} \exp(-\zeta^2/2). \tag{2.27}$$

The dispersion relation is established from the Vlasov equation in [58]

$$\omega = \sqrt{1 + 3k^2} - \frac{i}{k^3}\sqrt{\frac{\pi}{8}} \exp(-\frac{1}{2k^2}), \tag{2.28}$$

for small $k << 1$. The negative imaginary part corresponds to the Landau wave damping. In the following, we perform the dispersion analysis of the Landau wave damping using the three moments models.

2.5.1 M_1 model applied to an electron plasma wave

In this case, the two first moments are given by,

$$F_0(\zeta) = \zeta^2 \left(\frac{2}{\pi}\right)^{\frac{1}{2}} \exp(-\frac{\zeta^2}{2}), \quad F_{1x}(\zeta) = 0, \tag{2.29}$$

with $\mathcal{F} = 0$, $\chi(\mathcal{F}) = 1/3$ and $\chi'(\mathcal{F}) = 0$. Using the previous values in (2.26) we obtain that $D = \omega^2 - k^2\zeta^2/3$ and the dispersion relation (2.26) writes as follows,

$$1 + \int_0^\infty \frac{\zeta \partial_\zeta F_0(\zeta) - 2F_0(\zeta)}{3\omega^2 - k^2\zeta^2} d\zeta = 1 - \left(\frac{2}{\pi}\right)^{\frac{1}{2}} \int_0^\infty \frac{\zeta^4 \exp(-\frac{\zeta^2}{2})}{3\omega^2 - k^2\zeta^2} d\zeta = 0.$$

Using the Landau theory [58] we obtain an approximate dispersion relation assuming a large phase velocity $\omega/k >> 1$ and a weak damping $\mathcal{I}m(\omega) << Re(\omega) \approx 1$. The pole ω/k lies near the real ζ axis, and by using a contour prescribed by Landau with a small semicircle around the pole, the residue formula makes the previous equation equal to

$$1 = -\frac{\sqrt{2}}{\sqrt{\pi}k^2} \left[P \int_0^\infty \frac{\zeta^4 \exp(-\frac{\zeta^2}{2})}{\left(\zeta - \frac{\sqrt{3}\omega}{k}\right)\left(\zeta + \frac{\sqrt{3}\omega}{k}\right)} d\zeta + i\pi \left. \frac{\zeta^4 \exp(-\frac{\zeta^2}{2})}{\zeta + \frac{\sqrt{3}\omega}{k}} \right|_{\zeta = \frac{\sqrt{3}\omega}{k}} \right], \tag{2.30}$$

where P stands for the Cauchy principal value. As in the case of plasma waves, the main contribution to the integral comes from velocities $\zeta << \omega/k$, we perform a Taylor expansion for the rational fraction in

$$\frac{1}{\zeta^2 - \left(\frac{\sqrt{3}\omega}{k}\right)^2} = -\left(\frac{k}{\sqrt{3}\omega}\right)^2 \frac{1}{1 - \frac{\zeta^2}{\left(\frac{\sqrt{3}\omega}{k}\right)^2}} \approx -\left(\frac{k}{\sqrt{3}\omega}\right)^2 \left(1 + \frac{\zeta^2}{\left(\frac{\sqrt{3}\omega}{k}\right)^2}\right).$$

Equation (2.30) then reads

$$1 = \frac{1}{\omega^2} + \frac{5}{3}\frac{k^2}{\omega^4} - \frac{i\sqrt{2\,\pi}}{k^2} \left. \frac{\zeta^4 \exp(-\frac{\zeta^2}{2})}{\zeta + \frac{\sqrt{3}\omega}{k}} \right|_{\zeta = \frac{\sqrt{3}\omega}{k}}. \tag{2.31}$$

We consider the imaginary part of ω as a small perturbation and write

$$\omega = \omega_0 + i\delta\omega, \tag{2.32}$$

with $\delta\omega << \omega_0$. Inserting (2.32) into (2.31), neglecting the terms of order $(\delta\omega)^2$ leads to

$$\omega_0^2 + 2i\delta\omega\omega_0 = 1 + \frac{5k^2}{3\omega_0^2}(1 - \frac{2i\delta\omega}{\omega_0}) - if(\omega_0 + i\delta\omega, k), \tag{2.33}$$

where

$$f(\omega_0 + i\delta\omega, k) = \frac{3\sqrt{6\pi}(\omega_0 + i\delta\omega)^5}{k^5} \exp(\frac{-3\omega_0^2}{k^2}) \exp(-\frac{6i\delta\omega\omega_0}{k^2}).$$

Considering the following linearisation

$$f(\omega_0 + i\delta\omega, k) = f(\omega_0, k) + i\delta\omega f'(\omega_0, k)$$

into (2.33) and using the fact $\delta\omega << \omega_0$ gives

$$\omega_0^2 = 1 + 5k^2/3,$$

and

$$\delta\omega = -\frac{3\sqrt{6\pi}}{4k^5} \exp(-\frac{5}{2}) \exp(-\frac{3}{2k^2}) \approx -\frac{0.267}{k^5} \exp(-\frac{3}{2k^2}). \tag{2.34}$$

The dissipation found by the M_1 model (2.34) is significantly different from the Landau dissipation term (2.28) computed with the Vlasov equation. Indeed the pre-exponential factor varies in $0.267/k^5$ instead of $0.1398/k^3$ and the coefficient in the exponential is $1/2k^2$ instead of $3/2k^2$. Figure 2 displays the Landau dissipation coefficient as a function of k for the M_1 model (dotted curve) and the Vlasov equation (solid curve). The M_1 model clearly underestimates the Landau dissipation. This figure highlights the impossibility for the M_1 model to accurately model the Landau damping.

2.5.2 Two populations M_1 model: plasma wave dispersion

We propose here to study the possibility to model the Landau damping with the two populations M_1 model (2.2)-(2.18). The stationary solution for the two parts of the distribution function reads

$$f^{\pm}(v) = \frac{1}{(2\pi)^{\frac{3}{2}}} \exp(-\frac{v^2}{2}) \mathcal{H}(\pm\cos(\theta)),$$

where $\mathcal{H}$ is the Heaviside function. The corresponding reduced distribution functions are given by,

$$F_0^{\pm}(\zeta) = \zeta^2 \left(\frac{1}{2\pi}\right)^{\frac{1}{2}} \exp(-\frac{\zeta^2}{2}), \quad F_{1x}^{\pm}(\zeta) = \pm\frac{1}{2} F_0^{\pm}(\zeta). \tag{2.35}$$

The anisotropic coefficients are calculated using (2.13), $\chi(\mathcal{F}^-) = \chi(\mathcal{F}^+) = 7/16$ and $\chi'(\mathcal{F}^-) = -\chi'(\mathcal{F}^+) = -1/2$. The dispersion relation (2.26) writes as,

$$\begin{aligned}
0 = 1 \;&+\; \int_0^\infty \frac{1}{\beta^+ k} \left[(\omega - k\zeta\chi'(\mathcal{F}^+))\partial_\zeta F_1^+ + k\zeta\partial_\zeta(\chi(\mathcal{F}^+)F_0^+) - k(1-\chi(\mathcal{F}^+))F_0^+\right] d\zeta \\
&+\; \int_0^\infty \frac{1}{\beta^- k} \left[(\omega - k\zeta\chi'(\mathcal{F}^-))\partial_\zeta F_1^- + k\zeta\partial_\zeta(\chi(\mathcal{F}^-)F_0^-) - k(1-\chi(\mathcal{F}^-))F_0^-\right] d\zeta, \\
= 1 \;&+\; \int_0^\infty \frac{1}{k} \left[\frac{0.661\,\omega^2\zeta^2 + 0.079\,\zeta^6 k^2 + 0.063\,k^2\zeta^4 - 0.887\,\zeta^4\omega^2}{(\omega^2 - \omega_1^2 k^2\zeta^2)(\omega^2 - \omega_2^2 k^2\zeta^2)}\right] F_0^+ d\zeta,
\end{aligned}$$

where $\beta^{\pm} \approx \omega^2 - 0.199k^2\zeta^2 \mp 0.488\ \omega k\zeta \approx (\omega \pm \omega_1 k\zeta)(\omega \mp \omega_2 k\zeta)$ with $\omega_1 = 0.265$ and $\omega_2 = 0.753$.
As the phase velocity $\omega/k >> \zeta$, we perform a Taylor expansion of the previous expression to obtain the dispersion relation as for the M_1 model

$$\omega = \sqrt{1 + 2.916k^2} - i\left(\frac{0.19}{k^3} + \frac{0.085}{k^5}\right)\exp(-\frac{0.88}{k^2}),$$

which is close to the dispersion relation (2.28) obtained from the Vlasov equation. The real part of the dispersion relation is almost exact. Considering the imaginary part, the pre-exponential factor varies in $(0.19/k^3 + 0.085/k^5)$ instead of $0.1398/k^3$ and the coefficient in the exponential is $0.88/2k^2$ instead of $3/2k^2$. The representation of the dissipation coefficient in Fig.2.2 shows that the two populations M_1 model gives a more accurate result than the previous model for $k < 0.6$. The two populations M_1 model is then a good candidate to model the Landau damping.

2.5.3 M_2 model

In this part the dispersion relation is established using the M_2 model (2.20) and compared to the one obtained with the Vlasov equation. It is shown that the M_2 model gives more accurate results than the two populations M_1 model.

In the one dimensional electrostatic case, after normalisation the M_2 model (2.20) writes

$$\begin{cases} \partial f_0 + \zeta\partial_x(f_{1x}) - E_x\partial_\zeta(f_{1x}) = 0, \\ \partial_t f_{1x} + \zeta\partial_x(f_{2xx}) - E_x\partial_\zeta(f_{2xx}) + \frac{E_x}{\zeta}(f_0 - f_{2xx}) = 0, \\ \partial_t f_{2xx} + \zeta\partial_x(f_{3xxx}) - E_x\partial_\zeta(f_{3xxx}) + \frac{E_x}{\zeta}(2f_{1x} + 2f_{3xxx}) = 0. \end{cases} \tag{2.36}$$

The derivation is similar to the one performed for the M_1 model with an additional equation. The term f_{2xx} needs to be developed with the perturbative analysis

$$f_{2xx} = F_{2xx} + \delta f_{2xx}. \tag{2.37}$$

In this case F_{2xx} can be calculated by using the equilibrium state (2.27)

$$F_{2xx} = F_0/3,$$

with F_0 defined in equation (2.29). The term f_{3xxx} must be expressed as a function of the other terms. As opposed to the M_1 model closure (2.12), the M_2 model closure cannot be given explicitly. Nevertheless, using [4, 112, 160] and the equilibrium state (2.27), the first terms of the development of f_3 are determined. The linearisation of f_{3xxx} results in

$$f_{3xxx} = 0 + \frac{3}{5}\delta f_{1x}.$$

Then the linearisation of (2.36) gives

$$\begin{cases} \partial_t \delta f_0 + \zeta \partial_x(\delta f_{1x}), \\ \partial_t \delta f_{1x} + \zeta \partial_x(\delta f_{2xx}) - \frac{1}{3}\partial_\zeta(\delta E_x F_0) + \frac{2}{3\zeta}\delta E_x F_0 = 0, \\ \partial_t \delta f_{2xx} + \frac{3}{5}\zeta \partial_x(\delta f_{1x}) = 0. \end{cases} \tag{2.38}$$

Following a development similar to the one performed for the M_1 model, the dispersion relation for the M_2 model writes

$$1 = \frac{1}{3}\sqrt{\frac{2}{\pi}} \int_0^{+\infty} \frac{\zeta^4}{\omega^2 - k^2\zeta^2\lambda} \exp(-\frac{\zeta^2}{2}) \, d\zeta,$$

where the coefficient $\lambda = 3/5$.
Using a contour prescribed by Landau with a small semicircle around the pole, the residue formula applied to the previous equation leads to,

$$1 = \frac{1}{3}\sqrt{\frac{2}{\pi}} \left[P \int_0^{\infty} \frac{\zeta^4 \exp(-\frac{\zeta^2}{2})}{\omega^2 - k^2\zeta^2\lambda} d\zeta - \frac{i\pi}{2\omega k\lambda} \zeta^4 \exp(-\frac{\zeta^2}{2}) \Big|_{\frac{\omega}{k\sqrt{\lambda}}} \right]. \tag{2.39}$$

As the phase velocity $\omega/k >> \zeta$, the rational fraction is expanded with a Taylor series

$$\frac{1}{\omega^2 - k^2\zeta^2\lambda} = \frac{1}{\omega^2}\Big[1 + \frac{k^2\zeta^2\lambda}{\omega^2}\Big]. \tag{2.40}$$

Then the dispersion relation for the M_2 model reads.

$$\omega = \sqrt{1 + 3k^2} - i\frac{0.123}{k^5} \exp(-\frac{1.667}{2k^2}).$$

The real part of the dispersion relation is the same as the one obtained with the Vlasov equation. The imaginary part is different, the pre-exponential factor varies in $0.123/k^5$ instead of $0.1398/k^3$ and the coefficient in the exponential is $1.667/2k^2$ instead of $3/2k^2$ but its representation in Fig. 2.2 shows a good accuracy of the model.

In conclusion, the dispersion and dissipation of the plasma wave found by using the M_1 model are shown to be inaccurate. One notices in Fig. 2.2 a difference of behaviour between the M_1 model and the Vlasov equation. On the contrary, the two populations M_1 model gives much better results with the dissipation term close to the Vlasov dissipation. The M_2 model gives the exact real part of the dispersion relation and it reproduces more accurately than the two populations M_1 model the dissipation.

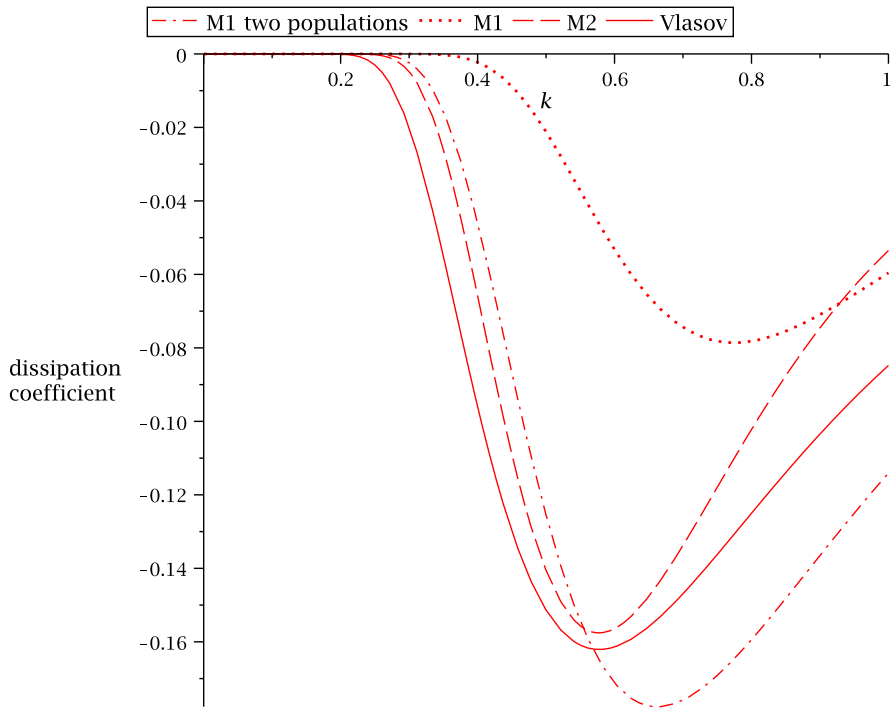

Figure 2.2: Representation of the dissipation coefficient as a function of k for the Vlasov equation and for the M_1, two populations M_1 and M_2 models.

2.6 Collisionless skin effect

In contrast to the electrostatic plasma waves, the electromagnetic waves are not damped in a homogeneous collisionless plasma. However, the dissipation appears if the plasma is inhomogeneous. We consider here the case of a plane electromagnetic wave, which is normally incident on a semi-infinite, overcritical plasma. Here the wave absorption is due to the electrons reflecting from the plasma boundary in a skin layer. The aim of this part is to study how the moments models are able to model such a more complicated situation with an electromagnetic field. The conductivity and absorption coefficient obtained with the M_1, two populations M_1 and M_2 models are compared to the conductivity and absorption coefficient obtained with the Vlasov equation. We consider a low amplitude electromagnetic wave of a frequency ω assuming the linear approach.

Consider a semi-infinite plasma with an electronic density n_0 higher than the critical density $n_c = m\varepsilon_0\omega^2/e^2$. The electromagnetic wave is reflected at the vacuum plasma interface. We propose here to compute the fraction of wave energy absorbed in the plasma [190]. There are two components of the electromagnetic fields E_y and B_z. We suppose the Debye length λ_{De} much smaller than the penetration depth and

then the electrons are reflected specularly at $x = 0$. In order to apply the Fourier transform we extend the plasma to the whole space by assuming that an electron coming from $x > 0$, which is reflected in $x = 0$, comes from the fictive region $x < 0$. The study is then extended to the entire space. The electrostatic field E_y is extended as an even function

$$E_y(x) = E_y(-x).$$

The Faraday equation gives

$$\frac{\partial B_z}{\partial t} = -\frac{\partial E_y}{\partial x},$$

the magnetic field is then to be extended as an odd function

$$B_z(x) = -B_z(-x).$$

In this model the electric field is continuous at the surface $x = 0$ but not its first derivative nor the magnetic field. As introduced in [190], the ratio of the electric and magnetic fields at the plasma boundary is characterised by the surface impedance $E(0)/B(0) = \mathcal{Z}$

$$Z = \frac{i\omega}{c\pi} \int_{-\infty}^{+\infty} \frac{dk}{\frac{\omega^2}{c^2} - k^2 + i\omega\mu_0\sigma_{yy}}, \tag{2.41}$$

where σ is the plasma conductivity. Knowing the impedance one can calculate the absorption coefficient

$$A = \frac{4Re(Z)}{|1+Z|^2}, \tag{2.42}$$

which is related to the real part of the impedance. We suppose that the equilibrium solution is given by the Maxwellian function (2.27).

2.6.1 M_1 model for the plasma skin effect

In this part, the conductivity σ and the absorption coefficient A are computed with the M_1 model (2.2)-(2.12)-(2.13). We show in this section that the M_1 model is not able to capture the absorption phenomenon.

There is no electromagnetic field and no electron current in the unperturbed plasma. We consider solutions with the perturbation theory. The angular moments are expanded

$$f_0(t,x,\zeta) = F_0(\zeta) + \delta f_0(t,x,\zeta), \tag{2.43}$$
$$f_{1x}(t,x,\zeta) = F_{1x}(\zeta) + \delta f_{1x}(t,x,\zeta), \tag{2.44}$$
$$f_{1y}(t,x,\zeta) = F_{1y}(\zeta) + \delta f_{1y}(t,x,\zeta). \tag{2.45}$$

where F_0 and F_{1x} are given in (2.29) and $F_{1y} = 0$. The following system corresponds to the M_1 linearised equations

$$\begin{cases} \dfrac{\partial \delta f_0}{\partial t} + \zeta \dfrac{\partial \delta f_{1x}}{\partial x} = 0, \\ \dfrac{\partial \delta f_{1x}}{\partial t} + \dfrac{\zeta}{3} \dfrac{\partial \delta f_0}{\partial x} = 0, \\ \dfrac{\partial \delta f_{1y}}{\partial t} + \dfrac{q \delta E_y}{3m} \dfrac{\partial F_0}{\partial \zeta} - \dfrac{2q \delta E_y F_0}{3m\zeta} = 0. \end{cases}$$

The Fourier transform of the last equation of (2.6.1) results in an explicit solution for f_{1y}

$$\delta f_{1y} = \frac{iq}{m\omega} \Big[\frac{2F_0}{3\zeta} - \frac{1}{3} \frac{\partial F_0}{\partial \zeta} \Big] \delta E_y. \tag{2.46}$$

Considering (2.18) and (2.46), the electric current is calculated

$$j_y = \frac{iq^2}{m\omega} \int_{\mathbb{R}^+} \Big[\frac{2F_0}{3} - \frac{\zeta}{3} \frac{\partial F_0}{\partial \zeta} \Big] d\zeta \; \delta E_y. \tag{2.47}$$

Introducing the conductivity tensor σ such that $j_y = \sigma_{yy} \delta E_y$, the integration by part in equation (2.47) provides

$$\sigma_{yy} = \frac{ie^2 n_0}{m\omega}. \tag{2.48}$$

Inserting this expression into equation (2.41) one obtains the impedance without any real part. Correspondingly there is no absorption,

$$A = 0. \tag{2.49}$$

Therefore, the M_1 model (2.2)-(2.12)-(2.13) is not able to correctly model the absorption phenomenon. After linearisation of the M_1 model, we note there is no contribution of the space derivative in the third equation of (2.6.1). Then the conductivity (2.48) does not depend on the wave number k and there is no absorption. This is an important result showing a limitation in the M_1 model for collisionless plasma physics applications. More accurate models need to be used for studies of the electromagnetic wave absorption. The aim of the next section is to make a calculation using the two populations M_1 model.

2.6.2 Two populations M_1 model

Here, the conductivity and the absorption coefficient are calculated using the two populations M_1 model (2.2)-(2.18). We show that this model is able to model the absorption phenomenon but does not capture it quantitatively. In this case

the first order moments in the perturbative development are given by (2.35) and $F_{1y}^{+} = F_{1y}^{-} = 0$.

$$\sigma_{yy} = i\frac{q^2}{2m}\int_{\mathbb{R}^+}\Big[\frac{\frac{(1+\chi)F_0}{\zeta} - (1-\chi)\frac{\partial F_0}{\partial \zeta} - \frac{F_0 k}{\omega}}{\omega + \zeta(3\chi-1)k} + \frac{\frac{(1+\chi)F_0}{\zeta} - (1-\chi)\frac{\partial F_0}{\partial \zeta} + \frac{F_0 k}{\omega}}{\omega - \zeta(3\chi-1)k}\Big]\zeta d\zeta. \tag{2.50}$$

The calculation of the previous equation leads to

$$\sigma_{yy} = \frac{i\omega_{pe}^2\varepsilon_0}{\sqrt{2\pi}v_{th}^3}\int_{\mathbb{R}}\frac{-\frac{1}{2} + \frac{3}{2}\chi + \frac{k\zeta}{2\omega} + \frac{\zeta^2(1-\chi)}{2v_{th}^2}}{\omega - \zeta(3\chi-1)k}\zeta^2\exp(-\frac{\zeta^2}{2v_{th}^2})d\zeta. \tag{2.51}$$

The conductivity (2.51) cannot be evaluated analytically. We consider the two limiting cases $\omega/k << v_{th}$ and $\omega/k >> v_{th}$.

5.2.1 Hot electron case

Following the method introduced in the previous section for the calculation of the integral in expression (2.51) in the limit $\omega/k << v_{th}$ one obtains the following expression for the plasma conductivity

$$\sigma_{yy} = \frac{i\omega_{pe}^2\varepsilon_0}{\sqrt{2\pi}v_{th}^3k^3}\Big[-\frac{4v_{th}^2k^2}{(3\chi-1)^4} - \frac{i\pi\omega^2[(3\chi-1)^2+1]}{2(3\chi-1)^4}\Big]. \tag{2.52}$$

It has to be compared to the one obtained with the Vlasov equation [190] σ_{yy}^{Vlasov}

$$\sigma_{yy}^{Vlasov} = \frac{i\omega_{pe}^2\varepsilon_0}{\sqrt{2\pi}v_{th}k}\Big[\frac{\omega\sqrt{2\pi}}{kv_{th}} - i\pi\Big]. \tag{2.53}$$

In contrast to the M_1 model case, the conductivity in this case depends on the wave number k. The conductivity obtained with the two populations M_1 model is different from the one obtained with the Vlasov equation. Indeed, ignoring the constant values, the real part of the conductivity varies in $\omega_{pe}^2/v_{th}k$ instead of $\omega_{pe}^2\omega/v_{th}^2k^2$ for the Vlasov equation and the imaginary part varies in $\omega_{pe}^2\omega^2/v_{th}^3k^3$ instead of $\omega_{pe}^2/v_{th}k$ for the Vlasov equation. Using the fact that $\omega << kv_{th}$ the calculation of the impedance Z leads to

$$Z = -\frac{2i\omega}{c\pi}\int_0^{+\infty}\frac{dk}{k^2 - i\frac{\tilde{K}}{k^3}}, \tag{2.54}$$

with

$$\tilde{K} = \frac{\pi\omega^3\omega_{pe}^2[(3\chi-1)^2+1]}{2\sqrt{2\pi}v_{th}^3c^2(3\chi-1)^4}.$$

The impedance computation results in

$$Z = \frac{2\omega e^{-i\frac{2\pi}{5}}}{5\sin(\frac{\pi}{5})c\sqrt[5]{\tilde{K}}}. \tag{2.55}$$

Inserting equation (2.55) into the definition of the absorption coefficient equation (2.42) leads to

$$A = \frac{K_1\Big(\frac{\omega}{\omega_{pe}}\Big)^{\frac{2}{5}}\Big(\frac{v_{th}}{c}\Big)^{\frac{3}{5}}}{\Big[1+\frac{K_1}{4}\Big(\frac{\omega}{\omega_{pe}}\Big)^{\frac{2}{5}}\Big(\frac{v_{th}}{c}\Big)^{\frac{3}{5}}\Big]^2+\Big[\frac{K_1}{4}\Big(\frac{\omega}{\omega_{pe}}\Big)^{\frac{2}{5}}\Big(\frac{v_{th}}{c}\Big)^{\frac{3}{5}}\Big]^2},$$

with

$$K_1 = \frac{8\cos(\frac{2\pi}{5})}{5\sin(\frac{\pi}{5})}\Big(\frac{2\sqrt{2\pi}(3\chi-1)^4}{\pi(3\chi-1)^2+1}\Big)^{\frac{1}{5}} \approx 0.434.$$

This absorption coefficient has to be compared to the one obtained with the Vlasov equation [190]

$$A^{Vlasov} = \frac{K_2\Big(\frac{\omega}{\omega_{pe}}\Big)^{\frac{2}{3}}\Big(\frac{v_{th}}{c}\Big)^{\frac{1}{3}}}{\Big[1+\frac{K_2}{4}\Big(\frac{\omega}{\omega_{pe}}\Big)^{\frac{2}{3}}\Big(\frac{v_{th}}{c}\Big)^{\frac{1}{3}}\Big]^2+\Big[\frac{K_2}{4}\Big(\frac{\omega}{\omega_{pe}}\Big)^{\frac{2}{3}}\Big(\frac{v_{th}}{c}\Big)^{\frac{1}{3}}\Big]^2}, \tag{2.56}$$

with

$$K_2 = \frac{16\sqrt{3}}{9}\Big(\frac{2}{\pi}\Big)^{\frac{1}{6}}\cos(\frac{\pi}{3}) \approx 1.428.$$

The coefficient ω/ω_{pe} varies as the power 2/5 instead of 2/3 for the Vlasov equation and v_{th}/c varies as the power 3/5 instead of 1/3 for the Vlasov equation.

5.2.2 Cold electron case

We now explore the limit $\omega >> kv_{th}$, where the conductivity equation (2.51) gives

$$\sigma_{yy} = \frac{i\omega_{pe}^2\varepsilon_0}{\sqrt{2\pi}v_{th}^3k^3}\Big[\frac{(3\chi+1)\sqrt{2\pi}k^3v_{th}^3}{2\omega} - \frac{i\pi\omega^4(1-\chi)}{(3\chi-1)^4v_{th}^2k^2}\exp\Big(-\frac{\omega^2}{2v_{th}^2k^2(3\chi-1)^2}\Big)\Big]. \tag{2.57}$$

This expression has to be compared with the one obtained with the Vlasov equation

$$\sigma_{yy}^{Vlasov} = \frac{i\omega_{pe}^2\varepsilon_0}{v_{th}k\sqrt{2\pi}}\Big[\frac{\sqrt{2\pi}kv_{th}}{\omega} - i\pi\exp\Big(-\frac{\omega^2}{2v_{th}^2k^2}\Big)\Big]. \tag{2.58}$$

Here, the real part of the conductivity varies as ω_{pe}^2/ω similarly to the Vlasov equation but the imaginary part varies as $\omega_{pe}^2\omega^4/v_{th}^5k^5$ instead of $\omega_{pe}^2/v_{th}k$ for the Vlasov equation. We also observe for the two populations M_1 model, a presence of the term $(3\chi-1)^2$ in the exponential factor instead of 1. Inserting equation (2.57) into the impedance equation (2.41) results in

$$Z = \frac{6\omega^6\omega_{pe}^2\beta}{c^3v_{th}^5\sqrt{2\pi}}\Big(\frac{\sqrt{2}v_{th}(3\chi-1)}{\omega}\Big)^8 - \frac{i\omega}{\sqrt{\omega_{pe}^2\alpha'-\omega^2}}.$$

Using the definition (2.42), the absorption coefficient is

$$A^{M_1} = \frac{K_3\left(\frac{v_{th}}{c}\right)^3\left(\frac{\omega_{pe}}{\omega}\right)^2}{\left[1+\frac{K_3}{4}\left(\frac{v_{th}}{c}\right)^3\left(\frac{\omega_{pe}}{\omega}\right)^2\right]^2+\left[\frac{\omega_{pe}^2}{\omega_0^2}\alpha'-1\right]^{-\frac{1}{2}}}, \tag{2.59}$$

where K_3 and α' are given by

$$K_3 = \frac{384(3\chi-1)^4(1-\chi)}{\sqrt{2\pi}} \approx 0.822,$$

$$\alpha' = \frac{(3\chi-1)}{2} \approx 0.156.$$

This expression has to be compared with the one obtained with the Vlasov equation [190]

$$A^{Vlasov} = \frac{K_4\left(\frac{v_{th}}{c}\right)^3\left(\frac{\omega_{pe}}{\omega}\right)^2}{\left[1+\frac{K_4}{4}\left(\frac{v_{th}}{c}\right)^3\left(\frac{\omega_{pe}}{\omega}\right)^2\right]^2+\left[\frac{\omega_{pe}^2}{\omega_0^2}-1\right]^{-\frac{1}{2}}}, \tag{2.60}$$

with

$$K_4 = \frac{16}{\sqrt{2\pi}} \approx 6.383.$$

The two expressions of the absorption coefficient are similar but the major difference originates from the parameter α' in the denominator of (2.59). The coefficient ω/ω_{pe} varies as the power 2 and v_{th}/c varies as the power 3 exactly like in the Vlasov absorption coefficient. The parameter α' in the denominator of the two populations M_1 model coefficient absorption makes a significant difference with the Vlasov equation absorption coefficient. While a pole is reached for $\omega/\omega_{pe} = 1$ for the Vlasov equation, the pole is reached when $\omega\alpha'/\omega_{pe} = 1$ for the two populations M_1 model. Even if in both limits the absorption phenomenon is captured qualitatively, the results are not satisfactory. This shows the limits of using the two populations M_1 model for studying laser plasma absorption. The aim of the next part is to see if these results can be improved using the M_2 model (2.20).

2.6.3 M_2 model

In this part the conductivity and the absorption coefficient are calculated with the M_2 model (2.20). In this case the first order moments in the perturbative development F_{1x}, F_{1y}, F_{2xx}, F_{2xy} and F_{2yy} are calculated using (2.1)

$$F_{1x} = F_{1y} = 0,$$

$$F_{2xx} = \frac{F_0}{3}, \qquad F_{2xy} = 0, \qquad F_{2yy} = \frac{F_0}{3},$$

where F_0 is given by equation (2.29). On the contrary to the M_1 model closure (2.12), the M_2 model closure cannot be given explicitly [4]. Nevertheless, only the component f_{3xyx} of the tensor f_3 is required in this study. Using [4, 112, 160], one can show that the linearisation of f_{3xyx} around the equilibrium state (2.27) gives

$$f_{3xyx} = 0 + \frac{\delta f_{1y}}{5}. \tag{2.61}$$

The linearisation of the M_2 model (2.20) leads to

$$\partial_t \delta f_{1y} + \partial_x(\zeta \delta f_{2xy}) + \frac{q}{3m}\partial_\zeta(F_0 \delta E_y) - \frac{2q\delta E_y F_0}{3m\zeta} = 0.$$

Performing a Fourier transform of the previous equation one finds

$$\delta f_{1y} = -i\frac{q\delta E_y}{3m}\frac{\dfrac{\partial F_0}{\partial \zeta} - 2\dfrac{F_0}{\zeta}}{\omega - \dfrac{\zeta^2 k^2}{5\omega}}.$$

Following the method introduced in the two populations M_1 model section, one obtains the conductivity

$$\sigma_{yy} = \frac{i\omega_{pe}^2 \varepsilon_0 \omega}{3v_{th}^5}\sqrt{\frac{2}{\pi}}\left[P\int_0^\infty \frac{\zeta^4 \exp(-\frac{\zeta^2}{2v_{th}^2})}{\omega^2 - k^2\zeta^2\lambda_1}d\zeta - \frac{i\pi\omega^3}{2k^5\sqrt[3]{\lambda_1}}\exp\left(\frac{-\omega^2}{2k^2\lambda_1 v_{th}^2}\right)\right], \tag{2.62}$$

where $\lambda_1 = 1/5$. The integral in this expression cannot be calculated analytically. In order to perform the complete calculation, two limiting cases are considered: $\omega/k << v_{th}$ and $\omega/k >> v_{th}$.

5.3.1 Hot electron case

Following the method introduced for the two populations M_1 model, the conductivity is

$$\sigma_{yy} = \frac{i\omega_{pe}^2 \varepsilon_0 \omega}{3v_{th}^5\sqrt{\pi}}\left[-\frac{v_{th}^3}{k^2} - \frac{i\pi\omega^3}{\lambda\sqrt{2\lambda}k^5}\right]. \tag{2.63}$$

This expression has to be compared with the one obtained with the Vlasov equation σ_{yy}^{Vlasov} (2.53). Ignoring the constant values, the real part of the conductivity varies in $\omega_{pe}^2\omega/v_{th}^2k^2$ exactly like for the Vlasov equation and the imaginary part varies in $\omega_{pe}^2\omega^4/v_{th}^5k^5$ instead of $\omega_{pe}^2/v_{th}k$ for the Vlasov equation. The expression for the M_2 model absorption coefficient reads

$$A = \frac{K_5\left(\dfrac{\omega}{\omega_{pe}}\right)^{\frac{2}{7}}\left(\dfrac{v_{th}}{c}\right)^{\frac{5}{7}}}{\left[1 + \dfrac{K_5}{4}\left(\dfrac{\omega}{\omega_{pe}}\right)^{\frac{2}{7}}\left(\dfrac{v_{th}}{c}\right)^{\frac{5}{7}}\right]^2 + \left[\dfrac{K_5}{4}\left(\dfrac{\omega}{\omega_{pe}}\right)^{\frac{2}{7}}\left(\dfrac{v_{th}}{c}\right)^{\frac{5}{7}}\right]^2},$$

with

$$K_5 = \frac{49.651\lambda^2\sqrt{\lambda}\cos(\frac{3\pi}{7})}{\pi\sqrt{2\pi}} \approx 0.025.$$

The coefficient ω/ω_{pe} varies as the power 2/7 instead of 2/3 for the Vlasov equation and v_{th}/c varies as the power 5/7 instead of 1/3 for the Vlasov equation.

5.3.2 Cold electron case

In the limit $\omega >> kv_{th}$, the conductivity (2.62) reads

$$\sigma_{yy} = \frac{i\omega_{pe}^2\varepsilon_0}{v_{th}^5}\Big[\frac{v_{th}^5}{\omega} - \frac{i\omega^4\sqrt{\pi}}{k^5 3\lambda^2\sqrt{2\lambda}}\exp(-\frac{\omega^2}{2k^2\lambda v_{th}^2})\Big]. \tag{2.64}$$

This expression has to be compared with the one obtained with the Vlasov equation (2.58). In this case the real part of the conductivity varies in ω_{pe}^2/ω like for the Vlasov equation. This good behavior was already obtained with the two populations M_1 model. The imaginary part varies as $\omega_{pe}^2\omega^4/v_{th}^5k^5$ like for the two populations M_1 model, instead of $\omega_{pe}^2/v_{th}k$ for the Vlasov equation but the exponential factor is obtained using the M_2 model contrarily to the two populations M_1 model. The expression for the M_2 model absorption coefficient reads

$$A = \frac{K_6\Big(\frac{v_{th}}{c}\Big)^3\Big(\frac{\omega_{pe}}{\omega}\Big)^2}{\Big[1+\frac{K_6}{4}\Big(\frac{v_{th}}{c}\Big)^3\Big(\frac{\omega_{pe}}{\omega}\Big)^2\Big]^2 + \Big[\frac{\omega_{pe}^2}{\omega^2}-1\Big]^{-\frac{1}{2}}},$$

with

$$K_6 = \frac{128}{5\sqrt{10\pi}} \approx 4.567.$$

This expression is compared with the one obtained from the Vlasov equation (2.60). The coefficient ω/ω_{pe} varies as the power 2 and v_{th}/c varies as the power 3 exactly like the Vlasov equation absorption coefficient. As opposed to the two populations M_1 model, the pole is reached at $\omega/\omega_{pe} = 1$ like for the Vlasov equation. In this limit, one observes the advantage in using the M_2 model compared to the two populations M_1 model.

The calculation of the impedance Z, has been performed using the conductivity expressions established in the hot and cold electron limits $\omega/k << v_{th}$ and $\omega/k >> v_{th}$. However, equation (2.41), implies the integration over all k from minus infinity to infinity. We can consider that the calculation of the impedance, using equation (2.41), holds if the main contribution of the integral comes from a set of wave numbers k where the limiting expressions for the conductivity are valid. In order to check this assumption, the parameters ω/ω_{pe} and v_{th}/c are fixed and the expression in the integral (2.41) is analysed as a function of k.

We present here an example with $\omega/\omega_{pe} = 0.1$ and $v_{th}/c = 0.8$ to illustrate how one can validate our approach for these parameters. The same steps can be used for any choice of parameters in order to verify if the calculated absorption is valid. The modulus integrand of the impedance for the Vlasov equation, the M_2 and M_1 two populations models are displayed in Fig.2.3, using the expressions derived in the limit $\omega/k << v_{th}$. In this case the dimensionless wave number kc/ω_{pe} must be larger than $(\omega/\omega_{pe})/(v_{th}/c) = 0.125$. Indeed, according to Fig.2.3 the main contribution to the integral comes from a set of wave numbers where the conductivity expressions are valid. Moreover, the position and the shape of integrand in the case of M_2 model agrees well with the Vlasov result. A second example is displayed in

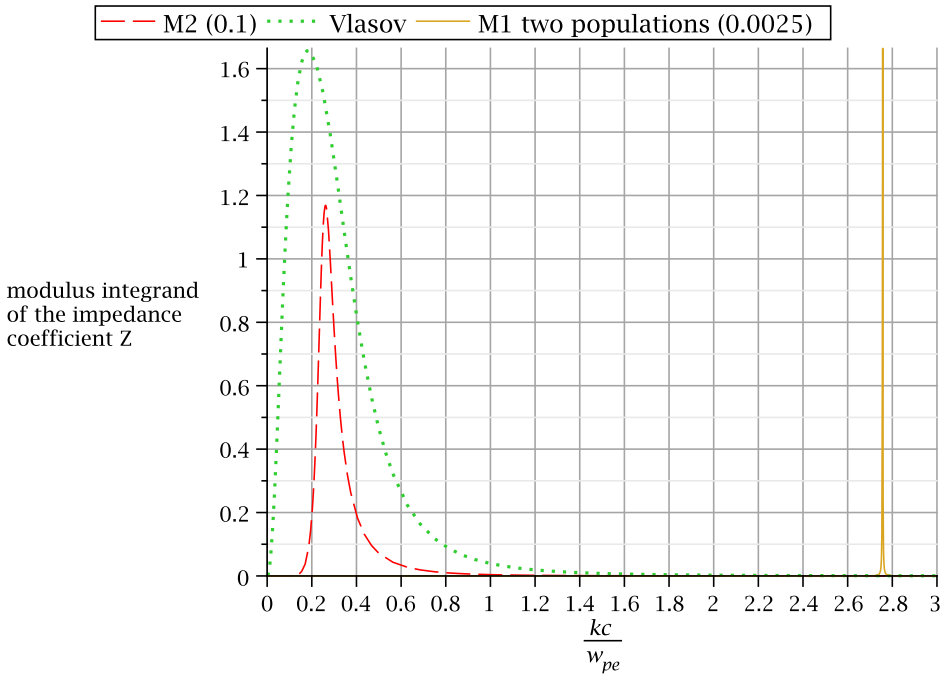

Figure 2.3: Representation of the modulus integrand of the impedance (2.41) as a function of k in the limit $\omega/k << v_{th}$ in the case $\omega/\omega_{pe} = 0.1$ and $v_{th}/c = 0.8$. The modulus integrand has been multiplied by a factor 0.1 for the M_2 model and by 0.0025 for the M_1 two populations model.

Fig.2.4, with $\omega/\omega_{pe} = 0.3$ and $v_{th}/c = 0.1$ using the expressions established in the limit $\omega/k >> v_{th}$. In this case, the dimensionless wave number kc/ω_{pe} must be smaller than $(\omega/\omega_{pe})/(v_{th}/c) = 3$. Indeed, one can verify in Fig.2.4 that the main contribution to the integral comes from a set of wave numbers where the conductivity expressions are valid.

In conclusion, it has been shown that the M_1 model (2.2)-(2.12)-(2.13) is not able to model the skin effect of an electromagnetic wave in an overdense plasma. In the limit $\omega/k << v_{th}$, the two populations M_1 (2.2)-(2.18) and the M_2 (2.20)

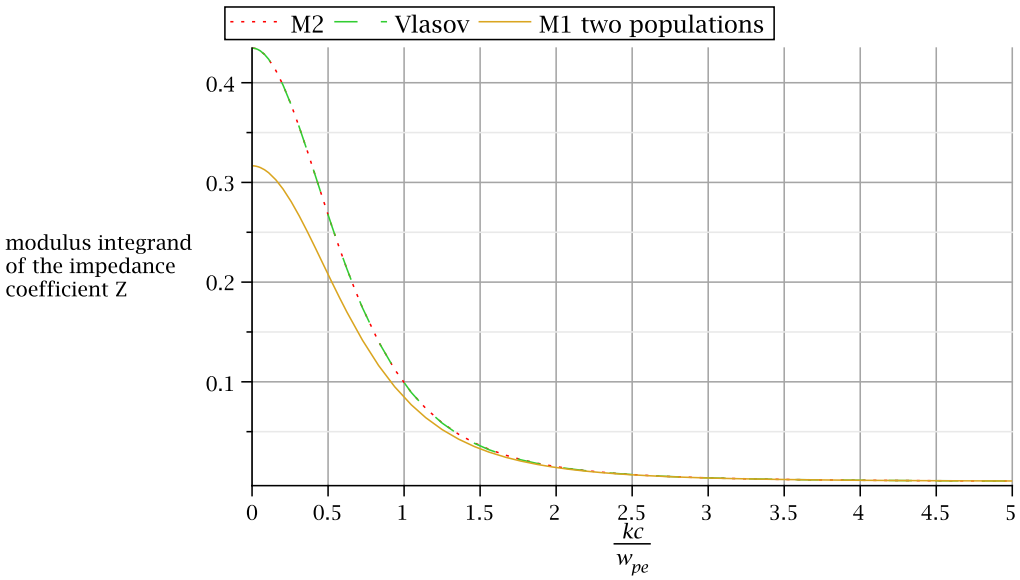

Figure 2.4: Representation of the modulus integrand of the impedance coefficient as a function of wave number in the limit $\omega/k >> v_{th}$ in the case $\omega/\omega_{pe} = 0.3$ and $v_{th}/c = 0.1$.

moments models both capture the absorption phenomenon qualitatively, but do not describe it correctly. In the opposite limit $\omega/k >> v_{th}$, the absorption phenomenon is not captured correctly by the two populations M_1 model. The M_2 model, on the contrary, correctly captures the phenomenon and the absorption expression obtained is very close to the one followed from the Vlasov equation. This study shows the limits of these three models for studies of laser plasma absorption. Higher moments models must therefore be used to correctly describe this phenomenon. In the hot electron limit, the M_3 model could be tested but the calculation is beyond the scope of this study.

2.7 Conclusion

Particle beams interaction, Landau damping and collisionless skin effect have been studied using the M_1, the two populations M_1 and M_2 moments models. By analytically deriving the dispersion relations, we have demonstrated that the particle beams interaction is correctly captured by the moments models. Landau damping is also captured by the three models, but the M_1 model is inaccurate while the two populations M_1 and M_2 moments models describe it accurately. The electromagnetic wave absorption coefficients in the case of collisionless skin effect have been calculated with the three models. We have shown that the M_1 model is not able

to model the absorption phenomenon. Two limit cases have been considered. In the case $\omega/k << v_{th}$, the two populations M_1 and the M_2 moments models both capture the absorption phenomena results but they are inaccurate. In the second case, $\omega/k >> v_{th}$, the two populations M_1 model does not describe correctly the absorption effect while the M_2 model is sufficiently accurate. Higher moments models such as the M_3 moments or full kinetic models can be used to correctly describe the absorption phenomenon in both limits. This work demonstrates through the Landau damping and the laser-plasma absorption that angular moments models have to be used carefully. These models do not always behave as a full kinetic model and can suffer from a severe lack of accuracy depending on the phenomenon studied. This study can be extended to other plasma effects and also to take into account collisional processes. In this direction, the next chapter is dedicated to the study of collisional operators for the electronic M_1 model.

Chapter 3

Classical transport theory for the collisional electronic M_1 model

The study introduced in this chapter has been published. The reference is: S. Guisset, S. Brull, E. d'Humières, B. Dubroca, V. Tikhonchuk. *Classical transport theory for the collisional electronic M1 model.* Physica A: Statistical Mechanics and its Applications, Volume 446, Pages 182-194 (2016).

3.1 Introduction

It was proposed to use laser pulses in order to compress a deuterium-tritium target and ignite nuclear fusion reactions. In this process the laser energy is deposited near the critical surface and than it is transported to denser parts of the plasma by electrons. This process plays a key role in the understanding of plasma phenomena such as, parametric [91, 173] and hydrodynamic [82, 191, 203] instabilities, laser-plasma absorption [117, 190], wave damping [58, 148], energy redistribution and hot spot formation [33, 170]. High energy, long pulse lasers produce a collisional ionised hot plasma, where the electron-ion mean free path is small compared to the plasma characteristic spatial size and the distribution function is close to the isotropic Maxwellian function. The physics of laser plasma interaction is described within the hydrodynamic plasma model. However, the moment extraction of the electron kinetic equation leads to an unclosed hydrodynamic set of equations. The closure of the system requires to express the fluxes in terms of the hydrodynamic variables and electron plasma transport coefficients. Spitzer and Härm first derived the electron plasma transport coefficients solving numerically the kinetic Fokker-Planck-Landau equation using the expansion of the electron mean free path over the temperature scale length. Their results have been reproduced in other works [9, 32, 192] using the early works of Chapman [55, 56] and Enskog [90] for neutral gases. However, the Spitzer-Härm theory is valid in the local regime where the electron flux is proportional to the temperature gradient. Indeed the electron transport plasma coefficients were derived in the case where the electron distribu-

tion function remains close to the isotropic Maxwellian function. However, in the context of inertial confinement fusion, the plasma particles may have the mean free path comparable with the temperature scale length so that the classical transport description is not adapted [179]. Moreover kinetic effects like the non local transport [33, 170], wave damping or the development of instabilities [82] can be important over time scales shorter than the collisional time so that the fluid description is insufficient. Therefore, a kinetic description is more appropriate for the study of inertial confinement fusion plasmas. However such a kinetic description is computationally expensive for describing real physical applications. Kinetic codes are limited to the time and length much shorter than those studied with fluid simulations. It is therefore an essential issue to describe kinetic effects by using reduced kinetic codes operating on fluid time scales.

It has been seen in Chapter 1, that angular moments models can be seen as a compromise between kinetic and fluid models. The collisional electronic M_1 model is derived by integrating with respect to the velocity direction the Fokker-Planck-Landau equation. However, since the electron-electron collision operator is nonlinear, the moments extraction is complex. A possibility could be to approximate the electron-electron collision operator assuming that the main contribution of the distribution function comes from its isotropic part [16]. However, as mentioned in [167], the collisional electronic M_1 model obtained by angular integration does not ensure the preservation of the admissibility states, that is, the angular moments derive from a positive underlying distribution function. Therefore, a new electron-electron collision operator was proposed in [167]. In this model, the angular integration leads to an electron-electron collision operator for the electronic M_1 model which preserves the admissible states. In this work, we start to recall the main results established in [166, 167] and complete them with an important result characterising the equilibrium states of the collision operators. Such fundamental properties make the model interesting for practical applications. In addition, to complete the validation of the considered collisional electronic M_1 model, we derive the electron transport coefficients. It is shown that in the high ion charge ($Z >> 1$) limit the electronic M_1 model and the Fokker-Planck-Landau equation coincide in the close-equilibrium case. The electron transport coefficients derived from the electron-electron collision operator used for the electronic M_1 model are compared with the ones obtained using the electron-electron collision operator for the Fokker-Planck-Landau equation.

This chapter is organised as follows: firstly the collisional operators for the electronic M_1 model are introduced. Then, their properties are presented and completed by the characterisation of the equilibrium state. In Section 3, the electron transport coefficients are derived using the collisional electronic M_1 model and compared with the ones obtained from the Fokker-Planck-Landau equation. The strategy proposed, based on an expansion on the Laguerre polynomials [32, 56], is particularly efficient since the stiffness in $1/\zeta^3$ in the electron-ion collision operator is removed. It is shown that accurate electron plasma transport coefficients are obtained. Finally, Section 4 presents our conclusions.

3.2 Collisional operators for the electronic M_1 model

This section provides a detailed description of the collisional operators used for the electronic M_1 model [83, 166].

3.2.1 Collisional electronic M_1 model

The derivation of the collisional operators, from the Fokker-Planck-Landau equation (1.10)-(1.26), for the electronic M_1 model is detailed in Annexe 1. However, the moment extraction of the electron-electron Landau collision operator (1.26) is complex because of its non-linearity [58] and some approximations are required. It has been pointed out in [166, 167] that the electron-electron collisional operator derived in Annexe 1, does not preserve the admissible states. Consequently, in order to overcome this major drawback the following collisional electronic M_1 model has been proposed [166, 167]

$$\begin{cases} \partial_t f_0(\zeta) + \nabla_{\vec{x}}.(\zeta \vec{f}_1(\zeta)) + \dfrac{q}{m}\partial_\zeta(\vec{f}_1(\zeta).\vec{E}) = Q_0(f_0), \\ \partial_t \vec{f}_1(\zeta) + \nabla_{\vec{x}}.(\zeta \bar{\bar{f}}_2(\zeta)) + \dfrac{q}{m}\partial_\zeta(\bar{\bar{f}}_2(\zeta)\vec{E}) - \dfrac{q}{m\zeta}(f_0(\zeta)\vec{E} - \bar{\bar{f}}_2(\zeta)\vec{E}) = \vec{Q}_1(\vec{f}_1) + \vec{Q}_0(\vec{f}_1), \end{cases} \tag{3.1}$$

where the collisional operators Q_0 and Q_1 are given by

$$Q_0(f_0) = \frac{2\alpha_{ee}}{3}\partial_\zeta\Big(\zeta^2 A(\zeta)\partial_\zeta(\frac{f_0}{\zeta^2}) - \zeta B(\zeta) f_0\Big), \tag{3.2}$$

$$\vec{Q}_0(\vec{f}_1) = \frac{2\alpha_{ee}}{3}\partial_\zeta\Big(\zeta^2 A(\zeta)\partial_\zeta(\frac{\vec{f}_1}{\zeta^2}) - \zeta B(\zeta)\vec{f}_1\Big), \tag{3.3}$$

$$\vec{Q}_1(\vec{f}_1) = -\frac{2\alpha_{ei}}{\zeta^3}\vec{f}_1. \tag{3.4}$$

The coefficients $A(\zeta)$ and $B(\zeta)$ write

$$A(\zeta) = \int_0^\infty \min(\frac{1}{\zeta^3}, \frac{1}{\omega^3})\omega^2 f_0(\omega)d\omega, \tag{3.5}$$

$$B(\zeta) = \int_0^\infty \min(\frac{1}{\zeta^3}, \frac{1}{\omega^3})\omega^3 \partial_\omega(\frac{f_0(\omega)}{\omega^2})d\omega. \tag{3.6}$$

Remark 3.1. *One remarks that contrarily to the M_1 collisional model derived in Annexe 1, the contribution of the electron-electron collisional operator appears in both equations of (3.1). This modification enables to obtain the admissibility requirement.*

Next we set,

$$F_0(\zeta) = \frac{f_0(\zeta)}{\zeta^2}, \qquad F_1(\zeta) = \frac{f_1(\zeta)}{\zeta^2}. \tag{3.7}$$

As remarked in [166], inserting expressions (3.5) and (3.6) into (3.2) and (3.4) gives the following equivalent expressions for $Q_0(f_0)$ and $\vec{Q}_0(\vec{f}_1)$

$$\begin{cases} Q_0(f_0) = \partial_\zeta\Big(\zeta\displaystyle\int_0^\infty J(\zeta,\zeta')\Big[\frac{F_0(\zeta')}{\zeta}\partial_\zeta F_0(\zeta) - \frac{F_0(\zeta)}{\zeta'}\partial_{\zeta'}F_0(\zeta')\Big]\zeta'^2 d\zeta'\Big), \\ \vec{Q}_0(\vec{f}_1) = \partial_\zeta\Big(\zeta\displaystyle\int_0^\infty J(\zeta,\zeta')\Big[\frac{F_0(\zeta')}{\zeta}\partial_\zeta \vec{F}_1(\zeta) - \frac{\vec{F}_1(\zeta)}{\zeta'}\partial_{\zeta'}F_0(\zeta')\Big]\zeta'^2 d\zeta'\Big), \end{cases} \tag{3.8}$$

with

$$J(\zeta,\zeta') = \frac{2\alpha_{ee}}{3}\min(\frac{1}{\zeta^3},\frac{1}{\zeta'^3})\zeta'^2\zeta^2.$$

In this work, both equivalent forms (3.5)-(3.6) and (3.8) are used. In [167], instead of using (1.26) the following electron-electron collision operator was proposed

$$Q_{ee}(f) = \frac{1}{\zeta^2}\partial_\zeta\Big(\zeta\int_0^\infty J(\zeta,\zeta')\Big[\frac{F_0(\zeta')}{\zeta}\partial_\zeta f(\zeta) - \frac{f(\zeta)}{\zeta'}\partial_{\zeta'}F_0(\zeta')\Big]\zeta'^2 d\zeta'\Big).$$

This operator satisfies mass and energy conservation properties and an entropy dissipation property. Also it preserves the realisability domain [167]. The angular integration of this operator leads to the definitions (3.8).

3.2.2 Properties of the collisional operators

In this part, we briefly recall important results established in [166, 167], then we characterise the equilibrium state of the collisional operators (3.2)-(3.4) which is given by an isotropic Maxwellian, similarly to the Landau collision operator. It is pointed out that this property is an important new result for the model. Firstly, it was demonstrated in [166, 167] that the realisability domain $\mathcal{A}$ is conserved by the collisional operators (3.2)-(3.4). Secondly, the quantity $E = \alpha_0 f_0 + \vec{\alpha}_1.\vec{f}_1$ is an entropy for the system in the case without electric field. More precisely, from system (3.1), in the case without electric field we can derive the following inequality

$$\partial_t E + \nabla_{\vec{x}}.\vec{F} \leq 0,$$

where $\vec{F}$ is the entropy flux given by $\vec{F} = \alpha_0\vec{f}_1 + \bar{\bar{f}}_2\vec{\alpha}_1$.
Thirdly, the collisional operators (3.2)-(3.4) satisfy mass and energy conservation properties. Here, we complete these results characterising the equilibrium state of the collisional operators (3.2)-(3.4) which corresponds to an isotropic Maxwellian function.

Theorem 3.2. *The solution $(f_0,\vec{f}_1)$ of the following system*

$$\begin{cases} Q_0(f_0) = 0, \\ \vec{Q}_0(\vec{f}_1) + \vec{Q}_1(\vec{f}_1) = \vec{0}, \end{cases} \tag{3.9}$$

is given by $f_0 = \zeta^2 K_1 \exp(-K_2\zeta^2)$ *and* $\vec{f_1} = \vec{0}$ *where* K_1 *and* K_2 *are two positive real constants.*

Proof. We first start to prove the following intermediate results

$$\int_0^{+\infty} \alpha_0 Q_0(f_0) d\zeta + \int_0^{+\infty} \vec{\alpha_1}.\vec{Q_0}(\vec{f_1}) d\zeta \leq 0, \tag{3.10}$$

and

$$\int_0^{+\infty} \vec{\alpha_1}.\vec{Q_1}(\vec{f_1}) d\zeta \leq 0. \tag{3.11}$$

The definition of $\vec{Q_1}(\vec{f_1})$ and the fact that $\vec{\alpha_1}.\vec{f_1} \geq 0$, (see [166]), directly lead to (3.11). Next, to prove (3.10) we use a Green formula in the expression of $\int_0^{+\infty} \alpha_0 Q_0(f_0) d\zeta$ to obtain

$$\begin{aligned} &\int_0^{+\infty} \partial_\zeta \left[\zeta \int_0^{+\infty} J(\zeta,\zeta') \left(\frac{f^0(\zeta')}{\zeta'^2} \frac{1}{\zeta} \partial_\zeta \left(\frac{f^0(\zeta)}{\zeta^2}\right) - \frac{f^0(\zeta)}{\zeta^2} \frac{1}{\zeta'} \partial_{\zeta'} \left(\frac{f^0(\zeta')}{\zeta'^2}\right) \right) \right. \\ &\qquad \left. (\zeta')^2 \, d\zeta' \right] \alpha_0 d\zeta \\ &= -\int_0^{+\infty} \int_0^{+\infty} J(\zeta,\zeta') \left(\frac{1}{\zeta} F^0(\zeta') \partial_\zeta F^0(\zeta) - \frac{1}{\zeta'} F^0(\zeta) \partial_{\zeta'} F^0(\zeta') \right) \partial_\zeta \alpha_0 \\ &\qquad \zeta \, (\zeta')^2 \, d\zeta d\zeta'. \end{aligned} \tag{3.12}$$

Next we compute $\frac{1}{\zeta} F^0(\zeta') \partial_\zeta F^0(\zeta) - \frac{1}{\zeta'} F^0(\zeta) \partial_{\zeta'} F^0(\zeta')$. From (3.7) and (2.1), we get the relation

$$\begin{aligned} \partial_\zeta F^0(\zeta) = &\int_{S^2} \partial_\zeta \alpha_0(\zeta) \exp(\alpha_0(\zeta) + \vec{\alpha_1}(\zeta).\vec{\Omega}) d\vec{\Omega} \\ &+ \int_{S^2} \vec{\Omega}.\partial_\zeta \vec{\alpha_1}(\zeta) \exp(\alpha_0(\zeta) + \vec{\alpha_1}(\zeta).\vec{\Omega}) d\vec{\Omega}. \end{aligned} \tag{3.13}$$

The expressions of F^0 and $\partial_\zeta F^0$ give

$$\begin{aligned} &\frac{1}{\zeta} F^0(\zeta') \partial_\zeta F^0(\zeta) - \frac{1}{\zeta'} F^0(\zeta) \partial_{\zeta'} F^0(\zeta') = \int_{S^2} \int_{S^2} \exp(\alpha_0(\zeta) + \vec{\alpha_1}(\zeta).\vec{\Omega}) \\ &\exp(\alpha_0(\zeta') + \vec{\alpha_1}(\zeta').\vec{\Omega}') \left(\frac{\partial_\zeta \alpha_0(\zeta)}{\zeta} + \frac{\vec{\Omega}}{\zeta}.\partial_\zeta \vec{\alpha_1}(\zeta) - \frac{\partial_{\zeta'} \alpha_0(\zeta')}{\zeta'} - \frac{\vec{\Omega}'}{\zeta'}.\partial_{\zeta'} \vec{\alpha_1}(\zeta') \right) d\vec{\Omega} d\vec{\Omega}'. \end{aligned}$$

Next by setting

$$K(\zeta,\zeta',\vec{\Omega},\vec{\Omega}') = J(\zeta,\zeta') \, \zeta^2 \zeta'^2 \exp(\alpha_0(\zeta) + \vec{\alpha_1}(\zeta).\vec{\Omega}) \exp(\alpha_0(\zeta') + \vec{\alpha_1}(\zeta').\vec{\Omega}'), \tag{3.14}$$

$$\delta(\zeta) = \frac{\partial_\zeta \alpha_0(\zeta)}{\zeta}, \quad \vec{\beta}(\zeta) = \frac{\partial_\zeta \vec{\alpha_1}(\zeta)}{\zeta}. \tag{3.15}$$

and by using equality (3.14) in (3.12) we get

$$
\begin{aligned}
&-\int_0^{+\infty}\zeta^2\int_0^{+\infty}\zeta'^2 J(\zeta,\zeta')\Big(\frac{1}{\zeta}F^0(\zeta')\partial_\zeta F^0(\zeta)-\frac{1}{\zeta'}F^0(\zeta)\partial_{\zeta'}F^0(\zeta')\Big)\frac{\partial_\zeta\alpha_0(\zeta)}{\zeta}\,d\zeta d\zeta'\\
&\qquad=-\int_0^{+\infty}\int_0^{+\infty}\int_{S^2}\int_{S^2}K(\zeta,\zeta',\vec{\Omega},\vec{\Omega}')\,(\delta(\zeta)-\delta(\zeta'))\delta(\zeta)d\zeta d\zeta' d\vec{\Omega}d\vec{\Omega}'\\
&\quad+\int_0^{+\infty}\int_0^{+\infty}\int_{S^2}\int_{S^2}K(\zeta,\zeta',\vec{\Omega},\vec{\Omega}')\left(\vec{\Omega}.\vec{\beta}(\zeta)-\vec{\Omega}'.\vec{\beta}(\zeta')\right)\delta(\zeta)d\zeta d\zeta' d\vec{\Omega}d\vec{\Omega}'.
\end{aligned}
$$

The change of variables $(\zeta,\zeta')\mapsto(\zeta',\zeta)$ leads to

$$
\begin{aligned}
&-\int_0^{+\infty}\zeta^2\int_0^{+\infty}\zeta'^2 J(\zeta,\zeta')\Big(\frac{1}{\zeta}F^0(\zeta')\partial_\zeta F^0(\zeta)-\frac{1}{\zeta'}F^0(\zeta)\partial_{\zeta'}F^0(\zeta')\Big)\frac{\partial_\zeta\alpha_0(\zeta)}{\zeta}\,d\zeta d\zeta'\\
&=-\frac{1}{2}\int_0^{+\infty}\int_0^{+\infty}\int_{S^2}\int_{S^2}K(\zeta,\zeta',\vec{\Omega},\vec{\Omega}')\,(\delta(\zeta)-\delta(\zeta'))^2\,d\zeta d\zeta' d\vec{\Omega}d\vec{\Omega}'\\
&\quad+\frac{1}{2}\int_0^{+\infty}\int_0^{+\infty}\int_{S^2}\int_{S^2}K(\zeta,\zeta',\vec{\Omega},\vec{\Omega}')\left(\vec{\Omega}.\vec{\beta}(\zeta)-\vec{\Omega}'.\vec{\beta}(\zeta')\right)(\delta(\zeta)-\delta(\zeta'))\,d\zeta d\zeta' d\vec{\Omega}d\vec{\Omega}'.
\end{aligned}
\tag{3.16}
$$

Next, for the remaining term

$$
\begin{aligned}
\int_0^{+\infty}\vec{Q}_0(\vec{f}_1).\vec{\alpha}_1(\zeta)d\zeta=-\int_0^{+\infty}\zeta^2\int_0^{+\infty}J(\zeta,\zeta')\Big(\frac{1}{\zeta}F^0(\zeta')\partial_\zeta\vec{F}^1(\zeta)-\frac{1}{\zeta'}\vec{F}^1(\zeta)\partial_{\zeta'}F^0(\zeta')\Big)\\
.\frac{\partial_\zeta(\vec{\alpha}_1)}{\zeta}(\zeta')^2\,d\zeta d\zeta'\,,
\end{aligned}
$$

we proceed as previously. The expression of $\vec{F}^1$ given in (3.7) leads to

$$
\begin{aligned}
\partial_\zeta\vec{F}^1(\zeta)=&\int_{S^2}\vec{\Omega}\partial_\zeta\exp(\alpha_0(\zeta)+\vec{\alpha}_1(\zeta).\vec{\Omega})d\vec{\Omega}\\
&+\int_{S^2}\vec{\Omega}^2\partial_\zeta\vec{\alpha}_1(\zeta)\,\exp(\alpha_0(\zeta)+\vec{\alpha}_1(\zeta).\vec{\Omega})d\vec{\Omega}.
\end{aligned}
\tag{3.17}
$$

Therefore by using expressions (3.13) and (3.17), we get

$$
\begin{aligned}
&-\int_0^{+\infty}\int_0^{\infty}J(\zeta,\zeta')\,\zeta^2\zeta'^2\left(F^0(\zeta')\frac{1}{\zeta}\partial_\zeta\vec{F}^1(\zeta)-\vec{F}^1(\zeta)\frac{1}{\zeta'}\partial_{\zeta'}F^0(\zeta')\right).\frac{\partial_\zeta(\vec{\alpha}_1)}{\zeta}d\zeta d\zeta'\\
&\qquad=\int_0^{+\infty}\int_0^{\infty}\int_{S^2}\int_{S^2}K(\zeta,\zeta',\vec{\Omega},\vec{\Omega}')\,(\delta(\zeta)-\delta(\zeta'))\,\vec{\Omega}.\vec{\beta}(\zeta)\,d\zeta d\zeta' d\vec{\Omega}d\vec{\Omega}'\\
&\quad+\int_0^{+\infty}\int_0^{\infty}\int_{S^2}\int_{S^2}K(\zeta,\zeta',\vec{\Omega},\vec{\Omega}')\left(\vec{\beta}(\zeta').\vec{\Omega}'-\vec{\beta}(\zeta).\vec{\Omega}\right)\vec{\Omega}.\vec{\beta}(\zeta)\,d\zeta d\zeta' d\vec{\Omega}d\vec{\Omega}'.
\end{aligned}
$$

Then the change of variables $(\zeta,\zeta')\mapsto(\zeta',\zeta)$ gives

$$-\int_0^{+\infty}\int_0^{\infty} J(\zeta,\zeta')\,\zeta^2\zeta'^2\left(F^0(\zeta')\frac{1}{\zeta}\partial_\zeta\vec{F}^1(\zeta)-\vec{F}^1(\zeta)\frac{1}{\zeta'}\partial_{\zeta'}F^0(\zeta')\right).\frac{\partial_\zeta(\vec{\alpha}_1)}{\zeta}d\zeta d\zeta'$$
$$=\frac{1}{2}\int_0^{+\infty}\int_0^{\infty}\int_{S^2}\int_{S^2} K(\zeta,\zeta',\vec{\Omega},\vec{\Omega}')\,(\delta(\zeta)-\delta(\zeta'))\left(\vec{\Omega}.\vec{\beta}(\zeta)-\vec{\Omega}'.\vec{\beta}(\zeta')\right)\,d\zeta d\zeta' d\vec{\Omega}d\vec{\Omega}'$$
$$-\frac{1}{2}\int_0^{+\infty}\int_0^{\infty}\int_{S^2}\int_{S^2} K(\zeta,\zeta',\vec{\Omega},\vec{\Omega}')\left(\vec{\beta}(\zeta').\vec{\Omega}'-\vec{\beta}(\zeta).\vec{\Omega}\right)^2 d\zeta d\zeta' d\vec{\Omega}d\vec{\Omega}'. \quad (3.18)$$

Finally, we add the right-hand sides of (3.16) and (3.18) and by using the inequality

$$(\delta(\zeta)-\delta(\zeta'))(\vec{\beta}(\zeta).\vec{\Omega}-\vec{\beta}(\zeta').\vec{\Omega}')\le\frac{1}{2}((\delta(\zeta)-\delta(\zeta'))^2+(\vec{\beta}(\zeta).\vec{\Omega}-\vec{\beta}(\zeta').\vec{\Omega}')^2), \quad (3.19)$$

we obtain (3.10).
Next, multiplying the first equation of (3.9) by α_0 and projecting the second on $\vec{\alpha}_1$, adding the two equalities and integrating over ζ gives

$$\int_0^{+\infty}\alpha_0 Q_0(f_0)d\zeta+\int_0^{+\infty}\vec{\alpha}_1.\vec{Q}_0(\vec{f}_1)d\zeta+\int_0^{+\infty}\vec{\alpha}_1.\vec{Q}_1(\vec{f}_1)d\zeta=0.$$

Since, we proved (3.10) and (3.11), it comes

$$\vec{\alpha}_1.\vec{Q}_1(\vec{f}_1)=0.$$

It follows that $\vec{f}_1=0$.
Multiplying the first equation of (3.9) by $\ln(F_0)$ and integrating over ζ gives

$$\int_0^{+\infty}\partial_\zeta(\zeta\int_0^{+\infty}J(\zeta,\zeta')\Big[\frac{\partial_\zeta F_0(\zeta)}{F_0(\zeta)\zeta}-\frac{\partial_{\zeta'}F_0(\zeta')}{F_0(\zeta')\zeta'}\Big]\zeta'^2F_0(\zeta)F_0(\zeta')d\zeta'\ln(F_0(\zeta))d\zeta=0.$$

By integration by part, it comes

$$-\int_0^{+\infty}\int_0^{+\infty}K(\zeta,\zeta')\Big[\frac{\partial_\zeta F_0(\zeta)}{F_0(\zeta)\zeta}-\frac{\partial_{\zeta'}F_0(\zeta')}{F_0(\zeta')\zeta'}\Big]\frac{\partial_\zeta F_0(\zeta)}{F_0(\zeta)\zeta}d\zeta'd\zeta=0.$$

with $K(\zeta,\zeta')=\zeta^2\zeta'^2F_0(\zeta)F_0(\zeta')$.
The change of variables $(\zeta,\zeta')\mapsto(\zeta',\zeta)$ leads to

$$-\int_0^{+\infty}\int_0^{+\infty}K(\zeta,\zeta')\Big[\frac{\partial_\zeta F_0(\zeta')}{F_0(\zeta')\zeta'}-\frac{\partial_\zeta F_0(\zeta)}{F_0(\zeta)\zeta}\Big]\frac{\partial_{\zeta'}F_0(\zeta')}{F_0(\zeta')\zeta'}d\zeta'd\zeta=0.$$

Summing the two previous equations gives

$$\int_0^{+\infty}\int_0^{+\infty}K(\zeta,\zeta')\Big[\frac{\partial_\zeta F_0(\zeta')}{F_0(\zeta')\zeta'}-\frac{\partial_\zeta F_0(\zeta)}{F_0(\zeta)\zeta}\Big]^2d\zeta'd\zeta=0.$$

It follows that

$$F_0(\zeta)=K_1\exp(-K_2\zeta^2),\qquad\text{and so}\qquad f_0(\zeta)=\zeta^2K_1\exp(-K_2\zeta^2).$$

Since the integral of f_0 in ζ must be positive and finite, K_1 and K_2 are positive real constants. □

These results demonstrate that the electron-electron collisional operator used for the electronic M_1 model satisfies fundamental properties. In the next section, the derivation of the plasma transport coefficients using this operator is investigated in the framework of the classical transport theory.

3.3 Derivation of the electronic transport coefficients

3.3.1 Electron collisional hydrodynamics

It has been shown that the equilibrium state of system (3.9) is given by an isotropic Maxwellian distribution function. Therefore, in this analytical derivation we consider a distribution function close to the equilibrium

$$f(t,\vec{x},\zeta,\vec{\Omega}) = M_f(\zeta,T_e(t,\vec{x}),n_e(t,\vec{x})) + \varepsilon F(t,\vec{x},\zeta,\vec{\Omega}), \tag{3.20}$$

where the Maxwellian distribution function reads

$$M_f(\zeta,T_e(t,\vec{x}),n_e(t,\vec{x})) = n_e(t,\vec{x})\Big(\frac{m_e}{2\pi T_e(t,\vec{x})}\Big)^{3/2}\exp\Big(-\frac{m_e\zeta^2}{2T_e(t,\vec{x})}\Big), \tag{3.21}$$

and the Knudsen number $\varepsilon = \lambda_{ei}/L$ is a small parameter which corresponds to the ratio between the mean free path λ_{ei} and the macroscopic scale length L. The perturbation F is seeked under the form

$$F(t,\vec{x},\zeta,\vec{\Omega}) = F_0(t,\vec{x},\zeta) + \vec{F}_1(t,\vec{x},\zeta).\vec{\Omega}, \tag{3.22}$$

According to the Chapman-Enskog approach, the density and temperature macroscopic quantities are defined as

$$n_e(t,\vec{x}) = 4\pi\int_0^{+\infty} f(t,\vec{x},\zeta,\vec{\Omega})\zeta^2 d\zeta, \tag{3.23}$$

$$T_e(t,\vec{x}) = \frac{4\pi m_e}{3n_e k_B}\int_0^{+\infty} f(t,\vec{x},\zeta,\vec{\Omega})\zeta^4 d\zeta. \tag{3.24}$$

Therefore the isotropic part of the perturbation verifies the following relations

$$\int_0^{+\infty} F_0(t,\vec{x},\zeta)\zeta^2 d\zeta = 0 \quad \text{and} \quad \int_0^{+\infty} F_0(t,\vec{x},\zeta)\zeta^4 d\zeta = 0.$$

Equations for the density and temperature are following from the integration over ζ of the electronic M_1 model (3.1) and definitions (3.23-3.24)

$$\begin{cases} \dfrac{\partial n_e}{\partial t} + \nabla_{\vec{x}}.(n_e\vec{u}_e) = 0, \\ \dfrac{\partial T_e}{\partial t} + \vec{u}_e.\nabla_{\vec{x}}(T_e) + \dfrac{2}{3}T_e\nabla_{\vec{x}}.(\vec{u}_e) + \dfrac{2}{3n_e}\nabla_{\vec{x}}.(\vec{q}) = \dfrac{2}{3n_e}\vec{j}.\vec{E} \end{cases} \tag{3.25}$$

where we retained only linear terms in the Knudsen number ε. The temporal evolution of n_e and T_e in these equations is driven by the fluxes of the particles and energy that are expressed through the electric current density and the electron heat flux defined by

$$\vec{j} = -en_e\vec{u}_e = -\frac{4\pi e\varepsilon}{3}\int_0^{+\infty}\vec{F}_1\zeta^3 d\zeta, \quad \vec{q} = \frac{2\pi m_e\varepsilon}{3}\int_0^{+\infty}\vec{F}_1\zeta^5 d\zeta. \tag{3.26}$$

In order to close the hydrodynamic system (3.25), one needs to express the electric current and the heat flux (3.26) in terms of the macroscopic variables n_e, T_e. More precisely, the term $\vec{F}_1$ should be derived explicitly in terms of the gradients of n_e and T_e, then definitions (3.26) give the electric current and the heat flux. In the quasi-stationary case ($\partial/\partial t << \nu_{ei}$) the second equation of the electronic M_1 model (3.1) reads

$$\nabla_{\vec{x}}\cdot(\zeta\bar{\bar{f}}_2) + \frac{q}{m}\partial_\zeta(\bar{\bar{f}}_2\vec{E}) - \frac{q}{m\zeta}(f_0\vec{E} - \bar{\bar{f}}_2\vec{E}) = \vec{Q}_1(\vec{f}_1) + \vec{Q}_0(\vec{f}_1).$$

Using the fact that $\bar{\bar{f}}_2 = f_0/3\bar{\bar{I}}_d$ according to equation (3.22), the previous equation leads to

$$\frac{\zeta}{3}\nabla_{\vec{x}}(f_0) - \frac{e\vec{E}}{3m_e}\frac{\partial f_0}{\partial\zeta} + \frac{2e\vec{E}}{3m\zeta}f_0 = \vec{Q}_1(\vec{f}_1) + \vec{Q}_0(\vec{f}_1),$$

which also rewrites

$$\frac{\zeta}{3}\nabla_{\vec{x}}f_0 - \frac{e\vec{E}\zeta^2}{3m_e}\frac{\partial}{\partial\zeta}\Big(\frac{f_0}{\zeta^2}\Big) = \vec{Q}_1(\vec{f}_1) + \vec{Q}_0(\vec{f}_1).$$

Then using in the place of f_0 the Maxwellian distribution (3.21), the previous equation gives

$$M_f\zeta\Big[\frac{e\vec{E}^*}{T_e} + \frac{1}{2T_e}\nabla_{\vec{x}}(T_e)\Big(\frac{m_e\zeta^2}{T_e} - 5\Big)\Big] = -\frac{2\alpha_{ei}\varepsilon}{\zeta^3}\vec{F}_1 + \frac{\varepsilon}{\zeta^2}\vec{Q}_0(\zeta^2\vec{F}_1), \tag{3.27}$$

with $\vec{E}^* = \vec{E} + (1/en_e)\nabla_{\vec{x}}(n_eT_e)$. In the following we note α_{ei} and α_{ee} instead of $\alpha_{ei}\varepsilon$ and $\alpha_{ee}\varepsilon$. In the dimensionless case a parameter $1/\varepsilon$ appears in front of the collisional operators, therefore considering the development (3.20), the parameter ε vanishes.
In order to obtain $\vec{F}_1$, one should solve the integro-differential equation (3.27). The resolution of this equation is challenging, however it is a linear equation in $\vec{F}_1$ and the form of the left hand side indicates that the solution is a linear combination of terms proportional to the generalised forces $\vec{E}^*$ and $\nabla(T_e)/T_e$ which can be represented as follows

$$\vec{F}_1 = \zeta\Big(\frac{e\vec{E}^*}{T_e}\phi^E + \nabla_{\vec{x}}(\ln T_e)\phi^Q\Big)M_f, \tag{3.28}$$

where ϕ^E and ϕ^Q are defined below. Inserting this expression into (3.26) one obtains the following relations [9]

$$\vec{j} = \sigma \vec{E}^* + \alpha \nabla_{\vec{x}} T_e, \tag{3.29}$$

$$\vec{q} = -\alpha T_e \vec{E}^* - \chi \nabla_{\vec{x}} T_e, \tag{3.30}$$

where α, σ and χ are called the plasma transport coefficients defined by

$$\sigma = -\frac{4\pi e^2}{3T_e} \int_0^\infty \zeta^4 \phi^E M_f d\zeta, \quad \chi = \frac{2\pi}{3} \int_0^\infty \zeta^4 (5 - \frac{m_e \zeta^2}{T_e}) \phi^Q M_f d\zeta, \tag{3.31}$$

$$\alpha = -\frac{4\pi e}{3T_e} \int_0^\infty \zeta^4 \phi^Q M_f d\zeta = \frac{2\pi e}{3T_e} \int_0^\infty \zeta^4 (5 - \frac{m_e \zeta^2}{T_e}) \phi^E M_f d\zeta. \tag{3.32}$$

The coefficients σ, α and χ are respectively called the electrical conductivity, the thermoelectric coefficient and the thermal conductivity. In the case of a homogeneous plasma (with no density nor temperature gradients) relation (3.29) simplifies into the Ohm's law $\vec{j} = \sigma \vec{E}$ and equation (3.30) leads to $\vec{q} = -\alpha T_e \vec{E}$. One can define the heat conductivity coefficient κ, which is a combination of the other three coefficients

$$\kappa = \chi - \alpha^2 T_e / \sigma. \tag{3.33}$$

Equation (3.27) has been established from the collisional electronic M_1 model (3.1). This equation is identical to the one obtained using the full Fokker-Planck-Landau equation (1.26), (see [9]) with the exception of the electron-electron collisional operator. Therefore, the possible differences in the plasma transport coefficients between the collisional electronic M_1 model (3.1) and the Fokker-Planck-Landau equation (1.10)-(1.26) are due to the electron-electron collisional operator. More precisely, the approximations made to derive the electron-electron collisional operator (3.2)-(3.3) for the electronic M_1 model (3.1) may lead to different plasma transport coefficients. The aim of the following subsections, is to derive the plasma transport coefficients using the collisional electronic M_1 model (3.1) and to compare them to the ones obtained using the Fokker-Planck-Landau equation (1.10)-(1.26).

3.3.2 Transport theory in Lorentzian plasma

In the case of a Lorentzian plasma the ions are highly charged therefore one can neglect the electron-electron collision operator in equation (3.27). As explained in the previous section, in this case ($Z >> 1$), the plasma transport coefficients are the same in the collisional electronic M_1 model (3.1) and in the Fokker-Planck-Landau equation (1.10)-(1.26). An explicit expression of $\vec{F}_1$ and the basic functions ϕ_E and ϕ_Q are easily derived

$$\vec{F}_1 = \zeta M_f \Big[\frac{e\vec{E}^*}{T_e} \Big(-\frac{\zeta^3}{2\alpha_{ei}} \Big) + \nabla_{\vec{x}} (\ln(T_e)) \frac{\zeta^3}{4\alpha_{ei}} \Big(5 - \frac{m_e \zeta^2}{v_{T_e}^2} \Big) \Big], \tag{3.34}$$

and

$$\phi^E = -\frac{\zeta^3}{2\alpha_{ei}}, \qquad \phi^Q = \frac{\zeta^3}{4\alpha_{ei}}\left(5 - \frac{m_e\zeta^2}{v_{T_e}^2}\right). \tag{3.35}$$

Inserting (3.35) into expressions (3.31) and (3.32) gives the transport coefficients for a high Z plasma [9]

$$\sigma_0 = \frac{32}{3\pi}\frac{e^2 n_e}{m_e\nu_{ei}}, \qquad \alpha_0 = \frac{16}{\pi}\frac{en_e}{m_e\nu_{ei}}, \qquad \chi_0 = \frac{200}{3\pi}n_e v_{T_e}\lambda_{ei}.$$

Here the subscript 0 corresponds to the high Z limit. In Figure 3.1, the electric current and heat flux are displayed in terms of $y = v/v_{T_e}$ using the definition (3.34).

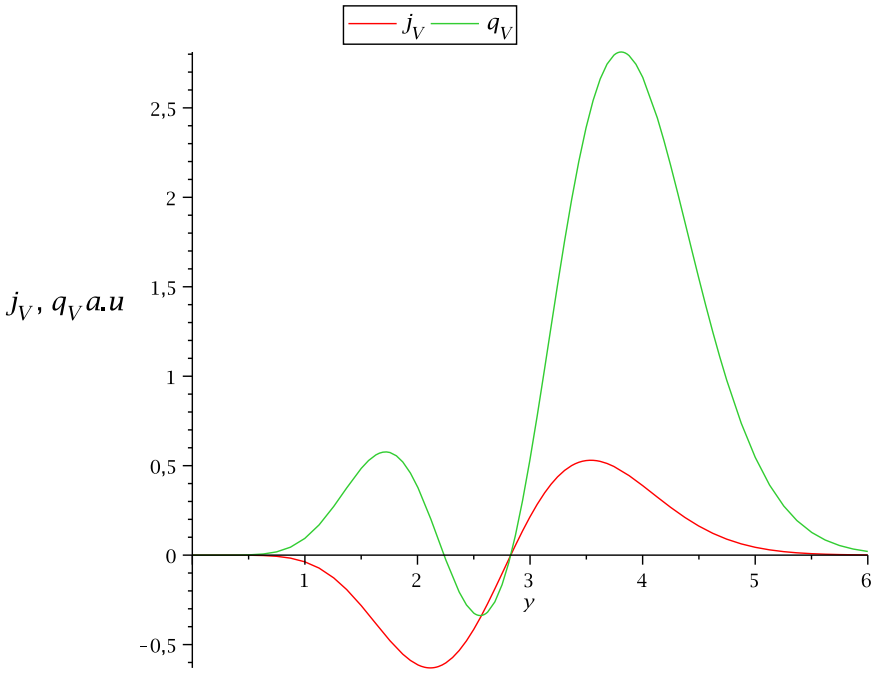

Figure 3.1: Representation of the velocity-dependent ($y = v/v_{T_e}$) particle flux, $\vec{j}_V = -\zeta^3\vec{f}_1$ in red and the electron energy flux $\vec{q}_V = m_e\vec{f}_1\zeta^5 - 5T_e\vec{f}_1\zeta^3$ in green in the case $Z >> 1$ (Lorentzian approximation).

3.3.3 Transport theory with electron-electron collisions

In the case of low Z plasmas the calculation presented in the previous section overestimates the transport coefficients because the electron-electron collision operator is not taken into account. In this case, one should solve the full equation (3.27). Spitzer and Härm [194] solved it numerically in the case of the Fokker-Planck-Landau

equation (1.10)-(1.26). Braginskii [32] derived an approximate analytical solution by expanding $\vec{F}_1$ onto a series of the Laguerre polynomials following ideas used in the kinetic theory of neutral gases [56]. In the present work, we apply the latter method for the case of the electronic M_1 model (3.1). Following (3.28), using a decomposition of $\vec{f}_1$ with the two functions ϕ^E and ϕ^Q in equation (3.27) reads

$$\frac{1}{\zeta^2}\vec{Q}_0(\zeta^2\zeta M_f\vec{\phi}^A) - \frac{2\alpha_{ei}}{\zeta^2}M_f\vec{\phi}^A = \zeta M_f\vec{S}^A, \tag{3.36}$$

where

$$\vec{S}^A = \Big[\frac{e\vec{E}^*}{T_e}S^E - \nabla_{\vec{x}}\ln(T_e)S^Q\Big],$$

with

$$S^E = 1, \qquad S^Q = \frac{1}{2}\Big(\frac{\zeta^2}{v_{T_e}^2} - 5\Big).$$

Following Chapman [56] and Braginskii [32], we expand $\vec{F}_1$ over the Laguerre polynomials [2] $L_n^{(3/2)}(x)$, with $x = \zeta^2/2v_{T_e}^2$. Indeed, the source term in the right hand side of (3.36) is a combination of the two first Laguerre polynomials $S^E = L_0^{3/2}(x)$ and $S^Q = -L_1^{3/2}(x)$. We represent the basic function ϕ^A as

$$\vec{\phi}^A(\zeta) = \sum_{m=0}^{+\infty}\vec{\phi}_m^A L_m^{(3/2)}(\zeta^2/2v_{T_e}^2),$$

multiply (3.36) by $\zeta^3 L_n^{(3/2)}(\zeta^2/2v_{T_e}^2)$ and integrate over ζ. The electron-ion collision term gives

$$\int_0^{+\infty} -\frac{2\alpha_{ei}}{\zeta^2}M_f\vec{\phi}^A\zeta^3 L_n^{(3/2)}(\zeta^2/2v_{T_e}^2)d\zeta = -2\alpha_{ei}\sum_{m=0}^{+\infty}\vec{\phi}_m^A\int_0^{+\infty} M_f v_{T_e}^2 L_m^{(3/2)}(x)L_n^{(3/2)}(x)dx.$$

Using the definition (3.21), it comes

$$\int_0^{+\infty} -\frac{2\alpha_{ei}}{\zeta^2}M_f\vec{\phi}^A\zeta^3 L_n^{(3/2)}(\zeta^2/2v_{T_e}^2)d\zeta = -2\alpha_{ei}\frac{n_e}{v_{T_e}(2\pi)^{3/2}}\sum_{m=0}^{+\infty}\vec{\phi}_m^A\int_0^{+\infty} L_m^{(3/2)}(x)L_n^{(3/2)}(x)e^{-x}dx.$$

The computation for the source term reads

$$\int_0^{+\infty}\zeta M_f\vec{S}^A\zeta^3 L_n^{(3/2)}\Big(\frac{\zeta^2}{2v_{T_e}^2}\Big)d\zeta = \frac{n_e v_{T_e}^2}{\pi\sqrt{\pi}}\int_0^{\infty} x\sqrt{x}e^{-x}\Big(\frac{e\vec{E}^*}{T_e} + \frac{1}{T_e}\nabla_{\vec{x}}(T_e)(x-\frac{5}{2})\Big)L_n^{(3/2)}(x)dx,$$

and using the orthogonality of the Laguerre polynomials, the previous equation reads

$$\int_0^{+\infty} \zeta M_f \vec{S}^A \zeta^3 L_n^{(3/2)}\Big(\frac{\zeta^2}{2v_{T_e}^2}\Big)d\zeta = \frac{n_e v_{T_e}^2}{\pi}\Big(\frac{3}{4}\frac{e\vec{E}^*}{T_e}\delta_{0n} - \frac{15}{8}\frac{1}{T_e}\nabla_{\vec{x}}(T_e)\delta_{1n}\Big)L_n^{(3/2)}(x)dx.$$

A similar derivation applies to the electron-electron collision operator

$$\int_0^{+\infty} \frac{1}{\zeta^2}\vec{Q}_0(\zeta^2\zeta M_f\vec{\phi}^A)\zeta^3 L_n^{(3/2)}\Big(\frac{\zeta^2}{2v_{T_e}^2}\Big)d\zeta = \frac{n_e v_{T_e}^2}{\pi\sqrt{\pi}}\sum_{m=0}^{+\infty}\vec{\phi}_m^A\int_0^{+\infty} L_n^{(3/2)}(x)Q_0(x\sqrt{x}e^{-x}L_m^{(3/2)}(x))dx.$$

A direct calculation finally gives the following set of equations

$$Z^{-1}\sum_{m=0}^{+\infty} ce_{nm}\vec{\phi}_m^A - \sum_{m=0}^{+\infty} ci_{nm}\vec{\phi}_m^A = \nu_{ei}^{-1}\vec{S}_n^A. \tag{3.37}$$

Here, ce_{nm} and ci_{nm} are the matrices of the integrals of the electron-electron and electron-ion collision operators. They are defined by

$$ci_{nm} = \int_0^{+\infty} L_n^{(3/2)}(x)L_m^{(3/2)}(x)e^{-x}dx, \tag{3.38}$$

$$ce_{nm} = \frac{2^{(3/2)}v_{T_e}^3}{Y_{ee}}\int_0^{+\infty} L_n^{(3/2)}(x)Q_0(x\sqrt{x}e^{-x}L_m^{(3/2)}(x))dx, \tag{3.39}$$

with $Y_{ee} = Z^{-1}Y_{ei}$ and $Y_{ei} = (3\pi/2)\nu_{ei}v_{T_e}^3$.
The term $\vec{S}_n^A$ reads

$$\vec{S}_n^A = \frac{e\vec{E}^*}{T_e}\delta_{0n} - \frac{5}{2}\frac{1}{T_e}\nabla_{\vec{x}}(T_e)\delta_{1n}.$$

The vector S_n^A has only two non-zero components. Therefore, only two first expansion coefficients ϕ_0^A and ϕ_1^A contribute to the transport coefficients (3.31)-(3.32)

$$\sigma = -\frac{e^2 n_e}{m_e}\phi_0^E, \qquad \alpha = -\frac{en_e}{m_e}\phi_0^Q = \frac{5}{2}\frac{en_e}{m_e}\phi_1^E,$$
$$\chi = \frac{5}{2}n_e v_{T_e}^2\phi_1^Q, \qquad \kappa = \frac{5}{2}n_e v_{T_e}^2(\phi_1^Q - \phi_0^Q\phi_1^E/\phi_0^E).$$

In the limit $Z >> 1$, the first term in (3.37) vanishes and the model simplifies into the case of a Lorentzian plasma. In this case the first expansion coefficients read $\phi_0^E = -32/3\pi\nu_{ei}$, $\phi_1^E = 32/5\pi\nu_{ei}$, $\phi_2^E = -32/35\pi\nu_{ei}$, $\phi_0^Q = \phi_2^Q = -16/\pi\nu_{ei}$ and $\phi_1^Q = 80/3\pi\nu_{ei}$.
Multiplying (3.27) by ζ^3 one obtains an equation more suitable for numerical integration. Indeed, the term $1/\zeta^3$ in the electron-ion collision operator makes the equation (3.27) very stiff when ζ becomes close to zero.

The computation of ci_{nm} using (3.38) is straightforward. However, the derivation of ce_{nm} using (3.39) is more challenging. The coefficients $A(\zeta)$ and $B(\zeta)$ in (3.5) and (3.6) are involved in the definition of the electron-electron collision operator Q_0. Using the variable $x = \zeta^2/2v_{T_e}^2$ a straight calculation gives

$$A(x) = \frac{n_e}{2\sqrt{\pi}x\sqrt{x}v_{T_e}}\Big[\frac{3\sqrt{\pi}}{\sqrt{2}}erf(\sqrt{x}) - e^{-x}(3\sqrt{2x} + 2\sqrt{2}x\sqrt{x})\Big] + \sqrt{\frac{2}{\pi}}\frac{n_e}{v_{T_e}}e^{-x}, \tag{3.40}$$

$$B(x) = -\frac{3n_e}{4\sqrt{\pi}v_{T_e}^3 x\sqrt{x}}\Big[\sqrt{2\pi}erf(\sqrt{x}) - 2\sqrt{2x}e^{-x}\Big] - \sqrt{\frac{2}{\pi}}\frac{n_e}{v_{T_e}^3}e^{-x}, \tag{3.41}$$

where erf is the error function. Next, inserting the definition of Q_0 (3.2) and expressions (3.40) and (3.41) into (3.39) a long but straight calculation leads to the following expression for ce_{nm}

$$\begin{aligned} ce_{nm} = \int_0^{+\infty} L_n^{(3/2)}(x)\sqrt{x}\partial_x\Big(\Big(2erf(\sqrt{x}) - \frac{4\sqrt{x}}{\sqrt{\pi}}e^{-x}\Big)\partial_x g(x) \\ + \Big(2erf(\sqrt{x}) - \frac{e^{-x}}{\sqrt{\pi}}[4\sqrt{x} - \frac{8}{3}x\sqrt{x}\,]\Big)g(x)\Big)dx, \end{aligned} \tag{3.42}$$

where $g(x) = \sqrt{x}e^{-x}L_m^{(3/2)}(x)$. Using definitions (3.38) and (3.42), each component of the matrices ci_{nm} and ce_{nm} can be computed numerically and the set of equations (3.37) can be solved.

The accuracy of the solution of (3.37) increases with the number of coefficients ϕ_n^A chosen. The minimum number is two since the first two coefficients ϕ_0 and ϕ_1 contribute to the transport coefficients. Such a two polynomial approximation was considered by Braginskii [32] for the Fokker-Planck-Landau equation (1.26). The four-polynomial approximation provides results beyond the need of experimental plasma physics. Kaneko [134] used 6 Laguerre polynomials and the high accuracy of transport coefficients he obtained was confirmed in [135] and [136] with 50 Laguerre polynomials. In this work, 6 Laguerre polynomials were used to ensure a high accuracy of the transport coefficients. The sixth polynomial expansion leads to the following approximations

$$\phi_0^E \approx -\nu_{ei}^{-1}\frac{670.42Z + 4467.79Z^2 + 3306.34Z^3 + 851.07Z^4 + 90.44Z^5 + 3.39Z^6}{173.69 + 2826.28Z + 3603.55Z^2 + 1604.84Z^3 + 320.28Z^4 + 29.31Z^5 + Z^6},$$

$$\phi_0^Q \approx -\frac{5}{2\nu_{ei}}\frac{29.38Z + 1611.93Z^2 + 1595.33Z^3 + 462.03Z^4 + 52.26Z^5 + 2.03Z^6}{173.69 + 2826.28Z + 3603.55Z^2 + 1604.84Z^3 + 320.28Z^4 + 29.31Z^5 + Z^6},$$

$$\phi_1^E \approx \nu_{ei}^{-1}\frac{-86.09Z + 1177.61Z^2 + 1414.61Z^3 + 437.38Z^4 + 51.18Z^5 + 2.03Z^6}{173.69 + 2826.28Z + 3603.55Z^2 + 1604.84Z^3 + 320.28Z^4 + 29.31Z^5 + Z^6},$$

$$\phi_1^Q \approx \frac{5}{2\nu_{ei}}\frac{163.98Z + 2155.57Z^2 + 2263.58Z^3 + 702.46Z^4 + 83.77Z^5 + 3.39Z^6}{173.69 + 2826.28Z + 3603.55Z^2 + 1604.84Z^3 + 320.28Z^4 + 29.31Z^5 + Z^6}.$$

The velocity-dependent flux functions presented in Figure 3.2 shows that the electron-electron contribution decreases as Z increases. We introduce the following dimensionless coefficients $\gamma_\sigma, \gamma_\alpha, \gamma_\chi, \gamma_\kappa$ defined by

$$\gamma_\sigma = \sigma/\sigma_0, \quad \gamma_\alpha = \alpha/\alpha_0, \quad \gamma_\chi = \chi/\chi_0, \quad \gamma_\kappa = \kappa/\kappa_0,$$

where the index 0 denotes the case of the Lorentzian approximation ($Z >> 1$). The computation of these coefficients shows that all of them are inferior to 1, that is, the Lorentzian approximation ($Z >> 1$) overestimates the electron transport coefficients for low-Z plasmas. The coefficients $\gamma_\sigma, \gamma_\alpha, \gamma_\chi, \gamma_\kappa$ are displayed in Figures 3.3 and 3.4 as a function of Z for the electron-electron Landau collision operator C_{ee} given in (1.27) and for the electron-electron M_1 collision operator (3.2)-(3.3) using six Laguerre polynomials.

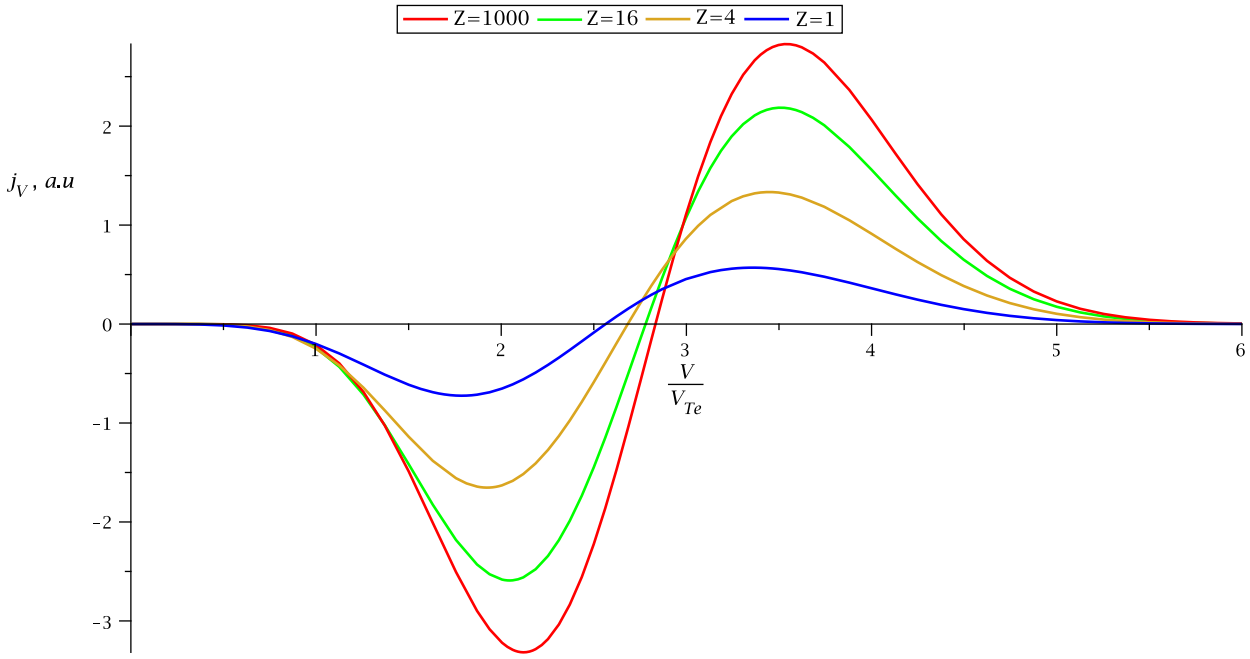

Figure 3.2: Representation of the velocity-dependent particle flux, $\vec{j}_V = -\zeta^3 \vec{f}_1$, in the case $Z = 1$ (blue), $Z = 4$ (yellow), $Z = 16$ (green) and $Z >> 1$ (Lorentzian approximation) in red.

According to Figure 3.3, the electron-electron collision operator (3.2)-(3.3) used for the electronic M_1 model underestimates the electric conductivity σ. In the large Z limit (Lorentzian approximation), the collisional M_1 model and the Fokker-Planck-Landau equation coincide. However, despite the correct tendency, the curve obtained using the M_1 collisional model underestimates the electric conductivity σ

with a largest error of 43% in the case $Z = 1$. Also, the two curves of γ_α, obtained with the M_1 model and the Fokker-Planck-Landau equation, as a function of Z are very close. In Figure 3.4, one observes that the curves representing the coefficients γ_χ and γ_κ overlap. The electron-electron collisional operator (3.2)-(3.3) recovers the correct χ and κ plasma transport coefficients.

In conclusion, the electron-electron collisional operator (3.2)-(3.3) used for the electronic M_1 model recovers the correct χ and κ plasma transport coefficients and is very accurate for the coefficient α. The main error is made with the coefficient σ with a maximum error of 43% in the case $Z = 1$. These results demonstrate the correct behaviour of the electron-electron collision operator (3.2)-(3.3) which can be used for practical applications.

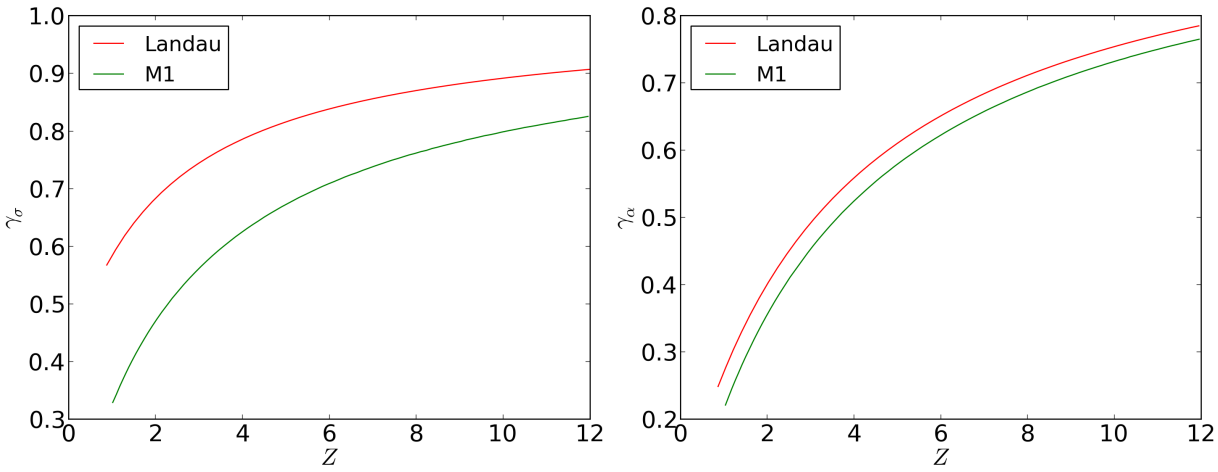

Figure 3.3: Representation of γ_σ (left) and γ_α (right) as a function of Z for the Landau (red) and the M_1 (green) collision operators using six Laguerre polynomials.

3.4 Conclusion

In this work, the fundamental properties of the electron-electron and electron-ion collision operators used for the electronic M_1 model have been studied. It is shown that their equilibrium states is given by an isotropic Maxwellian distribution function. In addition, in the Lorentzian approximation, the electronic M_1 model and the Fokker-Planck-Landau equation coincide. The electron transport coefficients are derived using the electron-electron collision operators proposed for the electronic M_1 model. Despite, the approximations used, accurate plasma transport coefficients have been obtained. The correct χ and κ plasma transport coefficients are recovered and the coefficient α is very close to the one obtained with the Fokker-Planck-Landau equation. The main error is made with the electric conductivity σ in the case $Z = 1$. In spite of this error, these results show that the electron-electron collision operator

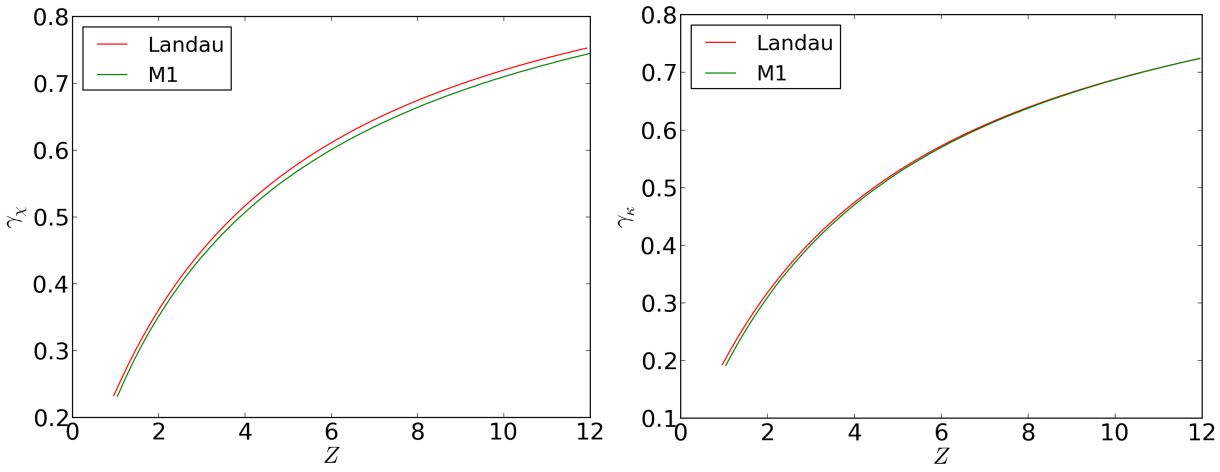

Figure 3.4: Representation of γ_χ (left) and γ_κ (right) as a function of Z for the Landau (red) and the M_1 (green) collision operators using six Laguerre polynomials.

is a good candidate for physical applications. It may be possible to improve this operator in order to obtain a more accurate σ coefficient. However, since the angular extraction of the kinetic electron-electron collision operator is complex, such an issue seems challenging.

Numerical methods for the study of the long time behavior particle transport

Chapter 4

Some basic concepts of numerical methods for nonlinear systems

The next chapters are devoted to the numerical resolution of the Maxwell-M_1 system introduced in the previous chapters. In particular, we are interested in the long time behaviour of the solutions of this system. More precisely, when the characteristic quantities of the problem become large compared to the plasma parameters, the studied model degenerates into a limit system. However, in general, the methods designed for the numerical resolution of the initial model are not able to correctly capture the limit problem. This point will be developed in detail in the next chapters.
The angular M_1 studied model is a nonlinear system. For this purpose, in this chapter, some concepts of numerical methods for nonlinear systems are given following the ideas of [52, 101, 102, 118, 159]. These methods are applied to the M_1 model. These elements will be used in the next chapters.

4.1 Godunov-type methods

In [102], Godunov proposed a numerical method for solving the Euler equations. The method is based on the fact that, even for nonlinear systems, the Riemann problem with piecewise constant initial data can be solved and the solution consists of a finite set of waves travelling at constant speeds. The Godunov method represents a major breakthrough for computational fluid dynamics. The wave structure is determined by the solution of the Riemann problem and shock waves can be correctly handled. In this section, we recall the derivation of Godunov-type methods.
We consider a given set of hyperbolic equations

$$\partial_t u + \partial_x f(u) = 0, \tag{4.1}$$

where $u \in \mathcal{U} \in \mathbb{R}^l$ and $f : \mathbb{R}^l \to \mathbb{R}^l, C^1$ with $l > 1$. We suppose there exists a strictly convex entropy-entropy flux pair (η, q) for (4.1)

$$\forall u \in \mathcal{U}, \;\; \eta'(u).f'(u) = q'(u).$$

We look for a weak entropy solution of (4.1), that is a weak solution of (4.1) such that

$$\partial_t \eta(u) + \partial_x q(u) \leq 0. \tag{4.2}$$

The eigenvalues of this system are written $\lambda^k(u)$ and we consider the associated initial condition u_0. We define a constant space step Δx and a constant time step Δt, the cell center coordinates $x_i = (i - \frac{1}{2})\Delta x$ and the mesh interfaces coordinates $x_{i+1/2} = i\Delta x$ for $i \in \mathbb{Z}$. At each time t^n, in the i^{th} cell interval $[x_{i-1/2}, x_{i+1/2}]$, $j \in \mathbb{Z}$, we compute u_j^n a numerical approximation of the solution of (4.1). Consequently, we define a piecewise constant approximate solution

$$u^h(x, t^n) = u_i^n \;\text{ for all }\; x \in [x_{i-1/2}, x_{i+1/2}[, \;\; i \in \mathbb{Z}, \;\; n \in \mathbb{N}. \tag{4.3}$$

At the initial time, in the i^{th} cell, we define

$$u_i^0 = \frac{1}{\Delta x} \int_{x_{i-1/2}}^{x_{i+1/2}} u_0(x)dx \;\text{ for all }\; i \in \mathbb{Z}.$$

Now, assuming a known numerical solution at time t^n we will detail the Godunov method to compute the numerical solution at time t^{n+1}.
Firstly, we solve the following Cauchy problem

$$\begin{cases} \partial_t w + \partial_x f(w) = 0, \; x \in \mathbb{R} \\ w(x, 0) = u^h(t^n, x), \end{cases} \tag{4.4}$$

where u^h is defined by (4.3). Considering the classical CFL condition

$$\Delta t \leq \frac{\Delta x}{2 \max\limits_{k,u}(|\lambda^{(k)}(u)|)},$$

it is known that the solution of (4.4) is given by

$$w(t, x) = u(\frac{x - x_{i+1/2}}{t - t^n}, u_i^n, u_{i+1}^n) \;\text{ for all }\; (x, t) \in [x_i, x_{i+1}] \times]t^n, t^{n+1}], \tag{4.5}$$

where $(t, x) \to u(x/t, u_L, u_R)$ is the unique weak entropic self-similar solution of the Riemann problem

$$\begin{cases} \partial_t u + \partial_x f(u) = 0, \; x \in \mathbb{R} \\ u(0, x) = \begin{cases} u^L \;\text{ if }\; x < 0, \\ u^R \;\text{ if }\; x > 0. \end{cases} \end{cases} \tag{4.6}$$

Then in order to compute a piecewise approximate solution on each cell at time t^{n+1}, we average the solution of (4.4) in each cell

$$u_i^{n+1} = \frac{1}{\Delta x}\int_{x_{i-1/2}}^{x_{i+1/2}} w(\Delta t, x)dx \text{ for all } i \in \mathbb{Z}. \tag{4.7}$$

Using (4.4) and (4.7) by Green's formula we obtain

$$u_i^{n+1} = u_i^n - \frac{\Delta t}{\Delta x}(f_{i+1/2}^n - f_{i-1/2}^n) \text{ for all } i \in \mathbb{Z},$$

where the numerical fluxes are given by

$$f_{i+1/2}^n = f(u(0, u_j^n, u_{j+1}^n)) \text{ for all } i \in \mathbb{Z}.$$

It is said that the Godunov method is exact since we consider an exact resolution of the Riemann problem (4.6). However, such a resolution can be challenging and one often prefers to use an approximate Riemann solver. In order to derive approximate Godunov-type method the exact solution of the Riemann problems considered at each interface (4.6) is replaced by an approximate solution. Following [28, 52, 101, 118] we detail the notion of consistency in the integral sense of an approximate Riemann solver.
Instead of solving exactly the Riemann problem (4.6) we consider the following an approximate Riemann solver made of $l+1$ constant states separated by l discontinuities which propagate at speed λ_k

$$\bar{w}(t,x) = u(x/t, u_l, u_R) = \begin{cases} u^0 = u^L \text{ if } x/t < \lambda_1, \\ \vdots \\ u^k \qquad \text{if } \lambda_k < x/t < \lambda_{k+1}, \\ \vdots \\ u^l = u^R \text{ if } x/t > \lambda_l. \end{cases} \tag{4.8}$$

We associate the usual CFL condition

$$\max_{1\le k\le l} |\lambda_k(u_L, u_R)| \frac{\Delta t}{\Delta x} \le \frac{1}{2}.$$

The approximate Riemann solver (4.8) is said to be consistent with the integral form of (4.1) if the integral of $w(., \Delta t)$ is equal to the integral of the exact solution on the space interval $[-\frac{\Delta x}{2}, \frac{\Delta x}{2}]$. There the approximate Riemann solver (4.8) satisfies

$$f(u_R) - f(u_L) = \sum_{k=1}^{l} \lambda_k(u_L, u_R)(u_k - u_{k-1}). \tag{4.9}$$

Then, the approximate Godunov method reads

$$\begin{cases} u_i^{n+1} = u_i^n - \dfrac{\Delta t}{\Delta x}(f_{i+1/2}^n - f_{i-1/2}^n) \\ f_{i+1/2}^n = f(u_j^n, u_{j+1}^n), \end{cases} \tag{4.10}$$

with

$$f(u_L, u_R) = \frac{1}{2}\Big(f(u_L) + f(u_R) - \sum_{k=1}^{l} |\lambda_k(u_L, u_R)|(u_k - u_{k-1})\Big).$$

Similarly, applying the same procedure with the entropy inequality (4.2), the approximate Riemann solver is said to be consistent with the integral form of (4.2) if

$$q(u_R) - q(u_L) \leq \sum_{k=1}^{l} \lambda_k(u_L, u_R)(\eta(u_k) - \eta(u_{k-1})).$$

Then, the numerical scheme (4.10) verifies a discrete entropy inequality

$$\begin{cases} \eta(u_i^{n+1}) = \eta(u_i^n) - \dfrac{\Delta t}{\Delta x}(q_{i+1/2}^n - q_{i-1/2}^n) \\ q_{i+1/2}^n = q(u_j^n, u_{j+1}^n), \end{cases} \tag{4.11}$$

with

$$q(u_L, u_R) = \frac{1}{2}\Big(q(u_L) + q(u_R) - \sum_{k=1}^{l} |\lambda_k(u_L, u_R)|(\eta(u_k) - \eta(u_{k-1}))\Big).$$

4.2 Application to angular moment models

In this section, we give an example of approximate Riemann solver, the Harten Lax van Leer's one (HLL) [118]. Then, we apply it to angular moment models and show that this approach enables to preserve the admissible sets.

4.2.1 HLL approximate Riemann solver

Here, we introduce the HLL scheme [118]. This approximate Riemann solver is obtained considering only one constant intermediate state. It writes

$$u(x/t, u_l, u_R) = \begin{cases} u^L & \text{if } x/t < \lambda_1, \\ u^* & \text{if } \lambda_1 < x/t < \lambda_2, \\ u^R & \text{if } x/t > \lambda_2. \end{cases} \tag{4.12}$$

The consistency relation (4.9) gives

$$u^* = \frac{\lambda_2 u_R - \lambda_1 u_L}{\lambda_2 - \lambda_1} - \frac{f(u_R) - f(u_L)}{\lambda_2 - \lambda_1}. \tag{4.13}$$

The structure of the approximate Riemann solver is displayed in Figure 4.1. This approximate Riemann solver is the simplest consistent with the integral form of (4.8). The wavespeeds λ_1 and λ_2 are chosen to satisfy the sub-characteristic condition [159]

$$\lambda_1 \leq \lambda^k \leq \lambda_2 \qquad \text{for all} \quad k. \tag{4.14}$$

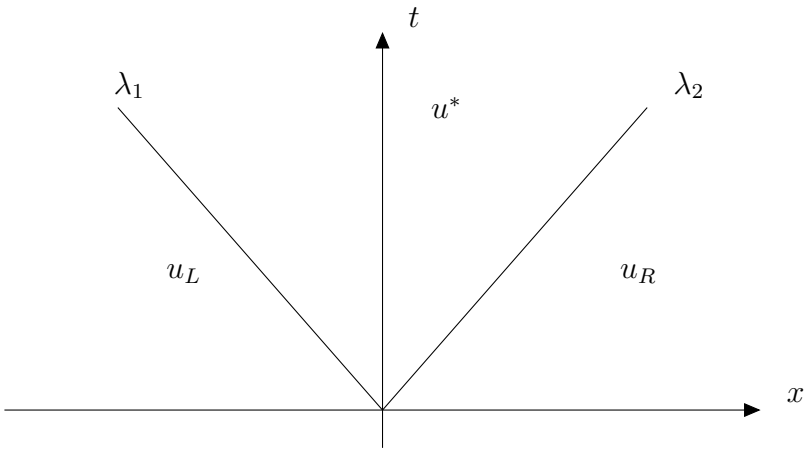

Figure 4.1: Structure of the HLL approximate Riemann solver.

4.2.2 Angular moment models

The HLL approximate Riemann solver is particularly interesting considering angular moment models. Indeed, this solver enables the preservation of the admissible sets. More precisely, considering an admissible numerical solution at time t^n, one can show that the numerical solution computed at time t^{n+1} remains admissible. In this section we detail this fundamental property. We note also that this solver is entropic [28]. These two properties are considered as nonlinear stability properties [28].
In the case of angular moments model, in a one dimensional framework, the moment vector u and the flux function $f(u)$ write

$$u =< fm >, \qquad f(u) =< fm\mu >, \tag{4.15}$$

where $m = (1, \mu, \mu^2, ..., \mu^k, ...)$ is the vector of basis functions used to defined the angular moments. The notation $< >$ represents the angular integration in μ defined by

$$< f >= \int_{-1}^{1} f(\mu) d\mu.$$

Equation (4.13) rewrites

$$u^* = \frac{1}{\lambda_2 - \lambda_1}(\lambda_2 u_R - f(u_R)) + \frac{1}{\lambda_2 - \lambda_1}(-\lambda_1 u_L + f(u_L)).$$

We remark that the terms $\lambda_2 u_R - f(u_R)$ and $-\lambda_1 u_L + f(u_L)$ are admissible. Indeed using the definitions (4.15) it follows that

$$\lambda_2 u_R - f(u_R) =< m f(\lambda_2 - \mu) > \quad \text{and} \quad -\lambda_1 u_L - f(u_L) =< m f(-\lambda_1 + \mu) > .$$

It will be shown that the eigenvalues of angular moment models based on an entropy minimisation principle are in the interval $[-1, 1]$. Therefore the condition (4.14) implies that

$$\lambda_1 \leq -1 \qquad \text{and} \qquad \lambda_2 \geq 1.$$

Then it follows that the two moments vectors $\lambda_2 u_R - f(u_R)$ and $-\lambda_1 u_L - f(u_L)$ are moments vectors of two positive distribution functions $f(\lambda_2 - \mu)$ and $f(-\lambda_1 + \mu)$. Therefore by definition there are admissible. Then since λ_2 is greater than λ_1 it follows that u^* is admissible. Finally using the Godunov approach detailed in the previous section, equation (4.7) gives the admissibility property for the numerical solution at time t^{n+1}.
To complete this explanation, we show that the eigenvalues of angular moment models based on an entropy minimisation principle are in absolute value smaller than 1. It has been seen in the first part of this manuscript, that in the case of angular moment models based on an entropy minimisation principle the form of the distribution function is given by a exponential of a polynomial function of μ. Therefore, using the definitions (4.15) it comes that

$$u =< \exp(\alpha.m) m >, \qquad f(u) =< \exp(\alpha.m) m\mu > .$$

Then it follows that

$$\partial_\alpha u =< \exp(\alpha.m) m \otimes m >, \qquad \partial_\alpha f(u) =< \exp(\alpha.m) m \otimes m\mu > .$$

Here, we are interested in the eigenvalues of the jacobian matrix $J(u)$ of (4.1) defined by

$$J(u) = \partial_u f(u).$$

This equation rewrites

$$J(u) = B(u)A(u)^{-1}, \tag{4.16}$$

where $A(u)$ and $B(u)$ are $l \times l$ matrices defined by

$$B(u) = \partial_\alpha f(u), \qquad A(u) = \partial_\alpha u.$$

We remark here, that $A(u)$ is regular since it is a positive definite symmetric matrix. By definition the eigenvalues of $J(u)$ verify

$$J(u)X = \lambda(u)X,$$

with $X \in \mathbb{R}^l$. Now, setting $Y = A^{-1}(u)X$ and using (4.16) it comes

$$B(u)Y = \lambda(u)A(u)Y.$$

Then

$$B(u)Y.Y = \lambda(u)A(u)Y.Y.$$

Finally it comes

$$\lambda(u) = \frac{B(u)Y.Y}{A(u)Y.Y}.$$

We recover the Rayleigh quotients

$$\lambda_{min}(u) = \min_{Y \in \mathbb{R}^l} \frac{B(u)Y.Y}{A(u)Y.Y},$$

$$\lambda_{max}(u) = \max_{Y \in \mathbb{R}^l} \frac{B(u)Y.Y}{A(u)Y.Y}.$$

Using the definitions (4.15) leads to

$$\lambda(u) = \frac{< \exp(\alpha.m)(m.Y)^2\mu >}{< \exp(\alpha.m)(m.Y)^2 >},$$

which is in absolute value smaller than 1.
In the next sections appropriate numerical schemes are designed for the M_1 angular moments model. In particular, one is interested in computing long time regimes. Therefore, the framework of asymptotic-preserving schemes is detailed.

Chapter 5

Asymptotic-Preserving scheme for the M_1-Maxwell system in the quasi-neutral regime

The study introduced in this chapter has been published. The reference is:
S. Guisset, S. Brull, E. d'Humières, B. Dubroca, S. Karpov, I. Potapenko. *Asymptotic-Preserving scheme for the M1-Maxwell system in the quasi-neutral regime.* Communications in Computational Physics, volume 19, issue 02, pp. 301-328 (2016).

5.1 Introduction

In this work we assume that the plasma consists of electrons and one ion species considered as immobile. This approximation is relevant due to the large mass of ions compared to the electron mass. This means the model studied is valid on time scales when the ion motion can be neglected.
For the study of collisional processes, the two important physical scales are the mean free path and the electron-ion collision frequency. The mean free path represents the average distance travelled by an electron between two collisions with an ion. The electron-ion collision frequency represents the number of electron-ion collisions per unit of time. When the electron plasma period is very small compared to the electron-ion collisional time and the Debye length is very small compared to the mean free path, the plasma is considered as quasi-neutral and the Maxwell-Gauss (also called Maxwell-Poisson) and Maxwell-Ampere equations degenerate into algebric equations on collisional time scales. Therefore to handle this type of situation a new class of methods, called Asymptotic-Preserving (AP) methods has been developed. Asymptotic-preserving schemes in the sense of Jin-Levermore [35, 36] are designed to handle multi-scale situations and behave correctly in the asymptotic limit considered. The literature on Asymptotic-preserving schemes is extensive and in this part we only consider the works dealing with the quasi-neutral limit. Consider a system (S_α) depending on a parameter α, and (S_0) being the corresponding limit

system when α tends to zero. In our case α is the ratio between the Debye length and the mean free path. A numerical scheme with time step Δt and space step Δx is called Asymptotic-Preserving in the limit α tends to zero for the system (S_α) if the scheme is stable independently of the values taken by α and if the limit scheme obtained for $\alpha = 0$ is consistent with the limit problem (S_0). In this work the system (S_α) corresponds to the Fokker-Planck-Landau-Maxwell (or the M_1-Maxwell) system and (S_0) corresponds to the Fokker-Planck-Landau-Maxwell system in the quasi-neutral limit.

This regime has been already studied in the context of fluid models [61, 63, 70]. For example in [63], the authors considered a two fluid isentropic Euler system coupled with the Poisson equation. It is shown that the Maxwell-Poisson equation can be reformulated into an elliptic equation which does not degenerate at the quasi-neutral limit. In [62], this approach is generalised to the Euler-Maxwell model with a strong magnetic field. A kinetic model consisting in a two fluid Vlasov-Poisson system has also been investigated in [68]. In [74], an Asymptotic-Preserving scheme is proposed for the Euler-Maxwell system in the quasi-neutral regime. The Maxwell equations are reformulated to enable the computation of the electrostatic field even in the limit regime. The development followed the approach for calculation of the electric field well known in the plasma physics [32, 58].

The present work deals with the construction of an Asymptotic-Preserving scheme or the M_1-Maxwell system in the quasi-neutral limit. The strategy adopted is similar to the one in [74], nevertheless to our knowledge, it is the first time that such schemes are considered for kinetic models with true collision operators. This fact is very important to deal with collisional plasma because the collision frequency ν must follow the Coulombian interaction law ($\nu \approx 1/|v|^3$). To perform realistic simulations in plasma physics, Coulombian interactions must be used. Therefore, relaxation operators are not relevant from the physical point of view. Moreover up to now, Asymptotic-Preserving schemes for the quasi-neutral limit have been developed either for fluid description of plasma or for collisionless plasmas.

The chapter is organised as follows. Section 5.2 introduces the Fokker-Planck-Landau-Maxwell system and its quasi-neutral limit. A reformulation of the Fokker-Planck-Landau-Maxwell system is presented in the case of one dimension in space and one dimension in velocity. The model is considered with electric fields and collision operators. Then, the method is generalised for full multi-dimensions problems with electromagnetic fields and collision operators. Section 5.3 introduces in detail the numerical construction of an Asymptotic-Preserving scheme for the reformulated system of section 5.2. Section 5.4 deals with the construction of an Asymptotic-Preserving scheme for the M_1 moments model from the kinetic one. Finally, section 5.5 presents two physically relevant numerical test cases for the M_1-Asymptotic-Preserving scheme for different regimes. The first one corresponds to a regime where electromagnetic effects are predominant whereas the second one on the contrary shows the efficiency of the Asymptotic-Preserving scheme in the collisional quasi-neutral regime. The numerical results are compared with kinetic and

hydrodynamic limits.

5.2 Fokker-Planck-Landau-Maxwell system in the quasi-neutral limit

In this section the Fokker-Planck-Landau-Maxwell system in the quasi-neutral limit is introduced. We consider a plasma constituted of electrons and of one fixed ion species. The description is performed with a non-negative distribution function for electrons $f_e(x, v, t)$, $x \in R^n$ represents the space variable, $v \in R^n$ is the velocity variable, $n = 1, 2$ or 3 and t is the time.

5.2.1 Scaling for the analysis of collisional processes.

For the analysis of collisional processes three important parameters are introduced: the mean free path λ_{ei} which represents the average distance travelled by an electron between two collisions, the thermal velocity v_{th} and the electron-ion collision frequency ν_{ei}. They satisfy the relations

$$v_{th} = \sqrt{\frac{k_B T}{m_e}}, \qquad \nu_{e,i} = \frac{v_{th}}{\lambda_{e,i}}.$$

These parameters enable us to scale time, space and speed

$$\tilde{t} = \nu_{e,i} t, \quad \tilde{x} = x/\lambda_{e,i}, \quad \tilde{v} = v/v_{th}.$$

In the same way, we scale the electric field, the magnetic field and the distribution function

$$\tilde{E} = \frac{eE}{m_e v_{th} \nu_{e,i}}, \quad \tilde{B} = \frac{eB}{m_e \nu_{e,i}}, \quad \tilde{f} = f_e \frac{v_{th}^3}{n_0}.$$

n_0 is the initial electronic density.
With these dimensionless quantities the Fokker-Planck-Landau-Maxwell system (1.10-1.26-1.15-1.18) becomes the following system where we have omitted the tildes

$$\begin{cases} \dfrac{\partial f}{\partial t} + v.\nabla_x f - (E + v \times B).\nabla_v f = \dfrac{1}{Z} C_{ee}(f, f) + C_{ei}(f) \ , \\ \dfrac{\partial E}{\partial t} - \dfrac{1}{\beta^2} \nabla_x \times B = -\dfrac{j}{\alpha^2}, \\ \dfrac{\partial B}{\partial t} + \nabla_x \times E = 0, \\ \nabla_x . E = \dfrac{1}{\alpha^2}(1 - n), \\ \nabla_x . B = 0, \end{cases} \tag{5.1}$$

where $\alpha = \frac{\nu_{e,i}}{\omega_{pe}}$, ω_{pe} represents the electronic plasma frequency, $\beta = v_{th}/c$, $n = n_e/n_0$ and Z the charge of the ions. In this work Z is taken equal to 1.

5.2.2 Electrostatic case

In the electrostatic case with only one dimension for space ($x \in \mathbb{R}$) and one for velocity ($v \in \mathbb{R}$), the system (5.1) can be written in the following form

$$\begin{cases} \dfrac{\partial f}{\partial t} + v\partial_x f - E\partial_v f = C_{ee}(f,f) + C_{ei}(f), \\ \dfrac{\partial E}{\partial t} = -\dfrac{j}{\alpha^2}, \end{cases} \tag{5.2}$$

where Maxwell-Poisson has to be satisfied at the initial time.

Remark 1. Notice that the fourth equation of system (5.1), called Maxwell-Gauss equation (or Poisson equation) is not used. Indeed, the second equation of (5.1), called Maxwell-Ampere equation and Poisson equation are equivalent if the Poisson equation is verified at the initial time. The limit system (S_0) is obtained when the parameter α tends to 0 and corresponds to the quasi-neutral limit. It can be written in the form

$$\begin{cases} \dfrac{\partial f}{\partial t} + v\partial_x f - E\partial_v f = C_{ee}(f,f) + C_{ei}(f), \\ j = 0, \end{cases}$$

with $n = 1$ at initial time. When α tends to zero the Maxwell-Poisson equation degenerates into the algebraic equation $n = 1$. This condition has to be satisfied at initial time. When α is equal to zero we lose the possibility to obtain the electric field from the Maxwell-Ampere equation on the collisional time scale. This limit is singular, because the Maxwell-Ampere equation degenerates into an algebraic equation.

5.2.3 Reformulation of the Maxwell-Ampere equation in the simplified case

The aim of this part is to provide a reformulation of the Maxwell-Ampere equation that is equivalent and contains explicitly the quasi-neutral limit as a particular case when $\alpha = 0$ for the electrostatic case with only one dimension for space and one for the velocity.
Multiplying the first equation of (5.2) by v, integrating in velocity and using the definition of the dimensionless current

$$j = -\int_{\mathbb{R}} f v dv, \tag{5.3}$$

we obtain

$$-\frac{\partial j}{\partial t}+\partial_x(\int_{\mathbb{R}} v^2 f dv)-E\int_{\mathbb{R}} v\partial_v f dv=\int_{\mathbb{R}} C_{ei} v dv. \tag{5.4}$$

Here we use the fact that

$$\int_{\mathbb{R}} v\, C_{ee}(f,f)dv=0.$$

Here, it is important to notice that the integral in velocity against v of the electron-ion collision operator $C_{e,i}$ does not vanish. The derivation in time of the Maxwell-Ampere equation in the electrostatic case leads to

$$\frac{\partial j}{\partial t}=-\alpha^2\frac{\partial^2 E}{\partial t^2}.$$

By using (5.4), we get

$$\alpha^2\frac{\partial^2 E}{\partial t^2}-E\int_{\mathbb{R}} v\partial_v f dv=-\partial_x(\int_{\mathbb{R}} v^2 f dv)+\int_{\mathbb{R}} C_{ei} v dv. \tag{5.5}$$

As

$$E\int_{\mathbb{R}} v\partial_v f\, dv=-nE,$$

the equation (5.5) becomes

$$\alpha^2\frac{\partial^2 E}{\partial t^2}+nE=-\partial_x(\int_{\mathbb{R}} v^2 f)dv+\int_{\mathbb{R}} C_{ei} v dv.$$

When the parameter α tends to 0, we find the limit problem

$$nE=-\partial_x(\int_{\mathbb{R}} v^2 f dv)+\int_{\mathbb{R}} C_{ei} v dv.$$

So the electrostatic field writes

$$E=\frac{-\partial_x(\int_{\mathbb{R}} v^2 f dv)+\int_{\mathbb{R}} C_{ei} v dv}{n}. \tag{5.6}$$

In this part we have shown that the Fokker-Planck-Landau-Maxwell system (5.2) is equivalent to the Fokker-Planck-Landau-Maxwell reformulated system

$$\begin{cases} \dfrac{\partial f}{\partial t}+\partial_x(vf)-\partial_v(Ef)=C_{ee}(f,f)+C_{ei}(f)\ , \\ \alpha^2\dfrac{\partial^2 E}{\partial t^2}+nE=-\partial_x(\displaystyle\int_{\mathbb{R}} v^2 f)dv+\int_{\mathbb{R}} C_{ei} v dv, \end{cases} \tag{5.7}$$

where Maxwell-Poisson has to be satisfied at initial time. The limit system when $\alpha\to 0$ is the following one

$$\begin{cases} \dfrac{\partial f}{\partial t}+\partial_x(vf)-\partial_v(Ef)=C_{ee}(f,f)+C_{ei}(f)\ , \\ E=\dfrac{-\partial_x(\int_{\mathbb{R}} v^2 f dv)+\int_{\mathbb{R}} C_{ei} v dv}{n}, \end{cases}$$

where $n = 1$ and $j = 0$ at initial time.
The second equation of (5.2) imposes $j = 0$ when $\alpha = 0$. This condition has to be satisfied at initial time.

5.2.4 Reformulation of the Maxwell-Ampere equation in the general case

In this section, we generalise previous method to a non-homogeneous collisional plasma with magnetic field in multiple dimensions.

Multiplying this first equation of (5.1) by $-v$, integrating in velocity and using the definition of the dimensionless current (5.3) we get

$$-\frac{\partial j}{\partial t} + div_x(\int_{\mathbb{R}^n} v \otimes v f dv) - \int_{\mathbb{R}^n} v(E + v \times B).\nabla_v f dv = \int_{\mathbb{R}^n} C_{ei}(f) v dv.$$

As

$$\int_{\mathbb{R}^n} (v \times B).\nabla_v f \, v \, dv = j \times B,$$

the same development as in the electrostatic case is performed.

The derivation in time of the Maxwell-Ampere equation in the general case leads to

$$\frac{\partial j}{\partial t} = -\alpha^2 \frac{\partial^2 E}{\partial t^2} + \frac{\alpha^2}{\beta^2}\big[\nabla_x \times \frac{\partial B}{\partial t}\big].$$

Finally the following form is obtained

$$\alpha^2 \frac{\partial^2 E}{\partial t^2} + n_e E - j \times B = -div_x(\int_{\mathbb{R}^n} v \otimes v f dv) + \frac{\alpha^2}{\beta^2}\big[\nabla_x \times \frac{\partial B}{\partial t}\big] + \int_{\mathbb{R}^n} C_{ei}(f) v dv. \quad (5.8)$$

When α tends to 0 in (5.8) we find the limit problem

$$n_e E = -div_x(\int_{\mathbb{R}^n} v \otimes v f dv) + \int_{\mathbb{R}^n} C_{ei}(f) v dv + j \times B.$$

So the electrostatic field writes

$$E = \frac{-div_x(\int_{\mathbb{R}^n} v \otimes v f dv) + \int_{\mathbb{R}^n} C_{ei}(f) v dv + j \times B}{n_e}.$$

In this part we have shown that the Fokker-Planck-Landau-Maxwell system (5.1) is equivalent to the Fokker-Planck-Landau-Maxwell reformulated system

$$\begin{cases} \dfrac{\partial f}{\partial t} + v.\nabla_x f - (E + v \times B).\nabla_v f = C_{ee}(f,f) + C_{ei}(f)\ , \\ \alpha^2 \dfrac{\partial^2 E}{\partial t^2} + n_e E - j \times B = -div_x(\displaystyle\int_{\mathbb{R}^n} v \otimes v f dv) + \frac{\alpha^2}{\beta^2}\Big[\nabla_x \times \frac{\partial B}{\partial t}\Big] \\ \qquad\qquad + \displaystyle\int_{\mathbb{R}^n} C_{ei}(f) v dv, \\ \dfrac{\partial B}{\partial t} + \nabla_x \times E = 0, \end{cases} \tag{5.9}$$

where the Maxwell-Poisson and Maxwell-Thomson equations have to be satisfied at the initial time.

Remark 2. The fifth equation of the system (5.1) called the Maxwell-Thomson equation is not used. Indeed the third and fifth equations (5.1) called the Maxwell-Faraday and Maxwell-Thomson equations are equivalent if the Maxwell-Thomson equation is verified at the initial time.

The limit system of (5.9) when $\alpha \to 0$ is the following one

$$\begin{cases} \dfrac{\partial f}{\partial t} + v.\nabla_x f - (E + v \times B).\nabla_v f = C_{ee}(f,f) + C_{ei}(f)\ , \\ n_e E - j \times B = -div_x(\displaystyle\int_{\mathbb{R}^n} v \otimes v f dv) + \displaystyle\int_{\mathbb{R}^n} C_{ei} v dv\ , \\ \dfrac{\partial B}{\partial t} + \nabla_x \times E = 0\ , \end{cases} \tag{5.10}$$

where $n = 1$ and $j = 0$ have to be satisfied at initial time.The second equation of (5.10) is called the Generalised Ohm's law.
In this part, a reformulation of the Maxwell-Ampere equation containing the limit case $\alpha = 0$ has been performed. This derivation enables us to construct an Asymptotic-Preserving numerical scheme for the quasi-neutral regime.

5.3 Discrete model

5.3.1 Limitation of the classical numerical scheme

A classical numerical scheme for the Maxwell-Ampere equation in the collisional regime writes

$$E_l^{n+1} = E_l^n - \frac{j_l^n \Delta t}{\alpha^2}. \tag{5.11}$$

The stability of this scheme depends directly on the parameter α. So, when α tends to 0, (5.11) can not be used to calculate the new electric field E_i^{n+1}.
The aim of the following part is to establish a numerical scheme which contains explicitly the quasi-neutral case when $\alpha = 0$. In this way, a new numerical scheme is developed for the reformulated Maxwell-Ampere equation.

5.3.2 Construction of an Asymptotic-Preserving Maxwell-Ampere numerical scheme

In this part the construction of an Asymptotic-Preserving scheme for the Maxwell-Ampere reformulated equation is explained. In this first part the numerical scheme is derived in the case of a non-homogeneous collisional plasma without magnetic field. The next part extends the method to the non-homogeneous collisional case with electromagnetic fields.

Case of a non-homogeneous collisional plasma without magnetic field.

In this part an Asymptotic-Preserving scheme is constructed for the second equation of (5.7). Let us define the primary mesh $\mathcal{M}$ for the velocity variable v, decomposed into a family of rectangles $\mathcal{M}_{p+\frac{1}{2}} =]v_p, v_{p+1}[\ \forall p \in \{-p_f; p_f\}$ where $v_p = p\Delta v$ and $p \in \mathbb{N}$ represents the number of points which discretize the velocity domain. Δv represents the energy discretisation step, which is fixed. Denote by $\mathcal{D}$ its associated dual mesh consisting of cells $\mathcal{D}_p =]v_{p-\frac{1}{2}}, v_{p+\frac{1}{2}}[$ where $v_{p-\frac{1}{2}} = (p-\frac{1}{2})\Delta v$. In the same way, a primary mesh $\mathcal{N}$ is defined for the space variable x, decomposed into a family of rectangles $\mathcal{N}_{l+\frac{1}{2}} =]x_l, x_{l+1}[\ \forall l \in \{1; l_f\}$ where $x_l = l\Delta x$ and $l \in \mathbb{N}$ represents the number of points which discretize the space domain. Δx represents the space discretisation step, which is fixed. We denote by $\mathcal{E}$ its associated dual mesh consisting of cells $\mathcal{E}_l =]x_{l-\frac{1}{2}}, x_{l+\frac{1}{2}}[$ where $x_{l-\frac{1}{2}} = (l-\frac{1}{2})\Delta x$. Let $h_{l,p}$ (resp. $h_{l+\frac{1}{2},p+\frac{1}{2}}$) be an approximation of $h(x_l, v_p)$ (resp $h(x_{l+\frac{1}{2}}, v_{p+\frac{1}{2}})$) for all distribution functions h. The velocity grid is chosen large enough to have $f_{l,p_f} = f_{l,-p_f} = 0 \ \forall l \in \{1; l_f\}$ which means that there are no particles with such velocities.

By using a conservative discretisation for the Fokker-Planck-Landau equation we obtain

$$\frac{f_{l,p}^{n+1} - f_{l,p}^n}{\Delta t} + \frac{(vf^n)_{l+\frac{1}{2},p} - (vf^n)_{l-\frac{1}{2},p}}{\Delta x} - \frac{(E^{n+1}f^n)_{l,p+\frac{1}{2}} - (E^{n+1}f^n)_{l,p-\frac{1}{2}}}{\Delta v} = C_{ee,l,p}^n + C_{ei,l,p}^n, \tag{5.12}$$

where the computation of the numerical fluxes is given by

$$(vf^n)_{l+\frac{1}{2},p} = v_p\left(\frac{f_{l,p}^n + f_{l+1,p}^n}{2}\right) - \frac{|v_p|}{2}(f_{l+1,p}^n - f_{l,p}^n), \tag{5.13}$$

$$(E^{n+1}f^n)_{l,p+\frac{1}{2}} = E_l^{n+1}(\frac{f_{l,p}^n + f_{l,p+1}^n}{2}) - \frac{|E_l^{n+1}|}{2}(f_{l,p+1}^n - f_{l,p}^n), \tag{5.14}$$

and

$$C_{ei,l,p}^n = \frac{1}{\Delta v}\Big[S_{p+\frac{1}{2}}\frac{f_{l,p+1}^n - f_{l,p}^n}{\Delta v} - S_{p-\frac{1}{2}}\frac{f_{l,p}^n - f_{l,p-1}^n}{\Delta v}\Big],$$

with

$$S_{p+\frac{1}{2}} = K(\frac{v_p + v_{p+1}}{\Delta v}).$$

The expression of K is given by (1.27). The numerical scheme for the operator $C_{ee,l,p}$ is not given, because this term cancels in the calculation. It is important to notice that the electrostatic field is calculated implicitly. It will be shown that this choice enables the calculation of the electrostatic field when $\alpha \to 0$. Using the above numerical fluxes, (5.12) reads

$$\begin{aligned}\frac{f_{l,p}^{n+1} - f_{l,p}^n}{\Delta t} &+ \frac{v_p\Big[f_{l+1,p}^n - f_{l-1,p}^n\Big] - |v_p|\Big[f_{l+1,p}^n - 2f_{l,p}^n + f_{l-1,p}^n\Big]}{2\Delta x} \\ &- \frac{E_l^{n+1}\Big[f_{l,p+1}^n - f_{l,p-1}^n\Big] - |E_l^{n+1}|\Big[f_{l,p+1}^n - 2f_{l,p}^n + f_{l,p-1}^n\Big]}{2\Delta v} \\ &= C_{ee,l,p}^n + C_{ei,l,p}^n.\end{aligned}$$

Multiplying the previous equation by $-v_p\Delta v$ and summing in p leads to

$$\begin{aligned}&\frac{-\sum_p v_p f_{l,p}^{n+1}\Delta v + \sum_p v_p f_{l,p}^n \Delta v}{\Delta t} \\ &\quad -\frac{\Delta v}{2\Delta x}\sum_p\Big[v_p^2\Big(f_{l+1,p}^n - f_{l-1,p}^n\Big) - v_p|v_p|\Big(f_{l+1,p}^n - 2f_{l,p}^n + f_{l-1,p}^n\Big)\Big] \\ &\quad +\frac{1}{2}\sum_p\Big[v_p E_l^{n+1}\Big(f_{l,p+1}^n - f_{l,p-1}^n\Big) - |E_l^{n+1}|v_p\Big(f_{l,p+1}^n - 2f_{l,p}^n + f_{l,p-1}^n\Big)\Big] \\ &\quad = -\sum_p C_{ei,l,p}^n v_p \Delta v.\end{aligned}$$

Then using the discrete definition of the current

$$j_l = -\sum_p v_p f_{l,p}\Delta v, \tag{5.15}$$

the computation of the previous equation leads to

$$\begin{aligned}\frac{j_l^{n+1} - j_l^n}{\Delta t} &- \frac{\Delta v}{2\Delta x}\sum_p\Big[v_p^2\Big(f_{l+1,p}^n - f_{l-1,p}^n\Big) - v_p|v_p|\Big(f_{l+1,p}^n - 2f_{l,p}^n + f_{l-1,p}^n\Big)\Big] \\ &+\frac{1}{2}\sum_p\Big[v_p E_l^{n+1}\Big(f_{l,p+1}^n - f_{l,p-1}^n\Big) - |E_l^{n+1}|v_p\Big(f_{l,p+1}^n - 2f_{1,l,p}^n + f_{l,p-1}^n\Big)\Big] \\ &= -\sum_p C_{ei,l,p}^n v_p \Delta v.\end{aligned}$$

The following scheme for the Maxwell-Ampere equation is used

$$\frac{E_l^{n+1} - E_l^n}{\Delta t} = -\frac{j_l^{n+1}}{\alpha^2}. \tag{5.16}$$

Contrarily to the classical scheme (5.11) the current j in (5.16) is chosen implicit. By using (5.16), we get

$$\begin{aligned}
&-\alpha^2 \frac{E_l^{n+1} - 2E_l^n + E_l^{n-1}}{\Delta t^2} \\
&\quad -\frac{\Delta v}{2\Delta x} \sum_p \Big[v_p^2 \Big(f_{l+1,p}^n - f_{l-1,p}^n \Big) - v_p |v_p| \Big(f_{l+1,p}^n - 2f_{l,p}^n + f_{l-1,p}^n \Big) \Big] \\
&\quad +\frac{1}{2} \sum_p \Big[v_p E_l^{n+1} \Big(f_{l,p+1}^n - f_{l,p-1}^n \Big) - |E_l^{n+1}| v_p \Big(f_{l,p+1}^n - 2f_{1,l,p}^n + f_{l,p-1}^n \Big) \Big] \\
&\quad = -\sum_p C_{ei,l,p}^n v_p \Delta v.
\end{aligned}$$

Remark 3. It is important to notice that

$$|E_l^{n+1}| \sum_p v_p \Big(f_{l,p+1}^n - 2f_{l,p}^n + f_{l,p-1}^n \Big) = 0.$$

Indeed a discrete integration by part gives

$$\begin{aligned}
&|E_l^{n+1}| \sum_p v_p \Big(f_{l,p+1}^n - 2f_{l,p}^n + f_{l,p-1}^n \Big) \\
&\qquad = |E_l^{n+1}| \Big[\sum_p v_p (f_{l,p+1}^n - f_{l,p}^n) - \sum_p v_{p+1} (f_{l,p+1}^n - f_{l,p}^n) \Big], \\
&\qquad = |E_l^{n+1}| \Big[\sum_p (v_p - v_{p+1}) (f_{l,p+1}^n - f_{l,p}^n) \Big], \\
&\qquad = -|E_l^{n+1}| \Delta v \Big[\sum_p (f_{l,p+1}^n - f_{l,p}^n) \Big], \\
&\qquad = 0,
\end{aligned}$$

because of boundary condition $f_{l,pf}^n = f_{l,-pf}^n = 0$. Therefore, no linearisation nor approximation is required to compute E_l^{n+1}.

Finally, the Asymptotic-Preserving scheme for the second equation of (5.7) writes

$$\begin{aligned}
-\alpha^2\frac{E_l^{n+1}-2E_l^n+E_l^{n-1}}{\Delta t^2}&\\
-\frac{\Delta v}{2\Delta x}\sum_p\Big[v_p^2\Big(f_{l+1,p}^n-f_{l-1,p}^n\Big)-v_p|v_p|\Big(f_{l+1,p}^n-2f_{l,p}^n+f_{l-1,p}^n\Big)\Big]&\\
+\frac{E_l^{n+1}}{2}\sum_p v_p\Big(f_{l,p+1}^n-f_{l,p-1}^n\Big)&\\
=-\sum_p C_{ei,l,p}^n v_p\Delta v,&
\end{aligned}$$

which is the numerical scheme for the reformulated Maxwell-Ampere equation in the case of a inhomogeneous collisional plasma. In the limit case when α tends to zero, the scheme becomes

$$E_l^{n+1}=\frac{\frac{\Delta v}{\Delta x}\sum_p\Big[v_p^2\Big(f_{l+1,p}^n-f_{l-1,p}^n\Big)-v_p|v_p|\Big(f_{l+1,p}^n-2f_{l,p}^n+f_{l-1,p}^n\Big)\Big]-2\sum_p C_{ei,l,p}^n v_p\Delta v}{\sum_p v_p\Big(f_{l,p+1}^n-f_{l,p-1}^n\Big)}.$$

In the case the expression obtained is well consistent with the limit equation (5.6), this is a key point to obtain the asymptotic preserving property.

Generalisation to a non-homogeneous collisional plasma with electromagnetic fields.

In this part we derive the numerical scheme for the reformulated Maxwell-Ampere equation in the simplified case of 1 dimension in space and 3 dimensions in velocity. The scheme can be extended to the case of 3 dimensions in space. We consider a cartesian case with an electric and a magnetic field of the form

$$E=(E_x(t,x,y),E_y(t,x,y),0),\quad B=(0,0,B_z(t,x,y)).$$

Following the same method as for the electrostatic case, we derive the following numerical scheme for the reformulated Maxwell-Ampere equation

$$\begin{aligned}
-\alpha^2\frac{E_{x,l}^{n+1}-2E_{x,l}^n+E_{x,l}^{n-1}}{\Delta t^2}&-\Delta v_x\Delta v_y\Delta v_z\sum_{i,j,k}\Big(E_{x,l}^{n+1}+j\Delta v_y B_{z,l}^{n+1}\Big)f_{l,i,j,p}^n\\
&-\Delta v_x^2\Delta v_z\sum_{i,j,k}v_{x,i}\Big(E_{y,l}^{n+1}-i\Delta v_x B_{z,l}^{n+1}\Big)f_{l,i,j,p}^n\\
=-\sum_{i,j,k}C_{ei,l,i,j,k}^n v_{x,i}\Delta v_x\Delta v_y\Delta v_z+\frac{\Delta v_x\Delta v_y\Delta v_z}{2\Delta x}&\sum_{i,j,k}\Big[v_{x,i}^2\Big(f_{l+1,i,j,k}^n-f_{l-1,i,j,k}^n\Big)\\
&-v_{x,i}|v_{x,i}|\Big(f_{l+1,j,k,p}^n-2f_{l,i,j,k}^n+f_{l-1,i,j,k}^n\Big)\Big],
\end{aligned}$$

$$
\begin{aligned}
-\alpha^2\frac{E_{y,l}^{n+1}-2E_{y,l}^{n}+E_{y,l}^{n-1}}{\Delta t^2} \; & -\Delta v_y^2\Delta v_z\sum_{i,j,k}\Big(E_{x,l}^{n+1}+j\Delta v_y B_{z,l}^{n+1}\Big)f_{l,i,j,p}^{n} \\
& -\Delta v_x\Delta v_y\Delta v_z\sum_{i,j,k}v_{x,i}\Big(E_{y,l}^{n+1}-i\Delta v_x B_{z,l}^{n+1}\Big)f_{l,i,j,p}^{n} \\
= -\sum_{i,j,k}C_{ei,l,i,j,k}^{n}v_{y,i}\Delta v_x\Delta v_y\Delta v_z+\frac{\alpha^2}{\beta^2\Delta t}\Big[\frac{B_{z,l+1}^{n+1}-B_{z,l-1}^{n+1}}{2\Delta x}-\frac{B_{z,l+1}^{n}-B_{z,l-1}^{n}}{2\Delta x}\Big] & \\
+\frac{\Delta v_x\Delta v_y\Delta v_z}{2\Delta x}\sum_{i,j,k}\Big[v_{y,i}v_{x,i}\Big(f_{l+1,i,j,k}^{n}-f_{l-1,i,j,k}^{n}\Big) & \\
-v_{y,i}|v_{x,i}|\Big(f_{l+1,i,j,k}^{n}-2f_{l,i,j,k}^{n}+f_{l-1,i,j,k}^{n}\Big)\Big], &
\end{aligned}
$$

where l is the index for space, i the index for the first coordinate in speed, j for the second and k for the third. Also Δt, Δx, Δv_x, Δv_y, Δv_z are respectively the time step, the space step, the velocity step in the first, second and third dimension. In this case there are two equations, we notice they are coupled.

5.3.3 Stability property

The asymptotic-preserving property also requires that the scheme is uniformly stable with respect to the parameter α. The rigorous proof of the asymptotic stability property is challenging and in general, the few results presented describe simplified linearised models where a linear stability study is conducted [70, 74]. In the present case, because of the dependence of the space and velocity variables in addition to the collisional operators such a property cannot be easily derived and a rigorous stability analysis of the method seems beyond the scope of this work. However, we can give some elements of the proof in a simplified linearised collisionless homogeneous case with one velocity dimension ($v \in \mathbb{R}$) without magnetic field. The model reads

$$
\begin{cases}
\dfrac{\partial f}{\partial t}-E\dfrac{\partial f}{\partial v}=0, \\
\alpha^2\dfrac{\partial E}{\partial t}=-j.
\end{cases}
$$

We consider the following linearisation around the equilibrium state given by a Maxwellian distribution function with no electric field

$$
f=f^m+f^1, \qquad E=0+E^1,
$$

with f^m a Maxwellian distribution function. The linearised system reads

$$\begin{cases} \dfrac{\partial f^1}{\partial t} + 2E^1 v f^m = 0, \\ \alpha^2 \dfrac{\partial E^1}{\partial t} = -j^1. \end{cases} \tag{5.17}$$

In the numerical method proposed, the electric field is chosen implicit as well as the electronic current. Then omitting the index 1 for simplicity, the numerical scheme reads

$$\begin{cases} \dfrac{f_p^{n+1} - f_p^n}{\Delta t} + 2E^{n+1} v_p f_p^m = 0, \\ \alpha^2 \dfrac{E^{n+1} - E^n}{\Delta t} = -j^{n+1} = \displaystyle\sum_{p=-p_f}^{p_f} f_p^{n+1} v_p \Delta v. \end{cases} \tag{5.18}$$

The previous system can also be written in the following linear system form

$$\begin{pmatrix} E \\ f_{-p_f} \\ f_{-p_f+1} \\ \vdots \\ f_{p_f-1} \\ f_{p_f} \end{pmatrix}^{n+1} = M^\alpha \begin{pmatrix} E \\ f_{-p_f} \\ f_{-p_f+1} \\ \vdots \\ f_{p_f-1} \\ f_{p_f} \end{pmatrix}^{n},$$

where the matrix M^α is given by

$$M^\alpha = \begin{pmatrix} \frac{A^\alpha \alpha^2}{\Delta t} & A^\alpha \Delta v v_{-pf} & \cdots & A^\alpha \Delta v v_{pf} \\ -\frac{B^\alpha_{-p_f} \alpha^2}{\Delta t} & 1 - B^\alpha_{-p_f} \Delta v v_{-p_f} & \cdots & -B^\alpha_{-pf} \Delta v v_{pf} \\ \vdots & \vdots & \ddots & \vdots \\ -\frac{B^\alpha_{p_f} \alpha^2}{\Delta t} & -B^\alpha_{p_f} \Delta v v_{-p_f} & \cdots & 1 - B^\alpha_{pf} \Delta v v_{pf} \end{pmatrix},$$

with

$$A^\alpha = \frac{\Delta t}{\alpha^2 + 2\Delta t^2 \displaystyle\sum_{p=-p_f}^{p_f} f_p^m v_p^2 \Delta v}, \qquad B_p^\alpha = \frac{2\Delta t^2 f_p^m v_p}{\alpha^2 + 2\Delta t^2 \displaystyle\sum_{p=-p_f}^{p_f} f_p^m v_p^2 \Delta v}.$$

The eigenvalues of the matrix M^α are given by

$$\underbrace{1, 1, ..., 1}_{2p_f - 1}, \;\; K + i\sqrt{K - K^2}, \;\; K - i\sqrt{K - K^2},$$

with $K = \dfrac{\alpha^2}{(\alpha^2 + 2\Delta t^2 \sum_{p=-p_f}^{p_f} f_p^m v_p^2 \Delta v)}$.

As $\alpha \in [0,1]$ one remarks that $K \in [0,1]$. It follows that the eigenvalues of M^α are in modulus less or equal than 1. The numerical scheme (5.18) for the simplified model (5.17) is then stable for all α. One remarks that in spite of the simplicity of the model (5.17), the form of the matrix M^α is not trivial and an extension to the general model seems challenging. However, in a more general case, the numerical tests for the wide range of input parameters, witness of the stability of the method. Kinetic codes are usually numerically expensive and limited to short time scales. Angular moments models can be seen as a compromise between kinetic and fluid models.

5.4 Asymptotic-Preserving scheme for the M_1-Maxwell moments model

This part presents an Asymptotic-Preserving scheme for the M_1 model associated to the system (5.1). The derivation of the M_1 model has been detailed in chapter 2 and chapter 3. Therefore, we directly give the system we use for the derivation of the scheme.

5.4.1 M_1 moment model

As detailed in the previous chapter, the M_1 moment model without electric field reads

$$\begin{cases} \partial_t f_0 + \nabla_x.(\zeta f_1) - \partial_\zeta(E f_1) = Q_0(f_0), \\ \partial_t f_1 + \nabla_x.(\zeta f_2) - \partial_\zeta(E f_2) + E\dfrac{(f_0 - f_2)}{\zeta} = Q_1(f_1) + Q_0(f_1), \end{cases} \tag{5.19}$$

where the collisional operators Q_0 and Q_1 are given by

$$Q_0(f_0) = \frac{2}{3}\partial_\zeta\Big(\zeta^2 A(\zeta)\partial_\zeta(\frac{f_0}{\zeta^2}) - \zeta B(\zeta) f_0\Big),$$
$$Q_1(f_1) = -\frac{2f_1}{\zeta^3}.$$

The coefficients $A(\zeta)$ and $B(\zeta)$ write

$$A(\zeta) = \int_0^\infty min(\frac{1}{\zeta^3}, \frac{1}{\omega^3})\omega^2 f_0(\omega) d\omega,$$
$$B(\zeta) = \int_0^\infty min(\frac{1}{\zeta^3}, \frac{1}{\omega^3})\omega^3 \partial_\omega(\frac{f_0(\omega)}{\omega^2}) d\omega.$$

5.4.2 Numerical scheme for the M_1 model

In this part the reformulation of the Maxwell-Ampere equation for the M_1 model is detailed. Considering a conservative scheme for the system (5.19) we write

$$\frac{f_{0,l,p}^{n+1}-f_{0,l,p}^{n}}{\Delta t}+\frac{(\zeta f_1^n)_{l+\frac{1}{2},p}-(\zeta f_1^n)_{l-\frac{1}{2},p}}{\Delta x}-\frac{(E^{n+1}f_1^n)_{l,p+\frac{1}{2}}-(E^{n+1}f_1^n)_{l,p-\frac{1}{2}}}{\Delta \zeta}=0, \tag{5.20}$$

$$\begin{aligned}\frac{f_{1,l,p}^{n+1}-f_{1,l,p}^{n}}{\Delta t}+&\frac{(\zeta f_2^n)_{l+\frac{1}{2},p}-(\zeta f_2^n)_{l-\frac{1}{2},p}}{\Delta x}-\frac{(E^{n+1}f_2^n)_{l,p+\frac{1}{2}}-(E^{n+1}f_2^n)_{l,p-\frac{1}{2}}}{\Delta \zeta}\\ &+\frac{E^{n+1}}{\zeta_p}(f_{0,l,p}^n-f_{2,l,p}^n)=Q_{1,l,p}^n+Q_{0,l,p}^n.\end{aligned} \tag{5.21}$$

The discrete collision operators involved in (5.21) are respectively given by

$$\begin{aligned}Q_{1,l,p}^n=&-\frac{2f_{1,l,p}^n}{\zeta_p^3},\\ Q_{0,l,p}^n=&\frac{2}{3\Delta\zeta_p}\Big[(\zeta_{p+\frac{1}{2}}^2A(\zeta_{p+\frac{1}{2}})\frac{1}{\Delta\zeta_{p+\frac{1}{2}}}\Big(\frac{f_{1,l,p+1}^n}{\zeta_{p+1}^2}-\frac{f_{1,l,p}^n}{\zeta_p^2}\Big)-\zeta_{p+\frac{1}{2}}B(\zeta_{p+\frac{1}{2}})f_{1,l,p+\frac{1}{2}}^n)\\ &-(\zeta_{p-\frac{1}{2}}^2A(\zeta_{p-\frac{1}{2}})\frac{1}{\Delta\zeta_{p-\frac{1}{2}}}\Big(\frac{f_{1,l,p}^n}{\zeta_p^2}-\frac{f_{1,l,p-1}^n}{\zeta_{p-1}^2}\Big)-\zeta_{p-\frac{1}{2}}B(\zeta_{p-\frac{1}{2}})f_{1,l,p-\frac{1}{2}}^n)\Big].\end{aligned}$$

Using HLL numerical fluxes in (5.20) and (5.21), it holds that

$$\begin{aligned}\frac{f_{0,l,p}^{n+1}-f_{0,l,p}^{n}}{\Delta t}+&\frac{\zeta_p\Big[f_{1,l+1,p}^n-f_{1,l-1,p}^n\Big]-|\zeta_p|\Big[f_{0,l+1,p}^n-2f_{0,l,p}^n+f_{0,l-1,p}^n\Big]}{2\Delta x}\\ &-\frac{E_l^{n+1}\Big[f_{1,l,p+1}^n-f_{1,l,p-1}^n\Big]-|E_l^{n+1}|\Big[f_{0,l,p+1}^n-2f_{0,l,p}^n+f_{0,l,p-1}^n\Big]}{2\Delta\zeta}=0,\end{aligned}$$

and

$$\begin{aligned}\frac{f_{1,l,p}^{n+1}-f_{1,l,p}^{n}}{\Delta t}+&\frac{\zeta_p\Big[f_{2,l+1,p}^n-f_{2,l-1,p}^n\Big]-|\zeta_p|\Big[f_{1,l+1,p}^n-2f_{1,l,p}^n+f_{1,l-1,p}^n\Big]}{2\Delta x}\\ &-\frac{E_l^{n+1}\Big[f_{2,l,p+1}^n-f_{2,l,p-1}^n\Big]-|E_l^{n+1}|\Big[f_{1,l,p+1}^n-2f_{1,l,p}^n+f_{1,l,p-1}^n\Big]}{2\Delta\zeta}\\ &+\frac{E_l^{n+1}}{\zeta_p}(f_{0,l,p}^n-f_{2,l,p}^n)=Q_{1,l,p}^n+Q_{0,l,p}^n.\end{aligned} \tag{5.22}$$

Multiplying the previous equation (5.22) by $-\zeta_p \Delta\zeta$ and summing in p leads to

$$\begin{aligned}
&\frac{-\sum_p \zeta_p f_{1,l}^{n+1}\Delta\zeta + \sum_p \zeta_p f_{1,l}^{n}\Delta\zeta}{\Delta t} \\
&-\frac{\Delta\zeta}{2\Delta x}\sum_p \left[\zeta_p^2\left(f_{2,l+1,p}^n - f_{2,l-1,p}^n\right) - \zeta_p^2\left(f_{1,l+1,p}^n - 2f_{1,l,p}^n + f_{1,l-1,p}^n\right)\right] \\
&+\frac{1}{2}\sum_p \left[\zeta_p E_l^{n+1}\left(f_{2,l,p+1}^n - f_{2,l,p-1}^n\right) - |E_l^{n+1}|\zeta_p\left(f_{1,l,p+1}^n - 2f_{1,l,p}^n + f_{1,l,p-1}^n\right)\right] \\
&-\sum_p E_l^{n+1}(f_{0,l,p}^n - f_{2,l,p}^n)\Delta\zeta = -\sum_p \zeta_p Q_{1,l,p}^n \Delta\zeta.
\end{aligned} \tag{5.23}$$

Here again, the term containing the electron-electron collision operator cancels. We use the definition of the dimensionless current j

$$j = -\int_{\mathbb{R}^+} f_1 \zeta d\zeta,$$

which can be written on the discrete form

$$j_l^n = -\sum_p f_{1,l,p}^n \zeta_p \Delta\zeta.$$

Therefore the scheme (5.23) becomes

$$\begin{aligned}
\frac{j_l^{n+1} - j_l^n}{\Delta t} \quad &- \quad \frac{\Delta\zeta}{2\Delta x}\sum_p \left[\zeta_p^2\left(f_{2,l+1,p}^n - f_{2,l-1,p}^n\right) - \zeta_p^2\left(f_{1,l+1,p}^n - 2f_{1,l,p}^n + f_{1,l-1,p}^n\right)\right] \\
&+ \quad \frac{1}{2}\sum_p \left[\zeta_p E_l^{n+1}\left(f_{2,l,p+1}^n - f_{2,l,p-1}^n\right) - |E_l^{n+1}|\zeta_p\left(f_{1,l,p+1}^n - 2f_{1,l,p}^n + f_{1,l,p-1}^n\right)\right] \\
&- \quad \sum_p E_l^{n+1}(f_{0,l,p}^n - f_{2,l,p}^n)\Delta\zeta = -\sum_p \zeta_p Q_{1,l,p}^n \Delta\zeta.
\end{aligned} \tag{5.24}$$

Using the scheme (5.16), expression (5.24) becomes

$$\begin{aligned}
&-\alpha^2 \frac{E_l^{n+1} - 2E_l^n + E_l^{n-1}}{\Delta t^2} \\
&-\frac{\Delta\zeta}{2\Delta x}\sum_p \left[\zeta_p^2\left(f_{2,l+1,p}^n - f_{2,l-1,p}^n\right) - \zeta_p^2\left(f_{1,l+1,p}^n - 2f_{1,l,p}^n + f_{1,l-1,p}^n\right)\right] \\
&+\frac{1}{2}\sum_p \left[\zeta_p E_l^{n+1}\left(f_{2,l,p+1}^n - f_{2,l,p-1}^n\right) - |E_l^{n+1}|\zeta_p\left(f_{1,l,p+1}^n - 2f_{1,l,p}^n + f_{1,l,p-1}^n\right)\right] \\
&-E_l^{n+1}\sum_p (f_{0,l,p}^n - f_{2,l,p}^n)\Delta\zeta = -\sum_p \zeta_p Q_{1,l,p}^n \Delta\zeta.
\end{aligned}$$

Like for the kinetic scheme in (5.3.2), it holds that

$$\sum_p |E_l^{n+1}|\zeta_p\Big(f_{1,l,p+1}^n - 2f_{1,l,p}^n + f_{1,l,p-1}^n\Big) = 0.$$

Therefore the final scheme obtained reads

$$E_l^{n+1} = \frac{-\alpha^2\dfrac{(2E_l^n - E_l^{n-1})}{\Delta t^2} + \beta_1(f_{0,l}^n, f_{1,l}^n)}{-\dfrac{\alpha^2}{\Delta t^2} + \beta_2(f_{0,l}^n, f_{1,l}^n)},$$

where the coefficients β_1 and β_2 are given by

$$\beta_1 = \frac{\Delta\zeta}{2\Delta x}\sum_p \Big[\zeta_p^2\Big(f_{2,l+1,p}^n - f_{2,l-1,p}^n\Big) - \zeta_p^2\Big(f_{1,l+1,p}^n - 2f_{1,l,p}^n + f_{1,l-1,p}^n\Big)\Big] - \sum_p \zeta_p Q_{1,l,p}^n \Delta\zeta,$$

$$\beta_2 = \frac{1}{2}\sum_p \Big[\zeta_p\Big(f_{2,l,p+1}^n - f_{2,l,p-1}^n\Big)\Big] - \sum_p (f_{0,p,l}^n - f_{2,p,l}^n)\Delta\zeta.$$

Remark 4. The stability of this new scheme does not depend on the parameter α. So, the electrostatic field can be obtained even if α becomes equal to zero.

Remark 5. Following the same procedure as for the Fokker-Planck-Maxwell system, this reformulation can be generalised for multi-dimension problems with magnetic fields.

5.5 Numerical test cases

This section presents two physically relevant numerical experiments where opposite regimes are considered. The first one consider two counter-propagating beams of electrons where the collective electrostatic effects are predominant. The second one deals with the relaxation of a localised temperature profile in the quasi-neutral regime. In this regime collisions between particles dominate.

5.5.1 Two electron beams interaction

In this part we study the interaction between two electron beams. This collisionless test case enables us to study the regime where electrostatic effects are predominant. Therefore for this test case we have $C_{ee} = C_{ei} = 0$.
Consider two electron beams propagating at velocity v_0 and v_1. The dispersion relation is given by

$$1 - \frac{1}{(\omega - kv_0)^2} - \frac{1}{(\omega - kv_1)^2} = 0,$$

where v_0 and v_1 denote the beams velocities.
This configuration can lead to electrostatic instabilities. Indeed, the solutions of the form $Ae^{-i\omega t+ikx}$ are unstable when ω_I the imaginary part of ω is strictly positive. In the case $v_0 = -v_1$ we can show that the solution is stable if $kv_0 \geq \sqrt{2}$.
This test is problematic for the M_1 model. Indeed, if we consider two electron beams propagating with equal but opposite velocities the distribution function is well defined. Nevertheless, the M_1 model considers only the angular moments f_0 and f_1. For the calculation of f_1 the contribution of two populations cancel out and we get $f_1 = 0$. The M_1 model sees an isotropic configuration which is not the reality. To overcome this problem we use the superposition principle that is valid because the model is linear. Two particle populations (one per beam) are considered. For each time step the M_1 problem is solved for the first population then for the second one. Hence the Maxwell equations are solved taking into account the two distribution functions.
In the case of two streams propagating with opposite velocities v_d and $-v_d$, the initial conditions are

$$f(t=0,x,v) = 0.5[(1+Acos(kx))M_{v_d}(v) + (1-Acos(kx))M_{-v_d}(v)],$$

with

$$M_{\pm v_d}(v) = n_e(\frac{m_e}{2\pi k_B T_e})^{3/2} exp\Big(\frac{-m_e(v \mp v_d)^2}{2k_B T_e}\Big).$$

The parameter A is introduced to perturb the initial condition in order to enable the development of the electrostatic instability. The velocity modulus goes from 0 to 12 v_{th} and the space scale from 0 to 25 λ_{De}. With 100 points for the space grid and 128 points for the velocity modulus grid the results are converged. In Figure 5.1 the distribution function is represented in the phase space for the initial time and the final time $t = 30$ plasma periods. In this example $v_d = 4$, $A = 0.001$ and periodical boundary conditions are used. In the second plot the interaction between the two streams is observed.

Our results have been compared with a kinetic code [87]. In Figure 5.2, the evolution of the electrostatic energy is represented as a function of time for the (M_1-AP) code in green and for a kinetic code in red. The first plot shows the results for A=0.001 and the second one for A=0.1. In the case of small perturbations (A=0.001), the M_1 model and the kinetic code give analogous results. In the case of strong perturbations (A=0.1), the (M_1-AP) code and the kinetic code show some differences after a long time. In the case of a strong perturbation, a non-linear regime is obtained and it is well-known that the M_1 model is not accurate enough [83].

This numerical experiment shows the good behaviour of the (M_1-AP) scheme in a regime where electrostatic effects are predominant.

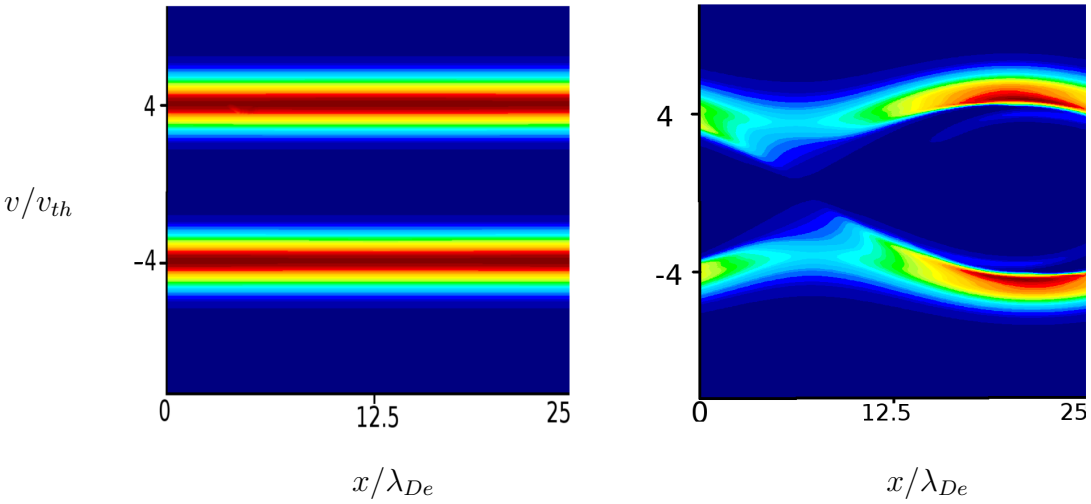

Figure 5.1: Distribution function as a function of space and velocity at initial time (left) and after 30 plasma periods (right).

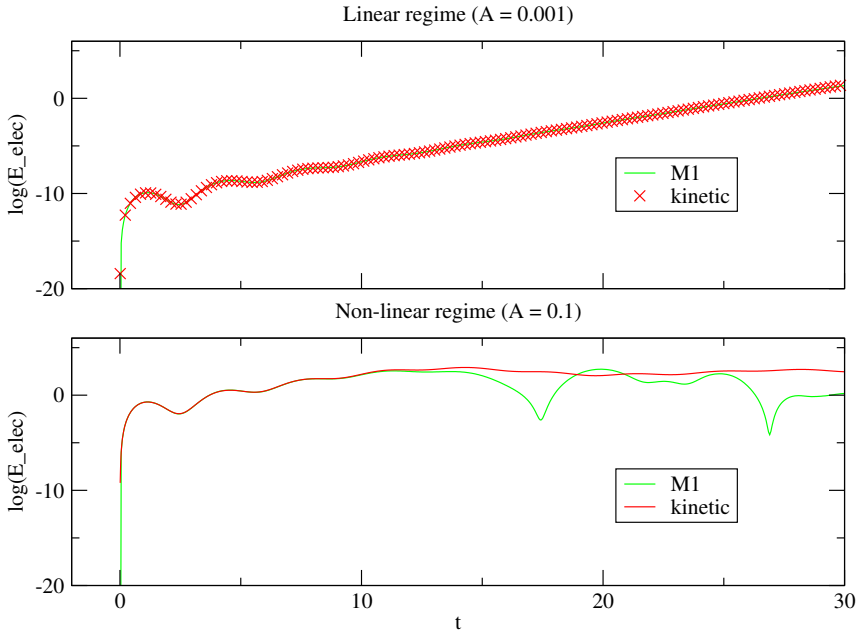

Figure 5.2: Temporal evolution of the electrostatic energy (dimensionless units) in the linear regime (top) and in the non-linear regime (bottom).

5.5.2 Hot spot relaxation

We now study the relaxation of a localised temperature perturbation generated, for example, by a short laser pulse. Suppose that the laser impulse duration

is shorter than the relaxation time. This phenomenon investigated in references [10],[33] corresponds physically to the heating of a plasma during a short time and to the relaxation phenomenon which follows. Steep temperature gradients due to the localised heating induce a non-local heat transport. Here, we consider the collisional regime. This configuration is particularly interesting because it enables to study the coupling of the M_1 model with the Maxwell-Ampere Asymptotic-Preserving scheme.

Initially the distribution function for electrons is a Maxwellian with a Gaussian temperature profile

$$T_e(x, t = 0) = T_0 + T_1 \exp(-\frac{x^2}{D^2}),$$

where the hot spot size D is a characteristic scale of inhomogeneity. First we make a few remarks on the formulation of the problem related to the ambipolar electric field. In the case of a smooth temperature gradient, the following formula for the electric field is obtained [179]

$$\frac{eE}{m_e} = -\frac{\nabla_x \int_{\mathbb{R}^3} F_0 v^7 dv}{6 \int_{\mathbb{R}^3} F_0 v^5 dv},$$

where F_0 is the isotropic part of the electron distribution function. For a Maxwellian distribution function, this field is expressed through the classical formula

$$eE = -T_e\Big(\frac{\nabla_x n_e}{n_e} + \frac{5}{2}\frac{\nabla_x T_e}{T_e}\Big).$$

The local heat flux is given by the Spitzer-Harm formula [194]

$$q_{SH} = -\kappa_{SH} \nabla_x T_e,$$

with conductivity

$$\kappa_{SH} = \frac{128}{3\pi}\frac{Z + 0.24}{Z + 4.2} n_e v_{th} \lambda_{ei}.$$

Note that already for $D^{-1}\lambda_{ei} > 0.06/\sqrt{Z}$, the classical transport theory is not applicable.
In a first simulation presented here, we choose typical parameters for ICF studies $T_0 = 1\text{KeV}$, $T_1 = 4\text{KeV}$ and $D = 8,44\lambda_{ei}$. There is no electric field at the initial time. We choose the specular reflection as the boundary conditions. The space scale goes from $-80\lambda_{ei}$ to $80\lambda_{ei}$. The velocity modulus scale goes from 0 to $50\, v_{th}$.

Figure 5.3 shows the evolution of the temperature and electric field profiles until 30 τ_{ei}. Then at $t = 2\ \tau_{ei}$, we observe that the temperature profile starts to relax to a colder temperature and the electric field, which is proportional to the gradient of temperature, also decreases. The numerical scheme reproduces a good behaviour of the hot spot relaxation phenomenon.

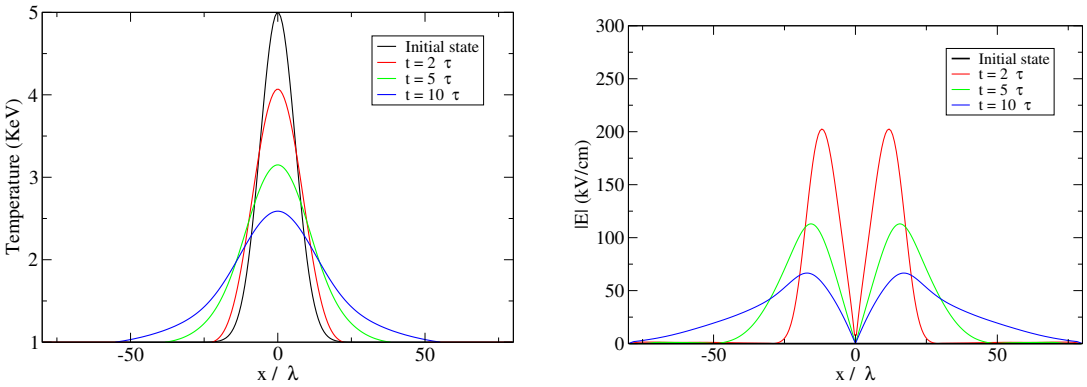

Figure 5.3: Representation of the temperature and electric field as function of space for different times.

The results of our M_1-Asymptotic-Preserving scheme (M_1-AP) have been compared with the ones obtained by a kinetic code [170]. In Figure 5.4, the temperature and the electrostatic field profiles are represented as a function of space for different times. The (M_1-AP) results are given in green while the kinetic results are in red. Both results show a good agreement. Small differences are observed concerning the amplitude of the temperature and the electric field. The relaxation phenomenon observed with the (M_1-AP) code is faster than the one with the kinetic code.
It is interesting to notice that there is a large difference of calculation time. The simulation with the kinetic code requires the use of 50 processes during several days while the (M_1-AP) code only needs few minutes with one processor. Moreover, thanks to the rapidity of the M_1 Asymptotic-Preserving code a mesh convergence study has been performed. With 500 points for the space grid and 80 points for the energy grid the results are converged. The time step used is $\Delta t = 10^{-3}\tau_{ei}$ in order to respect classical stability conditions.

Remark 6. In this case the parameter α which represents the ratio between the electron-ion collision frequency and the electron plasma frequency is equal to 4.10^{-4}. In order to avoid a severe constraint on the time step we use the new M_1-Asymptotic-Preserving scheme. With the same CFL conditions, the classic Maxwell-Ampere numerical scheme breaks down from the very first iterations.

Remark 7. It is important to notice that the Asymptotic-Preserving scheme is stable even in the case $\alpha = 0$.

In a second stage, a new simulation was performed in order to compare the results obtained using the (M_1-AP) scheme with the ones obtained using another kinetic code [24] and a hydrodynamic code based on the classical transport theory [179]-[194]. For the simulation presented, we choose the parameters $T_0 = 1$KeV, $T_1 = 2$KeV, $Z = 80$ and $D = 100\lambda_{ei}$. The results are given at time $t = 120\tau_{ei}$. The

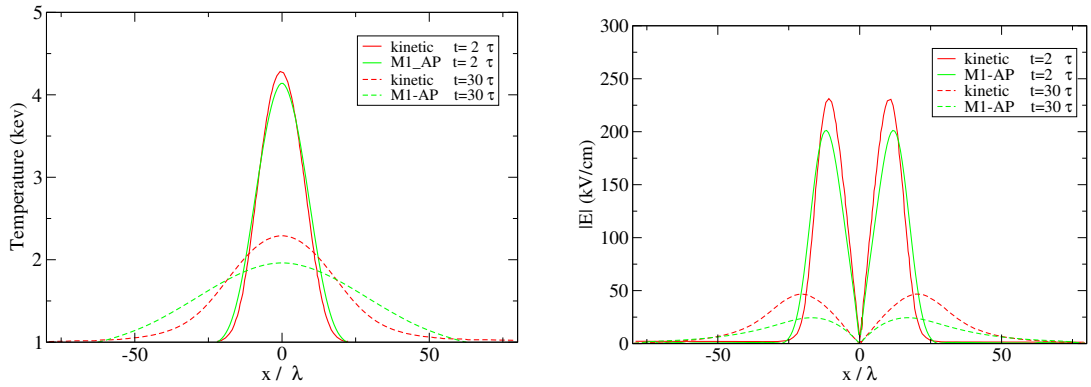

Figure 5.4: Comparison of the temperature (left) and electric field (right) for a kinetic code [170] and the M_1 Asymptotic-Preserving scheme.

space scale goes from $-2500\lambda_{ei}$ to $2500\lambda_{ei}$. In Figure 5.5, the temperature and the heat flux are represented for the three codes. Dimensionless quantities are used here. It appears that the three temperature profiles are very close. The hydrodynamic temperature is slightly smaller than the two others while the (M_1-AP) scheme and the kinetic scheme are in very good agreement. Different heat flux profiles are also compared in Figure 5.5. The (M_1-AP) flux and the kinetic flux are close and it appears that the (M_1-AP) flux is slightly more spread out. The hydrodynamic flux on the contrary is much larger than the two others and is also more localised. In this regime, one can again observe the good behaviour of the (M_1-AP) scheme. This scheme gives close results with the kinetic code while the hydrodynamic approach overestimates the heat flux.

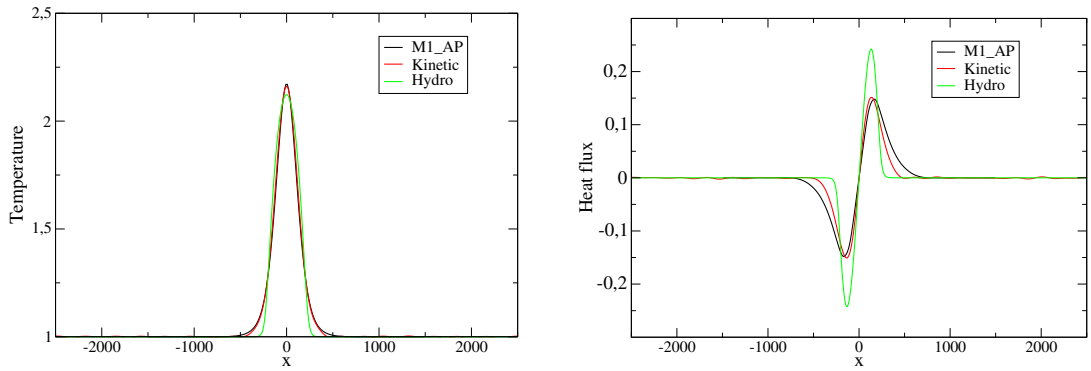

Figure 5.5: Comparison of the temperature (left) and heat flux (right) for a kinetic code [24], a hydrodynamic code and the M_1 Asymptotic-Preserving scheme.

5.6 Conclusion

In this chapter, we have constructed an Asymptotic-Preserving scheme for the full Fokker-Planck-Landau-Maxwell system, which handles the quasi-neutral limit without any contraction of time and space steps. We have first established a reformulated Fokker-Planck-Landau-Maxwell system then used it to construct the Asymptotic-Preserving scheme. The method has been extended to the general case of collisional plasmas in electromagnetic fields for multi-dimensions problems. An M_1-Asymptotic-Preserving scheme has been derived. Next, the M_1-Asymptotic-Preserving scheme has been implemented and two numerical test cases have been performed. The first one corresponds to a regime where electromagnetic effects are predominant. The second one on the contrary shows the efficiency of the Asymptotic-Preserving scheme in the quasi-neutral regime. The scheme, accurate and fast, works in both regimes. In this chapter, we have scaled the system studied with the collisional parameter to study the quasi-neutral regime. In the next chapter the electronic M_1 model is studied in the diffusive limit.

Chapter 6

Asymptotic-preserving scheme for the electronic M_1 model in the diffusive limit

The study introduced in this chapter has been submitted for publication.

6.1 Introduction

In inertial confinement fusion, nanosecond laser pulses are used to ignite a deuterium-tritium target. An accurate description of this process is necessary for understanding of laser-matter interactions and for the target design. Numerous physical phenomena such as, parametric [91, 173] and hydrodynamic [82, 191, 203] instabilities, laser-plasma absorption [190], wave damping [148], energy redistribution [180] inside the plasma and hot spots formation [33, 170] from which the thermonuclear reactions propagates depend on the electron heat transport. The most popular electron heat transport theory was developed by Spitzer and Härm [194] who first solved the electron kinetic equation by using the expansion of the electron mean free path to the temperature scale length (denoted ε in this work). Considering the distribution function of particles close to equilibrium, its deviation from the Maxwellian distribution function can be computed and the electron transport coefficients in a fully ionised plasma without magnetic field are derived. However, even if the electron heat transport is essential, it is not correctly described in large inertial confinement fusion tools. Indeed, when the electron mean free path exceeds about 2.10^{-3} times the temperature gradient length, the local electron transport model of Spitzer and Härm fails. The transport coefficients were derived in the case where the isotropic part of the electron distribution function remains close to the Maxwellian function. The results of Spitzer and Härm have been reproduced in several approaches [9, 32, 192] which develop another technique of solution to the integral equation for the electron distribution function introduced many years before by Chapman and Enskog [56] for neutral gases. Therefore, kinetic approaches seem

necessary in the context of inertial confinement fusion. In such multiscale issues, kinetic solvers are often very computationally expensive and usually limited to time and length much shorter than those studied with hydrodynamic simulations. It is then a challenge to describe kinetic effects using reduced kinetic code on fluid time scales.

In chapter 2, it has been seen that the angular moments models represent an alternative method situated between kinetic and fluid models. The M_1 model is largely used in various applications such as the radiative transfer [20, 57, 84, 186, 187, 201, 202] or electronic transport [83, 166]. The M_1 model is known to satisfy fundamental properties such as the positivity of the first angular moment, the flux limitation and conservation of total energy. Also, it correctly recovers the asymptotic diffusion equation in the limit of long time behaviour with important collisions [85]. One challenging issue is to derive numerical schemes satisfying fundamental properties. For example, the classical HLL scheme [118] ensures the positivity of the first angular moment and the flux limitation property. However, this scheme fails in recovering the correct limit diffusion equation in the asymptotic regime [7]. As explained in chapter 4, overcoming this major drawback a class of numerical schemes has emerged over the years called asymptotic-preserving schemes (AP). Asymptotic-preserving schemes in the sense of Jin-Levermore [128, 129] are designed to handle multi-scale situations and behave correctly in the asymptotic limit considered. In this context many works have been performed following different approaches in a one dimensional framework [6, 27, 30, 80, 92, 147, 155]. In particular, one of the most productive approach from the work of Gosse-Toscani [107] and which has been largely extended [20, 22, 38, 44, 53], is based on the modification of approximate Riemann solvers. Some works also deal with the two dimensional case [21, 45, 46]. In [20], an HLLC scheme is proposed to solve the M_1 model of radiative transfer in two space dimensions. The HLLC approximate Riemann solver is considered and a relevant numerical approximations of the extreme wavespeeds give the asymptotic-preserving property. Close ideas were also developed in [19], where a relaxation scheme is exhibited. In order to derive suitable schemes pertinent for transport and diffusion regimes, it was proposed to use the modified Godunov-type schemes in order to include sources terms [110]. The numerical viscosity is modified in [43, 44, 106, 107] to correctly recover the expected diffusion regimes but extensions seem to be challenging. In [22], the approximate HLL Riemann solver is modified to include collisional source term. The resulting numerical scheme satisfies all the fundamental properties and a clever correction enables to recover the good diffusion equation in the asymptotic limit.

In this work, we consider the M_1 model for the electron transport [83, 166, 167] in a Lorentzian plasma where ions are fixed. Omitting the x and t dependency, the first three angular moments f_0, f_1 and f_2 of the electron distribution function f are

defined by

$$f_0(\zeta) = \zeta^2 \int_{-1}^{1} f(\mu,\zeta)d\mu, \;\; f_1(\zeta) = \zeta^2 \int_{-1}^{1} f(\mu,\zeta)\mu d\mu, \;\; f_2(\zeta) = \zeta^2 \int_{-1}^{-1} f(\mu,\zeta)\mu^2 d\mu. \tag{6.1}$$

The moment system studied writes

$$\begin{cases} \partial_t f_0(t,x,\zeta) + \zeta \partial_x f_1(t,x,\zeta) + E(x)\partial_\zeta f_1(t,x,\zeta) = 0, \\ \partial_t f_1(t,x,\zeta) + \zeta \partial_x f_2(t,x,\zeta) + E(x)\partial_\zeta f_2(t,x,\zeta) \\ \qquad\qquad - \dfrac{E(x)}{\zeta}(f_0(t,x,\zeta) - f_2(t,x,\zeta)) = -\dfrac{2\alpha_{ei}(x) f_1(t,x,\zeta)}{\zeta^3}, \end{cases} \tag{6.2}$$

The coefficient α_{ei} is a positive function which may depend of x, E represents the electrostatic field as function of x and ζ is the velocity modulus. The fundamental point of the moments models is the definition of the closure which writes the highest moment as a function of the lower ones. This closure relation corresponds to an approximation of the underlying distribution function, which the moments system is constructed from. In the M_1 problem we need to define f_2 as a function of f_0 and f_1. As explained in chapter 2, the closure relation originates from an entropy minimisation principle [160, 175] and the moment f_2 can be computed [83, 84] as a function of f_0 and f_1

$$f_2(t,x,\zeta) = \chi\Big(\frac{f_1(t,x,\zeta)}{f_0(t,x,\zeta)}\Big) f_0(t,x,\zeta), \quad \text{with} \quad \chi(\alpha) \approx \frac{1+\alpha^2+\alpha^4}{3}. \tag{6.3}$$

The set of admissible states [83] is defined by

$$\mathcal{A} = \Big((f_0,f_1) \in \mathbb{R}^2, \;\; f_0 \geq 0, \;\; |f_1| \leq f_0\Big). \tag{6.4}$$

A challenging issue is to derive a numerical scheme for the electron M_1 model (6.2) satisfying all the fundamental properties and which handles correctly the diffusive limit recovering the good diffusion equation. Such a scheme could then have a direct access to all the nonlocal regimes and their related physical effects described above while the others numerical schemes fail in such regimes. Complications arise when considering such an issue. Firstly, the electron M_1 model (6.2) is nonlinear. Because, of the entropic closure, the angular moment f_2 is a nonlinear function of f_0 and f_1. Secondly, the approach undertaken must be sufficiently general to correctly take into account the source term $-E(x)(f_0(t,x,\zeta) - f_2(t,x,\zeta))/\zeta$. One must notice, that this term is closely related to the term $E\partial_\zeta f_2(t,x,\zeta)$, it plays an important role for low energies and cannot be treated as a collisional source term. Thirdly, for the purpose of realistic physical applications, one may require to correctly capture stationary states. In the case of near-equilibrium configurations a well-balancing property is then desired. Also, the physical parameter α_{ei} is a function of x and cannot be treated as a constant. Finally, the space and velocity modulus dependence of the

angular moments, leads to a very complex diffusion equation in the asymptotic limit with mixed derivatives.

In the first part of this chapter, the case without electric field and the homogeneous case with electric field are studied. The generalisation to the general problem requires a deep understanding of the two configurations studied here. An extension to the general model is proposed in a second part. The approach retained is noticeably different with [19, 20, 118]. The derivation of the numerical scheme is based on an approximate Riemann solver where the intermediate states are chosen consistent with the integral form of the approximate Riemann solver. This choice can be modified to enable the derivation of a scheme which also satisfies the admissibility conditions (6.4) and is well-suited for capturing stationary states. Moreover, it enjoys asymptotic-preserving properties and correctly handles the diffusive limit recovering the good diffusion equation.

In the first part of this work we introduce the M_1 model without electrostatic field and a homogeneous case with electric field. The classical HLL scheme [118] in the diffusive limit is briefly recalled before introducing the new numerical scheme. The asymptotic-preserving property is exhibited. In Section 6.3 for the homogeneous case with electric field, we point out difficulties encountered when using a relaxation approach in order to include the source term $-E(x)(f_0(t,x,\zeta)-f_2(t,x,\zeta))/\zeta$. Then, the derivation of an asymptotic-preserving scheme following the method introduced in the previous section is detailed and the well-balanced and asymptotic-preserving properties are analysed. In Section 6.4, different numerical tests are presented to highlight the efficiency of the present method.

The second part is extending these ideas and introduce a numerical scheme for the general electronic M_1 model. In section 6.6, the scheme is modified to ensure the admissibility conditions (6.4) and to capture the non isotropic diffusion then the asymptotic-preserving property is exhibited. The term $-E(x)(f_0 - f_2)/\zeta$ is finally included in the scheme. In Section 6.7, numerical examples are presented to demonstrate of the efficiency of the method. A conclusion is given in Section 6.8.

6.2 Case without electrostatic field

The first simplified case we consider is given by system (6.2) without electrostatic field E. In this case the M_1 model (6.2) writes

$$\begin{cases} \partial_t f_0 + \zeta \partial_x f_1 = 0, \\ \partial_t f_1 + \zeta \partial_x f_2 = -\dfrac{2\alpha_{ei}}{\zeta^3} f_1. \end{cases} \tag{6.5}$$

A very similar system was considered in [19] in the frame of radiative transfer and a relaxation scheme was proposed. The same procedure could be applied in this case, however we introduce a different approach based on approximate Riemann solvers.

6.2.1 Model and diffusive limit

We consider the following diffusion scaling

$$\tilde{t} = t/t^*, \quad \tilde{x} = x/x^*, \quad \tilde{\zeta} = \zeta/v_{th}, \quad \tilde{E} = Ex^*/v_{th}. \tag{6.6}$$

The parameters t^* and x^* are chosen such that $\tau_{ei}/t^* = \varepsilon^2$, $\lambda_{ei}/x^* = \varepsilon$, where τ_{ei} is the electron-ion collisional period , λ_{ei} the electron-ion mean free path and v_{th} the thermal velocity defined by $v_{th} = \lambda_{ei}/\tau_{ei}$. The positive parameter ε is devoted to tend to zero. In that case, omitting the tilde notation, system (6.5) rewrites

$$\begin{cases} \varepsilon \partial_t f_0^\varepsilon + \zeta \partial_x f_1^\varepsilon = 0, \\ \varepsilon \partial_t f_1^\varepsilon + \zeta \partial_x f_2^\varepsilon = -\dfrac{2\sigma}{\zeta^3} \dfrac{f_1^\varepsilon}{\varepsilon}, \end{cases} \tag{6.7}$$

where the coefficient σ represents a positive function of x defined as

$$\sigma(x) = \frac{\tau_{ei}\alpha_{ei}(x)}{v_{th}^3}.$$

Inserting the following Hilbert expansion of f_0^ε and f_1^ε

$$\begin{cases} f_0^\varepsilon = f_0^0 + \varepsilon f_0^1 + O(\varepsilon^2), \\ f_1^\varepsilon = f_1^0 + \varepsilon f_1^1 + O(\varepsilon^2), \end{cases} \tag{6.8}$$

into the second equation of (6.7) leads to

$$f_1^0 = 0. \tag{6.9}$$

Using the definition (6.3), it follows that

$$f_2^0 = f_0^0/3.$$

So, the second equation of (6.7) gives

$$f_1^1 = -\frac{\zeta^4}{6\sigma} \partial_x f_0^0. \tag{6.10}$$

Using the previous equation and the first equation of (6.7) finally leads to the diffusion equation for f_0^0

$$\partial_t f_0^0(t,x) - \partial_x \Big(\frac{\zeta^5}{6\sigma(x)} \partial_x f_0^0(t,x) \Big) = 0. \tag{6.11}$$

Here we have omitted the tilde notation, writing this diffusion equation in non-rescaled (dimensional) variables we obtain

$$\partial_t f_0^0(t,x) - \partial_x \Big(\frac{\zeta^5}{6\alpha_{ei}(x)} \partial_x f_0^0(t,x) \Big) = 0. \tag{6.12}$$

6.2.2 Numerical method

In this part, we first recall the limit of the HLL scheme, usually used for the electronic M_1 model, for the diffusive limit.

Limit of the HLL scheme

Introduce a uniform mesh with constant space step $\Delta x = x_{i+1/2} - x_{i-1/2},\ i \in Z$ and a time step Δt. We consider a piecewise constant approximate solution $U^h(x,t^n) \in \mathbb{R}^2$ at time t^n

$$U^h(x,t^n) = U_i^n \ \text{ if } \ x \in [x_{i-1/2}, x_{i+1/2}],$$

with $U_i^n = {}^t(f_{0i}^n, f_{1i}^n)$.
The classical HLL scheme [118] for the system (6.11), in the case where the minimum and maximum velocity waves involved in the approximate Riemann solver are chosen equal to $-\zeta$ and ζ, writes

$$\begin{cases} \varepsilon \dfrac{f_{0i}^{n+1,\varepsilon} - f_{0i}^{n,\varepsilon}}{\Delta t} + \zeta \dfrac{f_{1i+1}^{n,\varepsilon} - f_{1i-1}^{n,\varepsilon}}{2\Delta x} - \zeta \Delta x \dfrac{f_{0i+1}^{n,\varepsilon} - 2f_{0i}^{n,\varepsilon} + f_{0i-1}^{n,\varepsilon}}{2\Delta x^2} = 0, \\ \varepsilon \dfrac{f_{1i}^{n+1,\varepsilon} - f_{1i}^{n,\varepsilon}}{\Delta t} + \zeta \dfrac{f_{2i+1}^{n,\varepsilon} - f_{2i-1}^{n,\varepsilon}}{2\Delta x} - \zeta \Delta x \dfrac{f_{1i+1}^{n,\varepsilon} - 2f_{1i}^{n,\varepsilon} + f_{1i-1}^{n,\varepsilon}}{2\Delta x^2} = -\dfrac{2\sigma_i}{\zeta^3} \dfrac{f_{1i}^{n,\varepsilon}}{\varepsilon}. \end{cases} \tag{6.13}$$

We introduce the discrete Hilbert expansions

$$\begin{cases} f_{0i}^{\varepsilon} = f_{0i}^{n,0} + \varepsilon f_{0i}^{n,1} + O(\varepsilon^2), \\ f_{1i}^{n,\varepsilon} = f_{1i}^{n,0} + \varepsilon f_{1i}^{n,1} + O(\varepsilon^2). \end{cases} \tag{6.14}$$

At the order ε^{-1}, the second equation of (6.13) gives

$$f_{1i}^{n,0} = 0,$$

and using the definition (6.3), it follows that

$$f_{2i}^{n,0} = f_{0i}^{n,0}/3.$$

At the order ε^0, the second equation of (6.13) gives

$$f_{1i}^{n,1} = -\frac{\zeta^3}{3\sigma_i} \frac{f_{0i+1}^{n,0} - f_{0i-1}^{n,0}}{2\Delta x}.$$

However, because of the diffusive part of the HLL scheme, the first equation of (6.13) also leads to

$$\frac{f_{0i+1}^{n,0} - 2f_{0i}^{n,0} + f_{0i-1}^{n,0}}{\Delta x^2} = 0,$$

which is not the diffusion equation expected for f_0^0. The diffusive part of the HLL scheme gives an unphysical numerical viscosity and leads to the wrong asymptotic behaviour.

Derivation of the scheme

The ideas introduced in [19, 22, 28, 110] in order to include the contribution of source terms, urge to consider approximate Riemann solvers which own a stationary discontinuity (0-contact discontinuity). Therefore, we introduce the following approximate Riemann solvers at each cell interface, denoted by $U_{\mathcal{R}}(x/t, U^L, U^R)$, defined by

$$U_{\mathcal{R}}(x/t, U^L, U^R) = \begin{cases} U^L & if \;\; x/t < -a_x, \\ U^{L*} & if \;\; -a_x < x/t < 0, \\ U^{R*} & if \;\; 0 < x/t < a_x, \\ U^R & if \;\; a_x < x/t, \end{cases} \tag{6.15}$$

where $U^{L*} = {}^t(f_0^{L*}, f_1^*)$, $U^{R*} = {}^t(f_0^{R*}, f_1^*)$ and the minimum and maximum velocity waves $-a_x$ and a_x. Note, we choose the two velocity waves to be opposite. The structure solution of the approximate Riemann problem is displayed in Figure 6.1. At the interface $x_{i+\frac{1}{2}}$, the quantities U^L and U^R stand for $U_i = {}^t(f_{0i}, f_{1i})$ and $U_{i+1} = {}^t(f_{0i+1}, f_{1i+1})$. Contrarily to the classical HLL scheme [199] two intermediate states U^{L*} and U^{R*} are introduced. The second components of the two intermediate states are chosen equal, ie $f_1^{L*} = f_1^{R*} = f_1^*$. The approximate solution at time

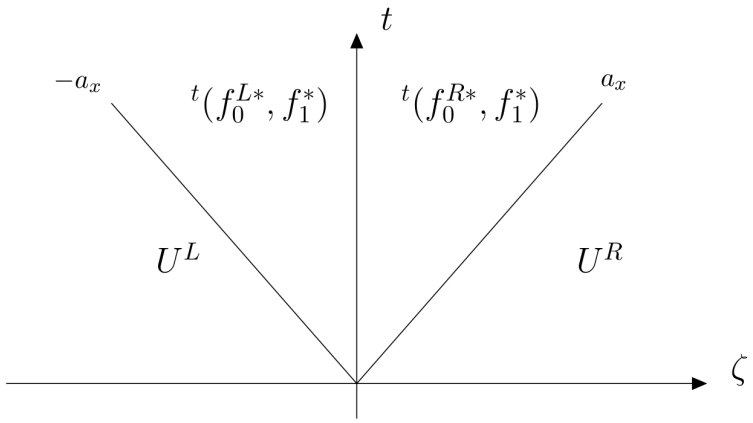

Figure 6.1: Structure solution of the approximate Riemann problem.

$t^n + \Delta t$ is chosen as

$$U^h(x, t^n + \Delta t) = U_{\mathcal{R}}\Big(\frac{x - x_{i+1/2}}{t^n + \Delta t}, U_i, U_{i+1}\Big) \;\text{ if }\; x \in [x_i, x_{i+1}].$$

As the following CFL condition is respected

$$\Delta t \leq \frac{\Delta x}{2a_x},$$

the piecewise constant approximate solution is then obtained

$$U_i^{n+1} = \frac{1}{\Delta x}\int_{x_{i-1/2}}^{x_{i+1/2}} U^h(x, t^{n+1})dx. \tag{6.16}$$

The intermediate states f_0^{L*}, f_0^{R*} and f_1^* must be defined. Integrating the first equation of (6.5) on $[-a_x\Delta t, a_x\Delta t]\times[0,\Delta t]$ and multiplying by $\frac{1}{2a_x\Delta t}$, gives the following consistency condition

$$\frac{f_0^{L*}+f_0^{R*}}{2} = \frac{f_0^L+f_0^R}{2} - \frac{1}{2a_x}[\zeta f_1^R - \zeta f_1^L]. \tag{6.17}$$

The unknowns f_0^{L*} and f_0^{R*} will be chosen in order to satisfy this consistency condition (6.17). The same procedure using the second equation of (6.5) gives

$$f_1^* = \frac{f_1^L+f_1^R}{2} - \frac{1}{2a_x}(\zeta f_2^R - \zeta f_2^L) - \frac{2}{\zeta^3}\frac{1}{2a_x\Delta t}\int_{-a_x\Delta t}^{a_x\Delta t}\int_0^{\Delta t}\alpha_{ei}(x)f_1(x,t)dtdx. \tag{6.18}$$

The following approximation is made

$$\frac{1}{2a_x\Delta t}\int_{-a_x\Delta t}^{a_x\Delta t}\int_0^{\Delta t}\alpha_{ei}(x)f_1(x,t)dtdx = \bar{\alpha}_{ei}\Delta t f_1^*, \tag{6.19}$$

with $\bar{\alpha}_{ei} = \alpha(0)$. Using (6.19) in (6.18), it follows that

$$f_1^* = \frac{\zeta^3}{\zeta^3 + 2\bar{\alpha}_{ei}\Delta t}\Big[\frac{f_1^L+f_1^R}{2} - \frac{1}{2a_x}(\zeta f_2^R - \zeta f_2^L)\Big].$$

Finally the following definition of f_1^* is chosen

$$f_1^* = \frac{2a_x\zeta^3}{2a_x\zeta^3 + 2\bar{\alpha}_{ei}\Delta x}\Big[\frac{f_1^L+f_1^R}{2} - \frac{1}{2a_x}(\zeta f_2^R - \zeta f_2^L)\Big]. \tag{6.20}$$

It will be shown in the next part, that this choice enables to obtain the good asymptotic-preserving property. Also, this definition recovers the formalism introduced in [20, 22]. In order to respect the consistency relation (6.17), the unknowns f_0^{L*} and f_0^{R*} are defined by

$$\begin{cases} f_0^{L*} = \tilde{f}_0 - \Gamma, \\ f_0^{R*} = \tilde{f}_0 + \Gamma, \end{cases}$$

with

$$\tilde{f}_0 = \frac{f_0^L+f_0^R}{2} - \frac{1}{2a_x}(\zeta f_1^R - \zeta f_1^L),$$

and the coefficient Γ is calculated using the classical Rankine-Hugoniot conditions

$$\begin{cases} f_0^{L*} = f_0^L - \dfrac{\zeta}{a_x}(f_1^* - f_1^L), \\ f_0^{R*} = f_0^R - \dfrac{\zeta}{a_x}(f_1^R - f_1^*). \end{cases} \tag{6.21}$$

It follows that

$$\Gamma = \frac{1}{2}[f_0^R - f_0^L - \frac{\zeta}{a_x}(f_1^L - 2f_1^* + f_1^R)]. \tag{6.22}$$

In order to satisfy the admissibility conditions (6.4), we propose to modify the states f_0^{L*} and f_0^{R*} such that

$$\begin{cases} f_0^{L*} = \tilde{f}_0 - \Gamma\theta, \\ f_0^{R*} = \tilde{f}_0 + \Gamma\theta, \end{cases} \tag{6.23}$$

where $\theta \in [0,1]$ is fixed to ensure the admissibility conditions.

Remark 6.1. *In the case $\theta = 0$, the admissibility requirements (6.4) are fulfilled.*

Indeed, in this case system (6.23) gives $f_0^{R*} = f_0^{L*} = \tilde{f}_0$ and f_1^* is given by (6.20). Since $2a_x\zeta^3/(2a_x\zeta^3 + \sigma\Delta x) \leq 1$ it follows that $f_1^* \leq f_0^{R*} = f_0^{L*}$. Then the parameter θ is computed as the largest possible such that

$$\begin{cases} f_0^{R*} - |f_1^*| \geq 0, \\ f_0^{L*} - |f_1^*| \geq 0, \\ f_0^{R*} \geq 0 \text{ and } f_0^{L*} \geq 0. \end{cases} \tag{6.24}$$

Equations (6.22), (6.23) and (6.24) lead to the following condition

$$\tilde{\theta} = \frac{\tilde{f}_0 - |f_1^*|}{|\Gamma|} \geq 0. \tag{6.25}$$

Finally, θ is chosen as $\theta = \min(\tilde{\theta}, 1)$.
Therefore the unknowns f_{0i}^{n+1} and f_{1i}^{n+1} are computed using (6.16)

$$\begin{cases} f_{0i}^{n+1} = \dfrac{a_x\Delta t}{\Delta x} f_{0i-1/2}^{R*} + (1 - \dfrac{2a_x\Delta t}{\Delta x}) f_{0i}^n + \dfrac{a_x\Delta t}{\Delta x} f_{0i+1/2}^{L*}, \\ f_{1i}^{n+1} = \dfrac{a_x\Delta t}{\Delta x} f_{1i-1/2}^{*} + (1 - \dfrac{2a_x\Delta t}{\Delta x}) f_{1i}^n + \dfrac{a_x\Delta t}{\Delta x} f_{1i+1/2}^{*}. \end{cases} \tag{6.26}$$

The wavespeed a_x is fixed using the ideas introduced in [19]. It is known that the electronic M_1 model without electric field is hyperbolic symmetrizable [160] and the eigenvalues of the Jacobian matrix always belong in the interval $[-\zeta, \zeta]$. Therefore, we set $a_x = \zeta$.

6.2.3 Asymptotic-preserving properties

In this part we prove the asymptotic-preserving property of the scheme (6.20)-(6.23)-(6.26). It is shown that when ε tends to zero, the scheme (6.20)-(6.23)-(6.26) is consistent with the limit diffusion equation (6.11).

Theorem 6.2. *When ε tends to zero, the unknown $f_{0i}^{n+1,0}$ given by the numerical scheme (6.26)-(6.23)-(6.20) satisfies the following discrete equation*

$$\frac{f_{0i}^{n+1,0}-f_{0i}^{n,0}}{\Delta t}-\frac{\zeta}{\Delta x}\Big[\frac{\zeta^3}{6\bar{\sigma}_{i+1/2}\Delta x}\Big[(\zeta f_{0i+1}^{n,0}-\zeta f_{0i}^{n,0})\Big]-\frac{\zeta^3}{6\bar{\sigma}_{i-1/2}\Delta x}\Big[(\zeta f_{0i}^{n,0}-\zeta f_{0i-1}^{n,0})\Big]\Big]=0. \tag{6.27}$$

Proof. Following the same approach as in [20, 22], using the diffusive scaling and equation (6.26) leads to

$$\begin{cases} \varepsilon\dfrac{f_{0i}^{n+1}-f_{0i}^{n}}{\Delta t}=\dfrac{a_x}{\Delta x}f_{0i+1/2}^{L*}-\dfrac{2a_x}{\Delta x}f_{0i}^{n}+\dfrac{a_x}{\Delta x}f_{0i-1/2}^{R*}, \\ \varepsilon\dfrac{f_{1i}^{n+1}-f_{1i}^{n}}{\Delta t}=\dfrac{a_x}{\Delta x}f_{1i+1/2}^{*}-\dfrac{2a_x}{\Delta x}f_{1i}^{n}+\dfrac{a_x}{\Delta x}f_{1i-1/2}^{*}, \end{cases} \tag{6.28}$$

where the intermediate states f_0^{L*} and f_0^{R*} are given by (6.23) and (6.20) rewrites

$$f_1^*=\frac{2a_x\zeta^3}{2a_x\zeta^3+2\bar{\sigma}\Delta x/\varepsilon}\Big[\frac{f_1^L+f_1^R}{2}-\frac{1}{2a_x}(\zeta f_2^R-\zeta f_2^L)\Big]. \tag{6.29}$$

As soon as ε tends to zero, we obtain $f_1^*=0$. We now suppose that $f_{1i}^n=0$ in the limit ε tends to zero. In this case, the definition (6.25) leads to

$$\tilde{\theta}=\frac{f_0^L+f_0^R}{|f_0^L-f_0^R|}\geq 1.$$

Then the parameter θ is equal to 1.

Remark 6.3. *In the diffusive regime when ε tends to zero, no limitation on the intermediates states (6.23) is required.*

Using the definition (6.23), it follows that the intermediate states f_0^{L*} and f_0^{R*} are given by

$$\begin{cases} f_0^{L*}=f_0^L-\dfrac{\zeta}{a_x}(f_1^*-f_1^L), \\ f_0^{R*}=f_0^R-\dfrac{\zeta}{a_x}(f_1^R-f_1^*). \end{cases} \tag{6.30}$$

The discrete Hilbert expansions (6.14) are now used. Inserting the previous expressions in the first equation of (6.28), considered at the order ε^0, gives no information since the terms cancel each other out. However, at the order ε^1, the expressions (6.30), (6.29) and the first equation of (6.28) lead to

$$\begin{cases} f_0^{L*,1}=f_0^{L,1}-\dfrac{\zeta}{a_x}(f_1^{*,1}-f_1^{L,1}), \\ f_0^{R*,1}=f_0^{R,1}-\dfrac{\zeta}{a_x}(f_1^{R,1}-f_1^{*,1}), \end{cases} \tag{6.31}$$

with

$$f_1^{*,1} = -\frac{\zeta^3}{6\bar{\sigma}\Delta x}\Big(\zeta f_0^{R,n,0} - \zeta f_0^{L,n,0}\Big), \tag{6.32}$$

and

$$\frac{f_{0i}^{n+1,0} - f_{0i}^{n,0}}{\Delta t} = \frac{a_x}{\Delta x} f_{0i+1/2}^{*,1} - \frac{2a_x}{\Delta x} f_{0i}^{n,1} + \frac{a_x}{\Delta x} f_{0i-1/2}^{*,1}. \tag{6.33}$$

Inserting expressions (6.31) into (6.33) leads to equation (6.27) which is consistent with the limit diffusion equation (6.11).
To complete the proof, it is necessary to show that f_1^n tends to zero, when ε tends to zero. Equation (6.16) gives

$$\Delta x U_i^{n+1} = \int_{x_{i-1/2}}^{x_i} U_{\mathcal{R}} dx + \int_{x_i}^{x_{i+1/2}} U_{\mathcal{R}} dx,$$

where $U_{\mathcal{R}}$ is computed with the approximate Riemann problem (6.15). Then

$$\int_{x_{i-1/2}}^{x_i} f_1(x, \Delta t) dx = a_x \Delta t f_{1i-1/2}^* + (\frac{\Delta x}{2} - a_x \Delta t) f_{1i}^n,$$

and

$$\int_{x_i}^{x_{i+1/2}} f_1(x, \Delta t) dx = (\frac{\Delta x}{2} - a_x \Delta t) f_{1i}^n + a_x \Delta t f_{1i+1/2}^*.$$

A long but classical calculation [22] leads to

$$\begin{aligned} &\frac{f_{1i}^{n+1} - f_{1i}^n}{\Delta t} + \frac{1}{\Delta x}\Big[\frac{2a_x}{2a_x + \bar{\sigma}_{i+1/2}\Delta x}\mathcal{F}_{i+1/2} - \frac{2a_x}{2a_x + \bar{\sigma}_{i-1/2}\Delta x}\mathcal{F}_{i-1/2}\Big] \\ &\quad + \frac{1}{\Delta x}\Big[\frac{\Delta x \bar{\sigma}_{i+1/2}}{2a_x + \bar{\sigma}_{i+1/2}\Delta x}(-a_x f_{1i}^n - \zeta f_{2i}^n) + \frac{\Delta x \bar{\sigma}_{i-1/2}}{2a_x + \bar{\sigma}_{i-1/2}\Delta x}(-a_x f_{1i}^n + \zeta f_{2i}^n)\Big] = 0, \end{aligned} \tag{6.34}$$

with

$$\mathcal{F}_{i+1/2} = \frac{1}{2}\Big[\zeta f_{2i+1}^n + \zeta f_{2i}^n - a_x(f_{1i+1}^n + f_{1i}^n)\Big].$$

Using the diffusive scaling we obtain that f_{1i}^n tends to zero when ε tends to zero. □

6.2.4 Stability property

The asymptotic-preserving property requires that the scheme should be uniformly stable with respect to the small parameter ε. In the case of an uniform stable scheme the CFL stability condition in diffusive regime should be that of a diffusion scheme $\Delta t \leq 3\alpha_{ei}\Delta x^2/\zeta^5$ (see Eq. 6.12). Also, in the case of a small collisional parameter α_{ei}, the time step should be chosen according to the hyperbolic CFL condition $\Delta t \leq \Delta x/\zeta$. An uniform stability property is proved in [141] or [164] in the framework of linear scalar equations. However, the model considered in this

work is a nonlinear system and the derivation of such a property is very challenging. Therefore, for the numerical test cases we consider the CFL condition

$$\Delta t \leq \max(\Delta x/a_x, 3\alpha_{ei}\Delta x^2/\zeta^5). \tag{6.35}$$

In practice, it has been observed that in the case of a very large collisional parameter α_{ei} the CFL stability condition is that of a diffusion scheme $\Delta t \leq 3\alpha_{ei}\Delta x^2/\zeta^5$ and the proposed AP scheme is not stable. More precisely, in a very diffusive regime when considering a parabolic CFL condition, it is observed that the quantity f_{1i}^n does not behave in $O(\varepsilon)$ in the long time regime as expected (see condition Eq. 6.9). To overcome this drawback, instead of using the second equation of (6.26), we propose to consider the classical following scheme to compute f_{1i}^n at each time step

$$\frac{f_{1i}^{n+1}-f_{1i}^n}{\Delta t}+\zeta\frac{f_{2i+1}^n-f_{2i-1}^n}{2\Delta x}-a_x\frac{f_{1i+1}^n-2f_{1i}^n+f_{1i-1}^n}{2\Delta x}=-\frac{2\alpha_{ei}}{\zeta^3}f_{1i}^{n+1}.$$

This scheme rewrites

$$f_{1i}^{n+1}=\frac{\zeta^3}{\zeta^3+2\alpha_{ei}\Delta t}\Big[f_{1i}^n-\Delta t\Big(\zeta\frac{f_{2i+1}^n-f_{2i-1}^n}{2\Delta x}-a_x\frac{f_{1i+1}^n-2f_{1i}^n+f_{1i-1}^n}{2\Delta x}\Big)\Big]. \tag{6.36}$$

Obviously this scheme is consistent with the second equation of (6.5) and captures the correct asymptotic limits (6.9) and (6.10). Here, it is important to notice that we still consider the first equation of (6.26) with the definitions (6.23)-(6.22)-(6.25) to compute f_{0i}^n at each time step. This choice enables to correctly capture the asymptotic limit and the use of the parabolic CFL condition in the diffusive regime. In addition, the numerical solution needs to satisfy the admissibility requirements (6.4). Indeed, the correction parameter θ defined in (6.25) was proposed considering the second equation of (6.26) which is now replaced by (6.36). However, it can be shown that the condition (6.25) also enables the admissibility of the numerical solution using (6.36).

Proposition 6.4. *The numerical scheme (6.22)-(6.23)-(6.25)-(6.26)-(6.36) preserves the admissibility of the numerical solutions.*

Proof. We remark that equation (6.36) rewrites

$$f_{1i}^{n+1}=\alpha\frac{a_x\Delta t}{\Delta x}\tilde{f}_{1i-1/2}+\alpha(1-\frac{2a_x\Delta t}{\Delta x})f_{1i}^n+\alpha\frac{a_x\Delta t}{\Delta x}\tilde{f}_{1i+1/2}, \tag{6.37}$$

with $\alpha=\zeta^3/(\zeta^3+2\alpha_{ei}\Delta t)\in[0,1]$ and

$$\tilde{f}_{1i+1/2}=\frac{f_{1i}^n+f_{1i+1}^n}{2}-\frac{1}{2a_x}(\zeta f_{2i+1}^n-\zeta f_{2i}^n).$$

Using the first equation of (6.26) and (6.37) a direct calculation shows that the condition (6.25) ensure the admissibility of the numerical solution. Also, it can be seen geometrically since the admissible set is a convex cone and α belongs to $[0,1]$. □

6.3 Homogeneous case with electric field

The second simplified model studied, is given by (6.2) which is homogeneous in space but considering an electric field. In this section, the difficulties encountered when using a relaxation-type method to include the source term $-\frac{E}{\zeta}(f_0 - f_2)$ are highlighted. Following the same procedure as in the case without electric field, a numerical scheme is proposed and the source term $-\frac{E}{\zeta}(f_0 - f_2)$ is taken into account. The scheme presented, satisfies a well-balanced property and is asymptotic-preserving. The collision coefficient α_{ei} is a function of x and is then constant in the present case. However, the method proposed here, is able to handle the case where α_{ei} depends on ζ. Without spatial dependence, the model (6.2) simplifies into

$$\begin{cases} \partial_t f_0 + E\partial_\zeta f_1 = 0, \\ \partial_t f_1 + E\partial_\zeta f_2 - \dfrac{E}{\zeta}(f_0 - f_2) = -\dfrac{2\alpha_{ei} f_1}{\zeta^3}. \end{cases} \tag{6.38}$$

Using the Hilbert expansions (6.8) as in the previous case, the following diffusion equation is obtained

$$\partial_t f_0^0(t,\zeta) - E\partial_\zeta\Big(\frac{E\zeta^3}{6\alpha_{ei}}\partial_\zeta f_0^0(t,\zeta) - \frac{E\zeta^2}{3\alpha_{ei}} f_0^0(t,\zeta)\Big) = 0. \tag{6.39}$$

6.3.1 Limit of the relaxation approach

Using the ideas introduced in [19], one can think of deriving a relaxation scheme for system (6.38). Even if the approach is similar, the relaxation scheme involved would be significantly different from the one proposed in [19] since the source term $-\frac{E}{\zeta}(f_0 - f_2)$ should be added. To assess such an issue, we first consider the collisionless case

$$\begin{cases} \partial_t f_0 + E\partial_\zeta f_1 = 0, \\ \partial_t f_1 + E\partial_\zeta f_2 - \dfrac{E}{\zeta}(f_0 - f_2) = 0. \end{cases} \tag{6.40}$$

Setting $\partial_\zeta z(\zeta) = 1/\zeta$, we propose the following relaxation model

$$\begin{cases} \partial_t f_0 + E\partial_\zeta \phi - E(f_1 - \phi)z'(\zeta) = 0, \\ \partial_t \phi + E\partial_\zeta f_0 - 2Ef_0 z'(\zeta) = \mu(f_1 - \phi), \\ \partial_t f_1 + E\partial_\zeta \pi - E(f_0 - \pi)z'(\zeta) = 0, \\ \partial_t \pi + E\partial_\zeta f_1 - 2Ef_1 z'(\zeta) = \mu(f_2 - \pi), \\ \partial_t z = 0, \end{cases} \tag{6.41}$$

where ϕ and π are relaxation variables. In the case $\mu = 0$, the previous system is hyperbolic, the eigenvalues are $-E$, 0, E and are associated with linearly degenerate fields. Hence, the Riemann problem can be solved.

Eigenvalue	Multiplicity	Riemann Invariants	Eigenvectors
E	2	$f_0+\phi,\ \ f_1+\pi,\ z$	${}^t(0,0,1,1,0),\ \ {}^t(1,1,0,0,0)$
$-E$	2	$-f_0+\phi,\ \ -f_1+\pi,\ z$	${}^t(0,0,-1,1,0),\ \ {}^t(-1,1,0,0,0)$
0	1	$\frac{f_1}{\zeta^2},\ \ \frac{f_0}{\zeta^2},\ \zeta(\pi-f_0/3),\ \zeta(\phi-f_1/3)$	${}^t(2f_0, f_1-\phi, 2f_1, f_0-\pi, 1)$

Table 6.1: Features of the Riemann problem

In order to be consistent with the notations [19], we introduce

$$w={}^t(f_0,\phi,f_1,\pi,z),\quad \mathcal{U}={}^t(f_0,f_1),\quad \mathcal{F}(\mathcal{U})={}^t\big(Ef_1,Ef_2(f_0,f_1)\big),$$

Lemme 6.5. *Let $w_{L,R}$ be equilibrium constant states with $\phi^{L,R}=f_1^{L,R}$ and $\pi^{L,R}=f_2^{L,R}$. Defining the initial condition of (6.41) by $w_0(x)=w_L$ if $x<0$ and $w_0(x)=w_R$ if $x>0$ for $\mu=0$, the solution of (6.41) writes*

$$w(x,t)=\begin{cases} w^L & if\ \ x/t<-E,\\ w^{L*} & if\ \ -E<x/t<0,\\ w^{R*} & if\ \ 0<x/t<E,\\ w^R & if\ \ E<x/t,\end{cases}\tag{6.42}$$

with

$$\begin{aligned} f_0^{L*,R*}=\frac{3(\zeta^{L,R})^2}{4(2(\zeta^R)^6+2(\zeta^L)^6+5(\zeta^R)^3(\zeta^L)^3)}\Big((-f_2^R-2f_1^R+3f_0^R)(\zeta^R)^4\\ +(-f_2^L+2f_1^L+3f_0^L)(\zeta^L)^4+(f_2^L+4f_1^L+3f_0^L)(\zeta^R)^3(\zeta^L)\\ +(f_2^R-4f_1^R+3f_0^R)(\zeta^R)(\zeta^L)^3\Big),\end{aligned}$$

$$\begin{aligned} f_1^{L*,R*}=\frac{3(\zeta^{L,R})^2}{4(2(\zeta^R)^6+2(\zeta^L)^6+5(\zeta^R)^3(\zeta^L)^3)}\Big((3f_2^R-2f_1^R-f_0^R)(\zeta^R)^4\\ +(-3f_2^L-2f_1^L+f_0^L)(\zeta^L)^4+(-3f_2^L-4f_1^L-f_0^L)(\zeta^R)^3(\zeta^L)\\ +(3f_2^R-4f_1^R+f_0^R)(\zeta^R)(\zeta^L)^3\Big),\end{aligned}$$

$$\begin{aligned} &z^{L*,R*}=z^{L,R},\\ &\phi^{L*}=f_0^L+f_1^L-f_0^{L*},\qquad \phi^{R*}=-f_0^R+f_1^R+f_0^{R*},\\ &\pi^{L*}=f_1^L+f_2^L-f_1^{L*},\qquad \pi^{R*}=-f_1^R+f_2^R+f_1^{R*},\end{aligned}$$

and $\mathcal{U}^{L*,R*}={}^t(f_0^{L*,R*},f_1^{L*,R*})$ satisfy the admissibility conditions (6.4).

The computation of the intermediate states $\mathcal{U}^{L*,R*}$ is straightforward using the Riemann invariants given in Table 6.1. A long but easy calculation, using the expressions gives the admissibility conditions (6.4).
The relaxation model (6.41) enables the computation of a numerical scheme [17, 28, 132] for the model (6.40). However, one notices the complexity of the intermediate states $\mathcal{U}^{L*,R*}$ and an extension including the collisional term $-2\alpha_{ei}f_1/\zeta^3$ is very challenging. Different relaxation models were tested in order to include the collisional source term, but, because of their complexity, they lead to configurations where a Riemann invariant is missing and the problem remains unclosed. In a recent work [79], the same issue is encountered and an additional relation is arbitrarily imposed. In the present situation, this strategy leads to particularly inconvenient solutions and the admissibility conditions are lost.

6.3.2 Numerical method

The numerical approach presented in the case without electric field is now considered. Contrarily to the relaxation-type procedure, this method enables to include the source term $-\frac{E}{\zeta}(f_0 - f_2)$ naturally.

Integrating the second equation of (6.38) by $\int_{-a_\zeta\Delta t}^{a_\zeta\Delta t}\int_0^{\Delta t}$ and multiplying by $\frac{1}{2a_\zeta\Delta t}$ gives the following expression

$$f_1^* = \frac{2a_\zeta\zeta^3}{2a_\zeta\zeta^3 + 2\alpha_{ei}\Delta\zeta}\Big[\frac{f_1^L + f_1^R}{2} - \frac{1}{2a_\zeta}(Ef_2^R - Ef_2^L) + \frac{\Delta\zeta}{2a_\zeta}S_{L,R}\Big], \tag{6.43}$$

with

$$S_{L,R} = \frac{1}{2}\Big[\frac{E}{\zeta_R}(f_0^R - f_2^R) + \frac{E}{\zeta_L}(f_0^L - f_2^L)\Big].$$

The unknowns f_0^{L*}, f_0^{R*}, f_0^{n+1} and f_1^{n+1} are computed following the same approach as in the first part

$$\begin{cases} f_{0i}^{n+1} = \dfrac{a_\zeta\Delta t}{\Delta\zeta}f_{0i-1/2}^{R*} + (1 - \dfrac{2a_\zeta\Delta t}{\Delta\zeta})f_{0i}^n + \dfrac{a_\zeta\Delta t}{\Delta\zeta}f_{0i+1/2}^{L*}, \\ f_{1i}^{n+1} = \dfrac{a_\zeta\Delta t}{\Delta\zeta}f_{1i-1/2}^{*} + (1 - \dfrac{2a_\zeta\Delta t}{\Delta\zeta})f_{1i}^n + \dfrac{a_\zeta\Delta t}{\Delta\zeta}f_{1i+1/2}^{*}, \end{cases} \tag{6.44}$$

where the unknowns f_0^{R*} and f_0^{L*} are given by

$$\begin{cases} f_0^{L*} = \tilde{f}_0 - \Gamma\theta, \\ f_0^{R*} = \tilde{f}_0 + \Gamma\theta, \end{cases} \tag{6.45}$$

with

$$\Gamma = \frac{1}{2}[f_0^R - f_0^L - \frac{\zeta}{a_\zeta}(f_1^L - 2f_1^* + f_1^R)],$$

and

$$\tilde{f}_0 = \frac{f_0^L + f_0^R}{2} - \frac{1}{2a_\zeta}[\zeta f_1^R - \zeta f_1^L].$$

Using, the same arguments as in the case without electric field, we set $a_\zeta = |E|$.

6.3.3 Properties

In this part, we are interested in the equilibrium solution of system (6.38). It is shown that the scheme (6.43)-(6.44)-(6.45) preserves this solution. Then, the asymptotic-preserving feature of the scheme is exhibited.

A stationary solution of system (6.38) satisfies

$$\begin{cases} E\dfrac{\partial f_1}{\partial \zeta} = 0, \\ E\dfrac{\partial f_2}{\partial \zeta} - \dfrac{E}{\zeta}(f_0 - f_2) = -\dfrac{2\alpha_{ei} f_1}{\zeta^3}. \end{cases} \tag{6.46}$$

The first equation of (6.46) implies that f_1 is independent of ζ. Using the definitions of the angular moments (2.1) and the definition (6.3), it follows that $f_1 = 0$ and $f_2 = f_0/3$. Indeed the definitions (2.1) imply $f_1 = 0$ in $\zeta = 0$. The second equation of the previous system is solved and gives the equilibrium solution of the model (6.38)

$$\begin{cases} f_0 = K\zeta^2, \\ f_1 = 0, \end{cases} \tag{6.47}$$

where K is a scalar constant.

Theorem 6.6. *The numerical scheme given by (6.43)-(6.44)-(6.45) is well-balanced in the sense that the stationary states (6.47) are exactly preserved by the scheme.*

Proof. Using the stationary states (6.47) into the definition (6.43) leads to

$$f_1^* = \frac{2a_\zeta \zeta^3}{a_\zeta \zeta^3 + 2\alpha_{ei}\Delta\zeta}\Big[-\frac{1}{3a_\zeta}(EK\zeta_R^2 - EK\zeta_L^2) + \frac{\Delta\zeta EK}{3a_\zeta}(\zeta_R + \zeta_L)\Big].$$

Since $(\zeta_R^2 - \zeta_L^2) = (\zeta_R + \zeta_L)(\zeta_R - \zeta_L) = (\zeta_R + \zeta_L)\Delta\zeta$, the calculation of the previous equation gives

$$f_1^* = 0.$$

Using the second equation of (6.44) leads to

$$f_1^{n+1} = 0.$$

With the definition (6.23) it follows that

$$\begin{cases} f_0^{R*} = \dfrac{1}{2}[f_{0L} - \theta f_{0L} + f_{0R} + \theta f_{0R}], \\ f_0^{L*} = \dfrac{1}{2}[f_{0R} - \theta f_{0R} + f_{0L} + \theta f_{0L}]. \end{cases} \tag{6.48}$$

The initial conditions (6.47) imply that $\theta = 1$ and inserting (6.48) into the first equation of (6.44) give

$$f_{0i}^{n+1} = \frac{a\Delta t}{\Delta\zeta} K\zeta_i^2 + (1 - \frac{2a\Delta t}{\Delta\zeta}) K\zeta_i^2 + \frac{a\Delta t}{\Delta\zeta} K\zeta_i^2.$$

Finally, the previous equation simplifies to give

$$f_{0i}^{n+1} = K\zeta_i^2.$$

The stationary solution (6.47) is then preserved by the scheme. □

Using the ideas introduced in the first section, we obtain that the scheme (6.43)-(6.44)-(6.45) is consistent with the limit diffusion equation (6.39) in the diffusive limit.

Theorem 6.7. *When ε tends to zero, the unknown f_0^{n+1} given by the numerical scheme (6.43)-(6.44)-(6.45) satisfies the following discrete equation*

$$\frac{f_{0i}^{n+1,0} - f_{0i}^{n,0}}{\Delta t} - \frac{E}{\Delta\zeta}\Big[\frac{\zeta_{i+1/2}^3}{6\sigma\Delta\zeta}\Big[(Ef_{0i+1}^{n,0} - Ef_{0i}^{n,0})\Big] - \frac{\zeta_{i-1/2}^3}{6\sigma\Delta\zeta}\Big[(Ef_{0i}^{n,0} - Ef_{0i-1}^{n,0})\Big] + \frac{\zeta_{i+1/2}^3 S_{i+1/2}^{n,0}}{2\sigma} - \frac{\zeta_{i-1/2}^3 S_{i-1/2}^{n,0}}{2\sigma}\Big] = 0,$$

with

$$S_{i+1/2}^{n,0} = \frac{E}{3}\Big[\frac{f_{0i+1}^{n,0}}{\zeta_{i+1}} + \frac{f_{0i}^{n,0}}{\zeta_i}\Big].$$

Proof. The proof is the same as in the case without electric field. □

As in the inhomogeneous case without electric field, in practice the following stability CFL condition is used

$$\Delta t \leq \max(\Delta\zeta/a_\zeta, 3\alpha_{ei}\Delta\zeta^2/E^2\zeta_{max}^3). \tag{6.49}$$

Similarly, using the ideas of the first part we consider the following scheme to compute f_{1i}^n at each time step

$$f_{1i}^{n+1} = \frac{\zeta_i^3}{\zeta_i^3 + 2\alpha_{ei}\Delta t}\Big[f_{1i}^n - \Delta t\Big(E\frac{f_{2i+1}^n - f_{2i-1}^n}{2\Delta\zeta} - a_\zeta\frac{f_{1i+1}^n - 2f_{1i}^n + f_{1i-1}^n}{2\Delta\zeta} + \frac{S_{i+1/2}^n + S_{i-1/2}^n}{2}\Big)\Big], \tag{6.50}$$

where

$$S^n_{i+1/2} = \frac{1}{2}\Big[\frac{E}{\zeta_{i+1}}(f^n_{0i+1} - f^n_{2i+1}) + \frac{E}{\zeta_i}(f^n_{0i} - f^n_{2i})\Big].$$

This scheme enables the use of the parabolic CFL condition (6.49) in the case of a large collisional parameter α_{ei}. In addition, the well-balanced property is ensured since the stationary state (6.47) is still preserved by this scheme.

6.4 Numerical examples

In this section we compare the asymptotic-preserving scheme to the standard HLL scheme [118] and to an explicit discretisation of the diffusion equation in different regimes. For all the numerical test cases the time step considered for the asymptotic-preserving scheme is taken as the maximum of the hyperbolic time step and the diffusion time step (see CFL condition Eq. 6.35). The numerical scheme is able to work with the diffusion time step when it becomes larger than the hyperbolic time step.

6.4.1 Free transport without electric field

We first consider system (6.5), without collisions, to validate the numerical scheme proposed in (6.20)-(6.23)-(6.26) on a simple advection of an initial profile. The solution is compared with the exact solution. Consider the initial conditions

$$\begin{cases} f_0(x,0) = \sqrt{\frac{2}{\pi}}\exp(-\frac{(x+5)^2}{2}), \\ f_1(x,0) = \sqrt{\frac{2}{\pi}}\exp(-\frac{(x+5)^2}{2}), \end{cases}$$

with periodical boundary conditions. In this case we have fixed $\zeta = 5$. In Figure 6.2, we compare the numerical solution obtained with the scheme (6.20)-(6.23)-(6.26) displayed in dashed blue with the exact solution in red at time t=6 using $\Delta x = 4 \cdot 10^{-3}$. In Table 6.2 the results of a convergence study are given. The scheme is first order accurate.

6.4.2 Temperature gradient with collisions without electric field

We now consider the system equation (6.5) with collisions to validate the numerical scheme (6.20)-(6.23)-(6.26) taking into account the collisional part. The solution obtained with the scheme presented in this paper is compared with the classical HLL scheme.

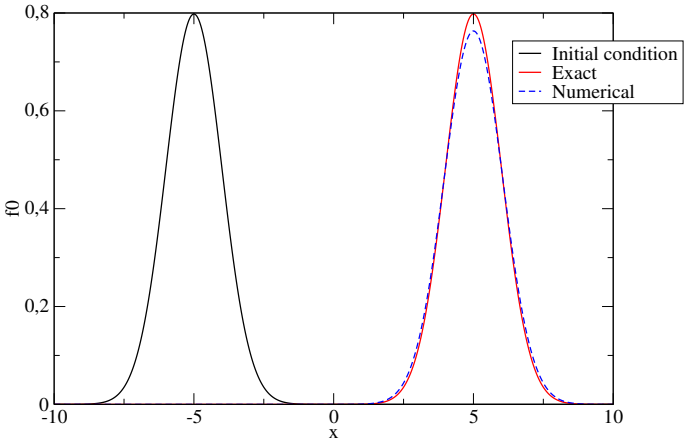

Figure 6.2: Free transport: comparison of the numerical solution for $\Delta x = 4 \cdot 10^{-3}$ and the exact solution (red) at time t=6.

Δx	L^1 **error**	L^1 **order**	L^2 **error**	L^2 **order**	L^∞ **error**	L^∞ **order**
$4 \cdot 10^{-2}$	0.63	-	0.27	-	0.22	-
$2 \cdot 10^{-2}$	0.36	0.77	0.17	0.7	0.14	0.65
$1 \cdot 10^{-2}$	0.20	0.88	0.09	0.83	0.08	0.84
$6.66 \cdot 10^{-2}$	0.14	0.88	0.06	0.9	0.06	0.87
$5 \cdot 10^{-3}$	0.11	0.84	0.05	0.92	0.04	0.91
$4 \cdot 10^{-3}$	0.08	1.09	0.04	0.95	0.03	0.93

Table 6.2: Convergence study of the method. The order of the method is given for the L^1, L^2 and L^∞ norms.

Consider the initial conditions

$$\begin{cases} f_0(x,\zeta,0) = \sqrt{\dfrac{2}{\pi}} \dfrac{\zeta^2}{T_{ini}(x)^{3/2}} \exp\Big(-\dfrac{\zeta^2}{2T_{ini}(x)}\Big), \\ f_1(x,\zeta,0) = 0, \end{cases}$$

with

$$T_{ini}(x) = 2 - \arctan(x),$$

and $\alpha_{ei} = 1$. On the right and left boundaries, we use a Neumann boundary condition: the values of f_0 and f_1 in the boundary ghost cells are set to the values in the corresponding real boundary cells. The energy range chosen is $[0, 12]$ with an energy step $\Delta\zeta = 0.1$ and the space range is $[-40, 40]$ with a space step $\Delta x = 0.2$. In Figure 6.3, we compare the numerical solution obtained with the AP scheme (6.20)-(6.23)-(6.26). The solution obtained with the Asymptotic-preserving scheme is displayed in continuous lines with the solution given by HLL scheme in dashed

lines at time 0.25 and 0.5. The Asymptotic-preserving numerical scheme and the HLL scheme gives comparable results.

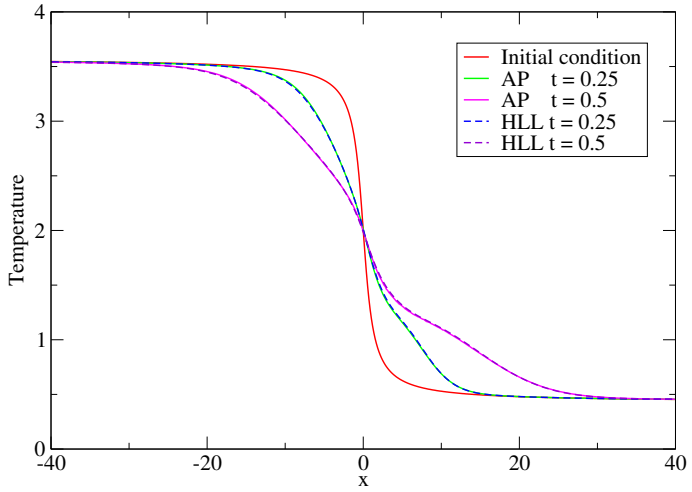

Figure 6.3: Temperature gradient: comparison of the temperature profile for the numerical solution (AP) and for the HLL scheme (HLL) at time 0.25 and 0.5.

6.4.3 Temperature gradient in the diffusive regime without electric field

In this numerical test, the same initial and boundary conditions that in the test case 3.2 are chosen. However, we consider a large collisional parameter and take $\alpha_{ei} = 10^4$. The scheme (6.20)-(6.23)-(6.26) is verified in the diffusive regime. The results are compared with the diffusion solution and with the one obtained with the HLL scheme.

In Figure 6.4, the numerical solution obtained with the scheme (6.20)-(6.23)-(6.26) is displayed. The results obtained with the asymptotic-preserving scheme are displayed in continuous green lines with the solution given by HLL scheme in continuous purple lines and the diffusion solution in dashed blue lines at time t=50, t=100, 500 and 1000. The AP numerical scheme and the diffusion solution match perfectly while we remark for time $t = 50$ and $t = 100$ that the HLL scheme gives very inaccurate results. The results obtained with the HLL scheme at time $t = 500$ and $t = 1000$ are completely wrong and are not displayed, however we notice that in the long time regime the AP numerical scheme and the diffusion solution still match.

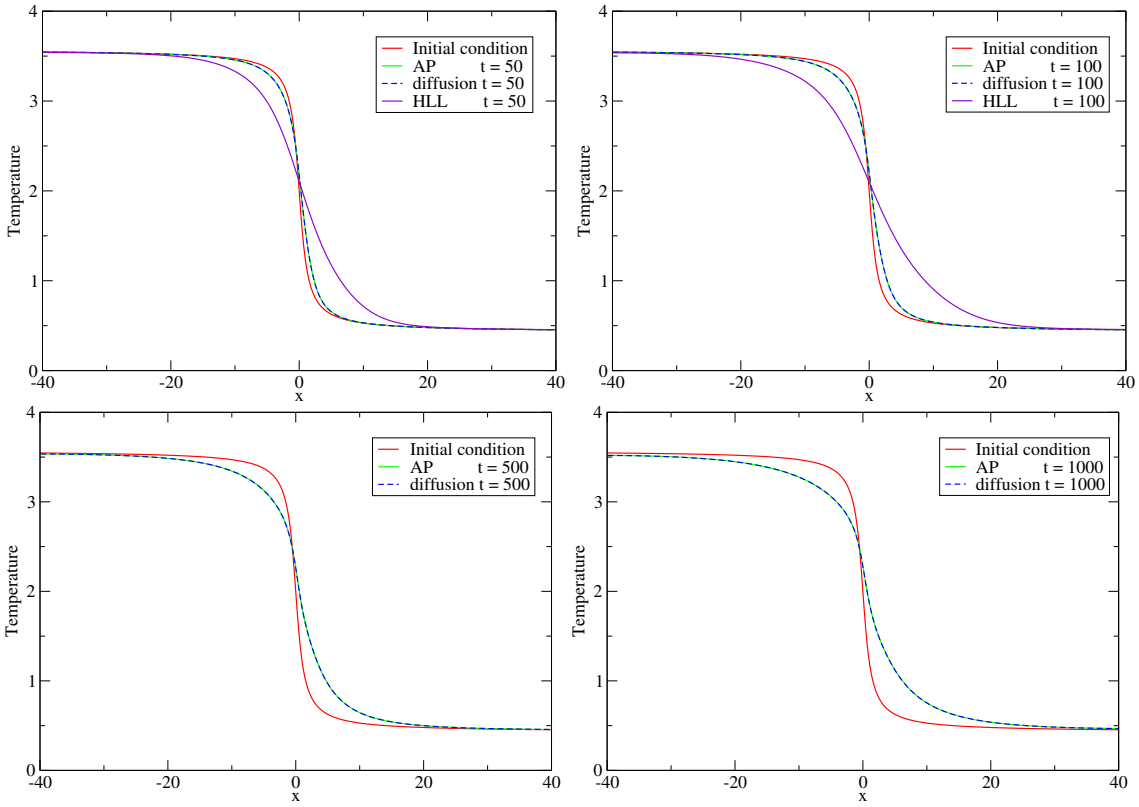

Figure 6.4: Temperature gradient in the diffusive limit: comparison of the temperature profile of the asymptotic-preserving scheme (AP), the HLL scheme (HLL) and the diffusion solution at time t=50, 100, 500 and 1000.

6.4.4 Discontinuous initial condition in the diffusive regime without electric field

In this case, a discontinuous initial condition in the diffusive regime without electric field is considered. The results are compared with the diffusion equation solution and the HLL scheme. The energy range chosen is $[0, 6]$ with an energy step $\Delta\zeta = 0.1$ and the space range L=$[-10, 10]$ with a space step $\Delta x = 5 \cdot 10^{-2}$.

Consider the initial conditions

$$\begin{cases} f_0(x,\zeta,0) = \begin{cases} 1 \text{ if } x \leq L/3, \\ 0 \text{ if } L/3 \leq x \leq 2L/3, \\ 1 \text{ if } L/3 \leq x, \end{cases} \\ f_1(x,\zeta,0) = 0, \end{cases}$$

with periodical boundary conditions and $\alpha_{ei} = 10^4$. In Figure 6.5, we compare the numerical solution obtained with the Asymptotic-preserving scheme displayed in red with the diffusion solution in dashed blue and the HLL scheme in green at time t=200. The AP and diffusion solutions match perfectly while the HLL scheme is very inaccurate. In Figure 6.6, the long time behaviour of the numerical solutions is considered. The AP scheme and the diffusion solution are compared at time t=500, the results match.

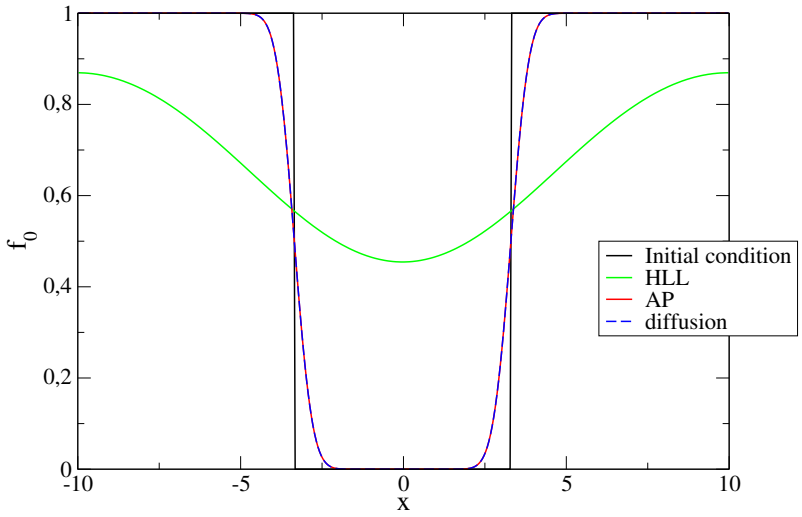

Figure 6.5: Comparison of the f_0 profile for the asymptotic-preserving scheme (AP), for the HLL scheme (HLL) and the diffusion solution at time t=200.

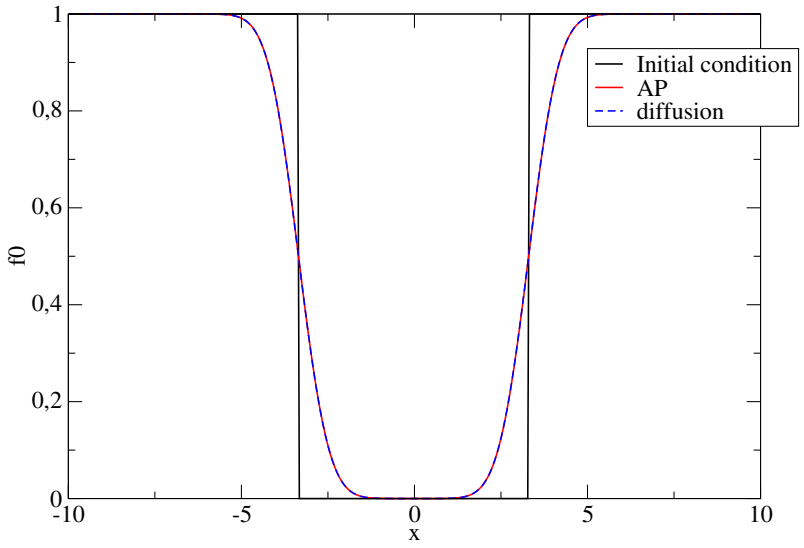

Figure 6.6: Comparison of the f_0 profile for the Asymptotic-preserving scheme (AP), and the diffusion solution at time t=500.

6.4.5 Relaxation of a Gaussian profile, in the homogeneous case in the diffusive regime with electric field

We consider system (6.38) with collisions and the source term $\frac{E}{\zeta}(f_0 - f_2)$ to validate the numerical scheme (6.43)-(6.44)-(6.45) in the diffusive limit. On the left and right boundaries, we use Neumann boundary conditions: the values of f_0 and f_1 in the boundary ghost cells are set to the values in the corresponding real boundary cells. Here $\alpha_{ei} = 10^4$ and the energy range chosen is $[0, 20]$ with an energy step $\Delta\zeta = 10^{-2}$. Here we have chosen $E = 1$ and considered the following initial conditions

$$\begin{cases} f_0(\zeta, 0) = \sqrt{\dfrac{2}{\pi}} \exp(-\dfrac{\zeta^2}{2}), \\ f_1(\zeta, 0) = 0. \end{cases}$$

In Figure 6.7, we compare the numerical solution obtained with the scheme (6.43)-(6.44)-(6.45) displayed in red with the diffusion solution in dashed blue and the HLL scheme at time t=20. The asymptotic-preserving and diffusion solutions match perfectly while the HLL scheme is very diffusive. In Figure 6.8, the results obtained with the AP scheme and the diffusion solution are compared in the long time regime at time t=80.

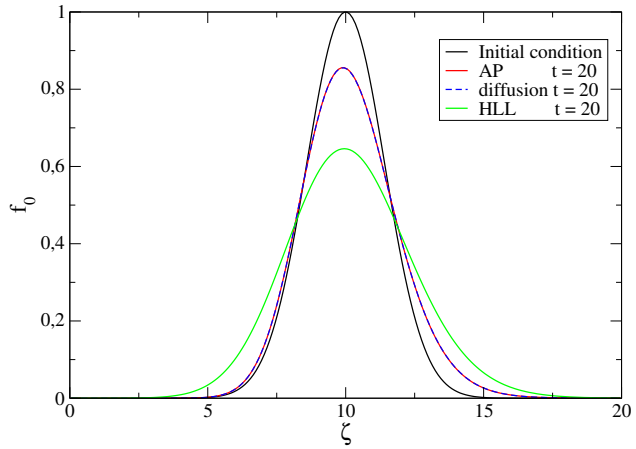

Figure 6.7: Relaxation of a Gaussian profile: comparison of the f_0 profile for the asymptotic-preserving scheme (AP), for the HLL scheme (HLL) and the diffusion solution at time t=20.

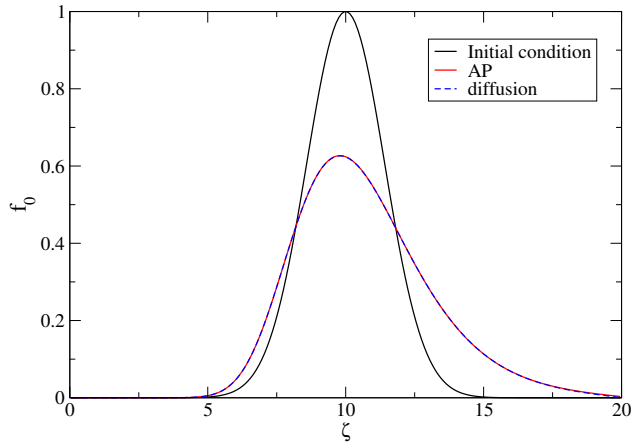

Figure 6.8: Relaxation of a Gaussian profile: comparison of the f_0 profile for the asymptotic-preserving scheme (AP) and the diffusion solution at time t=80.

6.4.6 Relaxation of a Gaussian profile in the diffusive regime without electric field in the case of a non-constant collisional parameter

In this example, the numerical scheme (6.20)-(6.23)-(6.26) is verified in the diffusive regime without electric field in a inhomogeneous collisional plasma. In this case the coefficient α_{ei} is not constant and follows the linear profile

$$\alpha_{ei}(x) = (5x/8 + 15/2) \cdot 10^3.$$

Then $\alpha_{ei}(-4) = 5 \cdot 10^3$ and $\alpha_{ei}(4) = 10^4$. On the left and right boundaries, we use Neumann boundary conditions: the values of f_0 and f_1 in the boundary ghost cells

are set to the values in the corresponding real boundary cells. The energy range chosen is $[0, 8]$ with an energy step $\Delta\zeta = 0.1$ and the space range $[-4, 4]$ with a space step $\Delta x = 5 \cdot 10^{-2}$. The initial conditions are the following

$$\begin{cases} f_0(x, \zeta, 0) = \zeta^2 \exp(-\frac{x^2}{2}), \\ f_1(x, \zeta, 0) = 0. \end{cases}$$

In Figure 6.9, we compare the numerical solution obtained with the asymptotic-preserving scheme displayed in red with the diffusion solution in dashed blue at time t=150. In this case, the asymptotic-preserving and diffusion solutions also match perfectly. The HLL scheme results are not given in Figure 6.9, since the final time t=150 is important the HLL results are completely wrong.

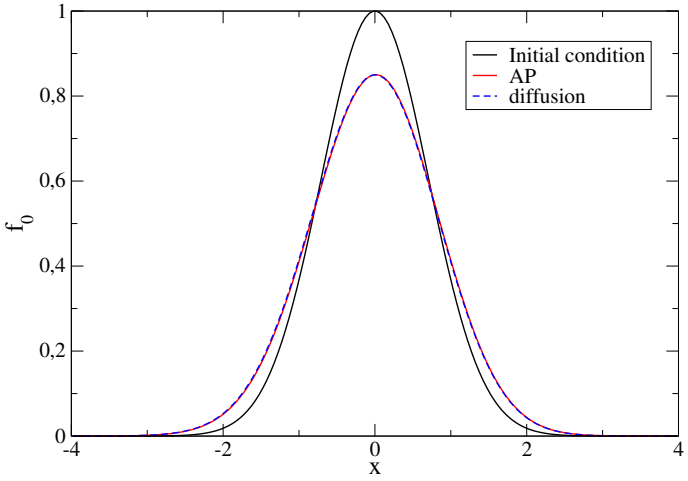

Figure 6.9: Relaxation of a Gaussian profile in the case of a linear collisional parameter: comparison of the f_0 profile for the asymptotic-preserving scheme (AP) and the diffusion solution at time t=150.

6.5 General model and diffusive limit

In the first part of this work, a numerical scheme was proposed for the electron M_1 model in a particular case without electric field and in the homogeneous case. The scheme derived using the consistency with the integral form of the approximate Riemann solver ensures the admissibility conditions (6.4) and correctly captures the limit diffusion equation. The method proposed naturally takes into account the source term $-E(x)(f_0 - f_2)/\zeta$, the non linearity of the model which comes from the M_1 model closure and the spatial dependencies of the electric field and the collisional parameter. However, the general model considering the x and ζ dependences has not

been considered. In such a general case, mixed derivatives arise in the diffusion limit leading to complex diffusion equation. In addition, the source term $-E(x)(f_0-f_2)/\zeta$ also contributes in the limit equation. In this part, the general electronic M_1 model (6.2) is considered. The aim is to propose a numerical scheme, extending the ideas of the first part, in order to take into account the mixed derivatives in the diffusive limit. Such a scheme must ensure the admissibility conditions (6.4) and include the contribution of the source term in the diffusion $-E(x)(f_0 - f_2)/\zeta$ limit.
After using the diffusive scaling (6.6), the general model (6.2) writes

$$\begin{cases} \varepsilon\partial_t f_0(t,x,\zeta) + \zeta\partial_x f_1(t,x,\zeta) + E(x)\partial_\zeta f_1(t,x,\zeta) = 0, \\ \varepsilon\partial_t f_1(t,x,\zeta) + \zeta\partial_x f_2(t,x,\zeta) + E(x)\partial_\zeta f_2(t,x,\zeta) \\ \qquad\qquad - \dfrac{E(x)}{\zeta}(f_0(t,x,\zeta) - f_2(t,x,\zeta)) = -\dfrac{2\sigma(x)}{\zeta^3}\dfrac{f_1(t,x,\zeta)}{\varepsilon}. \end{cases} \tag{6.51}$$

Inserting the Hilbert expansion (6.8) into the second equation of (6.51) gives at order ε^0

$$f_1^1 = -\frac{\zeta^4}{6\sigma}\partial_x f_0^0 - \frac{E\zeta^3}{6\sigma}\partial_\zeta f_0^0 + \frac{E\zeta^2}{3\sigma} f_0^0. \tag{6.52}$$

Finally, using the previous equation in the first equation of (6.2) at order ε^1, the following limit equation is obtained

$$\partial_t f_0^0 + \zeta\partial_x\Big(-\frac{\zeta^4}{6\sigma}\partial_x f_0^0 - \frac{E\zeta^3}{6\sigma}\partial_\zeta f_0^0 + \frac{E\zeta^2}{3\sigma} f_0^0\Big) + E\partial_\zeta\Big(-\frac{\zeta^4}{6\sigma}\partial_x f_0^0 - \frac{E\zeta^3}{6\sigma}\partial_\zeta f_0^0 + \frac{E\zeta^2}{3\sigma} f_0^0\Big) = 0. \tag{6.53}$$

In the case $E = 0$, one recognises a classical diffusion equation involving a second order space derivative with a diffusion coefficient of $-\zeta^5/6\sigma$. However, in the general case this limit equation involves mixed x and ζ derivatives leading to a non isotropic diffusion. In addition, the source term $E(f_0 - f_2)/\zeta$ also contributes in the diffusive limit adding the term $(E\zeta^2/(3\sigma))f_0^0$ in the right side of (6.52) and in the x and ζ derivatives of (6.53). Such an asymptotic limit is unusual compared to what has been studied in radiative transfer for example [19, 20]. The difference lies in the fact that here charged particles are considered. Then, the contribution of the electric field must be taken into account leading to these unexpected limit involving mixed derivatives.

6.6 Numerical scheme

The aim of this part is to propose a numerical scheme, generalising the ideas introduced in the first part, for the general model (6.2) and consistent, in the limit ε tends to zero, with equation (6.53). The main difficulty comes from the derivation of a numerical scheme consistent in the diffusive limit with equation (6.53) and in particular with the mixed-derivatives. The numerical scheme proposed must also be able to deal with the contribution of the source term $E(f_0 - f_2)/\zeta$.

6.6.1 Case without the source term $\frac{E}{\zeta}(f_0 - f_2)$

We first consider the case without the source term $\frac{E}{\zeta}(f_0 - f_2)$. With the present approach, it will be seen in part 6.6.1 that this term can be naturally taken into account, therefore, for clarity, we start without considering it. The electronic M_1 model then reads

$$\begin{cases} \partial_t f_0(t,x,\zeta) + \zeta \partial_x f_1(t,x,\zeta) + E(x)\partial_\zeta f_1(t,x,\zeta) = 0, \\ \partial_t f_1(t,x,\zeta) + \zeta \partial_x f_2(t,x,\zeta) + E(x)\partial_\zeta f_2(t,x,\zeta) = -\dfrac{2\sigma(x) f_1(t,x,\zeta)}{\zeta^3}, \end{cases} \tag{6.54}$$

and its diffusive limit equation

$$\partial_t f_0^0 + \zeta \partial_x \Big(-\frac{\zeta^4}{6\sigma}\partial_x f_0^0 - \frac{E\zeta^3}{6\sigma}\partial_\zeta f_0^0 \Big) + E\partial_\zeta \Big(-\frac{\zeta^4}{6\sigma}\partial_x f_0^0 - \frac{E\zeta^3}{6\sigma}\partial_\zeta f_0^0 \Big) = 0. \tag{6.55}$$

Derivation of the scheme

In this part the derivation of an numerical scheme for the model (6.54) is detailed. Let us consider an uniform mesh with a constant space step $\Delta x = x_{i+1/2} - x_{i-1/2}$, a constant energy step $\Delta\zeta = \zeta_{i+1/2} - \zeta_{i-1/2}$ and a time step Δt. Extending the ideas introduced in the first part, we propose to consider the following numerical scheme

$$\begin{aligned} \frac{U_{ij}^{n+1} - U_{ij}^n}{\Delta t} =& \frac{a_x}{\Delta x} U_{i-1/2j}^{R*} + \frac{2a_x}{\Delta x} U_{ij}^n + \frac{a_x}{\Delta x} U_{i+1/2j}^{L*} \\ &+ \frac{a_\zeta}{\Delta\zeta} U_{ij-1/2}^{R*} + \frac{2a_\zeta}{\Delta\zeta} U_{ij}^n + \frac{a_\zeta}{\Delta\zeta} U_{ij+1/2}^{L*}, \end{aligned} \tag{6.56}$$

where the intermediate states of the approximated Riemann solver (see Figure 6.10) $U_{i+1/2j}^{L*}$, $U_{i-1/2j}^{R*}$, $U_{ij+1/2}^{L*}$ and $U_{ij-1/2}^{R*}$ are defined by

$$U_{i-1/2j}^{R*} = \begin{pmatrix} f_{0i-1/2j}^{R*} \\ f_{1i-1/2j}^{*} \end{pmatrix}, \; U_{i+1/2j}^{L*} = \begin{pmatrix} f_{0i+1/2j}^{L*} \\ f_{1i+1/2j}^{*} \end{pmatrix}, \; U_{ij-1/2}^{R*} = \begin{pmatrix} f_{0ij-1/2}^{R*} \\ f_{1ij-1/2j}^{*} \end{pmatrix}, \; U_{ij+1/2}^{L*} = \begin{pmatrix} f_{0ij+1/2}^{L*} \\ f_{1ij+1/2}^{*} \end{pmatrix}.$$

The second components of the intermediate states at each interface are chosen equal, ie $f_{1i+1/2j}^{L*} = f_{1i+1/2j}^{R*} = f_{1i+1/2j}^{*}$ and $f_{1ij+1/2}^{L*} = f_{1ij+1/2}^{R*} = f_{1ij+1/2}^{*}$.

Following [19], the velocity waves a_x and a_ζ are fixed such that

$$a_x = \zeta_j, \qquad\qquad a_\zeta = |E_i|.$$

For clarity, in the following, we omit the dependency of the speed a_x in energy and a_ζ in space. However, the results presented hold in the general case. If the intermediate states are defined following the first part the numerical scheme (6.56) recovers only the second order space and energy derivatives in the diffusive limit. Therefore, in

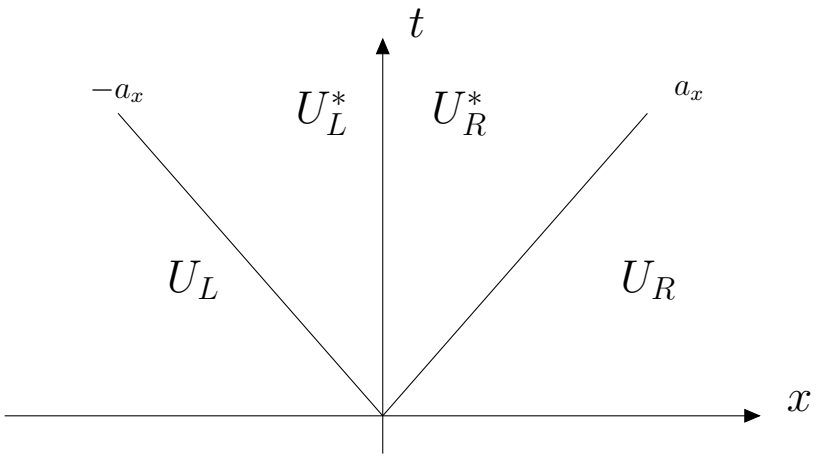

Figure 6.10: Structure of the approximate Riemann solver.

order to take into account the mixed-derivative terms in the diffusive limit leading to an anisotropic diffusion, we propose to modify the numerical viscosity of the intermediate state f_1^* used in equation (6.20) in the following way

$$f^*_{1i+1/2j} = \alpha_{i+1/2j}\Big[\frac{f_{1i+1j}+f_{1ij}}{2} - \frac{1}{2a_x}(\zeta_j f_{2i+1j} - \zeta_j f_{2ij}) - c_{i+1/2j}(\frac{\partial f_0}{\partial \zeta})_{i+1/2j}(1-\alpha_{i+1/2j})\Big], \tag{6.57}$$

$$f^*_{1ij+1/2} = \beta_{ij+1/2}\Big[\frac{f_{1ij+1}+f_{1ij}}{2} - \frac{1}{2a_\zeta}(E_i f_{2ij+1} - E_i f_{2ij}) - \bar{c}_{ij+1/2}(\frac{\partial f_0}{\partial x})_{ij+1/2}(1-\beta_{ij+1/2})\Big]. \tag{6.58}$$

with

$$\alpha_{i+1/2j} = \frac{2a_x\zeta_j^3}{2a_x\zeta_j^3 + \sigma_{i+1/2}\Delta x}, \qquad \beta_{ij+1/2} = \frac{2a_\zeta\zeta_{j+1/2}^3}{2a_\zeta\zeta_{j+1/2}^3 + \sigma_i\Delta\zeta}. \tag{6.59}$$

In this case, the numerical viscosity contributes in the x and ζ directions. The terms $(\frac{\partial f_0}{\partial \zeta})_{i+1/2j}$, $(\frac{\partial f_0}{\partial x})_{ij+1/2}$ and the coefficients c and $\bar{c}$ are fixed in order to obtained the relevant limit equation (6.53) in the diffusion regime. We set

$$c_{i+1/2j} = \frac{E_{i+1/2}\Delta x}{3a_x}, \qquad \bar{c}_{ij+1/2} = \frac{\zeta_{j+1/2}\Delta\zeta}{3a_\zeta}. \tag{6.60}$$

We use an upwind scheme for the discretisation of the terms $(\frac{\partial f_0}{\partial \zeta})_{i+1/2j}$ and $(\frac{\partial f_0}{\partial x})_{ij+1/2}$. The coefficient $\bar{c}$ is always positive then

$$\bar{c}_{ij+1/2}(\frac{\partial f_0}{\partial x})_{ij+1/2} \approx \bar{c}_{ij+1/2}\frac{f_{0i+1j+1} - f_{0ij+1} + f_{0i+1j} - f_{0ij}}{2\Delta x},$$

$$c_{i+1/2j}(\frac{\partial f_0}{\partial \zeta})_{i+1/2j} \approx \begin{cases} c_{i+1/2j}\dfrac{f_{0i+1j} - f_{0i+1j-1} + f_{0ij} - f_{0ij-1}}{2\Delta\zeta} & \text{if } c_{i+1/2j} < 0, \\ c_{i+1/2j}\dfrac{f_{0i+1j+1} - f_{0i+1j} + f_{0ij+1} - f_{0ij}}{2\Delta\zeta} & \text{if } c_{i+1/2j} > 0. \end{cases}$$

The previous two conditions rewrite

$$c_{i+1/2j}(\frac{\partial f_0}{\partial \zeta})_{i+1/2j} \approx c^-_{i+1/2j}\frac{f_{0i+1j} - f_{0i+1j-1} + f_{0ij} - f_{0ij-1}}{2\Delta\zeta} + c^+_{i+1/2j}\frac{f_{0i+1j+1} - f_{0i+1j} + f_{0ij+1} - f_{0ij}}{2\Delta\zeta},$$

with $(c)^+ = \max(c, 0)$ and $(c)^- = \min(c, 0)$. We introduce the following notations

$$\begin{aligned}\tilde{f}_{0i+1/2j} &= \frac{f_{1i+1j} + f_{1ij}}{2} - \frac{(\zeta_j f_{2i+1j} - \zeta_j f_{2ij})}{2a_x(2 - \alpha_{i+1/2j})},\\ \tilde{f}_{1i+1/2j} &= \frac{f_{1ij+1} + f_{1ij}}{2} - \frac{(E_i f_{2ij+1} - E_i f_{2ij})}{2a_\zeta(2 - \beta_{ij+1/2})}.\end{aligned} \tag{6.61}$$

In the first part of this work, the intermediate states of the considered approximate Riemann solvers were defined using consistency relations and a corrective coefficient to ensure the admissibility conditions. Extending these ideas, the intermediates states $f^{R*}_{0i+1/2j}$ and $f^{L*}_{0i+1/2j}$ are defined by

$$\begin{cases} f^{L*}_{0i+1/2j} = \tilde{f}_{0i+1/2j} - \Gamma_{i+1/2j}\theta_{1i+1/2j},\\ f^{R*}_{0i+1/2j} = \tilde{f}_{0i+1/2j} + \Gamma_{i+1/2j}\theta_{1i+1/2j},\end{cases} \tag{6.62}$$

with

$$\Gamma_{i+1/2j} = \frac{1}{2}[f_{0i+1j} - f_{0ij} - \frac{\zeta_j}{a_x}(f_{1ij} - 2f^*_{1i+1/2j} + f_{1i+1j})],$$

and the coefficient $\theta_{1i+1/2j}$ is fixed in order to ensure the admissibility conditions (6.4). Similarly, the definitions of $f^{R*}_{0ij+1/2}$ and $f^{L*}_{0ij-1/2}$ read

$$\begin{cases} f^{L*}_{0ij+1/2} = \tilde{f}_{0ij+1/2} - \Gamma_{ij+1/2}\theta_{2ij+1/2},\\ f^{R*}_{0ij+1/2j} = \tilde{f}_{0ij+1/2} + \Gamma_{ij+1/2}\theta_{2ij+1/2},\end{cases} \tag{6.63}$$

with

$$\Gamma_{ij+1/2} = \frac{1}{2}[f_{0ij+1} - f_{0ij} - \frac{\zeta_j}{a_\zeta}(f_{1ij} - 2f^*_{1ij+1/2} + f_{1ij+1})].$$

In order to ensure the admissibility conditions (6.4), the definitions of the intermediate states $f^*_{1i+1/2j}$ and $f^*_{1ij+1/2}$ given in (6.57) and (6.58) are modified such that

$$f^*_{1i+1/2j} = \alpha_{i+1/2j}\Big[\tilde{f}_{1i+1/2j} - \theta_{1i+1/2j}c_{i+1/2j}(\frac{\partial f_0}{\partial \zeta})_{i+1/2j}(1 - \alpha_{i+1/2j})\Big], \tag{6.64}$$

$$f^*_{1ij+1/2} = \beta_{ij+1/2}\Big[\tilde{f}_{1ij+1/2} - \theta_{2ij+1/2}\bar{c}_{ij+1/2}(\frac{\partial f_0}{\partial x})_{ij+1/2}(1 - \beta_{ij+1/2})\Big]. \tag{6.65}$$

Remark 6.8. *In the case $\theta_{1i+1/2j} = 0$ and $\theta_{2ij+1/2} = 0$, the admissibility requirements (6.4) are fulfilled.*

Then $\theta_{1i+1/2j}$ and $\theta_{2ij+1/2}$ are fixed in the interval $[0,1]$, the larger possible such that the admissibility requirements (6.4) are fulfilled. A simple calculation gives the following conditions

$$\tilde{\theta}_{1i+1/2j} = \frac{\tilde{f}_{0i+1/2j} - \alpha_{i+1/2j}|\tilde{f}_{1i+1/2j}|}{|\Gamma_{i+1/2j}| + |\alpha_{i+1/2j}(\frac{\partial f_0}{\partial \zeta})_{i+1/2j} c_{i+1/2j}|}, \tag{6.66}$$

and

$$\tilde{\theta}_{2ij+1/2} = \frac{\tilde{f}_{0ij+1/2} - \beta_{ij+1/2}|\tilde{f}_{1ij+1/2}|}{|\Gamma_{ij+1/2}| + |\beta_{ij+1/2}(\frac{\partial f_0}{\partial \zeta})_{ij+1/2} \bar{c}_{ij+1/2}|}. \tag{6.67}$$

Finally, $\theta_{1i+1/2j} = \min(\tilde{\theta}_{1i+1/2j}, 1)$ and $\theta_{2ij+1/2} = \min(\tilde{\theta}_{2ij+1/2}, 1)$.

Theorem 6.9. *(Admissibility) If for all $(i,j) \in \mathbb{N}^2$, $U^n_{i,j} \in \mathcal{A}$, then for all $(i,j) \in \mathbb{N}^2$, $U^{n+1}_{i,j} \in \mathcal{A}$ as soon as the following CFL condition holds*

$$\Delta t \leq \frac{\Delta\zeta \Delta x}{(2a_x \Delta\zeta + 2a_\zeta \Delta x)}.$$

Proof. The numerical scheme (6.56) also writes as a convex combination of vectors of $\mathcal{A}$

$$\begin{aligned} U^{n+1}_{ij} =& (1 - \frac{2a_x\Delta t}{\Delta x} - \frac{2a_\zeta \Delta t}{\Delta \zeta}) U^n_{ij} + \frac{a_x \Delta t}{\Delta x} U^{R*}_{i-1/2j} + \frac{a_x \Delta t}{\Delta x} U^{L*}_{i+1/2j} \\ &+ \frac{a_\zeta \Delta t}{\Delta \zeta} U^{R*}_{ij-1/2} + \frac{a_\zeta \Delta t}{\Delta \zeta} U^{L*}_{ij+1/2}, \end{aligned}$$

Using the definitions of θ_1 and θ_2 given in (6.66) and (6.67) the intermediate states $U^{R*}_{i-1/2j}$, $U^{L*}_{i+1/2j}$, $U^{R*}_{ij-1/2}$ and $U^{L*}_{ij+1/2}$ belong to $\mathcal{A}$. Since $\mathcal{A}$ is a convex space it follows that the updated states U^{n+1}_i belongs to $\mathcal{A}$. □

Asymptotic-preserving properties

In this part, the consistency in the classical regime and the asymptotic-preserving property of the scheme in the diffusive regime are exhibited.

Theorem 6.10. *(Consistency in the classical regime) The numerical scheme (6.56) is consistent, when Δt and Δx tend to zero, with the set of equation (6.54).*

Proof. Using the definitions (6.57) and (6.58), the second component of (6.56) reads

$$\begin{aligned}\frac{f_{1ij}^{n+1}-f_{1ij}^{n}}{\Delta t} =&\frac{a_x}{\Delta x}\Big[\alpha_{i+1/2j}\Big(\tilde{f}_{1i+1/2j}-\theta_{1i+1/2j}c_{i+1/2j}(\frac{\partial f_0}{\partial\zeta})_{i+1/2j}(1-\alpha_{i+1/2j})\Big)\Big]\\ &-\frac{2a_x}{\Delta x}f_{1ij}^{n}\\ &+\frac{a_x}{\Delta x}\Big[\alpha_{i-1/2j}\Big(\tilde{f}_{1i-1/2j}-\theta_{1i-1/2j}c_{i-1/2j}(\frac{\partial f_0}{\partial\zeta})_{i-1/2j}(1-\alpha_{i-1/2j})\Big)\Big]\\ &+\frac{a_\zeta}{\Delta\zeta}\Big[\beta_{ij+1/2}\Big(\tilde{f}_{1ij+1/2}-\theta_{2ij+1/2}\bar{c}_{ij+1/2}(\frac{\partial f_0}{\partial x})_{ij+1/2}(1-\beta_{ij+1/2})\Big)\Big]\\ &-\frac{2a_\zeta}{\Delta\zeta}f_{1ij}^{n}\\ &+\frac{a_\zeta}{\Delta\zeta}\Big[\beta_{ij-1/2}\Big(\tilde{f}_{1ij-1/2}-\theta_{2ij-1/2}\bar{c}_{ij-1/2}(\frac{\partial f_0}{\partial x})_{ij-1/2}(1-\beta_{ij-1/2})\Big)\Big].\end{aligned} \tag{6.68}$$

Inserting the definitions (6.61) into (6.68) and using the following expressions for $\alpha_{i+1/2j}$ and $\beta_{ij+1/2}$

$$\alpha_{i+1/2j}=\frac{2a_x\zeta_j^3}{2a_x\zeta_j^3+\sigma_{i+1/2}\Delta x}=1-\frac{\sigma_{i+1/2}\Delta x}{2a_x\zeta_j^3+\sigma_{i+1/2}\Delta x},$$

and

$$\beta_{ij+1/2}=\frac{2a_\zeta\zeta_{j+1/2}^3}{2a_\zeta\zeta_{j+1/2}^3+\sigma_i\Delta\zeta}=1-\frac{\sigma_i\Delta\zeta}{2a_\zeta\zeta_{j+1/2}^3+\sigma_i\Delta\zeta},$$

lead to the consistency with the second equation of (6.54) as Δx and Δt tend to zero. A similar calculation gives the consistency with the first equation of (6.54). □

Theorem 6.11. *(Consistency in the diffusive regime)*

In the diffusive limit, the numerical scheme (6.56) degenerates into

$$\begin{aligned}\frac{f_{0ij}^{n+1,0}-f_{0ij}^{n,0}}{\Delta t} =&\frac{\zeta_j}{\Delta x}\Big[\frac{\zeta_j^4}{6\sigma_{i+1/2}\Delta x}(f_{0i+1j}^{n,0}-f_{0ij}^{n,0})-\frac{\zeta_j^4}{6\sigma_{i-1/2}\Delta x}(f_{0i1j}^{n,0}-f_{0i-1j}^{n,0})\\ &+\frac{\zeta_j^3E_{i+1/2}}{6\sigma_{i+1/2}}(\frac{\partial f_0^{n,0}}{\partial\zeta})_{i+1/2j}-\frac{\zeta_j^3E_{i-1/2}}{6\sigma_{i-1/2}}(\frac{\partial f_0^{n,0}}{\partial\zeta})_{i-1/2j}\Big]\\ &+\frac{E_i}{\Delta\zeta}\Big[\frac{E_i\zeta_{j+1/2}^3}{6\sigma_i\Delta\zeta}(f_{0ij+1}^{n,0}-f_{0ij}^{n,0})-\frac{E_i\zeta_{j-1/2}^3}{6\sigma_i\Delta\zeta}(f_{0i1j}^{n,0}-f_{0ij-1}^{n,0})\\ &+\frac{\zeta_{j+1/2}^4}{6\sigma_i}(\frac{\partial f_0^{n,0}}{\partial x})_{ij+1/2}-\frac{\zeta_{j-1/2}^4}{6\sigma_i}(\frac{\partial f_0^{n,0}}{\partial x})_{ij-1/2}\Big].\end{aligned} \tag{6.69}$$

Proof. Following the same approach as in [20, 22, 113], using the diffusive scaling and equation (6.56) leads to

$$\begin{aligned}\varepsilon\frac{U_{ij}^{n+1,\varepsilon}-U_{ij}^{n,\varepsilon}}{\Delta t} =&\frac{a_x}{\Delta x}U_{i-1/2j}^{R*,\varepsilon}-\frac{2a_x}{\Delta x}U_{ij}^{n,\varepsilon}+\frac{a_x}{\Delta x}U_{i+1/2j}^{L*,\varepsilon}\\ &+\frac{a_\zeta}{\Delta\zeta}U_{ij-1/2}^{R*,\varepsilon}-\frac{2a_\zeta}{\Delta\zeta}U_{ij}^{n,\varepsilon}+\frac{a_\zeta}{\Delta\zeta}U_{ij+1/2}^{L*,\varepsilon},\end{aligned} \tag{6.70}$$

and equations (6.64) and (6.65) gives

$$\begin{aligned}f_{1i+1/2j}^{*,\varepsilon}&=\alpha_{i+1/2j}^{\varepsilon}\Big[\tilde{f}_{1i+1/2j}^{\varepsilon}-\theta_{1i+1/2j}c_{i+1/2j}(\frac{\partial f_0^{\varepsilon}}{\partial\zeta})_{i+1/2j}(1-\alpha_{i+1/2j}^{\varepsilon})\Big],\\ f_{1ij+1/2}^{*,\varepsilon}&=\beta_{ij+1/2}^{\varepsilon}\Big[\tilde{f}_{1ij+1/2}^{\varepsilon}-\theta_{2ij+1/2}\bar{c}_{ij+1/2}(\frac{\partial f_0^{\varepsilon}}{\partial x})_{ij+1/2}(1-\beta_{ij+1/2}^{\varepsilon})\Big].\end{aligned} \tag{6.71}$$

with

$$\alpha_{i+1/2j}^{\varepsilon}=\frac{2a_x\zeta_j^3}{2a_x\zeta_j^3+\sigma_{i+1/2}\Delta x/\varepsilon},\qquad \beta_{ij+1/2}^{\varepsilon}=\frac{2a_\zeta\zeta_{j+1/2}^3}{2a_\zeta\zeta_{j+1/2}^3+\sigma_i\Delta\zeta/\varepsilon}. \tag{6.72}$$

Then it follows that

$$f_{1i+1/2j}^{*,0}=0\qquad\text{and}\qquad f_{1ij+1/2}^{*,0}=0. \tag{6.73}$$

The second component of (6.70) reads

$$\begin{aligned}\varepsilon\frac{f_{1ij}^{n+1,\varepsilon}-f_{1ij}^{n,\varepsilon}}{\Delta t} =&\frac{a_x}{\Delta x}f_{1i-1/2j}^{*,\varepsilon}-\frac{2a_x}{\Delta x}f_{1ij}^{n,\varepsilon}+\frac{a_x}{\Delta x}f_{1i+1/2j}^{*,\varepsilon}\\ &+\frac{a_\zeta}{\Delta\zeta}f_{1ij-1/2}^{*,\varepsilon}-\frac{2a_\zeta}{\Delta\zeta}f_{1ij}^{n,\varepsilon}+\frac{a_\zeta}{\Delta\zeta}f_{1ij+1/2}^{*,\varepsilon}.\end{aligned}$$

At order ε^0 the previous equation leads to

$$f_{1ij}^{n,0}=0. \tag{6.74}$$

In the limit ε tends to zero, the results (6.73) and (6.74) give

$$\theta_{1i+1/2j}=1,\qquad\qquad \theta_{2ij+1/2}=1. \tag{6.75}$$

Indeed, when ε tends to zero, the definitions (6.66) and (6.67) lead to

$$\tilde{\theta}_{1i+1/2j}=\frac{f_{0i+1j}^{n,0}+f_{0ij}^{n,0}}{|f_{0i+1j}^{n,0}-f_{0ij}^{n,0}|}\geq 1,\qquad \tilde{\theta}_{2ij+1/2}=\frac{f_{0ij+1}^{n,0}+f_{0ij}^{n,0}}{|f_{0ij+1}^{n,0}-f_{0ij}^{n,0}|}\geq 1.$$

The first component of (6.70) reads

$$\begin{aligned}\varepsilon\frac{f_{0ij}^{n+1,\varepsilon}-f_{0ij}^{n,\varepsilon}}{\Delta t} =&\frac{a_x}{\Delta x}f_{0i-1/2j}^{R*,\varepsilon}-\frac{2a_x}{\Delta x}f_{0ij}^{n,\varepsilon}+\frac{a_x}{\Delta x}f_{0i+1/2j}^{L*,\varepsilon}\\ &+\frac{a_\zeta}{\Delta\zeta}f_{0ij-1/2}^{R*,\varepsilon}-\frac{2a_\zeta}{\Delta\zeta}f_{0ij}^{n,\varepsilon}+\frac{a_\zeta}{\Delta\zeta}f_{0ij+1/2}^{L*,\varepsilon}.\end{aligned}$$

Using the definitions (6.62) and (6.63), the result (6.75) and the previous equation considered at order ε^1 gives the numerical scheme (6.69).

□

6.6.2 General case with the term $\frac{E}{\zeta}(f_0 - f_2)$

As specified in part 3.1, in order to take into account the contribution of the source term $\frac{E}{\zeta}(f_0 - f_2)$, we simply propose to modify the intermediate states $f^*_{1i+1/2j}$ and $f^*_{1ij+1/2}$ given in (6.64) and (6.65) such that

$$f^*_{1i+1/2j} = \alpha_{i+1/2j}\Big[\tilde{f}_{1i+1/2j} - \theta_{1i+1/2j}c_{i+1/2j}\Big((\frac{\partial f_0}{\partial \zeta})_{i+1/2j} - \frac{\tilde{S}_{i+1/2j}}{2}\Big)(1-\alpha_{i+1/2j})\Big],$$
$$f^*_{1ij+1/2} = \beta_{ij+1/2}\Big[\tilde{f}_{1ij+1/2} + \frac{\Delta\zeta}{2a_\zeta}S_{ij+1/2} - \theta_{2ij+1/2}\bar{c}_{ij+1/2}(\frac{\partial f_0}{\partial x})_{ij+1/2}(1-\beta_{ij+1/2})\Big], \tag{6.76}$$

with

$$\tilde{S}_{i+1/2j} = \frac{\zeta_j^2}{3\sigma_i}\frac{f_{0i+1j} + f_{0ij}}{2} \qquad \text{and} \qquad S_{ij+1/2} = \frac{E_i}{2}\Big(\frac{f_{0ij+1} - f_{2ij+1}}{\zeta_{j+1}} + \frac{f_{0ij} - f_{2ij}}{\zeta_j}\Big).$$

In this case, as in the previous part the coefficients θ_1 and θ_2 are also fixed to ensure the admissibility requirements.

Theorem 6.12. *In the diffusive limit, the numerical scheme given by (6.56)-(6.62)-(6.63)-(6.76) is consistent with the limit equation (6.53).*

Proof. The proof is the same than for Theorem 3, considering the intermediate states $f^*_{1i+1/2j}$ and $f^*_{1ij+1/2}$ given in (6.76). A direct calculation using the Hilbert expansions leads to the result. The terms $S_{ij+1/2}$ are consistent with the term $\frac{E}{\zeta}(f_0 - f_2)$ while the terms $\tilde{S}_{i+1/2j}$ enable to correctly recover the contribution of the two terms $\frac{E\zeta^2}{3\sigma}f_0$ in the x and ζ derivatives of the limit equation. □

6.7 Numerical examples

In this section, the asymptotic-preserving scheme (6.56) is compared with the HLL scheme and an explicit discretisation of the diffusion equation (6.53) in the diffusive regime.

6.7.1 Relaxation of a Gaussian profile in the diffusive regime

In this example, the numerical scheme (6.56)-(6.62)-(6.63)-(6.76) is validated in the diffusive regime considering a inhomogeneous plasma with electric field. In this case, the initial conditions are the following

$$\begin{cases} f_0(t=0,x,\zeta) = \zeta^2\exp(-x^2)\exp(2(\zeta-3)^2), \\ f_1(t=0,x,\zeta) = 0. \end{cases}$$

The profile of f_0 at initial time as a function of x and ζ is displayed in Figure 6.11. For this test we have set $E = 1$, $\alpha_{ei} = 10^4$, the space range chosen is [-10,10] and the energy range [0,6]. In Figure 6.12, the solution obtained with the numerical scheme (6.56)-(6.62)-(6.63)-(6.76) is compared with the solution obtained with the HLL scheme and with an explicit discretisation of the limit diffusion equation (6.53) at different times. At time $t = 1$, one remark that the f_0 profile obtained with the HLL scheme is already seriously spread out while the profiles obtained with the AP scheme and the diffusion equation do not have changed. At time $t = 50$, the AP scheme and diffusion equation discretisation f_0 profiles are spread out while the profile obtained with the HLL scheme has vanished. As observed at time t=100, in the long time regime, the AP scheme and the discretisation of the diffusion equation behave identically.

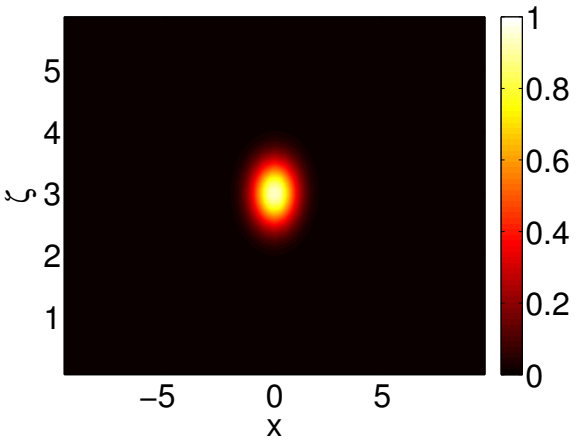

Figure 6.11: f_0 profile at the initial time.

6.7.2 Relaxation of a temperature profile in the diffusive regime with a self-consistent electric field

In this example, we consider the relaxation of a temperature profile in the diffusive regime considering a self-consistent electric field. The space range is [-40,40] and the energy range [0,6]. The initial conditions are the following

$$\begin{cases} f_0(t=0,x,\zeta) = \sqrt{\dfrac{2}{\pi}} \dfrac{\zeta^2}{T^{ini}(x)^{3/2}} \exp(-\dfrac{\zeta^2}{2T^{ini}(x)}), \\ f_1 = 0, \end{cases} \tag{6.77}$$

with $T^{ini}(x) = 2 - \arctan(x)$.

In this case the electric field is self-consistent meaning that at each time step it is calculated from the plasma profile. In this case we consider a Spitzer type model

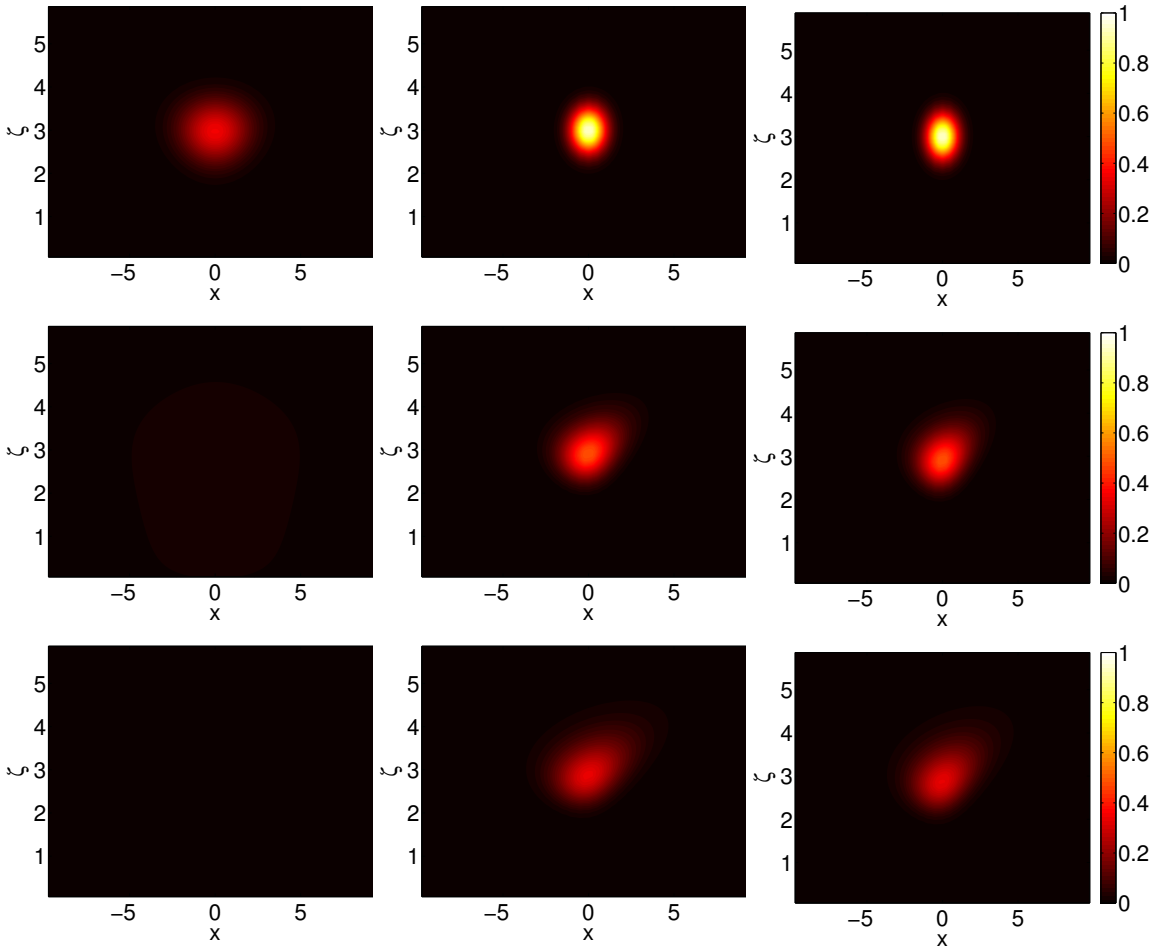

Figure 6.12: Representation of the f_0 profile as function of x and ζ at time t=1 (top), t=50 (middle), t=100 (bottom), for the HLL scheme (left), AP scheme (middle) and the diffusion equation.

[32, 194], to evaluate the electric field

$$E(x) = -\frac{dT(x)}{dx}, \tag{6.78}$$

where

$$T(x) = \frac{1}{3n_e}\Big(\int_0^{+\infty} \zeta^2 f_0 d\zeta - u^2 n_e\Big),$$

with

$$n_e = \int_0^{+\infty} f_0 d\zeta, \qquad \text{and} \qquad u = \frac{1}{n_e}\int_0^{+\infty} f_1 \zeta d\zeta.$$

In Figure 6.13, the temperature profile is displayed at the initial time and at time t=80. The temperature profiles obtained with the HLL scheme, the AP scheme

and a discretisation of the diffusion equation (6.53) are compared at time t=80. On one hand, one remark that the HLL temperature profile is excessively spread out compared to the AP and diffusion profiles while on the other hand the AP and diffusion profiles match exactly at time t=80. This example demonstrates the inability of the HLL scheme in capturing the correct temperature profile while the AP scheme presented handle perfectly the diffusive limit regime.

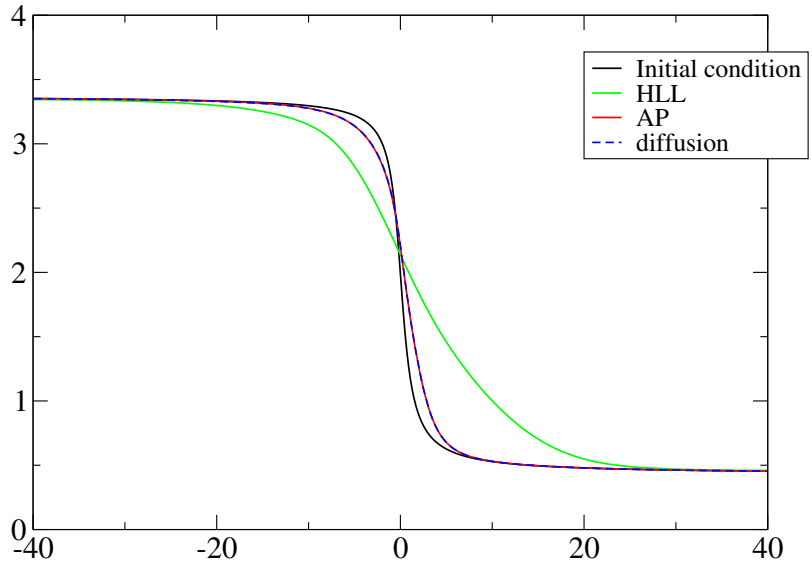

Figure 6.13: Temperature profile at time t=80.

6.7.3 Two electron beams interaction.

In this example the interaction between two electron beams is considered. This collisionless test case enables us to validate the AP scheme (6.56)-(6.62)-(6.63)-(6.76) in a regime where electrostatic effects are predominant compared to the collisional effects, therefore we set $\alpha_{ei} = 0$.
In the case of two streams propagating with opposite velocities v_d and $-v_d$, the initial electron distribution function is the following

$$f(t=0,x,v) = 0.5[(1 + A\cos(kx))M_{v_d}(v) + (1 - A\cos(kx))M_{-v_d}(v)],$$

with

$$M_{\pm v_d}(v) = \exp\Big(-\frac{(v \mp v_d)^2}{2}\Big).$$

The first corresponding angular moments f_0^1 and f_0^2 of the first and second population read

$$\begin{cases} f_0^1(t=0,x,\zeta) = 0.5(1 + A\cos(kx))\dfrac{\zeta}{v_d}\Big(\exp(-\dfrac{(\zeta - v_d)^2}{2}) - \exp(-\dfrac{(\zeta + v_d)^2}{2})\Big), \\ f_0^2(t=0,x,\zeta) = 0.5(1 - A\cos(kx))\dfrac{\zeta}{v_d}\Big(\exp(-\dfrac{(\zeta - v_d)^2}{2}) - \exp(-\dfrac{(\zeta + v_d)^2}{2})\Big). \end{cases}$$

The second angular moments f_1^1 and f_1^2 of the first and second population read

$$\begin{cases} f_1^1(t=0,x,\zeta) = 0.5(1+A\cos(kx))\dfrac{1-\zeta v_d}{v_d^2}\Big(\exp(-\dfrac{(\zeta-v_d)^2}{2}) - \exp(-\dfrac{(\zeta+v_d)^2}{2})\Big), \\ f_1^2(t=0,x,\zeta) = -0.5(1-A\cos(kx))\dfrac{1-\zeta v_d}{v_d^2}\Big(\exp(-\dfrac{(\zeta-v_d)^2}{2}) - \exp(-\dfrac{(\zeta+v_d)^2}{2})\Big). \end{cases}$$

At each time step, the electrostatic field is computed using the Maxwell-Ampere equation considering the contribution of the two population of particles

$$\frac{dE}{dt} = \int_0^{+\infty} f_1^1 \zeta d\zeta + \int_0^{+\infty} f_1^2 \zeta d\zeta.$$

The parameter A is introduced to perturb the initial condition in order to enable the development of the electrostatic instability. The energy range chosen is [0,12] and the space range is [0,25]. In this example we set $v_d = 4$, $A = 0.001$ and periodical boundary conditions are used. The results have been compared with a kinetic code [87]. In Figure 6.14, the evolution of the electrostatic energy is displayed as a function of time using the AP scheme in red and the kinetic code in dashed blue. The AP scheme and the kinetic code give analogous results. This numerical experiment shows the good behaviour of the AP scheme in a regime where electrostatic effects are predominant.

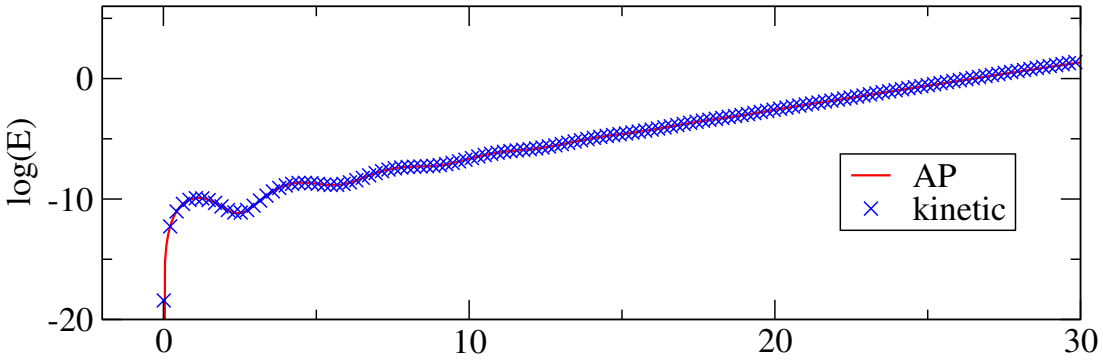

Figure 6.14: Temporal evolution of the electrostatic energy.

6.7.4 Relaxation of a temperature profile in the diffusive regime with a self-consistent electric field and non-constant collisional parameter

In this example, the initial conditions are the same than for the previous example where the initial temperature profile is given by (6.77) and the electric field is

computed using (6.78). In this case the collisional parameter α_{ei} is not constant and follows the linear profile

$$\sigma(x) = ax + b,$$

with $\alpha_{ei}(x_{min} = -40) = 5.10^3$ and $\alpha_{ei}(x_{max} = 40) = 10^5$. It follows that the coefficients a and b reads

$$a = \frac{10^5 - 5.10^3}{x_{max} - x_{min}}, \qquad b = 5.10^3 - a x_{min}.$$

The space range is [-40,40] and the energy range [0,6]. In Figure 6.15, the temperature profile is displayed at the initial time and at time t=5000 for the AP scheme and an explicit discretisation of the diffusion equation (6.53). After a long time (t=5000) and despite the strong spatial variation of the function α_{ei} the AP and diffusion profiles give very close result. One remark on the space interval [-40,0] the AP curve in red is slightly different to the diffusion curve in dashed blue while on the interval [0,40] the results match perfectly. This could be explained as the collisional parameter α_{ei} becomes larger for important x, therefore, the limit diffusive regime is fully reach for large x where the comparison with the diffusion equation is valid.

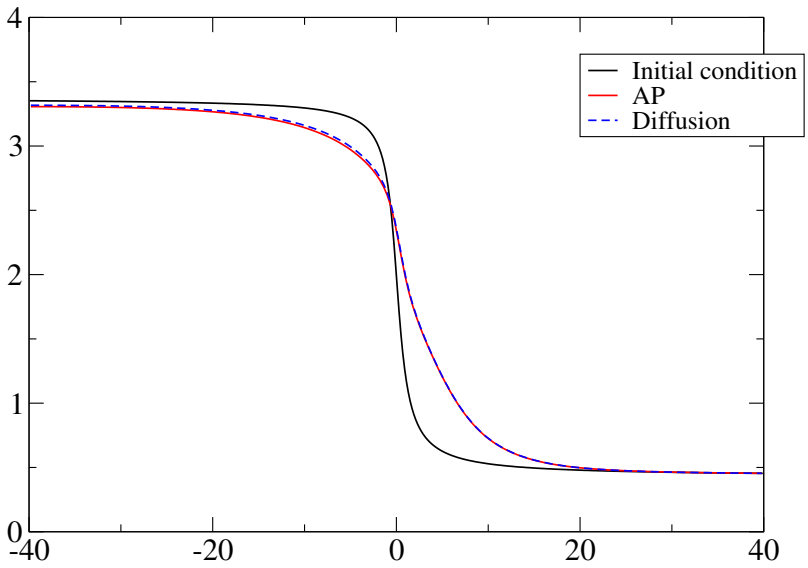

Figure 6.15: Temperature profile at time t=5000.

6.7.5 Case variable self-consistent collisional parameter

In the configurations occurring in plasma physics, the collisional parameter depends of the state of the plasma. The knowledge of the ion and electron distribution function is required to compute the collisional parameter. Therefore in this test case,

we choose to consider a nonlinear collisional parameter which depends of the solution itself

$$\alpha_{ei}(t,x,\zeta) = \exp(f_0(t,x,\zeta) + f_1(t,x,\zeta)).$$

In this case, $E = 1$, the space range chosen is [-10,10] and the energy range [0,6]. The initial condition is given by

$$\begin{cases} f_0(t=0,x,\zeta) = \zeta^2 \exp(-(\zeta-3)^2)) \exp(-x^2/10), \\ f_1 = 0. \end{cases}$$

We consider periodical boundary conditions. In Figure 6.16, the initial profile of f_0 is displayed at the initial time and at time t=3.

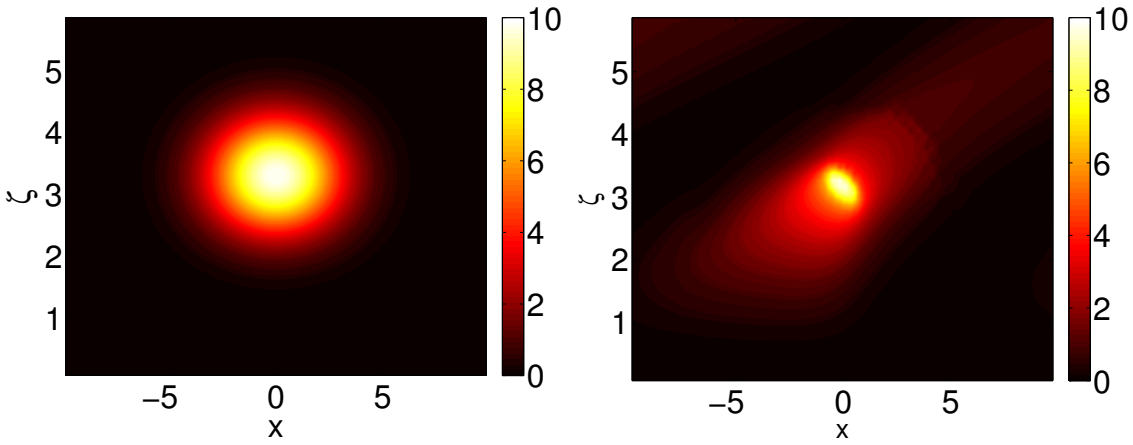

Figure 6.16: Representation of the f_0 profile as function of x and ζ at the initial time (left) and t=3 (right).

6.8 Conclusion

In the first part of this work, a numerical scheme has been proposed for the electron M_1 model in the case without electric field and in the homogeneous case with electric field. We have exhibited an approximate Riemann solver that satisfies the admissibility conditions. Contrarily to the HLL scheme, the proposed numerical scheme is asymptotic-preserving and recovers the correct diffusion equation in the diffusive limit. It has been shown, in the homogeneous case, that the method presented, enables to include the source term $-E(f_0 - f_2)/\zeta$, while a relaxation type method seems inconvenient. In addition, the scheme is well-balanced, capturing the steady state considered. Several numerical tests have been performed, it has been shown that the presented scheme behaves correctly in the classical regime and in the diffusive limit. Indeed, while, the HLL scheme is very inaccurate in the diffusive regime, the asymptotic-preserving scheme matches perfectly with the expected

diffusion solution. Also, the method correctly handles the case where the collisional parameter is not constant.

In the second part of this work, the approach has been extended to the general electronic M_1 model (6.2). In order to deal with the mixed derivatives which arise in the diffusive limit an anisotropic numerical viscosity has been considered. The numerical scheme preserves the realisibility domain and captures the correct limit equation. The contribution of the source term $E(f_0 - f_2)/\zeta$ is integrated and the cases of non constant electric field and collisional parameter are naturally included. Numerical examples have been performed in non-collisional and diffusive regimes. It has been observed that the present scheme behaves correctly in both regimes. A possible perspective could be to consider an electron-electron collisional operator or the study of the coupling with the Maxwell's equations.

First step towards multi-species modelling: the angular M_1 model in a moving frame

Chapter 7

Angular M_1 model in a moving reference frame

7.1 Introduction

This chapter is a first step towards the modelling and simulation of the multi-species particles transport. Previously, the electron transport studies were performed considering immobile ions [86, 168]. Indeed, because of their large mass compared to electrons, the ion motion could be neglected when considering small time intervals. However, if long time studies are considered, the ions motion needs to be taken into account. This would give access to a general and interesting physics relevant to the inertial confinement fusion applications. A significant work is then required in order to consider angular moments models for the multi-species particles transport studies. The long time perspective is to be able to work with charged particles of different species such as electrons and ions. In order to simplify the form of the electron-ion collisional operator and in order to ensure the galilean invariance property of angular moments models we will work in the framework of ions. This is significantly different with the previous studies, since the M_1 model [85, 115, 117] has always been considered in the framework of immobile ions.

However, before considering complex configurations dealing with charged particles interactions, in the present chapter, we only consider the case on species of non-charged particles and work in the frame of the mean velocity. Here, the velocity framework is centred on the particle mean velocity. Therefore, this study can be seen as a first step towards multi-species modelling since the problem investigated here contains some of the main difficulties encountered in the case of multi-species charged particles. Also, even if the long time perspective is the study of multi-species charged particles, the present approach is already relevant when considering neutral gas dynamics applications. Indeed, at our knowledge it is the first time that the M_1 angular moments model is used for the rarefied gas dynamic.

In order to derive the M_1 angular moments model in the mean velocity frame, a velocity change is considered to derived the kinetic equation in a moving frame.

Note, that rescaled velocity approaches are largely used in different context see [23, 96, 176] for example. However, the numerical treatment of the additional terms which appear when considering such a procedure on the kinetic equation can be challenging. In [95], in the context of granular flows, a numerical algorithm based on a relative energy scaling is proposed. Then, a clever de-coupling with the hydrodynamics equation is used to avoid the problems related to the change of scales in velocity variables. In this work the velocity framework is chosen centred on the mean velocity of the particles and enables the reduction of the velocity modulus grid. The Galilean invariance property for maximum entropy moments systems is discussed in details in [133]. It is shown that the choice of non-polynomial weight function leads to moments systems incompatible with the Galilean invariance property. In the present case, angular moments models are investigated, it is pointed out that working in the mean velocity enables to ensure the Galilean invariance property of the model.

The plan of this chapter is the following. First of all, the derivation of the angular M_1 moments model in the mean velocity frame is introduced. The choice of the mean velocity framework in order to enforce the Galilean invariance property of the model is highlighted. In addition, it is shown that the model rewritten in terms of the entropic variables is Friedrichs-symmetric. Also, the derivation of the associated conservation laws and the zero mean velocity condition are detailed. Secondly, a suitable numerical scheme, preserving the realisability requirement of the numerical solution for the angular M_1 moments model in the mean velocity frame is proposed. In order to enforce the correct discrete energy conservation and the zero mean velocity condition, a correction of the numerical solution is also presented. Thirdly, some numerical results obtained considering several test cases in different collisional regimes are displayed. Finally, some conclusion and perspectives are given.

7.2 Derivation of the model

Velocity change of variables procedures are used in various contexts (see [23, 95, 96, 176] for example) and can enable the simplification of a collisional operator form or the reduction of the velocity grid size used for numerical applications. In the context of angular moments models [83], it will be seen in the next section that moving frame formulations play an important role in enforcing the Galilean invariance property. In order to explain in details this point, in this section we introduce the kinetic formulation in a moving frame from which the M_1 angular moments model studied is derived.

7.2.1 Kinetic equation in a moving frame

We start considering the following kinetic equation written in the laboratory framework

$$\frac{\partial f(\alpha)}{\partial t} + div_x(vf(\alpha)) = C(f(\alpha)), \tag{7.1}$$

where f represents the particle distribution function and $\alpha = (t, x, v) \in \mathbb{R}_t^+ \times \mathbb{R}_x^3 \times \mathbb{R}_v^3$. The form of the collisional operator C is not detailed here but only the properties used in this study will be detailed.

We consider the vector $F(\alpha) \in \mathbb{R}_t^+ \times \mathbb{R}_x^3 \times \mathbb{R}_v^3$ defined as

$$F(\alpha) = \begin{pmatrix} f(\alpha) \\ vf(\alpha) \\ 0 \end{pmatrix},$$

then the kinetic equation (7.1) rewrites under the following form

$$div_\alpha(F(\alpha)) = C(f(\alpha)).$$

Introducing $\phi \in C_c^\infty(\mathbb{R}_t^+ \times \mathbb{R}_x^3 \times \mathbb{R}_v^3; \mathbb{R})$, we consider the associated weak formulation

$$\int_{\alpha \in \mathbb{R}_t^+ \times \mathbb{R}_x^3 \times \mathbb{R}_v^3} \Big(div_\alpha(F(\alpha)) - C(f(\alpha)) \Big) \phi(\alpha) d\alpha = 0,$$

which rewrites

$$\int_{\alpha \in \mathbb{R}_t^+ \times \mathbb{R}_x^3 \times \mathbb{R}_v^3} \partial_\alpha \phi(\alpha) F(\alpha) + C(f(\alpha)) \phi(\alpha) d\alpha = 0. \tag{7.2}$$

In order to derive the kinetic equation in a moving velocity frame the following set of coordinates is considered

$${}^t\beta = (\tau, y, c) = (t, x, v - u(t, x)),$$

where u is a relative velocity which depends of time and space. In particular, we define the C^1-diffeomorphism Φ as

$$\beta = \Phi(\alpha).$$

We remark here that only the velocity coordinates are transformed while time and space coordinates are kept unchanged. Eq. (7.2) considered in the new set of variables rewrites

$$\int_{\beta \in \mathbb{R}_t^+ \times \mathbb{R}_y^3 \times \mathbb{R}_c^3} \Big[\partial_\alpha \phi(\Phi^{-1}(\beta)) F(\Phi^{-1}(\beta)) + C(f(\Phi^{-1}(\beta))) \phi(\Phi^{-1}(\beta)) \Big] |\det J_{\Phi^{-1}}| d\beta = 0, \tag{7.3}$$

where $\det J_{\Phi^{-1}}$ is the determinant of the Jacobian matrix of the transformation. For this transformation $\det J_{\Phi^{-1}} = 1$, indeed the Jacobian matrix J_Φ reads

$$J_\Phi = \begin{pmatrix} 1 & 0 & 0 & 0 & 0 & 0 & 0 \\ 0 & 1 & 0 & 0 & 0 & 0 & 0 \\ 0 & 0 & 1 & 0 & 0 & 0 & 0 \\ 0 & 0 & 0 & 1 & 0 & 0 & 0 \\ -\partial_t u_1 & -\partial_{x_1} u_1 & -\partial_{x_2} u_1 & -\partial_{x_3} u_1 & 1 & 0 & 0 \\ -\partial_t u_2 & -\partial_{x_1} u_2 & -\partial_{x_2} u_2 & -\partial_{x_3} u_2 & 0 & 1 & 0 \\ -\partial_t u_3 & -\partial_{x_1} u_3 & -\partial_{x_2} u_3 & -\partial_{x_3} u_3 & 0 & 0 & 1 \end{pmatrix}.$$

The following quantities expressed in the mobile framework are introduced

$$G(\beta) = F(\Phi^{-1}(\beta)),\ \ g(\beta) = f(\Phi^{-1}(\beta)) \text{ and } \Psi(\beta) = \phi(\Phi^{-1}(\beta)).$$

In order to express $\partial_\alpha \phi(\Phi^{-1}(\beta))$, one remarks that

$$\partial_\beta \Psi(\beta) = \partial_\alpha \phi(\Phi^{-1}(\beta)) \partial_\beta (\Phi^{-1})(\beta).$$

Then by derivation of a reciprocal function

$$\partial_\beta \Phi^{-1}(\beta) = (\partial_\alpha \Phi(\Phi^{-1}(\beta)))^{-1},$$

it follows that

$$\partial_\alpha \phi(\Phi^{-1}(\beta)) = \partial_\beta \Psi(\beta)(\partial_\alpha \Phi(\Phi^{-1}(\beta))).$$

Using the two previous equations, equation (7.3) rewrites

$$\int_{\beta \in \mathbb{R}_t^+ \times \mathbb{R}_y^3 \times \mathbb{R}_c^3} \partial_\beta \Psi(\beta) \partial_\alpha \Phi(\Phi^{-1}(\beta)) G(\beta)) + C(g(\beta)) \Psi(\beta) d\beta.$$

Finally for all $\Psi(\beta) \in C_c^\infty(\mathbb{R}_\tau^+ \times \mathbb{R}_y^3 \times \mathbb{R}_c^3; \mathbb{R})$

$$\int_{\beta \in \mathbb{R}_t^+ \times \mathbb{R}_y^3 \times \mathbb{R}_c^3} \Big[div_\beta(\partial_\alpha \Phi(\Phi^{-1}(\beta)) G(\beta)) - C(g(\beta)) \Big] \Psi(\beta) d\beta = 0,$$

it follows that

$$div_\beta(\partial_\beta \Phi(\Phi^{-1}(\beta)) G(\beta)) = C(g(\beta)).$$

In the case of the present change of variables

$$\partial_\beta \Phi(\Phi^{-1}(\beta)) G(\beta) = \begin{pmatrix} g(\beta) \\ v g(\beta) \\ -(\dfrac{\partial u}{\partial t} + \dfrac{\partial u}{\partial x} v) g(\beta) \end{pmatrix}.$$

Finally, using the fact that $v = c + u(x,t)$, one obtains the kinetic equation in a moving velocity frame

$$\partial_\tau g(\beta) + div_y((c+u) g(\beta)) - div_c\Big[(\partial_\tau u + \partial_y u (c+u)) g(\beta)\Big] = C(g)(\beta).$$

Since time and space are unchanged by the change of variable

$$\partial_t g(t,x,c) + div_x((c+u)g(t,x,c)) - div_c\Big[(\partial_t u + \partial_x u(c+u))g(t,x,c)\Big] = C(g(t,x,c)). \tag{7.4}$$

This equation is used in the next sections to derive the angular M_1 moments model in a moving reference frame. Of course, an additional evolution equation is required to compute the velocity u. In this work, the velocity u is chosen as the particles mean velocity in the fixed frame (laboratory frame). In order to derive the evolution equation for u, the kinetic equation (7.1) is integrated in velocity. This leads to the following conservation laws

$$\begin{aligned} &\frac{\partial n}{\partial t} + div_x(nu) = 0, \\ &\frac{\partial (nu)}{\partial t} + div_x(\int_v fv \otimes v dv) = 0. \end{aligned} \tag{7.5}$$

Injecting the following expansion into (7.5)

$$v \otimes v = (v-u)\otimes(v-u) + (v-u)\otimes u + u \otimes (v-u) + u \otimes u,$$

and by using the following identities

$$\begin{aligned} &\int_v u \otimes u f dv = nu \otimes u, \\ &\int_v u \otimes (v-u) f dv = u \otimes \int_v (v-u) f dv = 0, \\ &\int_v (v-u) \otimes u f dv = \int_v (v-u) f dv \otimes u = 0, \end{aligned}$$

one obtains the evolution equation for u expressed in the new frame quantities

$$\frac{\partial (nu)}{\partial t} + div_x(nu \otimes u) + div_x(\int_v g(c) c \otimes c dc) = 0, \tag{7.6}$$

where

$$n = \int_c g(c) dc.$$

7.2.2 M_1 angular moments model in a moving frame

The M_1 angular moments model in a moving frame is derived by performing an angular moments extraction of the kinetic equation (7.4). One defines the following three first angular moments of the distribution function g

$$g_0(\zeta) = \zeta^2 \int_{S^2} g(\Omega,\zeta) d\Omega, \;\; g_1(\zeta) = \zeta^2 \int_{S^2} g(\Omega,\zeta)\Omega d\Omega, \;\; g_2(\zeta) = \zeta^2 \int_{S^2} g(\Omega,\zeta)\Omega\otimes\Omega d\Omega,$$

where S^2 is the unit sphere.
The complete derivation of the M_1 angular moments model in a moving frame is given in Appendix B. Removing the collisional operators contribution, the studied model reads

$$\begin{cases} \partial_t g_0 + div_x(\zeta g_1 + u g_0) - \partial_\zeta\Big(\dfrac{du}{dt}.g_1 + \zeta \partial_x u : g_2\Big) = 0, \\ \partial_t g_1 + div_x(\zeta g_2 + u \otimes g_1) - \partial_\zeta\Big(g_2 \dfrac{du}{dt} + \zeta g_3 \dfrac{\partial u}{\partial x}\Big) \\ \qquad\qquad + \dfrac{g_0 Id - g_2}{\zeta}\dfrac{du}{dt} + (\dfrac{\partial u}{\partial x} g_1 - g_3 \dfrac{\partial u}{\partial x}\Big) = 0, \end{cases} \tag{7.7}$$

where $\dfrac{du}{dt}$ is defined as

$$\frac{du}{dt} = \frac{\partial u}{\partial t} + \frac{\partial u}{\partial x} u,$$

and the third order moments g_3 as

$$g_3(\zeta) = \zeta^2 \int_{S^2} g(\Omega, \zeta)\Omega \otimes \Omega \otimes \Omega d\Omega. \tag{7.8}$$

The evolution law (7.6), expressed in terms of the angular moments rewrites

$$\frac{\partial (nu)}{\partial t} + div_x(nu \otimes u) + div_x(\int_0^{+\infty} g_2(\zeta)\zeta^2 d\zeta) = 0. \tag{7.9}$$

As explained in Chapter 2, one needs to close the set (7.7) by expressing the higher order moments g_2 and g_3 as function of g_0 and g_1. Using the M_1 minimisation problem introduced in Chapter 2, we recall that the distribution function from which the angular moments are derived writes

$$g(t, x, \zeta, \Omega) = \exp(a_0(t, x, \zeta) + a_1(t, x, \zeta).\Omega), \tag{7.10}$$

where a_0 is a scalar function and a_1 a vector valued function. Then extending the ideas of [83, 85, 160] one can show that the closure relation for g_2 is given by

$$g_2 = g_0\Big(\frac{3\chi(\alpha) - 1}{2}\frac{g_1}{|g_1|} \otimes \frac{g_1}{|g_1|} + \frac{1 - \chi(\alpha)}{2} Id\Big), \tag{7.11}$$

where

$$\chi(\alpha) = \frac{1 + |\alpha|^2 + |\alpha|^4}{3}, \qquad \alpha = g_1/g_0. \tag{7.12}$$

Similarly the higher order moment g_3 reads

$$g_3 = \Big(\frac{3|g_1| - \chi_2 g_0}{2}\Big)\frac{g_1}{|g_1|} \otimes \frac{g_1}{|g_1|} \otimes \frac{g_1}{|g_1|} + \frac{\chi_2 g_0 - |g_1|}{2}\Big(\frac{g_1}{|g_1|} \vee Id\Big), \tag{7.13}$$

with

$$\chi_2(\alpha) = \frac{3|\alpha| - |\alpha|^3 + 3|\alpha|^5}{5},$$

and

$$\begin{aligned}\frac{g_1}{|g_1|} \vee Id =& \frac{g_1}{|g_1|} \otimes e_1 \otimes e_1 + e_1 \otimes \frac{g_1}{|g_1|} \otimes e_1 + e_1 \otimes e_1 \otimes \frac{g_1}{|g_1|} \\ &+ \frac{g_1}{|g_1|} \otimes e_2 \otimes e_2 + e_2 \otimes \frac{g_1}{|g_1|} \otimes e_2 + e_2 \otimes e_2 \otimes \frac{g_1}{|g_1|} \\ &+ \frac{g_1}{|g_1|} \otimes e_3 \otimes e_3 + e_3 \otimes \frac{g_1}{|g_1|} \otimes e_3 + e_3 \otimes e_3 \otimes \frac{g_1}{|g_1|}.\end{aligned}$$

Before studying the models properties, the realisability conditions associated to the model (7.7) are introduced

$$\mathcal{A} = \Big((g_0, g_1) \in \mathbb{R}^2,\ g_0 \geq 0,\ \ |g_1| \leq g_0\Big). \tag{7.14}$$

Since the distribution function g is a nonnegative quantity the realisability conditions (7.14) naturally needs to be satisfied. In addition, these conditions are related to the existence of a nonnegative distribution function from which the angular moments can be derived [182].

7.3 Model properties

In this section the main properties of the angular M_1 model in a moving frame (7.7-7.9) are presented. It is first proved that the choice of working in the mean velocity frame enables to ensure the Galilean invariance property of the model. Secondly it is shown that this model, rewritten in terms of entropic variables, is Friedrichs-symmetric. Finally, the derivation of the conservation laws is detailed.

7.3.1 Galilean invariance property

Galilean invariance is a fundamental feature of the Boltzmann equation. Following [133], we start defining translational and rotational transformations. For any vector $s \in \mathbb{R}^d$ and any rotation matrix $R \in SO(d)$

$$(\mathcal{T}_s f)(v) = f(v - s), \qquad (\mathcal{T}_R f)(v) = f(Rv), \qquad v \in \mathbb{R}^d.$$

The following translational and rotational invariance properties of the collisional operator C are considered

$$\mathcal{T}_s C(f) = C(\mathcal{T}_s(f)), \qquad \mathcal{T}_R C(f) = C(\mathcal{T}_R(f)). \tag{7.15}$$

Note that the Boltzmann collision operator or the BGK collision operator satisfy such properties. Using equation (7.15) the Galilean invariance property of the kinetic

equation (7.1) can be shown. Indeed, the reference coordinates system (t, x, v) and a new set of coordinates $(t, \tilde{x}, \tilde{v})$ can be linked by the following relations

$$\tilde{x} = Rx - st, \qquad \tilde{v} = Rv - s, \tag{7.16}$$

for any constant vector $s \in \mathbb{R}^d$. Distribution function $\tilde{f}$ in the moving frame is defined as

$$\tilde{f}(t, \tilde{x}, \tilde{v}) = f(t, x, v).$$

Consequently the following relations can be derived

$$\partial_t f(t, x, v) = \partial_t \tilde{f}(t, \tilde{x}, \tilde{v}) - s.\partial_x \tilde{f}(t, \tilde{x}, \tilde{v}), \qquad \partial_x f(t, x, v) = R\partial_{\tilde{x}} \tilde{f}(t, \tilde{x}, \tilde{v}).$$

Therefore using (7.1), it follows that $\tilde{f}$ satisfies

$$\partial_t \tilde{f}(t, \tilde{x}, \tilde{c}) + div_{\tilde{x}}(\tilde{v}\tilde{f}(t, \tilde{x}, \tilde{c})) = C(\tilde{f}(t, \tilde{x}, \tilde{c})), \tag{7.17}$$

which shows the Galilean invariance of (7.1).

The same property cannot be directly obtained when considering angular moments models. Indeed, when integrating (7.1) on the unit sphere and applying the change of variables (7.16) on the resulting M_1 angular moments model gives nonlinear terms and one observes that the form of the M_1 model is not invariant. In order to overcome this drawback, in this study, we propose to not derive the M_1 angular moments model from the kinetic equation (7.1) but from the kinetic equation (7.4) which is expressed in a mobile reference frame. In particular, in this work the velocity u used in (7.4) is chosen as the particles mean velocity defined by

$$u = \frac{1}{n} \int_{\mathbb{R}^3} f(v) v dv. \tag{7.18}$$

In order to show the advantage in deriving the M_1 angular moments model from the kinetic equation (7.4), the kinetic equation (7.17) is rewritten in its mean velocity frame. This second kinetic equation expressed in a mobile frame reads

$$\begin{aligned} \partial_t \tilde{g}(t, \tilde{x}, \tilde{c}) + div_{\tilde{x}}((\tilde{c} + \tilde{u})\tilde{g}(t, \tilde{x}, \tilde{c})) - div_{\tilde{c}}\big[(\partial_t \tilde{u} + \partial_{\tilde{x}} \tilde{u}(\tilde{c} + \tilde{u}))\tilde{g}(t, \tilde{x}, \tilde{x})\big] \\ = C(\tilde{g}(t, \tilde{x}, \tilde{c})), \end{aligned} \tag{7.19}$$

where

$$\tilde{u} = \frac{1}{n} \int_{\mathbb{R}^3} \tilde{f}(\tilde{v}) \tilde{v} d\tilde{v}. \tag{7.20}$$

The key point which will be useful when considering angular moments models is the relation between the two kinetic equations (7.4) and (7.19). Indeed, the two relative velocities u and $\tilde{u}$ are linked through the following relation

$$\tilde{u} = Ru - s. \tag{7.21}$$

Therefore, we propose to consider the following change of variable

$$\tilde{x} = Rx - st, \quad \tilde{c} = Rc, \quad \tilde{u} = Ru - s. \tag{7.22}$$

Indeed, by injecting the change of variable (7.21-7.22) into (7.4) and using the following relations

$$\begin{aligned} \partial_t u &= {}^tR(\partial_t \tilde{u} - (\partial_{\tilde{x}} \tilde{u})s), \\ \partial_x u &= {}^tR(\partial_{\tilde{x}} \tilde{u})R, \end{aligned} \tag{7.23}$$

and

$$\begin{aligned} \partial_t g &= \partial_t \tilde{g} - (\partial_{\tilde{x}} \tilde{g})s, \\ \partial_x g &= (\partial_{\tilde{x}} \tilde{g})R, \\ \partial_c g &= (\partial_{\tilde{c}} \tilde{g})R, \end{aligned} \tag{7.24}$$

a direct calculation enables to recover equation (7.19). The relationships between the different studied framework are summarised on Fig 7.1. The starting point is the kinetic equation (7.1) expressed in the fixed frame, denoted A_0. Since this kinetic equation is Galilean invariant, one obtains (7.17) denoted B_0, by using (7.16). Secondly, the kinetic equation in a mobile frame (7.4) denoted A has been derived. In the present case u is the particles mean velocity defined in (7.18). The same procedure can be applied on (7.17) to obtain (7.19), denoted B. Finally, one remarks that (7.4) and (7.19), denoted A and B are linked by the change of variable (7.22). The change of variables (7.22) makes the link between equations (7.4) and (7.19)

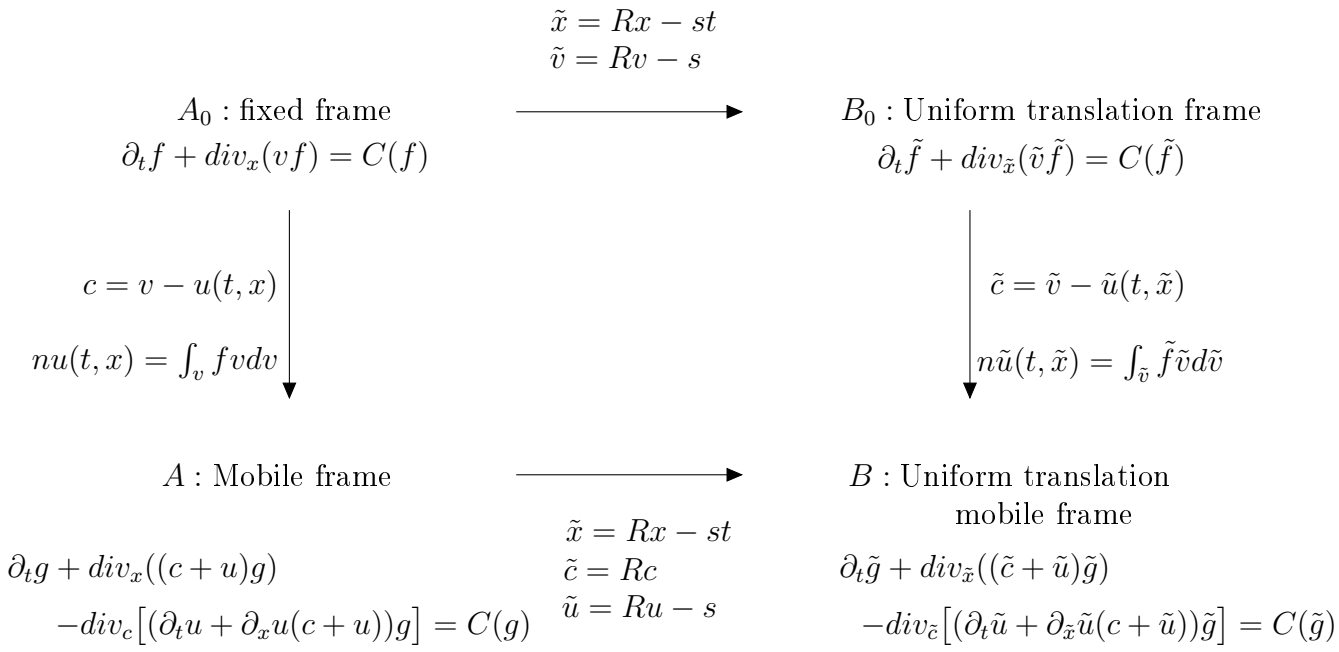

Figure 7.1: Diagram relation between the different frames

relevant when considering angular moments models. Indeed, this change of variable

also enables to link the angular M_1 model derived from the kinetic equation (7.4) to the angular M_1 model derived from the kinetic equation (7.19). This point is detailed in the following result.

Theorem 7.1. *(Galilean invariance property)*
The form of the M_1 angular moments model (7.7-7.9) expressed in the mean velocity frame is invariant by rotational and translational transformations.

Proof. Before showing the Galilean invariance property of the M_1 angular moments model (7.7-7.9), we define the quantities in the new frame. Consider the velocity modulus $\tilde{\zeta}$ and $\tilde{\Omega}$ the angular direction in the mobile frame

$$\tilde{\zeta} = |\tilde{c}|, \qquad \tilde{c} = \tilde{\zeta}\tilde{\Omega},$$

we define the two first angular moments $\tilde{g}_0$ and $\tilde{g}_1$ in the mobile frame

$$\tilde{g}_0 = \tilde{\zeta}^2 \int_{\tilde{S}_2} \tilde{g}(t,\tilde{x},\tilde{c}) d\tilde{\Omega}, \qquad \tilde{g}_1 = \tilde{\zeta}^2 \int_{\tilde{S}_2} \tilde{g}(t,\tilde{x},\tilde{c}) \tilde{\Omega} d\tilde{\Omega}.$$

Using the fact that

$$\tilde{\zeta} = \zeta, \qquad \tilde{\Omega} = R\Omega, \tag{7.25}$$

and the equations (7.24), the following relations can be derived

$$\begin{aligned} \tilde{g}_0 &= g_0, \\ \partial_t g_0 &= \partial_t \tilde{g}_0 - \partial_{\tilde{x}} \tilde{g}_0 s, \\ \partial_x g_0 &= \partial_{\tilde{x}} \tilde{g}_0 R, \\ \partial_\zeta g_0 &= \partial_{\tilde{\zeta}} \tilde{g}_0, \end{aligned} \tag{7.26}$$

and

$$\begin{aligned} g_1 &= R\tilde{g}_1, \\ \partial_t g_1 &= {}^tR(\partial_t \tilde{g}_1 - \partial_{\tilde{x}} \tilde{g}_1 s), \\ \partial_x g_1 &= {}^tR \partial_{\tilde{x}} \tilde{g}_1 R, \\ \partial_\zeta g_1 &= {}^tR \partial_{\tilde{\zeta}} \tilde{g}_1. \end{aligned} \tag{7.27}$$

Using the definition of $\tilde{g}_2$, we remark that

$$\begin{aligned} \tilde{g}_2 &= \tilde{\zeta}^2 \int_{\tilde{S}_2} \tilde{g}(t,\tilde{x},\tilde{c}) \tilde{\Omega} \otimes \tilde{\Omega} d\tilde{\Omega} \\ &= \zeta^2 \int_{\tilde{S}_2} \tilde{g}(t,\tilde{x},\tilde{c}) R\tilde{\Omega} \otimes \tilde{\Omega}\, {}^tR d\tilde{\Omega}. \end{aligned} \tag{7.28}$$

Then injecting (7.26-7.27) into the first equation of (7.7) and using (7.28) and (7.23) a direct calculation gives

$$\partial_t \tilde{g}_0 + div_x(\tilde{\zeta}\tilde{g}_1 + \tilde{u}\tilde{g}_0) - \partial_{\tilde{\zeta}}\Big(\frac{d\tilde{u}}{dt}.\tilde{g}_1 + \tilde{\zeta}\partial_{\tilde{x}}\tilde{u} : \tilde{g}_2\Big) = 0.$$

In order to deal with the second equation of (7.7), we remark that using (7.25) the ijk^{th} component of the higher order moments g_3 defined in (7.8) rewrites

$$g_{3ijk} = \sum_{l,m,n} \tilde{\zeta}^2 \int_{\tilde{S}_2} {}^tR_{il}\, {}^tR_{jm}\, {}^tR_{kn} (\tilde{\Omega} \otimes \tilde{\Omega} \otimes \tilde{\Omega})_{lmn} d\tilde{\Omega}. \tag{7.29}$$

Therefore, using (7.28) and (7.29) a direct calculation gives

$$div_x g_2 = {}^tR\, div_{\tilde{x}} \tilde{g}_2, \tag{7.30}$$

and

$$g_3 \frac{\partial u}{\partial x} = {}^tR\, \tilde{g}_3 \frac{\partial \tilde{u}}{\partial \tilde{x}}. \tag{7.31}$$

Consequently injecting (7.26-7.27) into the second equation of (7.7) and using the relations (7.23,7.30) and (7.31), one obtains

$$\begin{cases} \partial_t \tilde{g}_1 + div_{\tilde{x}}(\tilde{\zeta}\tilde{g}_2 + \tilde{u} \otimes \tilde{g}_1) - \partial_{\tilde{\zeta}} \Big(\tilde{g}_2 \dfrac{d\tilde{u}}{dt} + \tilde{\zeta}\tilde{g}_3 \dfrac{\partial \tilde{u}}{\partial \tilde{x}} \Big) \\ \qquad\qquad + \dfrac{\tilde{g}_0 Id - \tilde{g}_2}{\tilde{\zeta}} \dfrac{d\tilde{u}}{dt} + \Big(\dfrac{\partial \tilde{u}}{\partial \tilde{x}} \tilde{g}_1 - \tilde{g}_3 \dfrac{\partial \tilde{u}}{\partial \tilde{x}} \Big) = 0. \end{cases}$$

□

7.3.2 Symmetrization property

In this section it is shown that the M_1 model in a moving frame (7.7-7.9) written in terms of the entropic variables is Friedrichs symmetric. Following [160], the M_1 model in a moving frame (7.7) can be rewritten in terms of the entropic variables a_0 and a_1. This procedure is sometimes called a Godunov's symmetrisation [108].

Theorem 7.2. *The M_1 model in a moving frame (7.7-7.9) written in terms of the variables a_0 and a_1 is Friedrichs symmetric.*

Proof. Setting

$${}^tm = (1, \Omega), \qquad {}^t\alpha = (\alpha_0, \alpha_1),$$

the distribution function (7.10) reads

$$g(t, x, \zeta, \Omega) = \exp(\alpha.m),$$

and the solution of (7.7)-(7.11)-(7.13) writes

$${}^t(g_0, g_1) = \langle \zeta^2 \exp(\alpha.m) m \rangle,$$

where the notation $\langle . \rangle$ refers to the angular integration on the unit sphere. Consequently, after a direct calculation, the M_1 angular moments model in a moving frame (7.7) rewrites

$$A_0(\alpha)\partial_t \begin{pmatrix} \alpha_0 \\ \alpha_1 \end{pmatrix} + \sum_j A_j(\alpha)\partial_{x_j} \begin{pmatrix} \alpha_0 \\ \alpha_1 \end{pmatrix} + B(\alpha)\partial_\zeta \begin{pmatrix} \alpha_0 \\ \alpha_1 \end{pmatrix} + S(x,\zeta,\alpha) = \begin{pmatrix} 0 \\ 0 \end{pmatrix}, \quad (7.32)$$

where

$$\begin{aligned} A_0(\alpha) &=< \exp(\alpha.m) \begin{pmatrix} 1 & {}^t\Omega \\ \Omega & \Omega \otimes \Omega \end{pmatrix} >, \\ A_j(\alpha) &=< (\zeta\Omega_j + u_j) \exp(\alpha.m) \begin{pmatrix} 1 & {}^t\Omega \\ \Omega & \Omega \otimes \Omega \end{pmatrix} >, \\ B(\alpha) &=< -(\zeta^2 \frac{du}{dt}.\Omega + \zeta^3 \frac{\partial u}{\partial x} : \Omega \otimes \Omega) \exp(\alpha.m) \begin{pmatrix} 1 & {}^t\Omega \\ \Omega & \Omega \otimes \Omega \end{pmatrix} >, \end{aligned}$$

and

$$S(x,\zeta,\alpha) = \begin{pmatrix} (div_x u) g_0 - \frac{2}{\zeta}\frac{du}{dt}.g_1 - 3\frac{\partial u}{\partial x} : g_2 \\ \frac{\partial u}{\partial x} g_1 - \frac{2}{\zeta} g_2 \frac{du}{dt} - 3 g_3 \frac{\partial u}{\partial x} + \frac{g_0 Id - g_2}{\zeta}\frac{du}{dt} + (\frac{\partial u}{\partial x} g_1 - g_3 \frac{\partial u}{\partial x}) \end{pmatrix}.$$

Since $A_0(\alpha)$ is a positive-definite symmetric matrix and $A_j(\alpha)$ and $B(\alpha)$ are symmetric matrices, one obtains that the system (7.32) is Friedrichs-symmetric [15, 98]. □

7.3.3 Conservation laws

In this section the derivation of the conservation laws derived from the angular M_1 model in a moving frame (7.7) is detailed.
Before deriving the mass and energy conservation equations, we point out that in this work the velocity u is chosen as the particles mean velocity. Therefore, in the considered framework the mean velocity is equal to zero. This point is expressed by the following condition

$$\int_0^{+\infty} g_1(t,x,\zeta)\zeta d\zeta = 0. \quad (7.33)$$

Multiplying the second equation of (7.7) by ζ and integrating in ζ, one shows using Green's formula that all the terms vanish two by two and that condition (7.33) is preserved over times.
The derivation of the mass conservation equation can be directly obtained by direct integration in ζ. Indeed, integrating the first equation of (7.7) in ζ, one obtains

$$\partial_t n + div_x(nu) = 0, \quad (7.34)$$

where condition (7.33) has been used.
In order to derive the energy conservation equation, one starts multiplying the first

equation of (7.7) by $\frac{m}{2}\zeta^2$ and integrate in ζ to obtain the following internal energy equation

$$\partial_t(\frac{1}{2}\int_0^{+\infty} g_0\zeta^2 d\zeta) + div_x(\frac{1}{2}\int_0^{+\infty} g_1\zeta^3 d\zeta + u\frac{1}{2}\int_0^{+\infty} g_0\zeta^2 d\zeta) + (\partial_x u : \int_0^{+\infty} g_2\zeta^2 d\zeta) = 0. \tag{7.35}$$

One notices that since the mean velocity frame is considered, only an equation on the internal energy is obtained. The kinetic energy equation is derived from the evolution equation (7.9) and writes

$$\partial_t(nu^2) + div_x(\frac{nu^2}{2}u) + u.div_x(\int_0^{+\infty} g_2\zeta^2 d\zeta) = 0. \tag{7.36}$$

The energy conservation equation is directly obtained by summing equation (7.35) with equation (7.36).

7.4 Numerical scheme

In this part an appropriate numerical scheme is proposed for the M_1 model in a moving framework in an one dimensional spatial geometry considering a standard BGK collision operator [111]. In this case, the collisional operator $C(f)$ used in (7.1) is specified

$$C(f) = \frac{1}{\tau}(M_f - f),$$

with

$$M_f(v) = \frac{n}{(2\pi T)^{3/2}}\exp(-\frac{(v-u)^2}{2T}),$$

and τ is a collisional parameter which is fixed depending of the collisional regime studied. In this case the M_1 model in a moving framework (7.7) writes

$$\begin{cases} \partial_t g_0 + \partial_x(\zeta g_1 + u g_0) - \partial_\zeta\Big(\frac{du}{dt}g_1 + \zeta\frac{\partial u}{\partial x}g_2\Big) = \frac{1}{\tau}(M_{g_0} - g_0), \\ \partial_t g_1 + \partial_x(\zeta g_2 + u g_1) - \partial_\zeta\Big(\frac{du}{dt}g_2 + \zeta\frac{\partial u}{\partial x}g_3\Big) + \frac{du}{dt}\frac{g_0 - g_2}{\zeta} \\ \qquad\qquad + \frac{\partial u}{\partial x}(g_1 - g_3) = -\frac{1}{\tau}g_1, \end{cases} \tag{7.37}$$

where

$$M_{g_0} = 4\pi\zeta^2\frac{n}{(2\pi T)^{3/2}}\exp(-\frac{\zeta^2}{2T}).$$

7.4.1 Derivation of the numerical scheme

In order to derive a suitable numerical scheme for the model (7.37) which preserves the admissibility of the solution, the different terms of (7.37) are studied separately. Then the admissibility requirement of the complete scheme is shown under a reduced CFL condition.

Step 1: the first intermediate state is the following

$$\begin{cases} \partial_t g_0 + \partial_x(\zeta g_1 + u g_0) = 0, \\ \partial_t g_1 + \partial_x(\zeta g_2 + u g_1) = 0. \end{cases} \tag{7.38}$$

In order to derive a numerical scheme preserving the realisability of the numerical solution, we consider an underlying kinetic model from which the system (7.38) can be derived by direct angular moments extraction

$$\partial_t F(t,x) + \partial_x(a(x)F(t,x)) = 0, \tag{7.39}$$

with $F = \zeta^2 f$, $a(x) = \zeta\mu + u(x)$ and $\mu \in [-1,1]$. Note that μ is the angular variable in the case of one space dimension.

A natural conservative numerical scheme is proposed for the kinetic equation (7.39)

$$\frac{F_i^{n+1} - F_i^n}{\Delta t} + \frac{h_{i+1/2}^n - h_{i-1/2}^n}{\Delta x} = 0, \tag{7.40}$$

with

$$h_{i+1/2}^n = a_{i+1/2}^- F_{i+1}^n + a_{i+1/2}^+ F_i^n,$$

and $a^\pm = \dfrac{1}{2}(a \pm |a|)$.
Rewriting equation (7.40) as a convex combination

$$\begin{aligned} F_i^{n+1} = F_i^n &\Big(1 - \frac{\Delta t}{2\Delta x}(a_{i+1/2} - a_{i-1/2}) - \Delta t \frac{|a_{i+1/2}| + |a_{i-1/2}|}{2\Delta x}\Big) \\ &+ F_{i+1}^n \frac{2\Delta t}{\Delta x}\Big(|a_{i+1/2}| - a_{i+1/2}\Big) \\ &+ F_{i-1}^n \frac{2\Delta t}{\Delta x}\Big(|a_{i-1/2}| - a_{i-1/2}\Big), \end{aligned} \tag{7.41}$$

it follows that the positivity of the numerical distribution function is ensured under the following CFL condition

$$\Delta t_1 \leq \frac{\Delta x}{2||u||_\infty + \zeta}. \tag{7.42}$$

The numerical scheme (7.41) rewrites on the following viscous form

$$\begin{aligned}\frac{F_i^{n+1}-F_i^n}{\Delta t}+\frac{a_{i+1/2}F_{i+1}^n+(a_{i+1/2}-a_{i-1/2})F_i^n-a_{i-1/2}F_{i-1}^n}{2\Delta x}\\ -\frac{|a_{i+1/2}|F_{i+1}^n-(|a_{i+1/2}|+|a_{i-1/2}|)F_i^n+|a_{i-1/2}|F_{i-1}^n}{2\Delta x}=0.\end{aligned} \tag{7.43}$$

The angular integration can not be directly performed on the scheme (7.43) because of the angular variable μ which appears in the term $|a|$ in the numerical viscosity. Therefore we modify (7.43) and consider the following scheme which is suitable for the angular integration.

$$\begin{aligned}\frac{F_i^{n+1}-F_i^n}{\Delta t}+\frac{a_{i+1/2}F_{i+1}^n+(a_{i+1/2}-a_{i-1/2})F_i^n-a_{i-1/2}F_{i-1}^n}{2\Delta x}\\ -||a||_\infty\frac{F_{i+1}^n-2F_i^n+F_{i-1}^n}{2\Delta x}=0.\end{aligned} \tag{7.44}$$

Remark 7.3. *Considering (7.44), one observes that the numerical viscosity of the scheme is increased in order to enable the angular integration.Therefore the numerical scheme still preserves the nonnegativity of the numerical solution under CFL condition (7.42).*

The angular integration of the scheme (7.44) leads to a natural discretisation for the intermediate state (7.38)

$$\begin{aligned}&\frac{g_{0i}^{n+1}-g_{0i}^n}{\Delta t}\\ &+\frac{(\zeta g_{1i+1}^n+u_{i+1/2}g_{0i+1}^n)+((\zeta g_{1i}^n+u_{i+1/2}g_{0i}^n)-(\zeta g_{1i}^n+u_{i-1/2}g_{0i}^n))-(\zeta g_{1i}^n+u_{i-1/2}g_{0i-1}^n)}{2\Delta x}\\ &-(\zeta+||u||_\infty)\frac{g_{0i+1}^n-2g_{0i}^n+g_{0i-1}^n}{2\Delta x}=0,\end{aligned} \tag{7.45}$$

$$\begin{aligned}&\frac{g_{1i}^{n+1}-g_{1i}^n}{\Delta t}\\ &+\frac{(\zeta g_{2i+1}^n+u_{i+1/2}g_{1i+1}^n)+((\zeta g_{2i}^n+u_{i+1/2}g_{1i}^n)-(\zeta g_{2i}^n+u_{i-1/2}g_{1i}^n))-(\zeta g_{2i}^n+u_{i-1/2}g_{1i-1}^n)}{2\Delta x}\\ &-(\zeta+||u||_\infty)\frac{g_{1i+1}^n-2g_{1i}^n+g_{1i-1}^n}{2\Delta x}=0.\end{aligned} \tag{7.46}$$

Remark 7.4. *Computing $g_0^{n+1}+g_1^{n+1}$ and $g_0^{n+1}-g_1^{n+1}$, one can show the scheme (7.45-7.46) preserves the realisability requirement of the numerical solution under the CFL condition (7.42).*

Step 2: the second intermediate step we consider writes

$$\begin{cases}\partial_t g_0-\partial_\zeta(\dfrac{du}{dt}g_1+\zeta\partial_x u g_2)=0,\\ \partial_t g_1-\partial_\zeta(g_2\dfrac{du}{dt}+\zeta g_3\partial_x u)=0.\end{cases} \tag{7.47}$$

Following the same procedure than for the first intermediate state, the following underlying kinetic model is proposed

$$\partial_t F(\zeta) - \partial_\zeta((\frac{du}{dt}\mu + \zeta\partial_x u\mu^2)F(\zeta)) = 0,$$

with the following corresponding scheme

$$\begin{aligned}\frac{F_j^{n+1} - F_j^n}{\Delta t} + \frac{b_{j+1/2}F_{j+1}^n + (b_{j+1/2} - b_{j-1/2})F_j^n - b_{j-1/2}F_{j-1}^n}{2\Delta\zeta} \\ - ||b||_\infty \frac{F_{j+1}^n - 2F_j^n + F_{j-1}^n}{2\Delta\zeta} = 0,\end{aligned} \tag{7.48}$$

with $b = \frac{du}{dt}\mu + \zeta\partial_x u\mu^2$. The CFL condition associated reads

$$\Delta t_2 \leq \frac{\Delta\zeta}{2(||\frac{du}{dt}||_\infty + \zeta||\partial_x u||_\infty)}. \tag{7.49}$$

The angular integration of (7.48) leads to the following discretisation for the intermediate state (7.47)

$$\begin{aligned}&\frac{g_{0j}^{n+1} - g_{0j}^n}{\Delta t} \\ &+ \frac{(\frac{du}{dt}g_{1i+1}^n - \zeta_{j+1/2}\partial_x u g_{2j+1}^n) + ((\frac{du}{dt}g_{1j}^n - \zeta_{j+1/2}\partial_x u g_{2j}^n) - (\frac{du}{dt}g_{1j}^n - \zeta_{j-1/2}\partial_x u g_{2j}^n))}{2\Delta\zeta} \\ &- \frac{(\frac{du}{dt}g_{1j-1}^n - \zeta_{j-1/2}\partial_x u g_{2j-1}^n)}{2\Delta\zeta} - (|\frac{du}{dt}| + ||\zeta||_\infty|\partial_x u|)\frac{g_{0j+1}^n - 2g_{0j}^n + g_{0j-1}^n}{2\Delta\zeta} = 0,\end{aligned} \tag{7.50}$$

$$\begin{aligned}&\frac{g_{1j}^{n+1} - g_{1j}^n}{\Delta t} \\ &+ \frac{(\frac{du}{dt}g_{2j+1}^n - \zeta_{j+1/2}\partial_x u g_{3j+1}^n) + ((\frac{du}{dt}g_{2j}^n - \zeta_{j+1/2}\partial_x u g_{3j}^n) - (\frac{du}{dt}g_{2j}^n - \zeta_{j-1/2}\partial_x u g_{3j}^n))}{2\Delta\zeta} \\ &- \frac{(\frac{du}{dt}g_{2j-1}^n - \zeta_{j-1/2}\partial_x u g_{3j-1}^n)}{2\Delta\zeta} - (|\frac{du}{dt}| + ||\zeta||_\infty|\partial_x u|)\frac{g_{1j+1}^n - 2g_{1j}^n + g_{1j-1}^n}{2\Delta\zeta} = 0.\end{aligned} \tag{7.51}$$

Remark 7.5. *The scheme (7.50-7.51) preserves the realisability domain under the CFL condition (7.49).*

Step 3: the third state we consider is the following

$$\begin{cases}\partial_t g_0 = 0, \\ \partial_t g_1 + \frac{g_0 - g_2}{\zeta}\frac{du}{dt} = 0.\end{cases}$$

We choose the following classical scheme for this first model

$$\begin{cases} g_{0ij}^{n+1} = g_{0ij}^{n}, \\ g_{1ij}^{n+1} = g_{1ij}^{n} - \Delta t \dfrac{g_{0ij} - g_{2ij}}{\zeta_j} (\dfrac{du}{dt})_i. \end{cases}$$

Remark 7.6. *This scheme preserves the realisability conditions under CFL conditions*

$$\Delta t_3 \leq \frac{\zeta}{|\dfrac{du}{dt}|} \frac{1+\alpha}{1-\chi(\alpha)},$$

where α is defined by (7.12).

Proof. This result is directly obtained by computing $g_{0i}^{n+1} \pm g_{1i}^{n+1}$. □

Remark 7.7. *One remarks that the term $\dfrac{1+\alpha}{1-\chi(\alpha)}$ does not tend to zero as α tends to -1. Indeed, using the definition of χ given in (7.12), one can show that $\dfrac{1+\alpha}{1-\chi(\alpha)}$ tends to $1/2$ as α tends to -1.*

Step 4: the fourth intermediate step we consider writes

$$\begin{cases} \partial_t g_0 = 0, \\ \partial_t g_1 + \partial_x u (g_1 - g_3) = 0. \end{cases}$$

Following the third step we propose

$$\begin{cases} g_{0i}^{n+1} = g_{0i}^{n}, \\ g_{1i}^{n+1} = g_{1i}^{n} + \Delta t (\partial_x u)_i (g_{1i} - g_{3i}). \end{cases}$$

Remark 7.8. *This scheme preserves the realisability conditions under CFL conditions*

$$\Delta t_4 \leq \frac{1}{|\partial_x u|} \frac{1+\alpha}{\alpha - \chi_2(\alpha)}.$$

Using the definition of χ_2, we remark that $\dfrac{1+\alpha}{\alpha - \chi_2(\alpha)}$ tends to $-1/2$ as α tends to -1.

In order to derive a admissible numerical scheme for the complete model (7.37), we propose to consider the following time semi-discretisation

$$U^{n+1} = U^n + \Delta t \sum_{k=1}^{N} F_k(U^n), \tag{7.52}$$

where

$$U^{n+1} = \begin{pmatrix} g_0^{n+1} \\ g_1^{n+1} \end{pmatrix},$$

F_k represents the discretisation proposed for the k^{th} intermediate step and N is the number of intermediate step considered. Equation (7.52) rewrites under the form of a convex combination

$$U^{n+1} = \sum_{k=1}^{N} \frac{1}{N}[U^n + (N\Delta t)F_k(U^n)]. \tag{7.53}$$

Setting $\tilde{\Delta}t = N\Delta t$, one shows that if each intermediate step

$$\tilde{U}^{n+1} = U^n + \tilde{\Delta}tF_k(U^n),$$

preserves the realisability conditions of the numerical solution under CFL condition

$$\tilde{\Delta}t \leq C_k.$$

Therefore the general scheme (7.52) preserves the realisability conditions of the numerical solution under the following CFL condition

$$\Delta t \leq \min_k(\frac{C_k}{N}).$$

The following result is then obtained

Theorem 7.9. *The general scheme (7.52) preserves the realisability conditions under the following CFL condition*

$$\Delta t \leq \frac{1}{4}\min(\Delta t_1, \Delta t_2, \Delta t_3, \Delta t_4). \tag{7.54}$$

Proof. Each step preserves the realisability conditions under CFL condition. Therefore, by convexity of the admissible set, considering the convex combination (7.53) and using the condition (7.4.1), we directly obtain that the general scheme (7.52) preserves the realisability conditions under the CFL condition (7.54). □

The discretisation of the collision operator is performed by using a standard implicit scheme. For the numerical test presented in the next section, an usual second order Van Leer's slope limiter [154] is used.

7.4.2 Enforcement of the discrete energy conservation and zero mean velocity condition

In this section, the enforcement of the discrete energy conservation and zero mean velocity condition is discussed. In a recent work [185], a numerical scheme has been proposed to enforce the discrete zero mean velocity condition considering a kinetic equation. However, this strategy does not directly apply in the present case

since a nonlinear set of equations (7.37) is considered associated to the realisability conditions (7.14). The enforcement of the discrete energy conservation and the zero mean velocity condition while preserving realisability conditions (7.14) of the numerical solution is particularly challenging and beyond the scope of the present study. However, in order to be able to present numerical results, in this section a correction of the numerical solution is proposed.

In order to enforce the correct energy conservation, we start considering the following conservation laws associated to (7.37)

$$\begin{cases} \partial_t \rho + div_x(\rho u) = 0, \\ \partial_t(\rho u) + div_x(\rho u \otimes u + p - s) = 0, \\ \partial_t E + div_x((E + p - s)u + q) = 0, \end{cases} \tag{7.55}$$

where E is the total energy. The pressure tensor p, the stress tensor s and the heat flux q expressed in terms of the angular moments read

$$p - s = \frac{m}{2}\int_0^{+\infty} g_2 \zeta^2 d\zeta, \qquad q = \frac{m}{2}\int_0^{+\infty} g_1 \zeta^3 d\zeta.$$

At each time time step, the set of conservation laws (7.55) is numerically solved. Then the numerical solution is corrected by using

$$g_{0p} = \alpha \exp(\beta {\zeta_p}^2)\bar{g}_{0p}, \qquad \forall p \in \{1; ...; pf\},$$

where g_0 is the corrected solution and $\bar{g}_0$ the solution which requires a correction computed with the scheme (7.52). The coefficients α and β are numerically computed such that

$$m\sum_{p=1}^{pf} g_{0p}\Delta\zeta = \rho, \qquad \frac{m}{2}\sum_{p=1}^{pf} g_{0p}\zeta_p^2\Delta\zeta = E - \frac{\rho u^2}{2},$$

where the quantities E, $\frac{\rho u^2}{2}$ and ρ are known at each time step since the set (7.55) has been numerically solved. This procedure enables the enforcement of the correct energy conservation. As it will be shown in the next section this correction is important for the numerical results, in particular in order to numerically capture shock waves.

In order to enforce the zero mean velocity condition (7.33) at the discrete level, one could think in proposing an adapted discretisation for the source terms which appears in the second equation of (7.37). However, this procedure leads to an unsuitable CFL condition when considering the realisability requirements (7.14) for the numerical solution. Therefore the following correction is proposed based on the resolution of the convex optimisation problem

$$\min_{g_1 \in \mathbb{R}^{pf}} \frac{1}{2}||g_1 - \bar{g}_1||_{L^2}^2 = 0,$$

under equality constraint

$$\sum_{p=1}^{pf} g_{1p}\zeta_p \Delta\zeta = 0,$$

where g_1 is the corrected solution and $\bar{g}_1$ the solution before correction given by the scheme (7.52). One observes that this procedure does not enforce the realisable conditions of the numerical solutions. In such unfortunate case, g_1 is simply projected on the realisable set.

7.5 Numerical results

In this section, several test cases are presented. Depending on the regime considered, the numerical results obtained with the scheme introduced in the previous part for the angular M_1 moments model in a moving frame, denoted M_1 mobile, are compared either with an exact solution or with a kinetic reference solution. The results are given with and without the correction procedure. In the following, the kinetic solution has been obtained considering a standard kinetic 1D3V BGK model using an usual Lax-Friedrichs scheme with the second order Van Leer's slope limiter [154]. The results obtained with this scheme are denoted BGK 1D3V. In addition, the results obtained considering a second order HLL scheme for the Euler equations using the second order Van Leer's slope limiter are also given. These results obtained using this scheme are denoted Euler.

Test 1: Temperature gradient test case in different collisional regimes.

The first test case we study consists in considering a strong temperature gradient at initial time and studying the temporal evolution of density, velocity and temperature. The initial distribution function is supposed to be a Maxwellian distribution function defined by

$$f_{ini}(x,v) = \frac{n_{ini}(x)}{(2\pi T_{ini}(x))^{3/2}} \exp\Big(- \frac{(v-u_{ini}(x))^2}{2T_{ini}(x)}\Big),$$

with

$$n_{ini}(x) = 1, \;\; u_{ini}(x) = 0, \;\; T_{ini}(x) = 2 - \arctan(x).$$

The space range chosen is $[-40, 40]$, and the velocity range $[-15, 15]^3$. For the present test case, 400 cells in space and 200^3 cells in velocity have been considered for the 1D3V BGK kinetic approach. Also, 400 cells in space and 200 cells in velocity modulus have been considered for the M_1 mobile scheme. Finally, 400 cells in space have been considered for the Euler description.
Neumann boundary conditions are considered, the values in the boundary ghost cells set to the values in the corresponding real boundary cells.

1.a Fluid regime.
The first regime we consider is the fluid regime, then the collisional parameter τ is set equal to zero. In Figure 7.2, the density, velocity and temperature profiles are displayed at time $t = 10$ for the kinetic BGK 1D3V scheme in continuous blue, the M_1 mobile scheme in dashed green, the M_1 mobile scheme with correction in dashed blue and for the Euler scheme in dashed-point pink. It is observed that all the schemes converge towards the same solution. This behaviour is expected since working in fluid regime the distribution remains a Maxwellian distribution function and the three descriptions give the same solution.

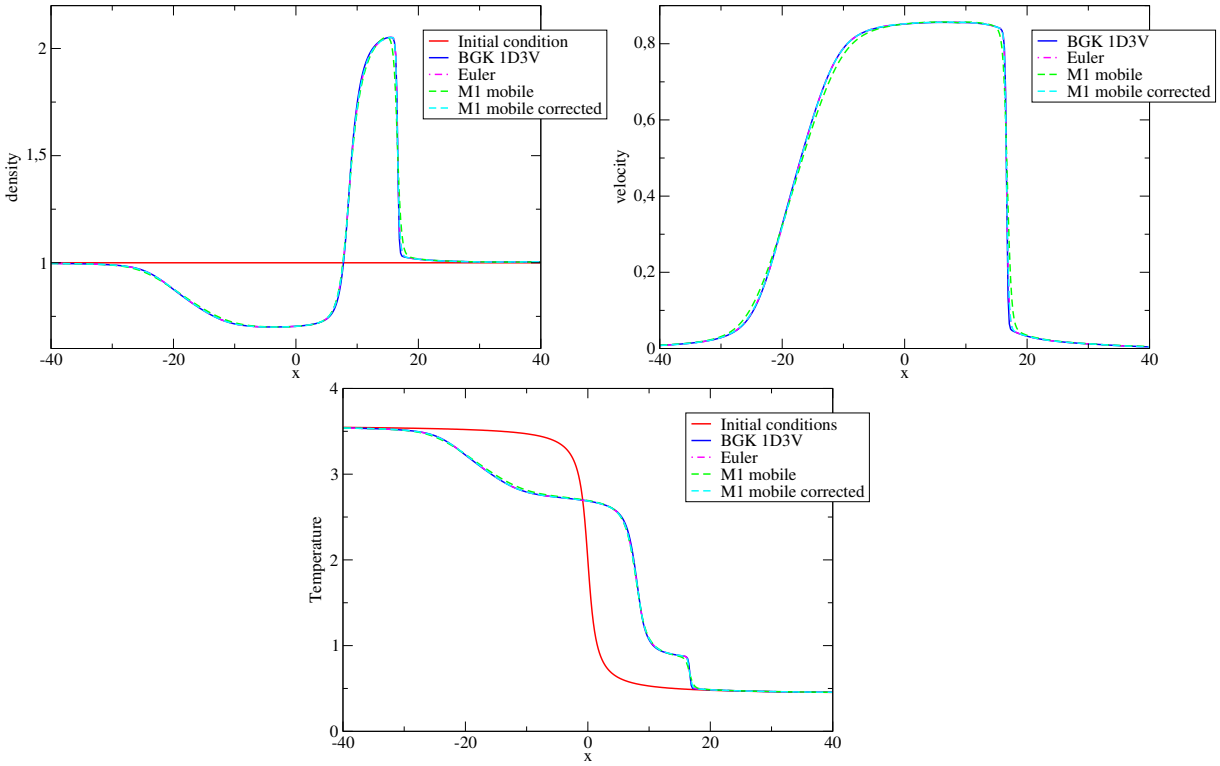

Figure 7.2: Test 1a - Solution profiles obtained for the temperature gradient test case with $\tau = 0$ at time $t = 10$.

1.b Rarefied regime.
The second regime we consider is a rarefied regime where the collisional parameter τ is set equal to 1. In Figure 7.3, the density, velocity, temperature and heat flux profiles are displayed at time $t = 10$ for the kinetic BGK 1D3V scheme in continuous blue, the M_1 mobile scheme in dashed green, the M_1 mobile scheme with correction in dashed blue and for the Euler scheme in dashed-point pink. The Euler scheme gives the same results than in the previous case 1a. This is expected since the description is not able to see the different regimes. In this case the heat flux is equal to zero. One observes that M_1 mobile scheme gives close results to the ones obtained with the kinetic BGK 1D3V scheme. When looking at the heat flux profiles, one observes

that the general trends are qualitatively similar with some notable differences in the amplitude reached. Since the heat flux is a high order velocity moment, the differences between the models are particularly visible. The M_1 model is accurate in collisional regimes, however as seen in Chapter 1 or in [117], it can be inaccurate in collisionless regimes. The differences observed here, are due to the inaccuracy to the M_1 model in rarefied regime.

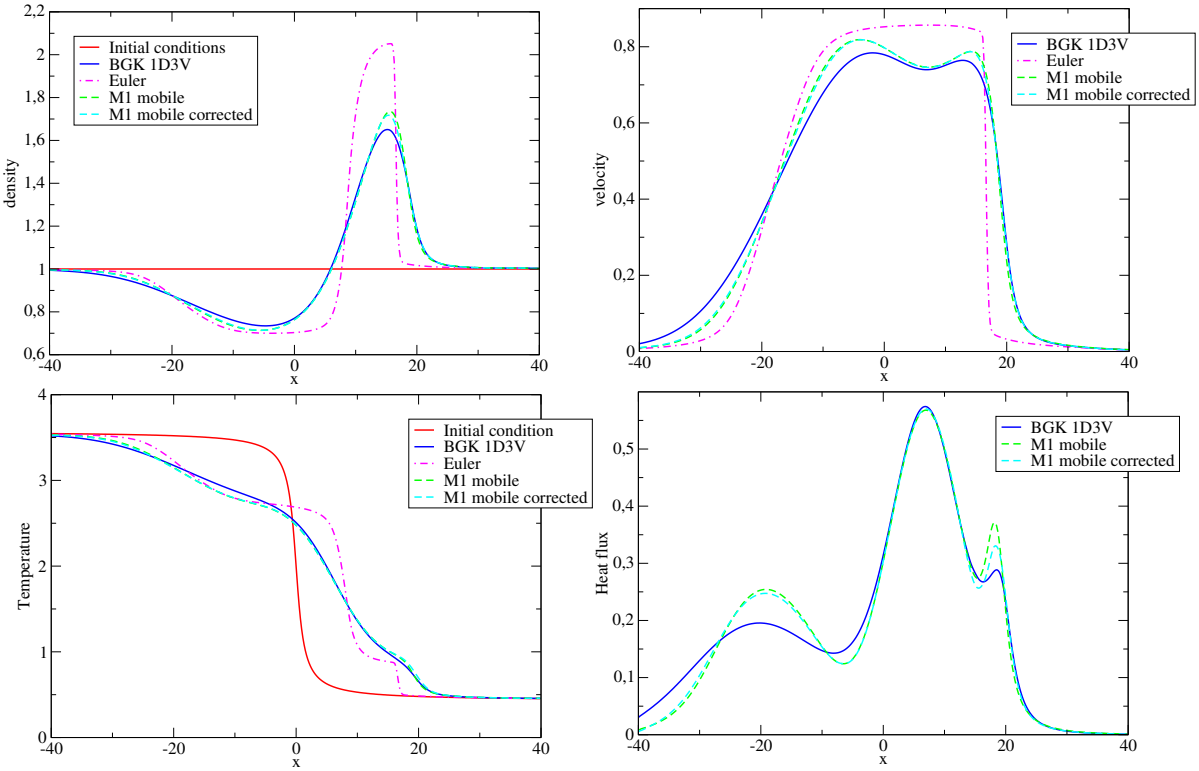

Figure 7.3: Test 1b - Solution profiles obtained for the temperature gradient test case with $\tau = 1$ at time $t = 10$.

1.c Non-homogeneous collisional parameter.
When considering realistic physical applications, the collisional parameter varies according to the gas conditions. Therefore, in the third case we consider the collisional parameter τ is variable in space and is defined by

$$\tau(x) = \frac{1}{2}(\arctan(1 + 0.1x) + \arctan(1 - 0.1x)).$$

In Figure 7.4, the density, velocity, temperature and heat flux profiles are displayed at time $t = 10$ for the kinetic BGK 1D3V scheme in continuous blue, the M_1 mobile scheme in dashed green and for the Euler scheme in dashed-point pink. It is observed that the profiles obtained using the M_1 mobile sheme and the BGK 1D3V scheme are very close. One also observes that even the heat flux profiles are very similar. These results show the interest in using an angular moment model.

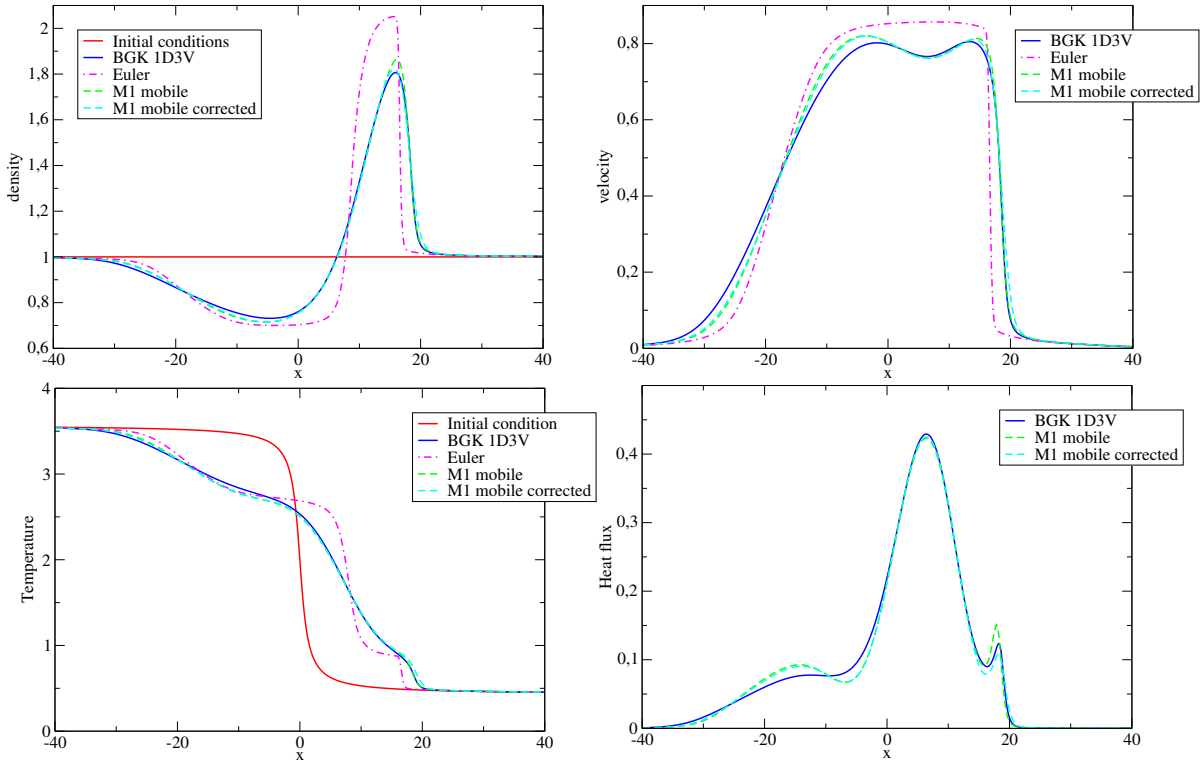

Figure 7.4: Test 1c - Solution profiles obtained for the temperature gradient test case with variable collisional parameter at time $t = 10$.

Test 2: Sod tube test case in fluid regime

The second test case we study is the Sod tube test case in fluid regime. The initial distribution function is supposed to be a Maxwellian distribution function defined by

$$f_{ini}(x,v) = \frac{n_{ini}(x)}{(2\pi T_{ini}(x))^{3/2}} \exp\Big(- \frac{(v - u_{ini}(x))^2}{2T_{ini}(x)}\Big),$$

with

$$(n_{ini}(x),\ u_{ini}(x),\ T_{ini}(x)) = \begin{cases} (1.00 \cdot 10^{-4},\ \ 0,\ \ 4.80 \cdot 10^{-3}) & \text{if } x < 0, \\ (1.25 \cdot 10^{-5},\ \ 0,\ \ 3.84 \cdot 10^{-3}) & \text{if } x > 0. \end{cases}$$

The space range chosen is $[0, 0.6]$, and the velocity range $[-20, 20]^3$. For the present test case, 200 cells in space and 200^3 cells in velocity have been considered for the 1D3V BGK kinetic approach. Also, 200 cells in space and 200 cells in velocity modulus have been considered for the M_1 mobile scheme. Finally, 200 cells in space have been considered for the Euler description. Neumann boundary conditions are considered, the values in the boundary ghost cells are set to the values in the corresponding real boundary cells. For this test case, we consider the fluid regime therefore the collisional parameter τ is set equal to 0. For this test case an

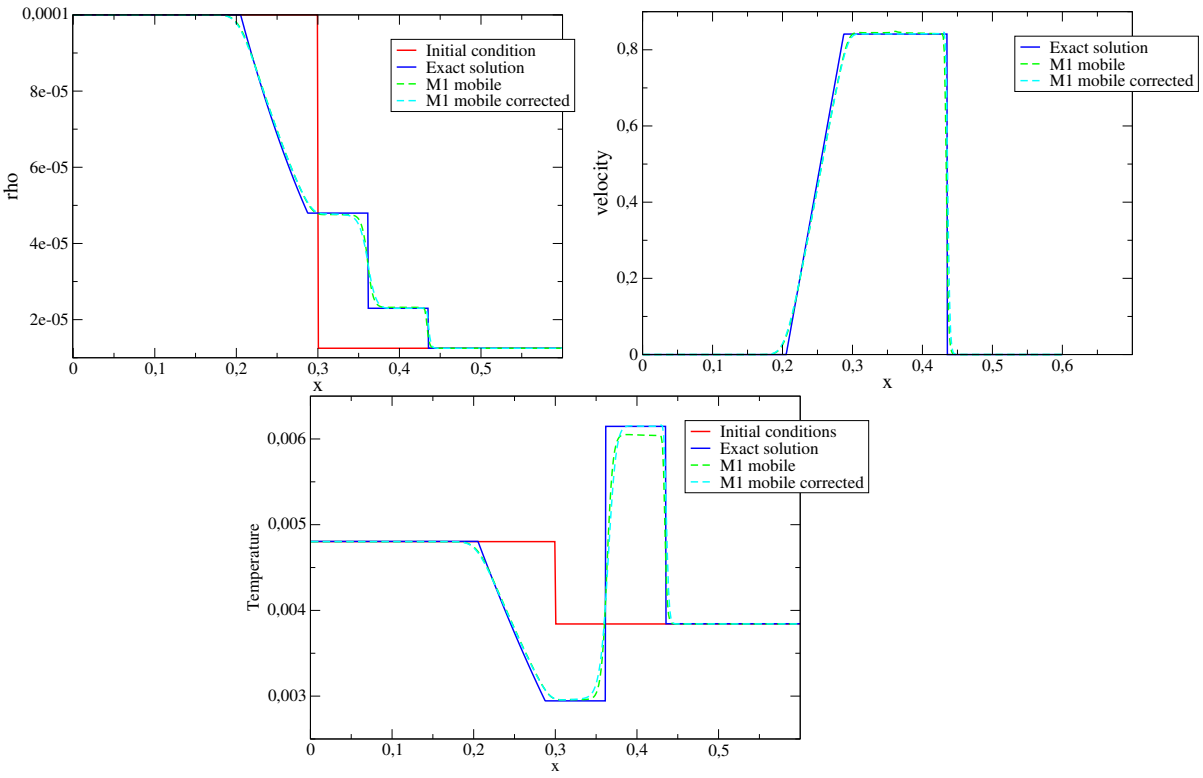

Figure 7.5: Test 2 - Sod tube test case with $\tau = 0$ at time $t = 7.34 \cdot 10^{-2}$.

exact solution is known, a rarefaction wave, a contact discontinuity and a shock wave appear. In Figure 7.5, the mass density, velocity and temperature solution profiles are displayed at time $t = 7.34 \cdot 10^{-2}$. It is observed that the rarefaction wave (left side) is correctly captured by the M_1 mobile scheme (solution displayed in dashed green). However, one remarks that the shock amplitude is not correctly captured. It has been observed that this incorrect behaviour is due to the wrong discrete energy conservation. Indeed, by using the correction procedure introduced in the previous part the results in dashed blue are obtained, in this case the correct amplitude is recovered. We notice, the importance of the correct discrete energy conservation for capturing shock waves. This point is highlighted in the next test case.

Test 3: Double shock wave test case

The third test case we study is the double shock wave test case in fluid regime. The initial distribution function is supposed to be a Maxwellian distribution function defined by

$$f_{ini}(x,v) = \frac{n_{ini}(x)}{(2\pi T_{ini}(x))^{3/2}} \exp\Big(- \frac{(v - u_{ini}(x))^2}{2T_{ini}(x)} \Big),$$

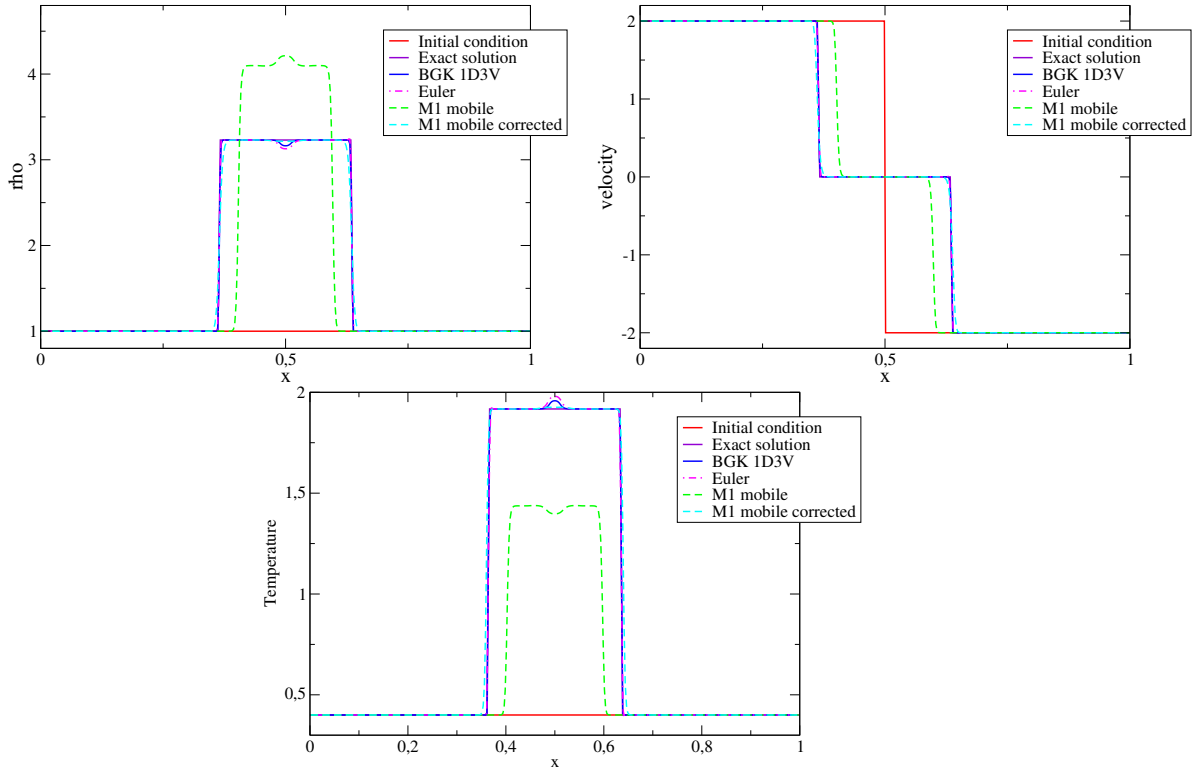

Figure 7.6: Test 3 - Double shock wave test case with $\tau = 0$ at time $t = 0.15$.

with

$$(\rho(x),\ u(x),\ T(x)) = \begin{cases} (1,\ \ 2, 0.4) & \text{if } x < 0, \\ (1, -2, 0.4) & \text{if } x > 0. \end{cases}$$

The space range chosen is $[0, 1]$, and the velocity range $[-15, 15]^3$. For the present test case, 200 cells in space and 200^3 cells in velocity have been considered for the 1D3V BGK kinetic approach. Also, 200 cells in space and 200 cells in velocity modulus have been considered for the M_1 mobile scheme. Finally, 200 cells in space have been considered for the Euler description. Neumann boundary conditions are considered, the values in the boundary ghost cells are set to the values in the corresponding real boundary cells. For this test case, we consider the fluid regime therefore the collisional parameter τ is set equal to 0. For this test case an exact solution is known, two shock waves are created. In Figure 7.6, the mass density, velocity and temperature solution profiles are displayed at time $t = 0.15$. Similarly as remarked in the previous test case, it is observed that the M_1 scheme does not capture the correct amplitude profile nor the correct shock positions (results in dashed green). The results displayed in dashed blue are obtained using the corrected scheme. It is observed that the correction enables to correctly captures the shock profiles. This example confirms the importance of the discrete energy conservation.

7.6 Conclusion

In this work, the M_1 angular moments model in a moving frame has been derived. Several fundamental properties of the model have been presented. In particular, the importance of working in the mean velocity frame has been highlighted. Indeed, this choice of framework is relevant when considering the Galilean invariance property of angular moments models. The derivation of the associated conservation laws has been detailed in addition to the zero mean velocity condition. A numerical scheme preserving the realisable sets has been proposed and validated with numerical test cases in different collisional regimes. Also, the importance of the correct discrete energy conservation has been emphasized.

As a short term perspective, one needs to derive a numerical scheme enforcing the discrete energy conservation and the zero mean velocity condition. Such an issue is challenging since it should be done preserving the realisable property of the numerical solution. As long term perspective, it would be interesting to study the electronic particle transport working in the ion mean velocity framework. This choice would enable a great simplification of the electron-ion collisional operator and an important step toward the multispecies particle transport for plasma physics applications.

Conclusion / Perspectives

The present work aimed at the development of models and numerical methods for the study of the charged particles transport in a hot plasma. In this context angular moments models based on an entropy minimisation principle have been introduced.

Questions addressed

First of all, one needs to understand the limits of angular moments models when considering plasmas physics or neutral gas dynamics applications. Indeed, the angular integration performed leads to reduced models which can be inaccurate depending on the physical phenomenon studied. The objective is to obtain a better understanding of the validity regimes of angular moments models.

A second issue deals with the design and validation of collisional operators for angular moments models. Indeed, relevant kinetic physical collisional operators such as the Landau collisional operator or the Boltzmann collisional operator are nonlinear. Therefore the angular moments extraction is not straightforward and some approximations are required. Of course, the collisional operators proposed need to satisfy fundamental properties such as the entropy dissipation or the realisability preservation of the angular moments.

A third issue concerns the derivation of appropriate numerical methods for angular moments models. Since angular moments models can be seen as intermediate models between kinetic and hydrodynamics descriptions, one can hope to capture more accurately physical processes studied compared to hydrodynamics models while keeping a computational cost more affordable compared to the ones required for kinetic models. This makes these models naturally attractive to study the kinetic effects on long time scales. Therefore, suitable numerical schemes with correct asymptotic behaviour are required to access such regimes. The design of these adapted methods needs to be done in the framework of the asymptotic-preserving schemes and ensuring the fundamental properties of the model such as the preservation of the realisable sets.

The last question we address deals with the development of models and numerical methods for the study of the transport of multiple particle species. When studying the electrons transport, the motion of ions is generally neglected because of their large mass compared to the one of electrons. However, when considering long time regimes this approximation may not be valid and the study of the transport of both

particle species is required. In addition, the study of the transport of electrons and ions would give access to a large variety of physical phenomena.

Our contribution

When investigating the validity limits of angular moments models, it has been shown that the M_1 model can be very inaccurate in collisionless regimes. Also, it has been seen that the M_2 angular moments model is much more accurate but remains unadapted when dealing with complex phenomena such as the laser-plasma absorption for example. However, the numerical experiments presented in this manuscript allow us to demonstrate the interest of using angular moments models in collisional regimes in order to capture kinetic effects.
In general it is then difficult to clearly define a validity domain for the use of angular moments models. It is observed that the results depend on the physical phenomenon and the collisionnality level considered.

In [166], collisional operators have been proposed for angular moments models. In this thesis, a work has been performed in order to validate them. After the study of the fundamental properties of the collisional operators proposed for the M_1 model, it has been shown that accurate transport plasma coefficients are recovered. This is an important result since it provides at our disposal a reliable model for the study of the collisional electronic transport. Therefore, this model represents a competitive tool which can be used for practical physical applications.

In this thesis a large amount of work has been devoted to the design and implementation of numerical schemes for the M_1 angular moments model. It has been shown that numerical schemes commonly used for angular moments models are not able to correctly capture some asymptotic regimes. Consequently, asymptotic-preserving schemes have been designed for the study of long time behaviours. The first regime studied corresponds to a quasi-neutral plasma. At this scale the characteristic quantities are large compared to the plasma parameters. In order to work without any restriction on the time step an appropriate reformulation of the Maxwell-Ampere equation has been considered. A natural discretisation of the scheme has been proposed and several test cases have been performed showing the interest of the method.

In order to be able to perform numerical simulations on larger time scales the diffusive limit has been studied. At this scale, the charateristic quantities are large compared to the collisional parameters. An asymptotic-preserving scheme has been proposed for the M_1 angular moments models in the diffusive regime. It has been shown that, since charged particles are considered, mixed derivatives arise in that limit leading to an anisotropic diffusion. The properties of the scheme have been studied and several test cases have been performed to show the interest of the method. Even if further details still need to be considered, this work represents an important step in the development of numerical methods for the study of long time regimes at an affordable numerical cost.

In the last part of this manuscript, the M_1 angular moments model in a mov-

ing non-inertial reference frame has been introduced. Before considering complex electron-ion interactions, the case of a single neutral particles specie has been considered. The equations are written in the mean velocity frame. This case applies to neutral gas dynamics studies. It represents an intermediate indispensable step before investigating multispecies configurations. This case allows to readily evaluate the mean difficulties that appear in the general case. The model properties have been studied and an appropriate numerical scheme proposed. Then, several test cases in different collisional regimes have been presented to show the major properties of the method. This work represents a first significant step towards the study of the multispecies particle transport and numerous perspectives can be considered.

Short and long time perspectives

Several perspectives can be considered following the results obtained in this thesis. First of all, other plasma instabilities can be studied within the formalism of angular moments models. In addition to the work performed in this thesis, collisional regimes may be considered since it has been shown that the M_1 and M_2 angular moments models are better adapted for collisionnal and weakly collisionnal regimes. This would further clarify the validity domain of angular moments models.

Secondly, following [31] the transport plasma coefficients need to be derived by taking into account the external and self-consistent electric and a magnetic fields. This study would be in the direct continuity of the work performed in this manuscript. It has been shown that, without an external electric field and in regimes close to the equilibrium regimes, accurate transport plasma coefficients are recovered by the collisional M_1 moments model. This provides a basis for extension of the present study to regimes with magnetic fields.

Concerning the numerical part of this manuscript, several directions can be considered. In the continuity of the work achieved in the diffusive regime, one can account for the contribution of the electron-electron collisional operator which was removed for simplicity. This is a challenging issue because of the complex form of this operator. Different approaches can be pursued by adapting the ideas introduced in [92] for example.

Also, a numerical study of the complete system M_1-Maxwell in the quasi-neutral and diffusive regime may be conducted. This work would be a direct extension of the studies presented in this thesis. This would lead to a complete and computationally cheap numerical tool for the electronic transport studies in long time regimes.

The last part of this manuscript opens interesting perspectives for physical applications levels. On a short time scale the design of appropriate numerical methods is needed for solving the M_1 angular moments model in a moving frame. As a long term perspective one could include the electromagnetic coupling terms in order to study the electron transport within the M_1 model while describing the ion motion with an usual hydrodynamic description. This would provide a performant hybrid tool for the multispecies transport studies in a plasma.

Appendix A

Derivation of the electron M_1 model

A.1 Derivation of the model for the angular moments f_0 and f_1

In this section we proove that in the case without collisional operators, the angular M_1 model writes under the following form

$$\begin{cases} \partial_t f_0 + \nabla_{\vec{x}}.(\zeta \vec{f_1}) + \dfrac{q}{m}\partial_\zeta(\vec{f_1}.\vec{E}) = 0, \\ \partial_t \vec{f_1} + \nabla_{\vec{x}}.(\zeta \bar{\bar{f}}_2) + \dfrac{q}{m}\partial_\zeta(\bar{\bar{f}}_2\vec{E}) - \dfrac{q}{m\zeta}(f_0\vec{E} - \bar{\bar{f}}_2\vec{E}) - \dfrac{q}{m}(\vec{f_1} \wedge \vec{B}) = 0. \end{cases} \tag{A.1}$$

Before beginning the proof, we can compute the divergence of the magnetic part of the Lorentz force,

$$\nabla_p.(v(p) \wedge B) = B \cdot \nabla_p \wedge v(p) - v(p) \cdot \nabla_p \wedge B = 0\,, \tag{A.2}$$

because $\nabla_p \wedge v(p) = 0$.
To proof these equalities, we can use duality approach. If we set $\zeta = |p| = m|v(p)|\gamma(|p|) = mv(\zeta)\gamma(\zeta)$, and we denote by φ some test function. Here, we suppose that the test function φ depends only of ζ. Therefore, multiplying the kinetic equation by φ and integrating in p gives

$$
\begin{aligned}
0 &= \int_{p\in\mathbb{R}^3} \left(\partial_t f + v(p)\cdot\nabla_x f + q\left(E + v(p)\wedge B\right)\cdot\nabla_p f\right)\varphi(\zeta)dp,\\
&= \int_{p\in\mathbb{R}^3} \left(\partial_t f + v(p)\cdot\nabla_x f\right)\varphi(\zeta)dp - \int_{p\in\mathbb{R}^3} \nabla_p\varphi(\zeta)\cdot\left(q\left(E + v(p)\wedge B\right)f\right)dp, \text{ from (A.2)},\\
&= \int_0^\infty \partial_t\left(\zeta^2\int_{S_2} f d\Omega\right)\varphi(\zeta)d\zeta + \int_0^\infty \nabla_x\cdot\left(v(\zeta)\zeta^2\int_{S_2}\Omega f d\Omega\right)\varphi(\zeta)d\zeta\\
&- \int_{p\in\mathbb{R}^3} \varphi'(\zeta)\frac{p}{\zeta}\cdot\left(q\left(E + v(p)\wedge B\right)f\right)dp, \text{ as } p=\zeta\Omega \text{ and } dp=\zeta^2 d\zeta d\Omega,\\
&= \int_0^\infty \left(\partial_t f_0 + \nabla_x\cdot\left(v(\zeta)f_1\right)\right)\varphi(\zeta)d\zeta - \int_{p\in\mathbb{R}^3}\varphi'(\zeta)\Omega\cdot\left(qEf\right)dp, \text{ as } p\cdot\left(v(p)\wedge B\right)=0,\\
&= \int_0^\infty \left(\partial_t f_0 + \nabla_x\cdot\left(v(\zeta)f_1\right)\right)\varphi(\zeta)d\zeta - \int_0^\infty \varphi'(\zeta)qE\cdot\left(\zeta^2\int_{S_2}\Omega f d\Omega\right)d\zeta,\\
&= \int_0^\infty \left(\partial_t f_0 + \nabla_x\cdot\left(v(\zeta)f_1\right)\right)\varphi(\zeta)d\zeta + \int_0^\infty \partial_\zeta\left(qE\cdot f_1\right)\varphi(\zeta)d\zeta,\\
&= \int_0^\infty \left(\partial_t f_0 + \nabla_x\cdot\left(v(\zeta)f_1\right) + \partial_\zeta\left(qE\cdot f_1\right)\right)\varphi(\zeta)d\zeta,
\end{aligned}
$$

which is verified for all test functions φ, hence the first equation of (A.1) is verified. Now if we consider the case of the vector f_1, we need to compute $\nabla_p\Omega$,

$$
\begin{aligned}
\nabla_p\Omega &= \nabla_p\left(\frac{p}{|p|}\right) = \frac{1}{|p|}I - \frac{1}{|p|^2}\nabla_p|p|\otimes p = \frac{1}{|p|}I - \frac{1}{|p|^2}\left(\frac{1}{|p|}p\right)\otimes p,\\
&= \frac{1}{|p|^3}\left(|p|^2 I - p\otimes p\right) = \frac{1}{\zeta}\left(I - \Omega\otimes\Omega\right),
\end{aligned}
\tag{A.3}
$$

where I is the identity matrix. Now, we can consider the proof of the second equation of (A.1). Multiplying the kinetic equation by $\varphi(\zeta)\Omega$, and integrating leads to

$$
\begin{aligned}
0 &= \int_{p\in\mathbb{R}^3} \left(\partial_t f + v(p)\cdot\nabla_x f + q\left(E + v(p)\wedge B\right)\cdot\nabla_p f\right)\Omega\varphi(\zeta)dp,\\
&= \int_{p\in\mathbb{R}^3} \left(\partial_t f + v(p)\cdot\nabla_x f\right)\Omega\varphi(\zeta)dp - \int_{p\in\mathbb{R}^3} \nabla_p\varphi(\zeta)\cdot\left(q\left(E + v(p)\wedge B\right)f\right)\Omega dp\\
&- \int_{p\in\mathbb{R}^3} \varphi(\zeta)\nabla_p\Omega\left(q\left(E + v(p)\wedge B\right)f\right)dp, \text{ from (A.2)},\\
&= \int_0^\infty \partial_t\left(\zeta^2\int_{S_2}\Omega d\Omega\right)\varphi(\zeta)d\zeta + \int_0^\infty \nabla_x\cdot\left(v(\zeta)\zeta^2\int_{S_2}\Omega\otimes\Omega f d\Omega\right)\varphi(\zeta)d\zeta\\
&- \int_{p\in\mathbb{R}^3} \varphi'(\zeta)\frac{p}{\zeta}\cdot\left(q\left(E + v(p)\wedge B\right)f\right)\Omega dp - \int_{p\in\mathbb{R}^3}\frac{1}{\zeta}\varphi(\zeta)q\left(E + v(p)\wedge B\right)f dp\\
&+ \int_{p\in\mathbb{R}^3}\frac{1}{\zeta}\varphi(\zeta)\Omega\otimes\Omega\left(q\left(E + v(p)\wedge B\right)f\right)dp, \text{ from (A.3)},\\
&= \int_0^\infty \left(\partial_t f_1 + \nabla_x\cdot\left(v(\zeta)f_2\right)\right)\varphi(\zeta)d\zeta - \int_{p\in\mathbb{R}^3}\varphi'(\zeta)\Omega\cdot\left(qEf\right)\Omega dp\\
&- \int_0^\infty \frac{q}{\zeta}\varphi(\zeta)\left(\zeta^2\int_{S_2} f d\Omega\, E + v(\zeta)\zeta^2\int_{S_2}\Omega f d\Omega\wedge B\right)d\zeta\\
&+ \int_0^\infty \frac{q}{\zeta}\varphi(\zeta)\left(\zeta^2\int_{S_2}\Omega\otimes\Omega f d\Omega\, E\right)d\zeta, \text{ because } \Omega\otimes\Omega\left(v\wedge B\right) = 0,\\
&= \int_0^\infty \left(\partial_t f_1 + \nabla_x\cdot\left(v(\zeta)f_2\right)\right)\varphi(\zeta)d\zeta - \int_0^\infty q\varphi'(\zeta)\left(\zeta^2\int_{S_2}\Omega\otimes\Omega f d\Omega\right)E d\zeta\\
&- \int_0^\infty \frac{q}{\zeta}\varphi(\zeta)\left(f_0\, E + v(\zeta)f_1\wedge B\right)d\zeta + \int_0^\infty \frac{q}{\zeta}\varphi(\zeta)\left(f_2\, E\right)d\zeta,\\
&= \int_0^\infty \left(\partial_t f_1 + \nabla_x\cdot\left(v(\zeta)f_2\right)\right)\varphi(\zeta)d\zeta + \int_0^\infty \partial_\zeta\left(qf_2 E\right)\varphi(\zeta)d\zeta\\
&- \int_0^\infty \frac{q}{\zeta}\varphi(\zeta)\left(f_0\, E + v(\zeta)f_1\wedge B\right)d\zeta + \int_0^\infty \frac{q}{\zeta}\varphi(\zeta)\left(f_2\, E\right)d\zeta,\\
&= \int_0^\infty \left(\partial_t f_1 + \nabla_x\cdot\left(v(\zeta)f_2\right) + q\left(\partial_\zeta\left(f_2 E\right) - \frac{1}{\zeta}\left(f_0\, E + v(\zeta)f_1\wedge B - f_2\, E\right)\right)\right)\varphi(\zeta)d\zeta,
\end{aligned}
$$

which is verified for all test functions φ, hence the second equation of (A.1) is verified.

A.2 Angular moment extraction for the collision operators C_{ee} and C_{ei}

In this section the angular integration of the collision operators is performed.

A.2.1 Angular integration for the electron-ion collision operator

Firstly, we start computing the electron-ion collision C_{ei} which is much simpler to compute. To establish this derivation we consider only the homogeneous case with the collision operator C_{ei},

$$\partial_t f = C_{ei}[f] = \alpha_{ei}\nabla_v \cdot \left[\frac{|v|^2 I - v\otimes v}{|v|^3}\nabla_v f(v)\right] = \alpha_{ei}\nabla_v \cdot [S(v)\nabla_v f(v)]\ , \tag{A.4}$$

where we have introduced $S(v)$ as,

$$S(v) = \frac{|v|^2 I - v\otimes v}{|v|^3} = \frac{1}{\zeta}\left(I - \Omega\otimes\Omega)\right)\cdot \tag{A.5}$$

The operator $S(v)$ is the projection operator on the orhogonal plane to the vector v and we have $S(v)v = 0$.

Now if we want to consider the influence of the C_{ei} operator for the equation about f_0, we can use duality approach. If we set $\zeta = |v|$, and we denote by φ some test function,

$$\begin{aligned}
0 &= \int_{v\in\mathbb{R}^3} \left(\partial_t f - \alpha_{ei}\nabla_v\cdot[S(v)\nabla_v f]\right)\varphi(\zeta)dv,\\
&= \int_0^\infty \partial_t\left(\zeta^2\int_{S_2} f d\Omega\right)\varphi(\zeta)d\zeta + \alpha_{ei}\int_{v\in\mathbb{R}^3}\nabla_v\varphi(\zeta)\cdot[S(v)\nabla_v f]\,dv,\\
&= \int_0^\infty \partial_t f_0\varphi(\zeta)d\zeta + \alpha_{ei}\int_{v\in\mathbb{R}^3}\varphi'(\zeta)\frac{v}{\zeta}\cdot[S(v)\nabla_v f]\,dv,\\
&= \int_0^\infty \partial_t f_0\varphi(\zeta)d\zeta + \alpha_{ei}\int_{v\in\mathbb{R}^3}\varphi'(\zeta)\left[S(v)\frac{v}{\zeta}\right]\cdot\nabla_v f dv,\ \text{as } S(v) \text{ is symmetric},\\
&= \int_0^\infty \partial_t f_0\varphi(\zeta)d\zeta,\ \text{as } S(v)v = 0,
\end{aligned}$$

which is verified for all test functions φ, hence,

$$\partial_t f_0 = 0,$$

and the C_{ei} operator has no influence on the equation for f_0.

Now, we consider the influence of the C_{ei} operator for the equation about f_1,

$$
\begin{aligned}
0 &= \int_{v\in\mathbb{R}^3} \left(\partial_t f - \alpha_{ei}\nabla_v\cdot\left[S(v)\nabla_v f\right]\right)\Omega\varphi(\zeta)dv,\\
&= \int_0^\infty \partial_t\left(\zeta^2\int_{S_2}\Omega f d\Omega\right)\varphi(\zeta)d\zeta + \alpha_{ei}\int_{v\in\mathbb{R}^3}\nabla_v\varphi(\zeta)\cdot\left[S(v)\nabla_v f\right]\Omega dv\\
&+ \alpha_{ei}\int_{v\in\mathbb{R}^3}\varphi(\zeta)\nabla_v\Omega\left[S(v)\nabla_v f\right]dv,\\
&= \int_0^\infty \partial_t f_1\varphi(\zeta)d\zeta + \alpha_{ei}\int_{v\in\mathbb{R}^3}\varphi'(\zeta)\frac{v}{\zeta}\cdot\left[S(v)\nabla_v f\right]\Omega dv\\
&+ \alpha_{ei}\int_{v\in\mathbb{R}^3}\varphi(\zeta)\frac{1}{\zeta}S(v)\left[S(v)\nabla_v f\right]dv,\ \text{from (A.3)},\\
&= \int_0^\infty \partial_t f_1\varphi(\zeta)d\zeta - \alpha_{ei}\int_{v\in\mathbb{R}^3}\varphi(\zeta)\nabla_v\cdot\left(\frac{1}{\zeta}S(v)\right)f dv,\\
&\quad \text{as } S(v) \text{ is symmetric, } S(v)S(v) = \frac{1}{\zeta}S(v) \text{ and } S(v)v = 0,\\
&= \int_0^\infty \partial_t f_1\varphi(\zeta)d\zeta - \alpha_{ei}\int_{v\in\mathbb{R}^3}\frac{\varphi(\zeta)}{\zeta^4}\nabla_v\cdot[\zeta^2 I - v\otimes v]f dv,\ \text{as } S(v)v = 0,\\
&= \int_0^\infty \partial_t f_1\varphi(\zeta)d\zeta + \alpha_{ei}\int_{v\in\mathbb{R}^3}\frac{\varphi(\zeta)}{\zeta^4}2v f dv,\ \text{as } \nabla_v\cdot[|v|^2 I - v\otimes v] = -2v,\\
&= \int_0^\infty \partial_t f_1\varphi(\zeta)d\zeta + \alpha_{ei}\int_0^\infty\frac{2}{\zeta^3}\left(\zeta^2\int_{S_2}\Omega f d\omega\right)\varphi(\zeta)d\zeta,\ \text{as } dv = \zeta^2 d\zeta d\Omega,\\
&= \int_0^\infty \left(\partial_t f_1 + \frac{2\alpha_{ei}}{\zeta^3}f_1\right)\varphi(\zeta)d\zeta,
\end{aligned}
$$

which is again verified for all test functions φ, hence,

$$\partial_t f_1 = -\frac{2\alpha_{ei}}{\zeta^3}f_1,$$

and in fact this gives exactly the operator Q_1. The electron-ion collisions are only relevant for the f_1 behavior, not the f_0.

A.2.2 Moment closure for the electron-electron collisions

To establish this closure we consider only the homogeneous case with the collision operator C_{ee},

$$\partial_t f = C_{ee}[f,f] = \alpha_{ee}\nabla_v\cdot\int_{v'\in\mathbb{R}^3} S(u)\left[f(v')\nabla_v f(v) - f(v)\nabla_{v'}f(v')\right]dv', \tag{A.6}$$

where $S(u)$ is given by (A.5) and $u = v' - v$. The moments of this operator is rather complicated, we will assume that the main contribution from this operator comes

from the isotropic part of f. In the remainder of this subsection, we will assume that f is isotropic, $f = f(|v|) = f(\zeta)$. This is a classical hypothesis useful in plasma physics.

We need introduce the notation $\Gamma(v)$ which is the term into the divergence in v,

$$\Gamma(v) = \int_{v' \in \mathbb{R}^3} S(u) \left[f(v') \nabla_v f(v) - f(v) \nabla_{v'} f(v') \right] dv'.$$

The $\Gamma(v)$ term satisfies $C_{ee}[f,f] = \alpha_{ee} \nabla_v \cdot \Gamma(v)$. Moreover if f is isotropic as we assume, $\Gamma(v)v$ is isotropic. In fact, in this case $\Gamma(v)v = g(|v|)$ doesnt depend on the direction of vector v. If we set $\zeta = |v|$, and we denote by φ some test function, then,

$$\begin{aligned}
0 &= \int_{v \in \mathbb{R}^3} \left(\partial_t f - \alpha_{ee} \nabla_v \cdot \Gamma(v) \right) \varphi(\zeta) dv, \\
&= \int_{v \in \mathbb{R}^3} \partial_t f \varphi(\zeta) dv + \alpha_{ee} \int_{v \in \mathbb{R}^3} \nabla_v \varphi(\zeta) \cdot \Gamma(v) dv, \\
&= \int_0^\infty \partial_t \left(\zeta^2 \int_{S_2} f d\Omega \right) \varphi(\zeta) d\zeta + \alpha_{ee} \int_0^\infty \frac{1}{\zeta} \varphi'(\zeta) \int_{S_2} \Gamma(v) \cdot v d\Omega \zeta^2 d\zeta, \\
&= \int_0^\infty \partial_t f_0 \varphi(\zeta) d\zeta + \alpha_{ee} \int_0^\infty \frac{1}{\zeta} \varphi'(\zeta) 4\pi \Gamma(v) \cdot v \zeta^2 d\zeta, \text{ as } \Gamma(v) \cdot v \text{ is isotropic}, \\
&= \int_0^\infty \left(\partial_t f_0 - 4\pi \alpha_{ee} \partial_\zeta \left(\zeta \Gamma(v) \cdot v \right) \right) \varphi(\zeta) d\zeta,
\end{aligned}$$

which imply that

$$\partial_t f_0 = 4\pi \alpha_{ee} \partial_\zeta \left(\zeta \Gamma(v) \cdot v \right). \tag{A.7}$$

Now to compute $\Gamma(v) \cdot v$, we introduce the notation $\zeta' = |v'|$, $v' = \zeta' \Omega'$, and we consider all the terms in $\Gamma(v)$,

$$\left[f(v') \nabla_v f(v) - f(v) \nabla_{v'} f(v') \right] dv' = \left[f(\zeta') \frac{v}{\zeta} \partial_\zeta f(\zeta) - f(\zeta) \Omega' \partial_{\zeta'} f(\zeta') \right] d\Omega' \zeta'^2 d\zeta', \tag{A.8}$$

and

$$\begin{aligned}
S(u) &= \frac{(v - \Omega'\zeta')I - (v - \Omega'\zeta') \otimes (v - \Omega'\zeta')}{(v - \Omega'\zeta')^3}, \\
&= \frac{(\zeta^2 + \zeta'^2 - 2\zeta' v \cdot \Omega')I - (v \otimes v + \zeta'^2 \Omega' \otimes \Omega' - \zeta'(\Omega' \otimes v + v \otimes \Omega'))}{(\zeta^2 + \zeta'^2 - 2\zeta' v \cdot \Omega')^{\frac{3}{2}}}.
\end{aligned} \tag{A.9}$$

Or $\Gamma(v) \cdot v$ involves the $S(u)v$ matrix-vector product, from (A.9) we can obtain,

$$\begin{aligned}
S(u)v &= \frac{(\zeta^2 + \zeta'^2 - 2\zeta' v \cdot \Omega')v - (\zeta^2 v + \zeta'^2 (\Omega' \cdot v)\Omega' - \zeta^2 \zeta' \Omega' - \zeta'(\Omega' \cdot v)v)}{(\zeta^2 + \zeta'^2 - 2\zeta' v \cdot \Omega')^{\frac{3}{2}}}, \\
&= \frac{(\zeta'^2 - \zeta' v \cdot \Omega')v - (\zeta'^2 (\Omega' \cdot v) - \zeta^2 \zeta')\Omega'}{(\zeta^2 + \zeta'^2 - 2\zeta' v \cdot \Omega')^{\frac{3}{2}}}.
\end{aligned}$$

To achieve the computation of $\Gamma(v)\cdot v$ we need to know some scalar product, $A_v = S(u)v\cdot v$ and $A_{\Omega'} = S(u)v\cdot\Omega'$. We introduce μ the cosine of that angle between of the vector Ω' and v, such that $\Omega'\cdot v = \zeta\mu$, and we obtain,

$$\begin{aligned} A_v &= S(u)v\cdot v = \frac{(\zeta'^2 - \zeta' v\cdot\Omega')\zeta^2 + \zeta'(\zeta^2 - \zeta'(\Omega'\cdot v))(\Omega'\cdot v)}{(\zeta^2+\zeta'^2-2\zeta' v\cdot\Omega')^{\frac{3}{2}}}, \\ &= \frac{\zeta'(\zeta'-\zeta\mu)\zeta^2 + \zeta\zeta'\mu(\zeta^2-\zeta\zeta'\mu)}{(\zeta^2+\zeta'^2-2\zeta\zeta'\mu)^{\frac{3}{2}}}, \\ &= \frac{\zeta^2\zeta'^2(1-\mu^2)}{(\zeta^2+\zeta'^2-2\zeta\zeta'\mu)^{\frac{3}{2}}}, \end{aligned} \tag{A.10}$$

$$\begin{aligned} A_{\Omega'} &= S(u)v\cdot\Omega' = \frac{\zeta'(\zeta'-v\cdot\Omega')(\Omega'\cdot v) + \zeta'(\zeta^2-\zeta'(\Omega'\cdot v))}{(\zeta^2+\zeta'^2-2\zeta' v\cdot\Omega')^{\frac{3}{2}}}, \\ &= \frac{\zeta'(\zeta'-\zeta\mu)\zeta\mu + \zeta'(\zeta^2-\zeta\zeta'\mu)}{(\zeta^2+\zeta'^2-2\zeta\zeta'\mu)^{\frac{3}{2}}}, \\ &= \frac{\zeta^2\zeta'(1-\mu^2)}{(\zeta^2+\zeta'^2-2\zeta\zeta'\mu)^{\frac{3}{2}}}. \end{aligned} \tag{A.11}$$

The comutation of the $\Gamma(v)\cdot v$ term can now be completed,

$$\begin{aligned} \Gamma(v)\cdot v &= \int_{v'\in\mathbb{R}^3} S(u)\left[f(v')\nabla_v f(v) - f(v)\nabla_{v'}f(v')\right]dv'\cdot v, \\ &= \int_{v'\in\mathbb{R}^3} S(u)v\cdot\left[f(v')\nabla_v f(v) - f(v)\nabla_{v'}f(v')\right]dv', \text{ by symmetry of } S(u), \\ &= \int_0^\infty\int_{\Omega'\in S_2} S(u)v\cdot\left[f(\zeta')\frac{v}{\zeta}\partial_\zeta f(\zeta) - f(\zeta)\Omega'\partial_{\zeta'}f(\zeta')\right]d\Omega'\zeta'^2 d\zeta', \text{ from (A.8)}, \\ &= \int_0^\infty\int_{\Omega'\in S_2}\left[f(\zeta')\frac{1}{\zeta}\partial_\zeta f(\zeta)A_v - f(\zeta)\partial_{\zeta'}f(\zeta')A_{\Omega'}\right]d\Omega'\zeta'^2 d\zeta', \\ &= \int_0^\infty\int_{-1}^{+1}\frac{\zeta^2\zeta'^2(1-\mu^2)}{(\zeta^2+\zeta'^2-2\zeta\zeta'\mu)^{\frac{3}{2}}}\left[f(\zeta')\frac{1}{\zeta}\partial_\zeta f(\zeta) - f(\zeta)\frac{1}{\zeta'}\partial_{\zeta'}f(\zeta')\right]2\pi d\mu\zeta'^2 d\zeta', \end{aligned}$$

from (A.10), (A.11) and $d\Omega' = 2\pi d\mu$. Or, as the integral in mu variable is very simple,

$$\int_{-1}^{+1}\frac{\zeta^2\zeta'^2(1-\mu^2)}{(\zeta^2+\zeta'^2-2\zeta\zeta'\mu)^{\frac{3}{2}}}d\mu = \frac{4}{3}\inf\left(\frac{1}{\zeta^3},\frac{1}{\zeta'^3}\right),$$

We can rewrite $\Gamma(v)\cdot v$ under the following form,

$$\Gamma(v)\cdot v = \int_0^\infty\frac{8\pi}{3}\inf\left(\frac{1}{\zeta^3},\frac{1}{\zeta'^3}\right)\zeta^2\zeta'^2\left[f(\zeta')\frac{1}{\zeta}\partial_\zeta f(\zeta) - f(\zeta)\frac{1}{\zeta'}\partial_{\zeta'}f(\zeta')\right]\zeta'^2 d\zeta'. \tag{A.12}$$

In this case, as we have assumed that f is isotropic, we have $f_0(\zeta) = \zeta^2 \int_{S_2} f(\zeta)\, d\Omega = 4\pi\zeta^2 f(\zeta)$, we can conclude from (A.7) and (A.12) that,

$$\begin{aligned}
\partial_t f_0 &= \alpha_{ee}\partial_\zeta \left(\zeta \int_0^\infty \frac{2}{3} \inf\left(\frac{1}{\zeta^3}, \frac{1}{\zeta'^3}\right) \zeta^2 \zeta'^2 \left[\frac{f_0(\zeta')}{\zeta'^2} \frac{1}{\zeta} \partial_\zeta \left(\frac{f_0(\zeta)}{\zeta^2} \right) - \frac{f_0(\zeta)}{\zeta^2} \frac{1}{\zeta'} \partial_{\zeta'} \left(\frac{f_0(\zeta')}{\zeta'^2} \right) \right] \zeta'^2 d\zeta' \right), \\
&= \frac{2\alpha_{ee}}{3}\partial_\zeta \left[\zeta^2 \left(\int_0^\infty \inf\left(\frac{1}{\zeta^3}, \frac{1}{\zeta'^3}\right) \zeta'^2 f_0(\zeta') d\zeta' \right) \partial_\zeta \left(\frac{f_0(\zeta)}{\zeta^2} \right) \right. \\
&- \left. \zeta \left(\int_0^\infty \inf\left(\frac{1}{\zeta^3}, \frac{1}{\zeta'^3}\right) \zeta'^3 \partial_{\zeta'} \left(\frac{f_0(\zeta')}{\zeta'^2} \right) d\zeta' \right) f_0(\zeta) \right], \\
&= \frac{2\alpha_{ee}}{3}\partial_\zeta \left(\zeta^2 A(\zeta) \partial_\zeta \left(\frac{f_0(\zeta)}{\zeta^2} \right) - \zeta B(\zeta) f_0(\zeta) \right), \\
&= \frac{2\alpha_{ee}}{3}\partial_\zeta \left(A(\zeta)\partial_\zeta f_0(\zeta) - \left(\zeta B(\zeta) + \frac{2A(\zeta)}{\zeta} \right) f_0(\zeta) \right),
\end{aligned}$$

where

$$A(\zeta) = \int_0^\infty \inf\left(\frac{1}{\zeta^3}, \frac{1}{\zeta'^3}\right) \zeta'^2 f_0(\zeta') d\zeta'$$

We finish computing the B coefficient

$$\begin{aligned}
B(\zeta) &= \int_0^\infty \min(\frac{1}{\zeta^3}, \frac{1}{w^3}) w^3 \partial_w \left(\frac{f_0(w)}{w^2} \right) dw, \\
&= \int_0^\zeta \frac{w^3}{\zeta^3} \partial_w \left(\frac{f_0(w)}{w^2} \right) dw + \int_\zeta^\infty \partial_w \left(\frac{f_0(w)}{w^2} \right) dw, \\
&= \left[\frac{w^3}{\zeta^3} \frac{f_0(w)}{w^2} \right]_0^\zeta - \int_0^\zeta \frac{3w^2}{\zeta^3} \frac{f_0(w)}{w^2} dw + \left[\frac{f_0(w)}{w^2} \right]_\zeta^\infty, \\
&= -\frac{3}{\zeta^3} \int_0^\zeta f_0(w) dw.
\end{aligned}$$

We retrieve exactly the formula (3.2) for the collision operators involved by the equation on f_0. We neglect the operator Q_{ee} for the equation on f_1 because we retain only the isotropic part of this operator and f_1 represent the anisotropic part of the distribution function.

Appendix B

Derivation of the angular M_1 model in a moving frame

In this part, the derivation of the angular M_1 model in a moving frame is detailed. The following kinetic equation will be considered for the angular moments integration

$$\partial_t g + div_x((c+u)g) - div_c\big((\frac{du}{dt} + \frac{\partial u}{\partial x}c)g\big) = 0,$$

where

$$\frac{du}{dt} = \partial_t u + (\partial_x u)u.$$

Introduce a test function ϕ, we consider the integral

$$\int_c \Big(\partial_t g + div_x((c+u)g) - div_c(\frac{du}{dt}g + \frac{\partial u}{\partial x}cg\Big)\phi(\zeta)dc = 0.$$

By using the Green formulae and $c = \zeta\Omega$

$$\int_c (\partial_t g + div_x((c+u)g))\phi(\zeta)dc + \int_c (\frac{du}{dt}g + \frac{\partial u}{\partial x} : \Omega \otimes \Omega\zeta g\zeta)\phi'(\zeta)dc = 0.$$

In spherical coordinates the previous equation leads to

$$\int_\zeta \int_{S^2} (\partial_t g + div_x((c+u)g))\phi(\zeta)\zeta^2 d\Omega d\zeta + \int_\zeta \int_{S^2} (\frac{du}{dt}.g\Omega + \frac{\partial u}{\partial x} : \Omega\otimes\Omega\zeta g)\phi'(\zeta)\zeta^2 d\Omega d\zeta = 0.$$

With the definitions of the angular moments

$$\int_\zeta (\partial_t g_0 + div_x(\zeta g_1 + u g_0))\phi(\zeta)d\zeta + \int_\zeta (\frac{du}{dt}.g_1 + \frac{\partial u}{\partial x} : \zeta g_2)\phi'(\zeta)d\zeta = 0.$$

Finally by integration by part,

$$\int_\zeta \Big(\partial_t g_0 + div_x(\zeta g_1 + u g_0) - \frac{\partial}{\partial\zeta}\Big[\frac{du}{dt}.g_1 + \frac{\partial u}{\partial x} : \zeta g_2\Big]\Big)\phi(\zeta)d\zeta = 0.$$

This holds true for all test function ϕ then one obtains the first equation for the M_1 model in a moving frame

$$\partial_t g_0 + div_x(\zeta g_1 + u g_0) - \frac{\partial}{\partial \zeta}\Big[\frac{du}{dt}.g_1 + \frac{\partial u}{\partial x} : \zeta g_2\Big] = 0.$$

Introduce a test function $\phi\Omega$, we consider the integral

$$\int_c \Big(\partial_t g + div_x((c+u)g) - div_c(\frac{du}{dt}g + \frac{\partial u}{\partial x}cg)\Big)\phi(\zeta)\Omega dc = 0.$$

By using the Green formulae

$$\int_c \Big(\partial_t g + div_x((c+u)g)\Big)\phi(\zeta)\Omega dc + \int_c \frac{\partial \phi(\zeta)\Omega}{\partial c}(\frac{du}{dt}g + \frac{\partial u}{\partial x}cg)dc = 0.$$

Using that

$$\frac{\partial \phi(\zeta)\Omega}{\partial c} = \phi'(\zeta)\Omega\otimes\Omega + \phi(\zeta)\frac{Id - \Omega\otimes\Omega}{\zeta}.$$

Then the second term of the left side of the equation gives

$$\begin{aligned}\int_c \frac{\partial \phi(\zeta)\Omega}{\partial c}(\frac{du}{dt}g + \frac{\partial u}{\partial x}cg)dc = &\int_c \frac{Id - \Omega\otimes\Omega}{\zeta}\frac{du}{dt}g\phi(\zeta)dc + \int_c \frac{Id - \Omega\otimes\Omega}{\zeta}\frac{\partial u}{\partial x}cg\phi(\zeta)dc\\ &+ \int_c \Omega\otimes\Omega\frac{du}{dt}\phi'(\zeta)g(c)dc + \int_c \Omega\otimes\Omega\frac{\partial u}{\partial x}cg(c)\phi'(\zeta)dc\end{aligned}$$

The first term of the right side reads

$$\int_c \frac{Id - \Omega\otimes\Omega}{\zeta}\frac{du}{dt}g\phi(\zeta)dc = \int_\zeta \frac{g_0 Id - g_2}{\zeta}\frac{du}{dt}\phi(\zeta)d\zeta.$$

The second term of the right side reads

$$\int_c \frac{Id - \Omega\otimes\Omega}{\zeta}\frac{\partial u}{\partial x}cg\phi(\zeta)dc = \int_\zeta (\frac{\partial u}{\partial x}g_1 - g_3\frac{\partial u}{\partial x})\phi(\zeta)d\zeta.$$

The third term of the right side gives

$$\int_c \Omega\otimes\Omega\frac{du}{dt}\phi'(\zeta)g(c)dc = -\int_\zeta \frac{\partial g_2}{\partial \zeta}\frac{du}{dt}\phi(\zeta)d\zeta.$$

The fourth term of the right side gives

$$\int_c \Omega\otimes\Omega\frac{\partial u}{\partial x}cg(c)\phi'(\zeta)dc = -\int_\zeta \frac{\partial \zeta g_3}{\partial \zeta}\frac{\partial u}{\partial x}\phi(\zeta)d\zeta$$

Finally one obtains the second equation for the M_1 model in a moving frame

$$\partial_t g_1 + div_x(\zeta g_2 + u\otimes g_1) - \partial_\zeta\Big(g_2\frac{du}{dt} + \zeta g_3\frac{\partial u}{\partial x}\Big) + \frac{f_0 Id - f_2}{\zeta}\frac{du}{dt} + (\frac{\partial u}{\partial x}g_1 - g_3\frac{\partial u}{\partial x}\Big) = 0.$$

The angular M_1 model in a moving frame reads

$$\begin{cases} \partial_t g_0 + div_x(\zeta g_1 + u g_0) - \partial_\zeta\Big(\dfrac{du}{dt}.g_1 + \zeta \partial_x u : g_2\Big) = 0, \\ \partial_t g_1 + div_x(\zeta g_2 + u \otimes g_1) - \partial_\zeta\Big(g_2 \dfrac{du}{dt} + \zeta g_3 \dfrac{\partial u}{\partial x}\Big) + \dfrac{f_0 Id - f_2}{\zeta}\dfrac{du}{dt} + (\dfrac{\partial u}{\partial x} g_1 - g_3 \dfrac{\partial u}{\partial x}\Big) = 0. \end{cases} \tag{B.1}$$

Bibliography

[1] A.Bermudez and M. E. Vazquez. Upwind methods for hyperbolic conservation laws with source terms. Computers and Fluids 23 (1994), no. 8, 1049–1071.

[2] M. Abramowitz and A. Stegun. Handbook of Mathematical functions. Dover Publications 1970.

[3] R. Alexandre and C. Villani. On the Landau approximation in plasma physics. Annales de l'Institut Henri Poincare (C) Non Linear Analysis, Volume 21, Issue 1, 2004, Pages 61-95, ISSN 0294-1449.

[4] G.W. Alldredge, C.D. Hauck, and A.L. Tits. High-order entropy-based closures for linear transport in slab geometry II: A computational study of the optimization problem. SIAM Journal on Scientific Computing Vol. 34-4 (2012), pp. B361-B391.

[5] J. Anderson. Hypersonic and High-Temperature Gas Dynamics. Second edition, AIAA Educ. Ser., American Institute of Aeronautics and Astronautics, 2006.

[6] D. Aregba-Driollet, M. Briani, and R. Natalini. Asymptotic High-Order Schemes for 2x2 Dissipative Hyperbolic Systems. SIAM Journal on Numerical Analysis 46 (2008), 869-894.

[7] E. Audit, P. Charrier, J.-P. Chièze, and B. Dubroca. A radiation hydrodynamics scheme valid from the transport to the diffusion limit. arXiv:astro-ph/0206281 (2002).

[8] R. Balescu. Phys. Fluids 3, 52 (1960).

[9] R. Balescu. Transport Processes in Plasma, Elsevier, (Amsterdam, 1988), Vol. 1.

[10] O.V. Batishchev, V.Yu. Bychenkov, F. Detering, W.Razmus, R. Sydera, C.E Copjack, and V.N.Novikov. Heat transport and electron distribution function in laser produced with hot spots. Physics of Plasmas 9 2302-2310, (2002).

[11] N. Bellomo and P. K. Maini. Preface (special issue on cancer modelling). Math. Mod. Math. Appl. Sci. 15 (2005), iii–viii.

[12] N. Bellomo and P. K. Maini. Preface (special issue on cancer modelling). Math. Mod. Math. Appl. Sci. 15 (2006), iii–vii.

[13] N. Bellomo and P. K. Maini. Preface (special issue on cancer modelling). Math. Mod. Math. Appl. Sci. 15 (2007), iii–vii.

[14] M. Bennoune, M. Lemou, and L. Mieussens. Uniformly stable numerical schemes for the Boltzmann equation preserving the compressible Navier–Stokes asymptotics. J. Comput. Phys. 227 (8) (2008) 3781–3803.

[15] S. Benzonie-Gavage and D. Serre. Multi-dimensonal Hyperbolic Partial Differential Equations. Oxford Science Publications.

[16] Yu. A. Berezin, V.N. Khudick, and M.S. Pekker. Conservative finite-difference schemes for the Fokker-Planck equation not violating the law of increasing entropy. J. Comput. Phy., 69, 163–174 (1987).

[17] C. Berthon. Numerical approximations of the 10-moment Gaussian closure. Math. Comp. 75 (2006) 1809-1831.

[18] C. Berthon, C. Buet, J.-F. Coulombel, B. Després, J. Dubois, T. Goudon, J. E. Morel, and R. Turpault. Mathematical models and numerical methods for radiative transfer. Volume 28 of Panoramas et Synthèses (Panoramas and Syntheses(. Société Mathématique de France, Paris, 2009.

[19] C. Berthon, P. Charrier, and B. Dubroca. An asymptotic preserving relaxation scheme for a moment model of radiative transfer. C. R. Acad. Sci. Paris, Ser. I 344 (2007).

[20] C. Berthon, P. Charrier, and B. Dubroca. An HLLC Scheme to Solve The M1 Model of Radiative Transfer in Two Space Dimensions. Journal of Scientific Computing, Vol. 31, No. 3, (2007).

[21] C. Berthon, G. Moebs, and R. Turpault. An Asymptotic-Preserving Scheme for Systems of Conservation Laws with Source Terms on 2D Unstructured Meshes. Finite Volumes for Complex Applications VII-Methods and Theoretical Aspects Volume 77 of the series Springer Proceedings in Mathematics and Statistics pp 107-115.

[22] C. Berthon and R.Turpault. Asymptotic preserving HLL schemes. Numerical Methods for Partial Differential Equations, 27 (6) (2011) 1396-1422.

[23] A. Bobylev, J. Carrillo, and I. Gamba. On some properties of kinetic and hydrodynamic equations for inelastic interactions. J. Stat. Phys. 98, 3 (2000), 743–773.

[24] A.V Bobylev and I.F Potapenko. Monte Carlo methods and their analysis for Coulomb collisions in multicomponent plasmas. J. Comp. Phys., 246, 123-144, 2013.

[25] N.N. Bogoliubov. Problems of Dynamical Theory in Statistical Physics. Studies in Statistical Mechanics, J. de Boer and G.E. Uhlenbeck eds., Interscience, New York, 1962.

[26] L. Boltzmann. Leçons sur la théorie des gaz. Gauthier-Villars (1902-1905). Réédition Jacques Gabay (1987).

[27] S. Boscarino, P.G. LeFloch, and G. Russo. High-order asymptotic-preserving methods for fully nonlinear relaxation problems. SIAM J. Sci. Comput. Vol. 36, No.2, pp.A377-A395.

[28] F. Bouchut. Nonlinear Stability of Finite Volume Methods for Hyperbolic Conservation Laws, and Well-Balanced Schemes for sources. Frontiers in Mathematics series, Birkhauser. (2004).

[29] F. Bouchut and T. Morales. A subsonic-well-balanced reconstruction scheme for shallow water flows. SIAM Journal on Numerical Analysis 48 (2010), no. 5, 1733–1758.

[30] F. Bouchut, H. Ounaissa, and B. Perthame. Upwinding of the source term at interfaces for Euler equations with high friction. Computers and Mathematics with Applications 53 (2007), 361-375.

[31] S.I. Braginskii. Reviews of Plasma Physics. M.A Leontovich, Ed., Consultants Bureau (New York, 1965), Vol. 1, p.205.

[32] S.I. Braginskii. Transport phenomena in a completely ionized two-temperature plasma. J. Exptl. Theoret. Phys. (U.S.S.R.) 33, 459-472 (1957).

[33] A.V. Brantov, V.Yu. Bychenkov, O.V. Batishchev, and W.Rozmus. Nonlocal heat wave propagation due to skin layer plasma heating by short laser pulses. Computer Physics communications 164 67, (2004).

[34] W. Braun and K. Hepp. The Vlasov dynamics and its fluctuations in the 1/n limit of interacting classical particles. Comm. Math. Phys. 56, 2 (1977), 101–113.

[35] S. Brull, P. Degond, and F. Deluzet. Degenerate anisotropic elliptic problems and magnetised plasma simulations. Commun. Comput. Phy., (2012).

[36] S. Brull, P. Degond, F. Deluzet, and A. Mouton. An asymptotic preserving scheme for a bi-fluid Euler-Lorentz system, Kinet. Rel. Models. Vol. 4, No. 4, (2011).

[37] C. Buet and S. Cordier. Asymptotic Preserving Scheme and Numerical Methods for Radiative Hydrodynamic Models. 951–956 C. R. Acad. Sci. Paris, Tome 338, Série I (2004).

[38] C. Buet and S. Cordier. Conservative and entropy decaying numerical scheme for the isotropic Fokker-Planck-Landau equation. J. Comput. Phys. 145, No.1, 228-245 (1998).

[39] C. Buet and S. Cordier. Numerical analysis of conservative and entropy schemes for the Fokker-Planck-Landau equation. SIAM J. Numer. Anal. 36, No. 3953-973, (1999).

[40] C. Buet, S. Cordier, P. Degond, and M. Lemou. Fast algorithm for numerical, conservative and entropy approximation of the Fokker-Planck-Landau equation. J. Comput. Physics 133 310-322, (1997).

[41] C. Buet, S. Cordier, and F. Filbet. Comparison of Numerical Schemes for Fokker-Planck-Landau Equation. ESAIM Proceedings, vol. 10, Soc. Math. Appl. Industry, Paris, pp. 161–181 (1999).

[42] C. Buet, S. Cordier, B. Lucquin-Desreux, and S. Mancini. Diffusion limit of the Lorentz model: asymptotic preserving schemes. M2AN Math. Model. Numer. Anal. 36 (4), 631–655, (2002).

[43] C. Buet and B. Després. Asymptotic analysis of fluid models for the coupling of radiation and hydrodynamics. J. Quant. Spectrosc. Radiat. Transfer, 85, 3-4, 385–418 (2004).

[44] C. Buet and B. Després. Asymptotic preserving and positive schemes for radiation hydrodynamics. J. Compt. Phy., 215, 717–740 (2006).

[45] C. Buet, B. Després, E. Franck, and T. Leroy. Proof of uniform convergence for a cell-centered AP discretization of the hyperbolic heat equation on general meshes. To appear in Math. of Comp.

[46] C. Buet, B. Després, and E. Franck. Design of asymptotic preserving finite volume schemes for hyperbolic heat equation on unstructured meshes. Numerische Mathematik, Volume 122, Issue 2, pp 227-278 (2012).

[47] O. Buneman. Dissipation of Currents in Ionized Media. Phys. Rev.115, 503 (1959).

[48] F. C. Buet, S. Cordier. Comparison of numerical scheme for Fokker-Planck-Landau equation. ESAIM Proc. 10 161-181, (1999).

[49] P. Cargo and A.-Y. Le Roux. Un schéma équilibre adapté au modèle d'atmosphère avec termes de gravité. Comptes rendus de l'Académie des sciences. Série 1, Mathématique 318 (1994), no. 1, 73–76.

[50] J.A. Carrillo, T. Goudon, P. Lafitte, and F. Vecil. Numerical schemes of diffusion asymptotics and moment closures for kinetic equations. J. Sci. Comput. 36 (1) (2008) 113–149.

[51] C. Cercignani, R. Illner, and M. Pulvirenti. The Mathematical Theory of Dilute Gases. Springer, New York NY, 1994.

[52] C. Chalons and F. Coquel. Modified Suliciu relaxation system and exact resolution of isolated shock waves. Math. Models Methods Appl. Sci. (M3AS), Vol. 24, No. 5 937–971 (2014).

[53] C. Chalons, F. Coquel, E. Godlewski, P.-A. Raviart, and N. Seguin. Godunov-type schemes for hyperbolic systems with parameter-dependent source. The case of Euler system with friction. Math. Models Methods Appl. Sci. 20 (2010), no. 11, 2109–2166. MR 2740716 (2011m:65179).

[54] C. Chalons, F. Coquel, and C. Marmignon. Well-balanced time implicit formulation of relaxation schemes for the euler equations. SIAM Journal on Scientific Computing 30 (2008), no. 1, 394–415.

[55] S. Chapman. On the Law of Distribution of Molecular Velocities, and on the Theory of Viscosity and Thermal Conduction, in a Non-Uniform Simple Monatomic Gas. Phil. Trans. Roy. Soc. London 216 (1916) 279.

[56] S. Chapman and T. G. Cowling. The Mathematical Theory of Non-Uniform Gases. Cambridge University Press, Cambridge, England, 1995.

[57] P. Charrier, B. Dubroca, G. Duffa, and R. Turpault. Multigroup model for radiating flows during atmospheric hypersonic re-entry. Proceedings of International Workshop on Radiation of High Temperature Gases in Atmospheric Entry, pp. 103–110. Lisbonne, Portugal. (2003).

[58] F. Chen. *Introduction to Plasma Physics and Controlled Fusion, (1984).* Plenum Press, New York.

[59] J.P. Chièze and R. Teyssier. Gas and Dark Matter Spherical Dynamics. The Astrophysical Journal, 484:40–52, 1997.

[60] F. Coron and B. Perthame. Numerical passage from kinetic to fluid equations. SIAM J. Numer. Anal. 28 (1991) pp. 26-42.

[61] P. Crispel, P. Degond, and M.-H. Vignal. A plasma expansion model based on the full Euler-Poisson system. Math. Models Methods Appl. Sci. 17 1129-1158, (2007).

[62] P. Crispel, P. Degond, and M.-H. Vignal. An Asymptotic Preserving scheme for the Euler equations in a strong magnetic field. Math. Models Methods Appl. Sci. 17 1129-1158, (2007).

[63] P. Crispel, P. Degond, and M.-H. Vignal. An asymptotic preserving scheme for the two-fluid Euler-Poisson model in the quasi-neutral limit. J. Comput. Phys. 223 (2007) 208-234, (2007).

[64] P. Crispel, P. Degond, and M.-H. Vignal. Quasi-neutral fluid models for current-carrying plasmas. Journal Comp. Phys. 205 408-438, (2005).

[65] N. Crouseilles and F. Filbet. Numerical approximation of collisional plasmas by high order methods. Journal Comp. Phys 201 546-572, (2004).

[66] N. Crouseilles, M. Lemou, and F. Méhats. Asymptotic Preserving schemes for highly oscillatory Vlasov Poisson equations. Volume 248, Pages 287–308, 1 September 2013.

[67] R. Dautray and J.P. Watteau. La fusion thermonucléaire Inertielle par Laser. Collection du CEA, série synthèse, Eyrolles, Paris, (1993).

[68] P. Degond, F. Deluzet, L. Navoret, A. Sun, and M. Vignal. Asymptotic-Preserving Particle-In-Cell method for the Vlasov-Poisson system near quasineutrality. J. Comput. Phys, 229 no 16, 5630-5652, (2010).

[69] P. Degond, F. Deluzet, A. Sangam, and M.-H. Vignal. An Asymptotic Preserving scheme for the Euler equations in a strong magnetic field. J. Comput. Phys. Volume 228, Issue 1, (2009).

[70] P. Degond, H. Liu, D. Savelief, and M-H. Vignal. Numerical approximation of the Euler-Poisson-Boltzmann model in the quasineutral limit. C. R. Acad. Sci. Paris, Ser. I 341 323–328, (2005).

[71] P. Degond, A. Lozinski, J. Narski, and C. Negulescu. An Asymptotic-Preserving method for highly anisotropic elliptic equations based on a micro-macro decomposition. J. Comp. Phys., 231 (2012), pp. 2724-2740.

[72] P. Degond and B. Lucquin-Desreux. An entropy scheme for the Fokker-Planck collision operator of plasma kinetic theory. Nummer. Math 68 (1994) 239-262.

[73] P. Degond and B. Lucquin-Desreux. The Fokker-Planck asymptotics of the Boltzmann collision operator in the Coulomb case. M3AS vol 2 (1992) 167-182.

[74] P. Degond, D. Savelief, and F. Deluzet. Numerical approximation of the Euler-Maxwell model in the quasineutral limit. J. Comput. Phys. 231 (2012) 1917–1946.

[75] J.-L. Delcroix and A. Bers. Physique des plasmas. InterEditions, Paris, 1994, V.2.

[76] J.-L. Delcroix and A. Bers. Physique des plasmas 1. CNRS editions-EDP Sciences, Paris (1998).

[77] J.-L. Delcroix and A. Bers. Physique des plasmas 2. CNRS editions-EDP Sciences, Paris (1998).

[78] S. Dellacherie. Contribution à l'analyse et a la simulation numérique des equations cinétiques décrivant un plasma chaud. PhD thesis from Univ. Denis Diderot Paris VII, CEA BIII (1998).

[79] V. Desveaux, M. Zenk, C. Berthon, and C. Klingenberg. Well-balanced schemes to capture non-explicit steady states. Part 1: Ripa model. Math. Comp. 85 (2016), 1571-1602.

[80] G Dimarco and L Pareschi. Asymptotic Preserving Implicit-Explicit Runge–Kutta Methods for Nonlinear Kinetic Equations. SIAM Journal on Numerical Analysis 51 (2013), 1064-1087.

[81] R. L. Dobrushin. Vlasov equations. Funktsional Anal. i Prilozhen 13, 2 (1979), 48–58.

[82] J.F. Drake, P.K. Kaw, Y.C. Lee, G. Schmidt, C.S. Liu, and M.N. Rosenbluth. Parametric instabilities of electromagnetic waves in plasmas. Phys. Fluids 17, 778, 1974.

[83] B. Dubroca, J.-L. Feugeas, and M. Frank. Angular moment model for the Fokker-Planck equation. European Phys. Journal D, 60, 301, (2010).

[84] B. Dubroca and J.L. Feugeas. Entropic moment closure hierarchy for the radiative transfert equation. C. R. Acad. Sci. Paris Ser. I, 329 915, (1999).

[85] B. Dubroca and J.L. Feugeas. Étude théorique et numérique d'une hiéarchie de modèles aux moments pour le transfert radiatif. C. R. Acad. Sci. Paris, t. 329, SCrie I, p. 915-920, (1999).

[86] R. Duclous. *Modélisation et Simulation Numérique multi-échelle du transport cinétique électronique*. PhD thesis, Université Bordeaux 1, 2009.

[87] R. Duclous, B. Dubroca, F. Filbet, and V. Tikhonchuk. High order resolution of the Maxwell-Fokker-Planck-Landau model intended for ICF applications. J. Comput. Phys. 228(14): 5072-5100 (2009).

[88] R. Duclous, B. Dubroca, and M. Frank. Deterministic Partial Differential Equation Model for Dose Calculation in Electron Radiotherapy. Phys. Med. Biol. 55 3843-3857., 2010.

[89] J.J. Duderstadt and G.A. Moses. Inertial Confinement Fusion. Wiley-Interscience Publication, (1982).

[90] D. Enskog. Kinetische Theorie der Vorgänge in Mässig Verdünnten Gasen. Uppsala, 1917.

[91] E. Epperlein and R. Short. Phys. Fluids B 4, 2211 1992.

[92] F. Filbet and S. Jin. A class of asymptotic preserving schemes for kinetic equations and related problems with stiff sources. J. Comp. Phys. vol. 229, no 20 (2010).

[93] F. Filbet and L. Pareschi. A Numerical Method for the Accurate Solution of the Fokker-Planck-Landau Equation in the Non Homogeneous Case. J. Comput. Physics vol. 179 no. 1, pp. 1-26 (2002).

[94] F. Filbet and T. Rey. A hierarchy of hybrid numerical methods for multi-scale kinetic equation. SIAM J. Sci. Computing, 37 Issue: 3 Pages: A1218-A1247 (2015).

[95] F. Filbet and T. Rey. A Rescaling Velocity Method for Dissipative Kinetic Equations - Applications to Granular Media. J. Comput. Physics, vol 248, pp. 177-199 (2013).

[96] F. Filbet and G. Russo. A Rescaling Velocity Method for Kinetic Equations: the Homogeneous Case. In Proceedings Modelling and Numerics of Kinetic Dissipative Systems (Lipari, 2004), Nova-Science, p. 11.

[97] M. Franck, A. Klar and. E. W. Larsen, and S. Yasuda. Approximate models for radiative transfer. Bulletin-institute of mathematics academia sinica, 2(2), 409. (2007).

[98] K.0. Friedrichs and P.D. Lax. Systems of Conservation Equations with a Convex Extension. Proc. Nat. Acad. Sci. USA Vol. 6S, No. 8, pp. 1686-1688, 1971.

[99] I. Gallagher, L. Saint-Raymond, and B. Texier. From Newton to Boltzmann : the case of hard spheres and short-range potentials. Zürich Lectures in Advanced Mathematics, Eur. Math. Soc., Zürich, 2013.

[100] G. Gallice. Positive and entropy stable Godunov-type schemes for gas dynamics and MHD equations in Lagrangian or Eulerian coordinates. Numer. Math. 94 (2003), no. 4, 673–713. MR 1990589 (2004e:65094).

[101] E. Godlewski and P.-A. Raviart. Numerical approximation of hyperbolic system of conservation laws. Springer (1995).

[102] S. K. Godunov. A difference method for numerical calculation of discontinuous solutions of the equations of hydrodynamics. Mat. Sb., 47 (1959), pp. 271-306.

[103] D. M. Goebel and I. Katz. Fundamentals of electric propulsion: ion and Hall thrusters. John Wiley & Sons. (Vol. 1), (2008).

[104] M. Gonzáles. Contribution a l'étude numérique de l'hydrodynamique radiative: des expériences de chocs radioatifs aux jets astrophysiques. PhD thesis of Paris-Sud XI Univ, (2006).

[105] L. Gosse. Computing qualitatively correct approximations of balance laws. SEMA SIMAI Springer Series.

[106] L. Gosse and G. Toscani. An asymptotic-preserving well-balanced scheme for the hyperbolic heat equations. C. R. Math. Acad. Sci. Paris 334 (4) (2002) 337–342.

[107] L. Gosse and G. Toscani. Space localizaion and well-balanced schemes for discrete kinetic models in diffusive regimes. SIAM J. Numer. Anal. 41 (2) (2003) 641–658.

[108] T. Goudon and C. Lin. Analysis of the M1 model: well-posedness and diffusion asymptotics. J. Math. Anal. Appl. 402 (2) (2013) 579–593.

[109] H. Grad. On the kinetic theory of rarefied gases. Commun. Pure Appl. Math. 2, 331-407 (1949).

[110] J. M. Greenberg and A. Y. Leroux. A well-balanced scheme for the numerical processing of source terms in hyperbolic equations. SIAM J. Numer. Anal., 33, 1–16 (1996).

[111] E.P. Gross, P.L. Bathnagar, and M. Krook. A Model for Collision Processes in Gases. I. Small Amplitude Processes in Charged and Neutral One-Component Systems. Phys. Rev. 94 (1954), 511.

[112] C.P.T. Groth and J.G. McDonald. Towards physically-realizable and hyperbolic moment closures for kinetic theory. Continuum Mech. Thermodyn. 21, 467-493 (2009).

[113] S. Guisset, S. Brull, E. d'Humières, and B. Dubroca. Asymptotic-preserving well-balanced scheme for the electronic M_1 model in the diffusive limit: particular cases. Submitted.

[114] S. Guisset, S. Brull, B. Dubroca, E. d'Humières, S. Karpov, and I. Potapenko. Asymptotic-preserving scheme for the Fokker-Planck-Landau-Maxwell system in the quasi-neutral regime. Communications in Computational Physics, volume 19, issue 02, pp. 301-328 (2016).

[115] S. Guisset, S. Brull, E. d'Humières, B. Dubroca, and V. Tikhonchuk. Classical transport theory for the collisional electronic M1 model. Physica A: Statistical Mechanics and its Applications, Volume 446, Pages 182-194 (2016).

[116] S. Guisset, M. Gutnic, P. Helluy, M. Massaro, L. Navoret, N. Pham, and M. Roberts. agrangian/Eulerian solvers and simulations for Vlasov-Poisson. ESAIM: proceedings and surveys, March 2016, Vol. 53, p. 120-132.

[117] S. Guisset, J.G. Moreau, R. Nuter, S. Brull, E. d'Humières, B. Dubroca, and V.T. Tikhonchuk. Limits of the M1 and M2 angular moments models for kinetic plasma physics studies. J. Phys. A: Math. Theor. 48, 335501 (2015).

[118] A. Harten, P.D. Lax, and B. Van Leer. On upstream differencing and Godunov-type schemes for hyperbolic conservation laws. SIAM Review 25 (1983), 35-61.

[119] C. Hauck and R. McLarren. Positive P_N closures. Siam J. Sci. Comp. 32, 2603, pp. 2603–2626, (2010).

[120] C.D. Hauck. High-order entropy-based closures for linear transport in slab geometry. Commun. Math. Sci 9 (1), 187-205 (2011).

[121] M. Hauray and P.E. Jabin. N-particles approximation of the Vlasov equation with singular potential. Arch. Ration. Mech. Anal. 183, 3 (2007), 489–524.

[122] Philippe Helluy, Michel Massaro, Laurent Navoret, Nhung Pham, and Thomas Strub. Reduced Vlasov-Maxwell modeling. PIERS Proceedings, August 25-28, Guangzhou, 2014, Aug 2014, Gunagzhou, China. pp.2622-2627, 2014.

[123] F.L. Hinton. Collisional transport in plasma. Basics Plasma Physics I, 147-197, (1983).

[124] O. E. Lanford III. Time evolution of large classical systems. Dynamical Systems, theory and applications. J. Moser éd.. Lecture Notes in Physics 38, 1–111, Springer-Verlag, Heidelberg, 1975.

[125] R. Illner and M. Pulvirenti. Global validity of the Boltzmann equation for a two-dimensional rare gas in vacuum. Erratum and improved result. Commun. Math. Phys. 105 (1986), 189–203.

[126] R. Illner and M. Pulvirenti. Global validity of the Boltzmann equation for two and three dimensional rare gas in vacuum. Commun. Math. Phys. 121 (1989), 143–146.

[127] P. Lafitte J.A. Carrillo, T. Goudon. Simulation of fluid and particles flows: asymptotic preserving schemes for bubbling and flowing regimes. J. Comput. Phys. 227 (16) (2008) 7929–7951.

[128] S. Jin and C.D. Levermore. Fully discrete numerical transfer in diffusive regimes. Transport Theory Statist. Phys. 22 (6) 739–791. (1993).

[129] S. Jin and C.D. Levermore. The discrete-ordinate method in diffusive regimes. Transport Theory Statist. Phys. 20 (5–6) 413–439. (1991).

[130] S. Jin and L. Pareschi. Discretization of the multiscale semiconductor Boltzmann equation by diffusive relaxation scheme. J. Comput. Phys. 161, 312-330, (2000).

[131] S. Jin, L. Pareschi, and G. Toscani. Uniformly accurate diffusive relaxation schemes for multiscale transport equations. SIAM J. Numer. Anal. 38 (3), 913–936, (2000).

[132] S. Jin and Z. Xin. The relaxation scheme for systems of conservation laws in arbitrary space dimension. Comm. Pure Appl. Math. 45, (1995) 235–276.

[133] M. Junk and A. Unterreiter. Maximum entropy moment systems and Galilean invariance. Contin. Mech. Thermodyn. 14 (2002), no. 6, 563–576.

[134] S. Kaneko. J. Phys. Soc. Jpn. 15 (1960) 1685.

[135] S. Kaneko and M. Tagushi. J. Phys. Soc. Jpn. 45 (1978) 1380.

[136] S. Kaneko and A. Yamao. J. Phys. Soc. Jpn. 48 (1980) 2098.

[137] F. KING. BBGKY hierarchy for positive potentials. Mémoire de Ph.D., Département de Mathématiques, Univ. of California, Berkeley, 1975.

[138] A. Klar. An asymptotic-induced scheme for nonstationary transport equations in the diffusive limit. SIAM J. Numer. Anal. 35 (3), 1073–1094, (1998).

[139] A. Klar. An asymptotic preserving numerical scheme for kinetic equations in the low Mach number limit. SIAM J. Numer. Anal. 36, 15071527, (1999).

[140] A. Klar and C. Schmeiser. Numerical passage from radiative heat transfer to nonlinear diffusion models. Math. Models Methods Appl. Sci. 11 (5), 749–767, (2001).

[141] A. Klar and A. Unterreiter. Uniform stability of a finite difference scheme for transport equations in the diffusion limit. SIAM J. Numer. Anal. 40 (3) (2002) 891-913.

[142] Y. L. Klimontovich. The kinetic theory of electromagnetic processes. Zh. Eksp. Teor. Fiz. 33, 928 (1958) [Sov. Phys. JETP 6, 753 (1958)]; (translated by A. Dobroslavsky, Springer-Verlag, 1983).

[143] N. Krall and A. Trivelpiece. Principles of Plasma Physics, McGraw Hill, New York 1973.

[144] N. Krall and A. Trivelpiece. *Principles of Plasma Physics.* San Francisco Press.

[145] Eriksson L.-G. and Helander P. Simulation of runaway electrons during tokamak dis- ruptions. Computer Physics communications, (2003), 154, 175.

[146] Eriksson L.-G., Helander P., Andersson F., Anderson D., and Lisak M. Current Dynamics during Disruptions in Large Tokamaks. Physical Review Letter, (2004), 92, 20.

[147] P. Lafitte and G. Samaey. Asymptotic-preserving projective integration schemes for kinetic equations in the diffusion limit. SIAM Journal on Scientific Computing , 34(2):A579– A602, 2012.

[148] L. Landau. On the vibration of the electronic plasma. J. Phys. USSR 10 (1946).

[149] L.D. Landau. Kinetic equation for the case of Coulomb interaction. Phys. Zs. Sov. Union, 10, 154-164 (1936).

[150] A.W. Larsen and J.E. Morel. Asymptotic solutions of numerical transport problems in optically thick, diffusive regimes II. J. Comput. Phys. 83 (1), 212–236, (1989).

[151] A.W. Larsen, J.E. Morel, and W.F. Miller Jr. Asymptotic solutions of numerical transport problems in optically thick, diffusive regimes. J. Comput. Phys. 69 (2), 283–324, (1987).

[152] G. Laval. La fusion thermonuclaire inertielle par laser, Partie 1: L'interaction laser-matière. Eyrolles editions, Paris 1993.

[153] J. D. Lawson. Some Criteria for a Power Producing Thermonuclear Reactor. Proceedings of the Physical Society. Section B, vol. 70 (1957) 6-10.

[154] B. Van Leer. Towards the ultimate conservative difference scheme III. Upstream-centered finite-difference schemes for ideal compressible flow. J. Comput. Phys. 23, 3 (Mar. 1977), 263–275.

[155] M. Lemou and L. Mieussens. A new asymptotic preserving scheme based on Micro-Macro formulation for linear kinetic equations in the diffusion limit. SIAM J. Sci. Comput., 31(1), 334–368, 2008.

[156] M. Lemou and L. Mieussens. Fast implicit schemes for the Fokker-Planck-Landau equation. C. R. Math. Acad. Sci. Paris, 338, no. 10, 809-814, (2004).

[157] M. Lemou and L. Mieussens. Implicit schemes for the Fokker-Planck-Landau equation. SIAM J. Sci. Comput., Vol. 27, No. 3, pp. 809-830, (2005).

[158] A. Lenard. Ann. Phys. (N.Y.) 3, 390 (1960).

[159] R.J. Leveque. Finite volume methods for hyperbolic problems. Cambridge texts in applied mathematics.

[160] C.D. Levermore. Moment closure hierarchies for kinetic theories. J. Stat. Phys. 83, 1021-1065 (1996).

[161] E.M. Lifchitz and L.P. Petaevski. Kinetic theory. MIR, Moscow (1979).

[162] E. M. Lifshitz and L. P. Pitaevskii. Plasma Kinetics, Pergamon Press, 1981.

[163] J.D. Lindl. Inertial Confinement Fusion. AIP Press, Springer-Verlag, 1998.

[164] J. Liu and L. Mieussens. Analysis of an asymptotic preserving scheme for linear kinetic equations in the diffusion limit. SIAM J. Numer. Anal. 48 (4) (2010) 7561-7586.

[165] D. Lynden-Bell. Statistical mechanics of violent relaxation in stellar systems. Mon. Not. R. Astr. Soc., 136 (1967), 101–121.

[166] J. Mallet, S. Brull, and B. Dubroca. An entropic scheme for an angular moment model for the classical Fokker-Planck-Landeau equation of electrons. Comm. Comput. Phys., 422, (2013).

[167] J. Mallet, S. Brull, and B. Dubroca. General moment system for plasma physics based on minimum entropy principle. Kinetic and Related Models, vol. 8, No.3, 533-558, (2015).

[168] Jessy Mallet. *Contribution à la modélisation et à la simulation numérique multi-échelle du transport cinétique électronique dans un plasma chaud.* PhD thesis, Université Bordeaux 1, 2012.

[169] J. H. Malmberg and C. B. Wharton. Phys. Rev. Lett. 13, 184 (1964).

[170] A. Marocchino, M. Tzoufras, S. Atzeni, A. Schiavi, Ph. D. Nicolaï, J. Mallet, V. Tikhonchuk, and J.-L. Feugeas. Nonlocal heat wave propagation due to skin layer plasma heating by short laser pulses. Phys. Plasmas 20, 022702, (2013).

[171] J. C. Maxwell. A Dynamical Theory of the Electromagnetic Field. Philosophical Transactions of the Royal Society of London 155, 459–512 (1865).

[172] J.G. McDonald and C.P.T. Groth. Towards realizable hyperbolic moment closures for viscous heat-conducting gas flows based on a maximum-entropy distribution. Continuum Mech. Thermodyn. 25, 573-603 (2012).

[173] N. Meezan, L. Divol, M. Marinak, G. Kerbel, L. Suter, R. Stevenson, G. Slark, and K. Oades. Phys. Plasmas 11, 5573 2004.

[174] D. Mihalas and B. W. Mihalas. Foundations of Radiation Hydrodynamics. New York: Oxford University Press, 1984.

[175] G.N. Minerbo. Maximum entropy Eddigton Factors. J. Quant. Spectrosc. Radiat. Transfer, 20, 541, (1978).

[176] S. Mischler and C. Mouhot. Cooling process for inelastic Boltzmann equations for hard spheres, Part II: Self-similar solutions and tail behavior. J. Stat. Phys. 124, 2 (2006), 703–746.

[177] I. Muller and T. Ruggeri. Rational Extended Thermodynamics. Springer, New York (1998).

[178] Dwight R. Nicholson. Introduction to plasma theory. John Wiley and Sons.

[179] Ph. D. Nicolai, J.-L. A. Feugeas, and G. P. Schurtz. A practical nonlocal model for heat transport in magnetized laser plasmas. Phys. Plasmas 13, 032701, (2006).

[180] Ph. Nicolaï, M. Vandenboomgaerde, B. Canaud, and F. Chaigneau. Effects of self-generated magnetic fields and nonlocal electron transport in laser produced plasmas. Phys. Plasmas 7, 4250 2000.

[181] T. Pichard, D. Aregba, S. Brull, B. Dubroca, and M. Franck. Relaxation schemes for the M1 model with space-dependent flux: application to radiotherapy dose calculation. Communications in Computational Physics, vol 19, 1, 168–191 (2016).

[182] G.C. Pomraning. Maximum entropy Eddington factors and flux limited diffusion theory. J. of Quantitative Spectroscopy and Radiative Transfer, 26 5 385-388 (1981).

[183] M. Pulvirenti, C. Saffirio, and S. Simonella. On the validity of the Boltzmann equation for short range potentials. prépublication arXiv:1301.2514.

[184] S. Jin R. Caflish and G. Russo. Uniformly accurate schemes for hyperbolic systems with relaxation. SIAM J. Numer. Ana. 34, 24628, (1997).

[185] T. Rey and C. Tan. An Exact Rescaling Velocity Method for some Kinetic Flocking Models. To appear in SIAM J. Num. Anal.

[186] J.-F. Ripoll. An averaged formulation of the M1 radiation model with presumed probability density function for turbulent flows. J. Quant. Spectrosc. Radiat. Trans. 83 (3–4), 493–517. (2004).

[187] J.-F. Ripoll, B. Dubroca, and E. Audit. A factored operator method for solving coupled radiation-hydrodynamics models. Trans. Theory. Stat. Phys. 31, 531–557. (2002).

[188] M.N. Rosenbluth, W.M. MacDonald, and D.L. Judd. Fokker-Planck equation for an inverse-square force. Phys. Rev., 107, 1-6 (1957).

[189] W. Rozmus, V. T. Tikhonchuk, and R. Cauble. A model of ultrashort laser pulse absorption in solid targets. Phys. Plasmas 3, 360 (1996).

[190] K. Shigemori, H. Azechi, M. Nakai, M. Honda, K. Meguro, N. Miyanaga, H. Takabe, and K. Mima. Phys. Rev. Lett. 78, 250 1997.

[191] I.P. Shkarofsky, T.W. Johnston, and The Particle Kinetics of Plasmas M.P. Bachynski. Addison-Wesley (Reading, Massachusetts, 1966).

[192] J.S Shrimpton, S. Haeri, and S.S Scott. Statistical treatment of turbulent polydisperse particle systems. Springer.

[193] L. Spitzer and R. Härm. Phys. Rev. 89 (1953) 977.

[194] H. Struchtrup. Macroscopic Transport Equations for Rarefied Gas Flows. Springer, Berlin (2005).

[195] S. Subramaniam. Statistical representation of a spray as a point process. *Physics of Fluids*, 12(10):2413–2431, 2000.

[196] A. Sunahara, J. Delettrez, C. Stoeckl, R. Short, and S. Skupsky. Phys. Rev. Lett. 91, 095003 2003.

[197] A.G.R. Thomas, M. Tzoufras, A.P.L. Robinson, R.J. Kingham, C.P. Ridgers, M. Sherlock, and A.R. Bell. A review of vlasov-fokker-planck numerical modeling of inertial confinement fusion plasma. *Journal of Computational Physics*, 231(3):1051–1079, 2012.

[198] E.F. Toro. *Riemann Solvers and Numerical Methods for Fluids dynamics.* Springer, Berlin, 1999.

[199] M. Touati, J.L. Feugeas, P. Nicolaï, J.J. Santos, L. Gremillet, and V.T. Tikhonchuk. New Journal of Physics 16 (2014).

[200] R. Turpault. A consistent multigroup model for radiative transfer and its underlying mean opacity. J. Quant. Spectrosc. Radiat. Transfer 94, 357–371 (2005).

[201] R. Turpault, M. Frank, B. Dubroca, and A. Klar. Multigroup half space moment appproximations to the radiative heat transfer equations. J. Comput. Phys. 198 363 (2004).

[202] A. Velikovich, J. Dahlburg, J. Gardner, and R. Taylor. Phys. Plasmas 5, 1491 1998.

[203] C. Villani. A review of mathematical topics in collisional kinetic theory. Handbook of mathematical fluid dynamics, 1, 71-305, (2002).